Aus dem Institut für Humanernährung und Lebensmittelkunde

der Christian-Albrechts-Universität zu Kiel

Influence of process factors on the formation and fragmentation of amyloid and amyloid-like aggregates from beta-lactoglobulin

Dissertation

zur Erlangung des Doktorgrades

der Agrar- und Ernährungswissenschaftlichen Fakultät

der Christian-Albrechts-Universität zu Kiel

vorgelegt von

M.Sc. Timon Robert Heyn

aus Hamburg

Kiel, 2020

Dekan: Prof. Dr. Dr. Christian Henning

1. Berichterstatter: Prof. Dr. Karin Schwarz

2. Berichterstatter: Assist. Prof. Dr. Julia Keppler

Tag der mündlichen Prüfung: 15. Mai 2020

Gedruckt mit Genehmigung der Agrar- und Ernährungswissenschaftlichen Fakultät der
Christian-Albrechts-Universität zu Kiel

Acknowledgement

I am indebted to the **German research foundation** (**DFG**) who funded the conducted research of this thesis within the priority program SPP1934 “Dispersitäts-, Struktur- und Phasenänderungen von Proteinen und biologischen Agglomeraten in biotechnologischen Prozessen”.

I am deeply grateful to my doctoral supervisor **Prof. Karin Schwarz**, for the opportunity to deepen my scientific education in the department of food technology and who intervened with remarkable precision at the necessary points and supported me with tips and advice in the development of my dissertation.

My greatest thanks go to **Dr. Julia Keppler**, who infected me with her exemplary passion for science and the research of beta-lactoglobulin already during my bachelor's studies and implemented the nucleus of curiosity for the scientific field of whey proteins in me. The nucleus grew and led to a combination of new possibilities to go deeper into this field of research. It has now becomes a stable fibril of expertise, to which development Julia has contributed significantly with her talent for constructive ideas, motivating words and the right questions at the right time.

Many thanks go to my cooperation partners from the *Institute of Particle Technology in Braunschweig*: **Prof. Kwade, Dr. Kampen, Herr Mayer** and **Frau Michel**. From the *Institute of Particle Technology in Erlangen*: **Prof. Peukert** and **Herr Uttinger**. From the *Institute of Material Science in Kiel*: **Prof. Selhuber-Unkel** and **Dr. Neumann**. And from the *Centre of Coastal Research in Geesthacht*: **Dr. Garamus.**

The successful buildup of the thesis at hand was also possible, due to numerous talented students. Therefore, I would like to thank **Monique Heuer, Monica Gamba, Jesco Reimer, Lisiane Petersen, Katja Kasper-Gempfer, Anika Ziemer and Bisher Eymsh**.

During the course of the doctoral period the office or laboratory tends to become a second home. How wonderful, when this house is filled with shared laughter, warm words and mutual helpfulness. Thank you **to the team of the food technology Kiel**. I am grateful for each and every one of you with whom I was able to share this house full of warmth. A special thank goes to my fibril buddy **Jacqueline Lux**, for sharing travels, office and amyloid conversations.

At some point during the day you have enough of fibrils and co. and then its fine that colleagues and research partners associate to the common circle of friends and you can have another off-topic conversation about all the really important things in life. Thanks to **Eva, Jacqueline, Fynn, Jule, Jonas, Laura, Philipp, Max, Therese and Neeskea** for sharing good times and laughter

Doing a promotion presents you with new challenges you have to master every day. The art is to take the challenges for personal development. Many thanks to **Thomas, Heike, Sören, Daniel, Anna, Babsi, Mark, Stephan, Ute, Lea** and **Anja** for your reflections during the enneagrammatic talks and discussions, as well as the joint philosophizing and journeys.

I would like to extend an especially warm thank you to my family. Dear **Papa**, dear **Mama**, dear **Ina** and dear **Tonia**, I am so incredibly grateful that I grew up in your sheltered and warm circle and thus could simply face the challenges of this work with much trust and confidence.

Finally, I want to thank my dear wife **Charlotte** for always being by my side.

Abstract

Protein amyloid-aggregation is increasingly being recognized to expand, broaden and enrich protein functionalities. A large number of very different proteins, including the whey protein beta-lactoglobulin (BLG) have been shown to convert into amyloid fibrils under properly designed conditions. At high temperatures and acid conditions, BLG forms semi-flexible amyloid fibrils (at pH 2) or flexible amyloid-like aggregates (at pH 3.5). It was mentioned, that the interfacial properties of amyloid aggregates are different from those of non-aggregated BLG. For example, the application of fibrils leads to a higher physical and chemical stabilization of oil-water emulsions and foams. However, in the production of emulsions the protein structures are exposed to high shear forces and cavitation in combination with a high specific surface area of the oil-water interface. These process factors can contribute to the degradation of the amyloid aggregates. Otherwise, shear and interfaces also have a high relevance for the formation of amyloid structures. To date, no comparison of the different morphologies with respect to physico-chemical properties, as well as formation kinetics and stability as a function of mechanical stress or interfaces has been performed. This information is relevant to estimate the value of the respective aggregates for different applications.

In order to obtain this information, several studies were conducted in this thesis. The investigation of the aggregate building blocks have shown that pH 2 fibrils build from peptides, while worm-like aggregates formed from unhydrolysed BLG. Analysis of the physico-chemical properties revealed a higher proportion of beta-sheets, a higher compactness, a higher zeta-potential and a lower hydrophobicity of the fibrils compared to the worm-like aggregates. Using a statistically designed experiment, it was possible to identify the temperature as the most important factor for aggregation kinetics. Interactions of temperature with pH value and stirring speed were determined. The nucleation supporting effect of mechanical energy input and surfaces on the amyloid aggregation kinetics was demonstrated by using chemically modified glass beads in the shaking incubator. The impact on the length of the aggregates was investigated in more detail in shearing experiments with rotor-stator and ultra-sonication in the presence and absence of a dispersed oil-phase. A dependence of the fibril fragmentation on the amount of shear stress and the presence of oil was found, while the worm-like aggregates remained unaffected to rotor-stator-shear. In summary, this thesis demonstrates that amyloid and amyloid-like aggregates have different characteristics with respect to structure, physico-chemical properties, formation kinetics and process stability, which makes them suitable for different technological applications.

Publications

Peer reviewed journals

Accepted:

Heyn, T. R.; Garamus, V. M.; Neumann, H. R.; Uttinger, M. J.; Guckeisen, T.; Heuer, M.; Selhuber-Unkel, C.; Peukert, W.; Keppler, J.K. (2019): Influence of the polydispersity of pH 2 and pH 3.5 beta-lactoglobulin amyloid fibril solutions on analytical methods. In: *European Polymer Journal.* 120, 109211. DOI*:* 10.1016/j.eurpolymj.2019.08.038.

Heyn, T. R.; Mayer, J.; Neumann, H. R.; Kwade, A.; Selhuber-Unkel, C.; Schwarz, K.; Keppler, J.K. (2020): The threshold of amyloid aggregation of beta-lactoglobulin: Relevant factor combinations. In: *Journal of Food Engineering.* Article reference: JFOE_110005.

Keppler, J. K.; Heyn, T. R.; Meissner, P. M.; Schrader, K.; Schwarz, K. (2019): Protein oxidation during temperature-induced amyloid aggregation of beta-lactoglobulin. In: *Food chemistry.* 289, S. 223–231. DOI: 10.1016/j.foodchem.2019.02.114.

Uttinger, M. J.; Heyn, T. R.; Jandt, U.; Wawra, S. E.; Winzer, B.; Keppler, J.K.; et al. (2020): Measurement of length distribution of beta-lactoglobulin fibrils by multiwavelength analytical ultracentrifugation. In: *European Biophysics Journal*. DOI: 10.1007/s00249-020-01421-4.

Eymsh, B.; Drobny, A.; Heyn, T. R.; Xiang, W.; Lucius, R.; Schwarz, K. et al. (2020): Toxic Metamorphosis-How Changes from Lysosomal to Cytosolic pH Modify the Alpha-Synuclein Aggregation Pattern. In: Biomacromolecules 21 (12), S. 4673–4684. DOI: 10.1021/acs.biomac.0c00629.

Lux, J.; Heyn, T. R.; Kampen, I.; Schwarz, K.; Keppler, J. K.; Steffen-Heins, A. (2021): Amyloid aggregation of spin-labeled β-lactoglobulin. Part I. Influence of spin labeling on amyloid aggregation. In: Food Hydrocolloids 112, S. 106178. DOI: 10.1016/j.foodhyd.2020.106178.

Keppler, J. K.; Heyse, A.; Scheidler, E.; Uttinger, M. J.; Fitzner, L.; Jandt, U. et al. (2021): Towards recombinantly produced milk proteins. Physicochemical and emulsifying properties of engineered whey protein beta-lactoglobulin variants. In: Food Hydrocolloids 110, S. 106132. DOI: 10.1016/j.foodhyd.2020.106132.

Under review:

Heyn, T. R.; Uttinger, M. J.; Kwade, A.; Peukert, W.; Keppler, J.K.; Schwarz, K. (2020): Whey protein (amyloid)-aggregates in oil-water systems: The process-related comminution effect. In: *Journal of Food Engineering.* Article reference: JFOODENG-D-21-00032.

Oral and poster presentations:

Heyn, T. R.; Keppler J. K.; Schwarz K. (2018): Funktionalisierung von Proteinen zur Stabilisierung von Emulsionen und Schäumen mit Milch und Molkenprotein. At: *Protein Symposium ZDS*, Kiel, Germany [oral]

Heyn, T. R.; Keppler J. K.; Schwarz K. (2018): Amyloide Aggregate aus Molkenprotein. At: *Kieler Milchtage*, Kiel, Germany [oral]

Heyn, T. R.; Lux, J.; Steffen-Heins, A.; Schwarz K.; Keppler J. K. (2018): Determination of critical process parameters for the onset of amyloid aggregation of whey protein beta-lactoglobulin. At: *ProcessNet Jahrestagung*, Aachen, Germany [oral] DOI: doi.org/10.1002/cite.201855441

Heyn, T. R.; Lux, J.; Neumann, H. R.; Steffen-Heins, A.; Schwarz, K.; Selhuber-Unkel, C.; Keppler J. K. (2019): Physico-chemical properties of different fractions of whey protein beta-Lactoglobulin amyloid aggregates. At: *Delivery of Functionality*, Porto, Portugal [poster]

Heyn, T. R; Lux, J.; Uttinger, M. J.; Schrader, M.; Kwade, A.; Peukert, W.; Steffen-Heins, A.; Schwarz, K.; Keppler, J. K. (2019): High pressure homogenisation affects the length distribution and functionality of amyloid aggregates from whey. At: *NIZO Dairy Conference*, Papendal, Netherlands [poster]

Heyn, T. R.; Lux, J.; Steffen-Heins, A.; Schwarz, K. Keppler, J.K. (2019): Hochschultagung 31. Januar 2019 - Verhalten von amyloiden Aggregaten aus Molkenprotein in technologischen Prozessen. At: *Hochschultagung der Agrar- und Ernährungswissenschaftlichen Fakultät*, Kiel, Germany [Poster]

Table of contents

Figures

Tables

Equations

List of abbreviations

Å, Ångstrom = 0.1 nm

AFM, atomic force microscopy

Arg, arginine

Asp, asparagine

ATR-FTIR, attenuated total reflection Fourier transform infrared spectroscopy

AUC, analytical ultracentrifugation

BLG, beta-lactoglobulin

BLG A, beta-lactoglobulin genetic variant A

BLG B, beta-lactoglobulin genetic variant B

BSE, bovine spongiform encephalopathy

CFD, computational fluid dynamics

Cys, cysteine

DBLG, dissociated beta-lactoglobulin

DEM, Discrete Element Method

DHS, dissociated heated solution

DTT, dithiothreitol

DLBLG, dissociated lyophilised beta-lactoglobulin

DLF, dissociated lyophilised filtrate

DLHS, dissociated lyophilised heated solution

DLR, dissociated lyophilised retentate

DLS, dynamic light scattering

DOE, design of experiments

DSC, differential scanning calorimetry

H^+, proton

HS, heated solution

LBLG, lyophilised beta-lactoglobulin

LF, lyophilised filtrate

LHS, lyophilised heated solution

LR, lyophilised retentate

pI, isoelectric point

PTFE, polytetrafluorethylene

SAXS, small angle X-ray scattering

SEC, size exclusion chromatography

ThT, thioflavin-T

TRP, tryptophan

UF, ultrafiltration

VOF, volume of fluid

1. Motivation and objectives

The milk protein beta-lactoglobulin (BLG) forms so-called fibrils under certain conditions (Loveday et al. 2017; Cao and Mezzenga 2019; van der Linden and Venema 2007). These fibrils can be described as long semi-flexible aggregate strands, which have a length of more than 10 µm and a maximum thickness of 10 nm (Adamcik et al. 2010). Not only this high aspect ratio, but also the specific cross beta-sheet structure, which is typical for amyloid aggregates (Nelson et al. 2005; Riek and Eisenberg 2016) contribute to special functional properties of these aggregates (Knowles and Mezzenga 2016). In addition to the potential use for new materials such as hybrid sensors (Li et al. 2012; Sasso et al. 2014), filter membranes (Bolisetty et al. 2015) and textiles (Ling et al. 2014), the amyloid structures build from whey protein and could therefore possibly be used in novel foods (Loveday et al. 2017). It has already been shown that their application improves the physical (Gao et al. 2017; Moro et al. 2013) and chemical stability (Serfert et al. 2014) of oil in water emulsions and the rheology of protein gels (Mohammadian and Madadlou 2016; Gosal et al. 2004), but also of air-water interfaces (Jung et al. 2010), as they are formed during foaming (Moro et al. 2013; Peng et al. 2017). However, the application associated processing of protein aggregates can lead to their possible degradation. Various research groups have already shown that homogenisation led to a shortening of the fibril length (Oboroceanu et al. 2011; Mantovani et al. 2018; Kroes-Nijboer et al. 2010), which may have consequences for its functionality (Koo et al. 2018). On the other hand, food processing sometimes offers conditions that could also be conducive to the formation of amyloid aggregates. Relevant formation factors were found to be temperature induced protein denaturation (Loveday et al. 2012b) and low pH value, but also other interacting process parameters (Loveday et al. 2011). Also shear forces or the large specific oil-water interface—which is found present in emulsions for example—could potentially have a constructive (Akkermans et al. 2006; Ng et al. 2016; Bolder et al. 2007; Pronchik et al. 2010) or degrading (Akkermans et al. 2008a; Jung and Mezzenga 2010; Rühs et al. 2012) effect on amyloid aggregates. This is important to understand in order to implement appropriate changes to the process.

While amyloid fibrils from BLG formed at a pH value of < 3.0 (Nicolai et al. 2011), short, worm-like aggregates are formed at a pH of 3.5, and—due to the Thioflavin-T (ThT) assay—also have an amyloid-like structure (Serfert et al. 2014). These aggregates seem to exhibit a more flexible behavior (Mudgal et al. 2011a), but have not been investigated much in terms of

structure and the factors that build up and break down the amyloid. It is possible that these morphologies also offer a high potential for industrial application, due to their greater proximity to food-relevant pH values and different process behavior.

Because amyloid aggregates have a high potential for the use as emulsifier, this thesis aims to investigate in more detail the factors that are potentially found in the process chain of emulsion production and that can have a constructive or destructive effect on amyloid or amyloid-like aggregates of BLG. At the same time, this research should lead to an answer regarding the structural and process-relevant differences between the semi-flexible fibrils at pH 2 and the worm-like aggregates at pH 3.5.

The results can thus provide a better assessment of the potential value of amyloid and amyloid-like structures for food applications. In addition, the specific investigation of the constituent factors can provide information on whether amyloid or amyloid-like aggregates could be formed spontaneously in food processes. Based on these findings, whey protein or amyloid(-like) aggregates manufacturing processes can be modified to support or prevent their formation or degradation.

Hypothesis 1:

The fibrils and worm-like aggregates formed at pH 2 and pH 3.5, respectively, consist of different building blocks.

Background:
The acid hydrolysis depends on the existing proton activity in the solution. At pH 2, in combination with high temperatures, BLG peptides are formed which are the building blocks for the fibril structures (Akkermans et al. 2008b; Ye et al. 2018). At pH 3.5 a faster increase in aggregation has been described (Serfert et al. 2014) despite a presumably reduced hydrolysis rate, which could be explained by the possibility that at pH 3.5 unhydrolysed protein material assembles.

Experimental approach:
The BLG solutions are adjusted to a pH value of 2 or 3.5 and then heated for 5 hours at 90 °C. To investigate the degree of hydrolysis, the formed aggregates are dissociated into their building blocks with guanidine HCl and dithiothreitol (DTT) and their size is analysed by size exclusion chromatography (SEC) and analytical ultracentrifugation (AUC). For better evidence aggregated and non-aggregated fraction will be separated by ultrafiltration (UF).

Hypothesis 2:

Isolated non-amyloid and amyloid materials have different physico-chemical properties and vary between the different aggregates observed at pH 2 and pH 3.5 due to the different building blocks. The differences in sample composition (pH 2 vs. pH 3.5) interfere with the analysis of the aggregates.

Background:
The fibril solution incubated at pH 2 and 90 °C is composed of amyloid aggregates and unaggregated BLG monomers and peptides (polydispersity) (Akkermans et al. 2008b). When this solution is measured by analytical methods it is not possible to determine from which fraction a signal, absorption or fluorescence is generated. However, this is of high relevance to assess the functional properties and potential of fibrillar and worm-like aggregates as well as of smaller aggregates and the non-aggregated fractions.

Experimental approach:
The aggregate solutions obtained after 5 hours incubation are separated into aggregated and non-aggregated material by ultrafiltration. The success of the separation is examined by ThT-assay and atomic force microscopy (AFM). The obtained fractions are concentrated by lyophilisation to meet the analytical standards. Phyico-chemical properties of purified and unpurified fraction will be analysed by small angle X-ray scattering (SAXS), Fourier- transform infrared spectroscopy (FTIR), intr. tryptophan (Trp) fluorescence, zeta-potential, ThT- and Nile red assay. Effects of lyophilisation will be monitored by comparison with unlyophilised samples.

Hypothesis 3:

Among the relevant fibril formation process parameters—such as pH value, shear stress, protein and ion concentration—temperature is the most important, due to its relation for BLG denaturation and assembling kinetics. However, interacting process parameters may affect the aggregation kinetics at different temperatures.

Background:
Population balance models and aggregation kinetics studies gave evidence that fibril formation kinetics depends on the temperature (Arosio et al. 2012). However, there is no information available about the threshold of fibril formation. So far, only fibril formation was described for temperature > 75 °C (Loveday et al. 2012b; Kroes-Nijboer et al. 2011), which is in the range

of the irreversible denaturation temperature of BLG (~70 °C) (Loveday 2016; Belloque and Smith 1998; Harwalkar 1980). As denaturation of proteins can be shifted by the parameters of the environment (Wang et al. 2010; Bekard et al. 2011), the threshold of fibril formation < 70 °C might be shifted too.

Experimental approach:
A screening of the relevant process parameters temperature, pH value, stirring speed, protein and ion concentration will be conducted to find the threshold of fibril formation. A statistical design of experiments (DOE) will be created for this onset and conducted to find relevant interactions. Statistical relevant parameters are then further investigated by additional methods to receive explanation of the observed effects.

Hypothesis 4:

The application of additional mechanical energy and increase in specific surface area by agitated particles can accelerate the formation of aggregates. This effect could be different for pH 2 fibrils and pH 3.5 worm-like aggregates.

A) Different particle sizes and agitation degree can alter the level and type of mechanical stress and therefore its influence on fibril formation kinetics.

Background:
Stirring and shearing can increase the formation kinetics of BLG fibril formation by shear flow and secondary nucleation effects (Akkermans et al. 2006; Ng et al. 2016; Bolder et al. 2007; Dunstan et al. 2009). Energy intake by agitated non BLG-protein solutions was described earlier to have a similar effect (Ladner-Keay et al. 2014; Macchi et al. 2011; Arosio et al. 2012). However, the type of stress affecting the proteins is different when glass beads are agitated with the solution and varying with the used particle size and agitation velocity (Schrader et al. 2019).

Experimental approach:
The BLG solutions adjusted to pH 2 or pH 3.5 will be agitated at 180 RPM and 280 RPM with glass beads of four different diameter distributions (0 – 20 µm, 100 – 200 µm, 400 – 600 µm and 750 – 1000 µm) in an incubation system at an effective temperature of ~70 °C. Further experiments at other agitation velocities will be conducted to find the optimal combination of particle size and agitation velocity. Amyloid (like) aggregation will be monitored by ThT-assay and AFM.

B) Different specific particle surface area and polarities can have different effects on aggregation kinetics of BLG.

Background:
Particle surfaces were found earlier to be the decisive effect of enhancing fibril formation of alpha-synuclein (Pronchik et al. 2010). Increased nucleation supporting effects were described by hydrophobic polytetrafluorethylene (PTFE) compared to glass bead surfaces (Pronchik et al. 2010; Shezad et al. 2016). However, as the density of PTFE and glass beads is different, their flow behaviour in agitated solution and therefore the implicated mechanical stress can be altered (**hypothesis 4 A**). Chemical modification of the nano-particle properties were described earlier by covalent bounding of carbon acids (Kockmann et al. 2015) and gives the opportunity to create glass beads with different surface polarity, but similar flow behaviour in agitated systems.

Experimental approach:
Glass beads of different size distributions (**see hypothesis 4 A**) will be modified by covalent bounding of stearic acid to their surface. Incubation with pH 2 and pH 3.5 BLG solution at ~70 °C will then performed. Fibril formation will be monitored by ThT-assays and AFM. Surfaces will be characterized by AFM and attenuated total reflection - FTIR (ATR-FTIR). Absorbance of aggregated and non-aggregated material will be analysed by ATR-FTIR and monitoring of the protein concentration by UV/VIS spectroscopy. The comparison to findings with unmodified glass beads (**hypothesis 4 A**) gives answers about the proportion of the surface effect and the proportion bases on mechanical energy input.

Hypothesis 5:

Application of shear stress and cavitation in the absence or presence of an oil phase affects the degradation of amyloid(-like) aggregates to a different extent.

Background:
It was mentioned that processing by homogenisation of semiflexible and flexible fibrils at pH 2 led to fibril fragmentation (Serfert et al. 2014; Jung et al. 2010; Jung and Mezzenga 2010; Oboroceanu et al. 2011; Oboroceanu et al. 2014). However, there is still no evidence if the effect is based on shear flow, cavitation and/or oil-water interfaces. Because the distribution of length is highly relevant for the functionality in food, the specific factor which leads to the fibril destruction should have been clearified. Due to possible differences in structure of amyloid(-

like) aggregates formed at pH 2 or pH 3.5 (**hypothesis 2**), there might also be differences in stability against destructive forces.

Experimental approach:

Protein solution of matured semiflexible fibrils (pH 2) and flexible worm-like aggregates (pH 3.5) will be stressed at increasing levels shear flow by a rotor-stator-dispersion system (Ultra-turrax). Ultra-sonication of increasing amplitudes will be applied to investigate the effect of cavitation. Processes will be conducted with and without a specific amount of oil to investigate the influence of the oil phase during the process. Effects on morphology will be measured with AFM and AUC. Influences on size distribution will also be monitored by dynamic light scattering (DLS). Effects on structure will be examined by ThT-assay and FTIR.

2. Theoretical background

2.1. Beta-lactoglobulin

The basic fundament of all experiments and the resulting materials described or produced, analysed and characterised in this work is the whey protein beta-lactoglobulin (BLG). Due to its specific calyx-like structure, which gives its physiological transport abilities for mammalian organisms, BLG is classified as a lipocalin (Sawyer and Kontopidis 2000). As the name of the protein suggests, BLG is a globular storage protein of milk. The term "globulin" indicates the solubility at low salt concentrations. The "beta" is probably due to the high occurrence of beta sheets in the native protein structure. BLG consists of 162 amino acids, which together form a molecule size of ~18,400 Da (Kontopidis et al. 2004). The eight different genetic variants A, B, C, D, H, I, J, and W have been described so far, with A and B being the most abundant species in cow's milk (Farrell et al. 2004). The isoelectric point of BLG is pI 5.13 (Farrell et al. 2004).

2.1.1. Structure

The **primary structure** of the genetic variant A of BLG consists of 162 alpha-amino acids and was sequenced for the first time by (Braunitzer et al. 1973). The genetic variant A has a molecular mass of 18,362 Da. BLG B has two different residues: Asp-64 and Val-118 are replaced by glycine and alanine and therefore the molecular mass amounts for 18,276 Da. (Wong et al. 1996). The sequence contains five cysteine molecules, which enable two disulphide bridges each between Cys-66 and Cys-160, as well as Cys-106 and Cys-119 (Léonil et al. 1995), while the Cys-121 stays free.

As shown in **FIG 2-1**, 11 % of all amino acid residues are involved in helical structures and 31 % in beta sheets. The total **secondary structure** of the native BLG thus contains 10 % alpha-helix, 50 – 54 % beta-sheet and 10 – 25 % beta-turns and 6 – 27 % random coil investigated by FTIR (Creamer et al. 1983; Ngarize et al. 2004; Bhattacharjee et al. 2005). The proportion of alpha-helix is amounted with up to 28 % when analysed by circular dichroism method (Qi et al. 1997). However, alpha-helical structures can be overestimated, when using circular dichroism, due to a transient formation of a non-native alpha-helical intermediate structure, during the return to the native state after thermal unfolding (Hamada et al. 1996).

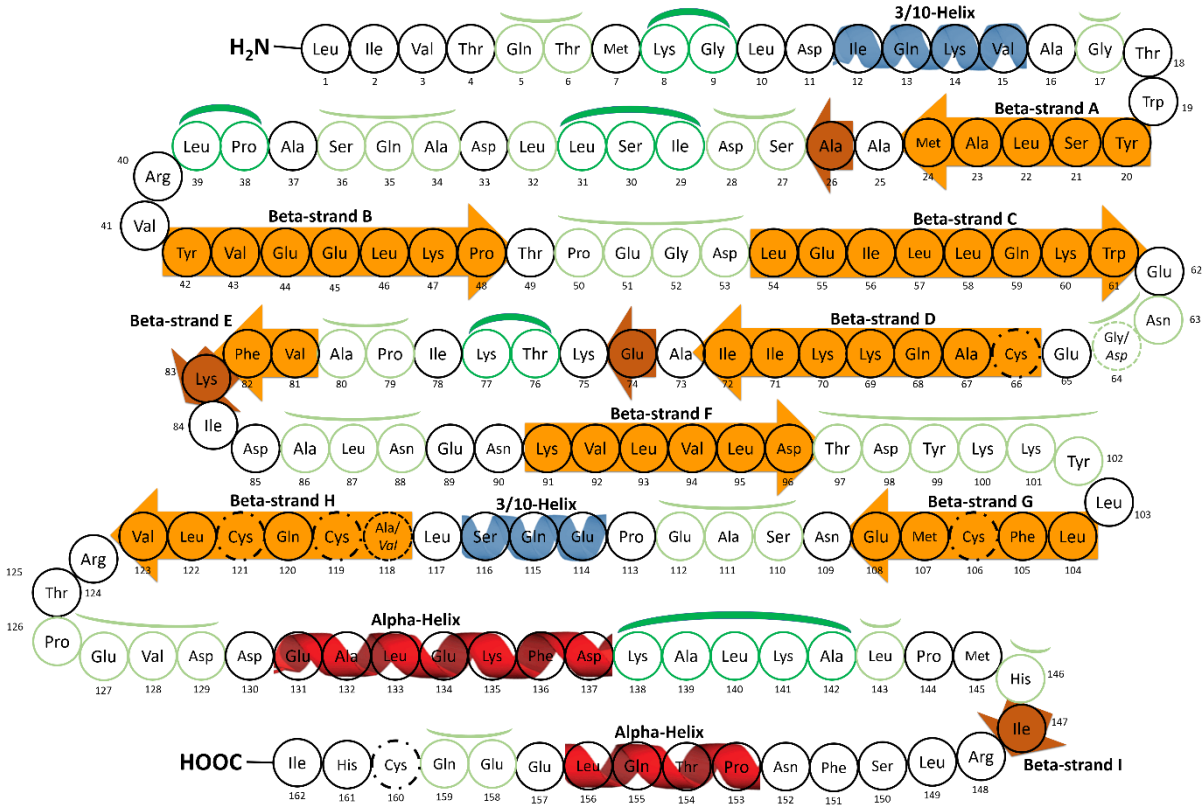

FIG 2-1 Amino acid sequence of beta-lactoglobulin A/B and their involvement in secondary structure elements according to McKenzie et al. (1972), Murzin et al. (1995) and Sakurai et al. (2009).

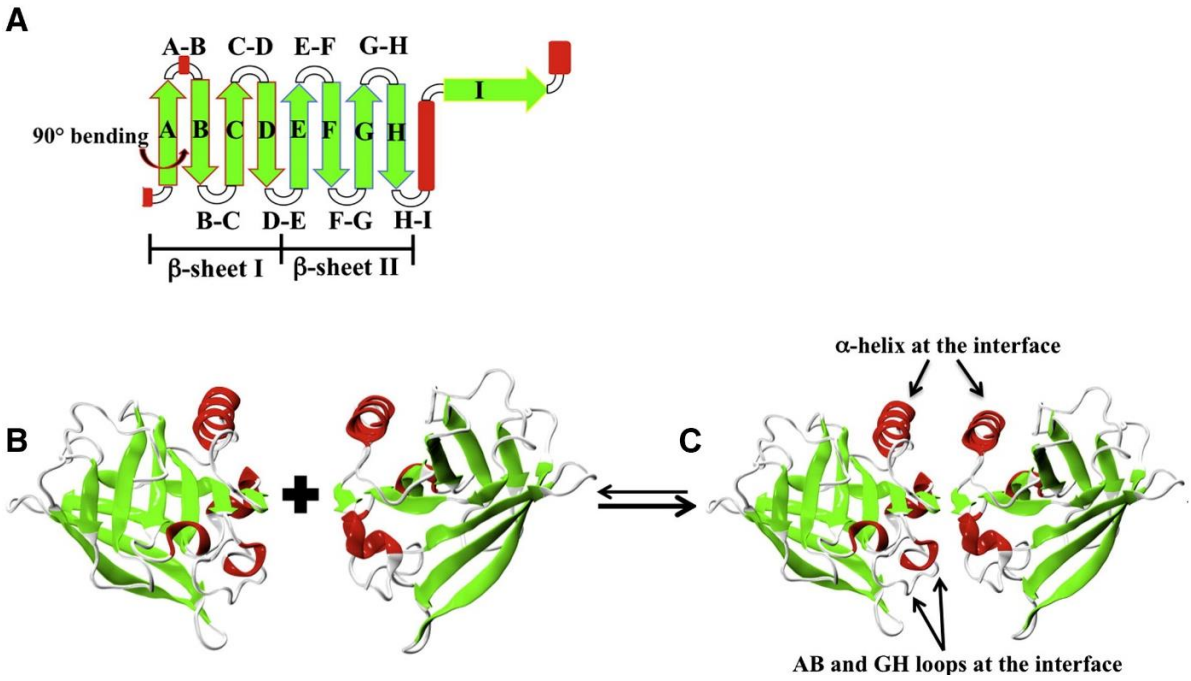

FIG 2-2 Secondary (A), tertiary (B) and dimeric structure (C) of beta-lactoglobulin A (Mercadante et al. 2012).

The **tertiary structure** is formed by eight antiparallel beta strands (strand A to strand H) (**FIG 2-2**). The strands A–D forming one sheet and E–H a second, which together form a central cavity, the so-called beta-barrel, which is closed by the interaction (DE-loop) of two strand on one side (Kontopidis et al. 2002; Qin et al. 1998). The E–F-loop acts as a gate over the binding site, which is latched at low pH by Glu-89 (Qin et al. 1998). On the outer surface there is a three-turn alpha-helix and the ninth beta-strand I (Kontopidis et al. 2004). The monomer has a hydrodynamic radius of 1.75 nm (Sawyer and Kontopidis 2000).

The **quaternary structure** of BLG is a mixture of monomer and dimer forms with a condition depending equilibrium (Aymard et al. 1996) (**FIG 2-2**). In its natural habitat of milk (pH 5.7) BLG is predominantly dimer (Wit 2009). This dimeric form keeps BLG also over a wide pH range from pH 3 to pH 8, as long as a moderate ionic strength (< 100mM) and a temperature above 20 °C is present (Mercadante et al. 2012), whereas at below pH 3 and ionic strength of < 10 mM BLG is predominantly monomeric (Townend et al. 1960). In this acid solution the equilibrium between the monomeric and dimeric is shifted to monomeric form when the temperature is increased (Aymard et al. 1996). The interaction between two BLG monomers is induced by the antiparallel attachment of the beta-strand I. A second dimer-stabilizing interaction is triggered by Asp-33 of one monomer in the AB loop, which interacts with Arg-40 of the other subunit (Sakurai and Goto 2002). Therefore the interaction region is next to the alpha-helix and close to the free thiol group Cys-121 (Wit 2009).

Around pH 4.7 BLG dimers associate to octamers. BLG A shows a higher tendency for this association then BLG B (Verheul et al. 1999).

A heating of neutral BLG solutions in combination with a certain ion concentration induces the formation of spherical oligomer structures with a size of up to 50 nm (Carrotta et al. 2001), while association of oligomer sizes can also be favoured by higher protein concentration (> 30 mg/ml) (Verheul et al. 1999). The structure remains similar to that of the native protein, but with a less tight packing of the side chains (Bauer et al. 2000).

2.1.2. Denaturation of BLG

Depending on the environmental conditions, proteins adopt the state of the lowest free energy. This specific conformation, which usually prevails under the natural physiological conditions of the protein, is defined as the native state. The loss of this native state, including loss of native quaternary, tertiary and/or secondary structure, without change in molecular weight, is defined

as “denaturation” (Tanford 1997). The denaturation of BLG can be induced by various factors such as heat, pH value, chemicals, shear, ion concentration, pressure or interfaces.

Thermal denaturation

The temperature-dependent denaturing process is well studied (Wit 2009), although it does show some interaction with other factors such as pH (Ananthanarayanan et al. 1977), protein concentration (Qi et al. 1995), ion concentration or ligand binding status (Considine et al. 2014).

As in the native state BLG is dimeric (N2), thermal denaturation starts with a reversible dissociation of BLG-dimers to monomers (N) between 30-55 °C (Qi et al. 1995; Rytkönen 2006). Further heat denaturation can be characterized as two consecutive first-order transition reactions (Sawyer et al. 1971), inducing a reversible (R) up to 70 °C and an irreversible (S) transition above (Wit 2009; Iametti et al. 1996), which leads to aggregation (A).

N2	⇔	N	⇔	R	⇔	S	⇔	A
<30°C	⇔	< 55 °C	⇔	< 70 °C	⇔	> 70 °C		

From 40 °C on, a Tanford-like thermal transition occurs (not likely to be identical to the classic Tanford transition observed at room temperature by pH-adjustment), which describes a reversible conformation rearrangement to monomers, in which the free thiol Cys-121 and hydrophobic patch expose (Loveday 2016; Qi et al. 1995). At 55 °C strand E and the A-B loop unfold and strand A became partially flexible (Belloque and Smith 1998). With further increasing temperature BLG shows a significant loss of its beta-sheet structure and at 65 °C an abrupt loss of helical conformation (Qi et al. 1997; Belloque and Smith 1998).

Above 65 °C BLG reaches the so-called molten globule status, where region of local disorder and increased flexibility are existent (Molinari et al. 1996), caused by the destabilization of the beta-strand I and the loss of the alpha-helix (Qi et al. 1997; Seo et al. 2010), while the calyx formed beta-strands remain resistant (Belloque and Smith 1998). The conformational changes expose the Trp-61 reversible (Bhattacharjee and Das 2000; Mills 1976). This first state of unfolding is determined by a denaturation enthalpy of ΔH = 142 kJ7mol (Dupont 1965).

At 75 °C the internal hydrophobic face is partially exposed (Belloque and Smith 1998; Iametti et al. 1996). Exposure of reactive thiol groups and adhesive hydrophobic surfaces causes non-native dimers and small oligomers mainly by oxidation of the thiols (Wit 2009; Iametti et al.

1996; Schokker et al. 2000) and to a smaller extent by disulphide exchange reactions (Wit 2009). It is assumed that the free thiol group Cys-121 of one monomer may oxidize a disulphide bond of another monomer and form a stable bond with a Cys-66, but leaving a free thiol group Cys-160 as a result (Gezimati et al. 1997; Creamer et al. 2004). The dimers formed can then enlarge to trimers, tetramers (Bauer et al. 2000) and between 75 °C and 85 °C to bigger oligomer species, by a combination of non-covalent (hydrophobic and salt induced associations) and thiol/disulphide exchange reactions (Sawyer et al. 1971; Schokker et al. 1999; Wang et al. 2010).

Solution conditions

As already mentioned, all these temperature-dependent unfolding, interaction, and association processes show a strong but complex dependence on the pH of the aqueous solution.

A denaturation rate ~5.5 times higher with an increase in the pH value from pH 7 ($k = 2.65\ s^{-1} \times 10^3$) to pH 8.8 ($k = 14.63\ s^{-1} \times 10^3$) has already been described (Law and Leaver 2000). Reasons might be the repelling forces of negatively charged residues.

At pH 3 – 4 BLG was described to be most stable to heat-induced denaturation (Dissanayake et al. 2013; Wada et al. 2006), due to buried hydrophobic surface area (García-Hernández et al. 1998).

At acid pH values (pH < 2.5) the thermal denaturation of BLG involves different mechanism, since the denatured BLG-molecules are stable forms with no apparent accompanying aggregation compared to denatured BLG at neutral pH (Harwalkar 1980).

Extreme acid or basic pH values are able to denature BLG without thermal treatment (Casal et al. 1988). As the concentration of H^+ in the solution determines the type and distribution of surface charges on the protein, intramolecular folding interactions and intermolecular protein-protein interactions are affected (Wang et al. 2010; Taulier and Chalikian 2001). Heavily dense surface charges lead to increased repulsive intramolecular and intermolecular interactions, which are able to unfold the protein partially (Wang et al. 2010; Fang and Dalgleish 1997). Below pH values of pH 3.5 BLG dissociate to monomers, due to electrostatic repulsion (Townend et al. 1960). The protein charge-charge repulsion is minimal at its pI, having an effect on the association behaviour and protein solubility (Yan et al. 2013; Dissanayake et al. 2013). Above pH 9, BLG undergoes irreversible base-induced unfolding (Taulier and Chalikian 2001; Casal et al. 1988).

Just like the pH value, the ion strength of the solution determines protein interactions. The positive or negative ions of the solution influence the electrostatic charge of the protein surface (Yan et al. 2013). Thus, these ions influence the charge-charge interactions or rejections between the protein monomers, which might promote the aggregation. In addition, the specific protein conformation depends on the ionic strength, since charges—as already described—are important for the specific folding or stability of the protein (Wang et al. 2010). Certain conformations in which the hydrophobic protein structures emerge can also lead to aggregation. All these effects also depend on the ion type (Xiong et al. 1993), the respective pH value (Renard et al. 1998; Xiong et al. 1993) and the degree of glycosylation (Høiberg-Nielsen et al. 2006). For example a certain concentration of NaCl is necessary for BLG to be dimerized at a neutral pH value (Renard et al. 1998). Furthermore, the ion concentration at acid pH value effect the extent of association reactions (Renard et al. 1998).

Processing

A protein solution can experience an energy input through various mechanical process factors. Shearing, e.g. during stirring, shaking or flowing of the solution, but also pressurization, cavitation or oil-water interfaces can stress and unfold the protein (Bekard et al. 2011).

Shear stress describes the internal stress of a body in the course of an external force. Accordingly, the unit of shear stress is force (F) per unit area (m^2). Since the real shear stress of a system depends on many other factors, such as viscosity, density etc. the shear rate (s^{-1}) is usually listed as a characterization of the shear stress.

In the literature, effects of moderate shear (< 400 s^{-1}) on BLG aggregates have been observed but not on native BLG so far (Erabit et al. 2014). However, light conformational changes—which effect the antigenicity of BLG—were described when using shear rates up to (1000 s^{-1}) (Rahaman et al. 2015). Furthermore, for shear rates up to 250 000 s^{-1} only moderate association of some proteins were described (Bee et al. 2009). However, application of shear has an immense effect on the size distribution of BLG aggregates formed by thermal treatment (Erabit et al. 2014; Gaaloul et al. 2009; Simmons et al. 2007; Spiegel and Huss 2002).

In many cases shearing is accompanied by the creation of air-water interfaces. In the case of emulsion production, however, oil-water interfaces are also present. The more hydrophobic properties of air or oil in relation to water can lead to BLG adsorption at the interface with increased adsorption, especially of lipophilic amino acid residues (Bouyer et al. 2012). The resulting exposure of the hydrophobic components from the interior of BLG induces a partial

unfolding of the protein (A. Bos and van Vliet 2001), but can also enable aggregation (Wang et al. 2010).

The treatment of native whey proteins in micro fluidisers leads to an increase in the particle size distribution (Dissanayake and Vasiljevic 2009). However, for this altered associating potential the high pressure during the process might have a decisive role. Among other things, this can disturb the sensitive balance of forces between the amino acid residues and the interactions associated with them and lead to their unfolding (Considine et al. 2007). This effect has also been observed by dynamic pressure treatment (Iordache and Jelen 2003).

It has not yet been investigated whether the interactions of the different process factors influencing BLG can induce an amyloid aggregation or at least lead to a faster amyloid aggregation under milder conditions (**see hypothesis 3 and 4**, **manuscript 2 and 3**).

2.2. Amyloid aggregates from beta-lactoglobulin

The term "amyloid" is derived from the Greek "ἄμυλον", pronounced ámylon, which is translated as starch. Amyloid therefore means starch-like and goes back to the discovery made by Rudolf Virchow in 1854, who had first discovered such atypical material in the liver of deceased people. He observed that these structures, similar to starch, are blue-coloured by iodine.

The term “fibril” is a diminutive form of the word "fibre", which derives from the Latin-word "fibra". Fibrils are elongated structures, which in turn are often combined into larger bundles. Myofibrils in muscle tissue (Fyrberg and Beall 1990) or microfibrils in the cell wall of plants (Thomas et al. 2013) are just two examples.

Amyloid fibrils are structures in which proteins or polypeptides in a certain order aggregate to form an elongated strand, i.e. fibril, and thus obtain amyloid properties. The common feature of all amyloid fibrils is the cross beta core structure (Cao and Mezzenga 2019), in which the polypeptide chains run perpendicular to the fibrillar axis. It is known that different forms of appearance, i.e. so-called morphologies of amyloid structures, can occur (Loveday et al. 2017). If no fibrillar morphology is recognizable, these are generally characterized as amyloid or amyloid-like aggregates.

2.2.1. Relevance of amyloid structures

Origin

Amyloid structures were characterized for the first time in the course of pathologically conditioned post-mortem investigations. It has been found that these structures are due to misfolded proteins and related to the pathogenesis of many diseases known as amyloidosis (Eisenberg and Sawaya 2017). True amyloidosis are diseases in which such amyloids have accumulated extracellularly and there is no clinical or pathological evidence that this disease can occur without this accumulation (Pepys 2006). In 1984, Glenner first isolated the amyloid fibril from the so-called "beta-protein", which is associated with Alzheimer's disease (Hansen et al. 2005; Hardy 1997). However, there is no clear evidence that Alzheimer's disease or other diseases such as diabetes mellitus type 2 or Parkinson's disease—which are linked to amyloidosis—are really caused by amyloid fibril plaque (Pepys 2006). It was observed that degenerate protein structures—associated with amyloidosis—are partly able to degenerate other proteins—like in crystallization—and thus promote their amyloid aggregation. Because of this mechanism a connection between amyloid structures and prion diseases such as bovine spongiform encephalopathy (BSE) (Gibbs 1996) or Creutzfeldt-Jakob disease (Liberski et al. 1991) was also discussed.

Originally, it was assumed that there are only a few proteins or peptides that are able to form amyloid structures. Finally, however, a comprehensive genome study revealed that almost all proteins (> 98.7 %) have self-complementary short sequences, which potentially enable them to form amyloid fibrils (Goldschmidt et al. 2010). For this, only protein-specific conditions are required, which can be physiologically e.g. alpha-synuclein (37 °C, pH 5) or relatively extreme e.g. BLG (90 °C, < pH 3).

Functionality

In fact, many amyloid structures also have natural physiological functions. For example, amyloid fibrils have been found in the biofilms of E.coli and pseudomonas (Chapman et al. 2002). The silk moth protects its eggs with an amyloid tissue (Iconomidou et al. 2000), catalytic functions of amyloids were observed in melanin synthesis in the melanosome (Fowler et al. 2006) and release of human peptide hormones are controlled by them (Maji et al. 2008).

Due to their extreme aspect ratio, multitude of functional groups on the fibril surface and their high stiffness amyloid fibrils have increasingly been applied as new materials (Knowles and Mezzenga 2016; Cao and Mezzenga 2019; Bolisetty et al. 2019; Wei et al. 2017). Prototypes have already been developed from BLG amyloid fibrils, which can be used as biosensors (Li et

al. 2012; Li et al. 2013), photovoltaics (Bolisetty et al. 2012), hybrid membranes for continuous catalysis (Bolisetty et al. 2015) or water purification (Bolisetty and Mezzenga 2016), as means of transport for cancer-fighting nanoparticles (Bolisetty et al. 2014), or as new silk-like textiles (Ling et al. 2014).

The attractivity of whey protein for nanomaterials is caused by the natural, regenerative source of the starting material. BLG is proven to be non-toxic and very well studied. Some attractive functional properties, such as the ability to bind ligands or generally interact with other molecules (Keppler et al. 2015; Wilde et al. 2016), could be transferred to the amyloid aggregates. In addition, the parameters leading to the formation of amyloid structures and their modification are already well investigated (Cao and Mezzenga 2019; Loveday et al. 2017). The long, semi-flexible or short, worm-like fibrils can be provided depending on the particular application system (Nicolai and Durand 2013). All these capabilities make BLG fibrils not only particularly valuable for material science purposes, but also for food technology applications. *However, there is still a great lack of clarity about the exact structural differences of the various morphologies, their physico-chemical properties and the resulting process and food suitability* **(see hypothesis 2, manuscript 1).**

Use of amyloid aggregates in food

As mentioned before, food sources provide protein material that is usually non-toxic, and the formed amyloid fibrils can therefore potentially be used in food application. At the same time, their supply through agricultural processes has already been well tested. The formation conditions of amyloid fibrils from a wide variety of different food related proteins have already been described. From milk these are in addition to BLG: alpha-lactalbumin (Goers et al. 2002; Yang et al. 2006), alpha$_{S2}$- (Thorn et al. 2008), kappa- (Thorn et al. 2005) and beta-casein (Pan and Zhong 2015); from egg: ovalbumin (Pearce et al. 2007), lysozyme (Arnaudov and Vries 2005) and ovotransferrin (Wei and Huang 2019); from blood: ferritin (Jurado et al. 2019), bovines serum albumin (Usov et al. 2013) and haemoglobin (Jayawardena et al. 2017); from cereals: rice albumin and globulin (Zhang and Huang 2014), wheat gluten and gliadin (Mackintosh et al. 2009); from legumes: soy protein, glycinin (Tang and Wang 2010), peas protein (Munialo et al. 2014), and vicilin from kidney bean, red bean and mungo bean (Lassé et al. 2016; Liu and Tang 2013).

The BLG fibrils have already been tested for various food technology applications. The forming fibril network enhances the gel-forming properties in comparison to unfibrillar protein (Mohammadian and Madadlou 2016; Loveday et al. 2012). In addition, the foam-forming

(Moro et al. 2013; Oboroceanu et al. 2014) and emulsion-forming (Gao et al. 2017; Humblet-Hua et al. 2013) properties are improved. *So far, there is no comparison of the physico-chemical and functional properties with worm-like aggregates from BLG* **(see hypothesis 2, manuscript 1).**

2.2.2. Structure

The common feature of all amyloid fibrils is the cross-beta-sheet structure. Cross-beta-sheets describe beta-sheets stacked parallel to the fibril axis (**FIG 2-3**). The beta-sheets consist of beta-strands, which are arranged perpendicular to the fibrillar axis and are formed by N-H---O=C hydrogen bonds between the peptides (Riek and Eisenberg 2016). The distance between the beta-strands is about 4.8 Å, while the distance between the beta-sheets is 6 – 12 Å (Astbury et al. 1935; Sunde et al. 1997), depending on the size of the inner side groups and the specific arrangement (Cao and Mezzenga 2019). Amino acid residues can form bonds between the layers of beta-sheets, so-called ladders, which strongly stabilize the fibrils (Eisenberg and Sawaya 2017). For example, the amide-containing amino acids glutamine and asparagine can form hydrogen bonds between beta-sheets, while tyrosine, serine and threonine are involved in hydrogen-free inter-sheet bonds (Nelson et al. 2005). This creates an interdigitated dual sheet structure described as steric zipper spine (Eisenberg and Sawaya 2017). In addition to the Van der Waals forces between the beta-sheets, the hydrogen bonds running parallel to the axis stabilize with a binding energy of -9.1 kcal mol^{-1} per hydrogen-bond resulting in extreme fibril stability (Tsemekhman et al. 2007; Messens et al. 1997). For comparison, ice has only -6.7 kcal mol^{-1} per hydrogen-bond.

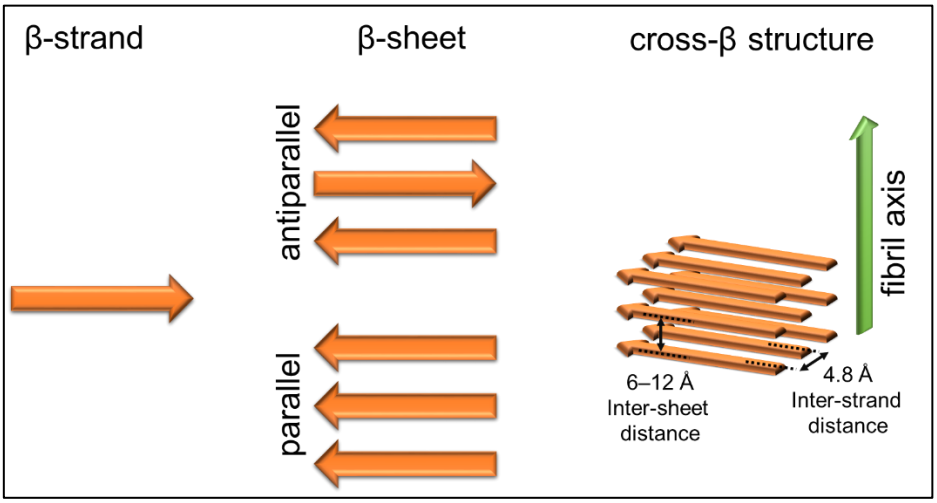

FIG 2-3 Beta-strands form beta-sheets (antiparallel or parallel arrangement) which assemble into an amyloid fibril cross beta-structure with an inter-strand distance of about 4.8 Å and an inter-sheet distance of 6 – 12Å. Beta-sheets are arranged parallel, while beta-strands lay perpendicular to the main fibril axis. Own illustration according to Cao and Mezzenga (2019).

The beta-sheet stacks form the core of protofibrils. These protofibrils can already be recognized as single stranded, several micrometre long threads. Depending on the protein and the assembly process, the protofibril can be surrounded by a coat of protein side chains that are not part of the structuring beta-sheet arrangement (**FIG 2-4**) and leads again to additional stabilization (Eisenberg and Sawaya 2017). The protofibrils in turn twist with other protofibrils to form two or more stranded twisted ribbons, which are then called fibrils or mature fibrils. Some flexible aggregates formed at pH 2 and high protein or ion concentration, were classified as fibrils, too.

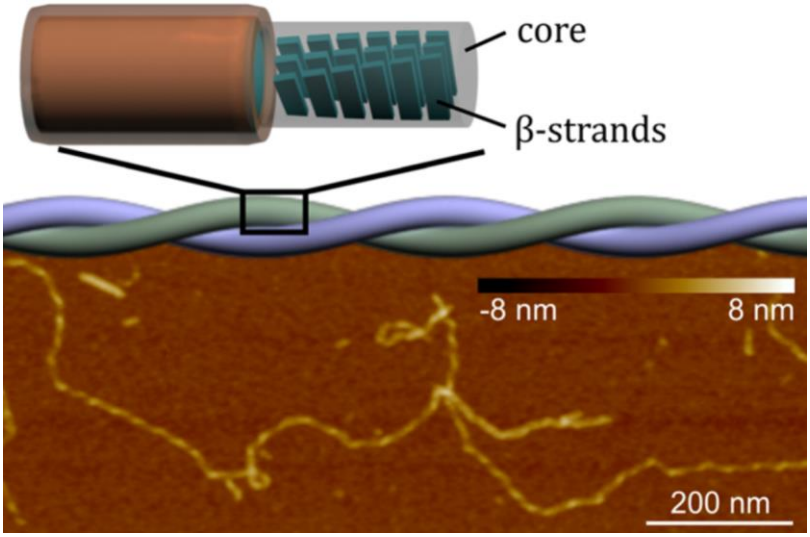

FIG 2-4 Schematic illustration of the internal cross-beta-structure of the protofibrils. The protofibrils of beta-lactogloblin can be arranged to twisted ribbons (AFM image shows fibrils from bovine serum albumin). Illustration adapted from Usov and Mezzenga (2014).

2.2.3. Amyloid fibril polymorphism

Even though all amyloid aggregates in the nucleus have a cross-beta structure, several different manifestations, so-called morphologies, can occur depending on the protein or the environmental and formation factors (Hoyer et al. 2002; Adamcik et al. 2010; Lara et al. 2011; Meinhardt et al. 2009; Pedersen et al. 2006; Usov and Mezzenga 2014). This polymorphism can occur on different levels. The molecular polymorphism describes different molecular arrangements in the formation of the cross-beta-sheet structure (Cao and Mezzenga 2019; Pedersen et al. 2010). Fibrillation-prone segments within a polypeptide can for example be packed with various density (Colvin et al. 2016), the stacks can be built up from interactions of different segments (Gremer et al. 2017; Wälti et al. 2016) or the interacting segments can originate from different or the same polypeptide (Eisenberg and Sawaya 2017).

Structural polymorphism describes the way in which protofilaments are assembled into fibrils. The fibril usually appears as a twisted ribbon (Adamcik et al. 2010; Meinhardt et al. 2009; Usov

and Mezzenga 2014). Depending on the number of filaments that make up the fibril, the diameter of the fibril increases and so does the pitch, i.e. the distance between a twist (Adamcik et al. 2010). However, helical ribbons or nanotubes or completely untwisted crystals have also been observed for different proteins (**FIG 2-5**) (Usov and Mezzenga 2014; Lara et al. 2013; Reynolds et al. 2017; Lara et al. 2011). The transition from twisted ribbons to helical ribbons occurs after a critical exceeding of the number of associated protofibrils. The transition from helical morphology into nanotubes allows the free energy to be reduced by releasing the line tension of externally associated protofibrils. The more rarely observed polymorphic transition in the amyloid polymorph crystal occurs by unfolding the twisted ribbons by thermal fluctuation, at which the level of free energy must first be temporarily increased. The resulting crystal morphology, however, is located in a deep energetic funnel, through the lateral aggregation of many untwisted protofilaments, the very low specific surface area, and interfacial energy (Adamcik and Mezzenga 2018). The self-assembly into twisted ribbons and a later transformation into helical ribbons of up to 17 protofibrils have been shown for BLG (Lara et al. 2011).

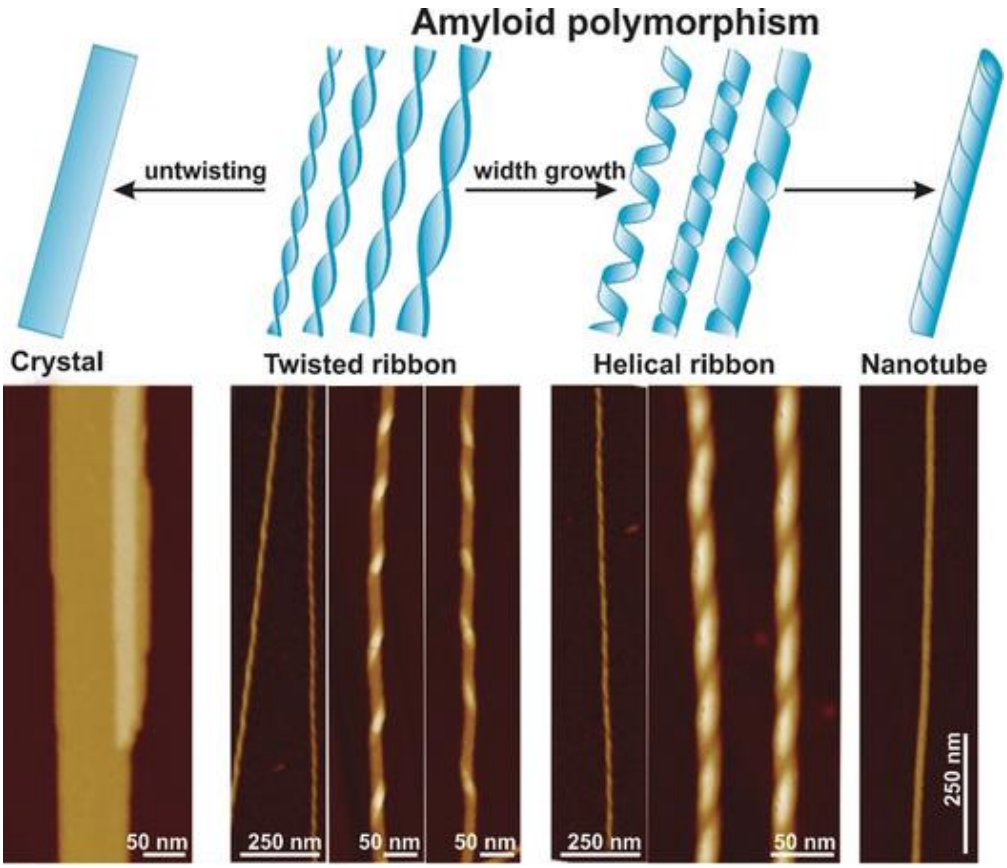

FIG 2-5 structural polymorphism of amyloid fibrils. Illustration adapted from Adamcik and Mezzenga (2018).

Some flexible aggregates formed at pH 2 and high protein or ion concentration, were classified as fibrils, too. Thus, another kind of amyloid polymorphism might be classified due to the flexibility and length of the fibril. Regarding to this classification worm-like aggregates at pH 3.5 might be distinguished from fibrils. *However, there is still no clear evidence these worm-like structures can be classified as fibrils or just as amyloid-like structures* (**see hypothesis 2, manuscript 1**).

2.2.4. Formation

Unfolded proteins such as alpha-synuclein, beta-peptide, kappa-casein can form fibrils under physiological conditions (Pronchik et al. 2010; Pan and Zhong 2015; Valiente-Gabioud et al. 2012). Globular proteins such as BLG require partial unfolding of the tertiary structure as an initial step, since the fibrillation-prone beta-sheets are part of the inner protein structure (van der Linden and Venema 2007). However, the unfolding of BLG, in turn, can lead to the formation of amyloid fibrils, worm-like or amorphous aggregates or a mixture thereof, depending on the conditions (Cao and Mezzenga 2019). For the association of BLG in long, semiflexible fibrils, a pH value of < 3, a temperature of > 75 °C and a low ion concentration are generally described (Serfert et al. 2014; Krebs et al. 2009; Loveday et al. 2012b). The low pH value in combination with the low ion strength provides electrostatic repulsion between the strongly positively charged peptides or monomers and thus prevents the random aggregation to amorphous aggregates (Loveday et al. 2017). At the same time, the low pH value combined with the high temperatures ensures partial hydrolysis of the protein (Dave et al. 2013).

After the unfolding or hydrolysis of the protein, nucleation of the peptides or protein monomers occurs. Self-assembly of the building blocks proceeds when the nuclei grow to a critical size, below which the association is reversible (Akkermans et al. 2006; Aymard et al. 1999). Especially N-terminal peptides self-assemble to weak-associated nuclei, which can dissociate again by cooling. Fibril growth takes place by a linear addition of the monomers to the nucleus (Usov and Mezzenga 2014). When the concentration of fibrillogenic peptides is sufficiently high enough that the rate of assembly and growth of the nuclei exceeds the rate of disassembly, the initial lag phase is overcome, and the growth phase begins. This critical point is characterized by a sharp increase in ThT-fluorescence (Dave et al. 2013). Assuming that the semiflexible BLG fibrils consist of peptides (Akkermans et al. 2008b), the duration of the lag phase and the aggregation kinetics during the growth phase depend on the availability of the building blocks and thus on the hydrolysis rate (Kroes-Nijboer et al. 2011; Ye et al. 2018). Dave et al. (2014b) were able to show, that chemical reduction of hydrolysis also inhibit the fibril

growth. However, other studies indicate that fibril growth is independent of the amount of hydrolysate (Loveday et al. 2017). For example, unhydrolysed BLG can also be incorporated into fibrils (Hettiarachchi et al. 2012), whereby a dependency between hydrolysis and assembly rate is probably caused by the lower steric hindrance of smaller peptides (Dave et al. 2014a). During the further heating process, the parts that are not components of the core—the so-called coat (**FIG 2-4**)—can also be hydrolysed further, i.e. form "shaved" fibrils (Usov and Mezzenga 2014). After the lag and growth phase a stationary phase occurs leading to a sigmoidal fit of the growth curve (Dave et al. 2014b; Kroes-Nijboer et al. 2011; Loveday et al. 2010). The common theory is, that this plateau is determined by the exhaustion of the building blocks (peptides or BLG monomers) (Loveday et al. 2017).

Formation of worm-like aggregates at pH 3.5 was described to have no lag-phase (Serfert et al. 2014). However, there is still no clarity about their building blocks and their way of assembling. **(see hypothesis 1, manuscript 1).**

2.3. Relevant processing factors

2.3.1. Processing factors which influence the fibril formation

In order to produce fibrils from BLG, a pH value of < 3, a temperature of > 80 °C, the lowest possible ion concentration and light stirring are generally used. After 5 to 7 hours the stationary phase and thus the maximum fibril yield is reached. The selected parameters can influence the aggregation kinetics, the structural and molecular morphology as well as the functionality of the amyloid aggregates for different reasons.

pH value

The pH value describes the reverse negative decadic logarithm of the hydrogen ions (i.e. protons) activity (Norby 2000). The proton activity has two different effects on the formation of fibrils. The first effect is the hydrolysis of the protein at particularly acid pH values in combination with the high temperatures. The first step of hydrolysis is the protonation of the carbonyl oxygen, followed by the nucleophilic attachment of an oxygen from water to the amide carbon and the associated cleavage of the peptide amide between two amino acids (Zahn 2004). With a diluted acid (pH 1 – 3), this cleavage takes place predominantly in the immediate vicinity of aspartic acid. Accordingly, N-terminal peptides of the BLG sequence 1 – 32, 1 – 33 (Asp-33), 1 – 52 and 1 – 53 (Asp-53) were found in fibrillary structures at pH 2 (Akkermans et al. 2008b) (**FIG 2-6**). Although this sequence as part of the beta strands A and B as part of the Calyx are obscured (Mercadante et al. 2012), the unfolding and cleavage destabilizes the BLG

to such an extent that these fibrillization prone peptide segments become accessible (van der Linden and Venema 2007). The pH value not only controls the degree of hydrolysis, but the proton activity also influences the electrostatic interactions between the peptides (or at lower degrees of hydrolysis of the BLG monomers) (Cao and Mezzenga 2019; Loveday et al. 2011). At pH values below the isoelectric point, the surface charge of the monomers is positive. The combination of strong (positive) intramolecular repulsion and hydrophobic and Van der Waals attraction leads to an ordered aggregation as already described for the formation of long semi flexible fibrils at pH 1.6 to 3 (Loveday et al. 2017; Cao and Mezzenga 2019; Serfert et al. 2014; Loveday et al. 2011). From a pH value of 3 up to pH value 3.5 the building blocks aggregate to more flexible and worm-like morphologies (Serfert et al. 2014; Nicolai and Durand 2013). This is attributed as the state of knowledge to the weaker electrostatic repulsion forces due to low charge density and the steric limits of the less hydrolysed material (Cao and Mezzenga 2019). At pH values close to the isoelectric point, spherical amorphous aggregates are formed (Serfert et al. 2014). *However, it is yet unclear, if these structures consist of the same building blocks as the straight fibrils at pH 2, considering a reduced acid hydrolysis rate* **(see hypothesis 2, manuscript 1).**

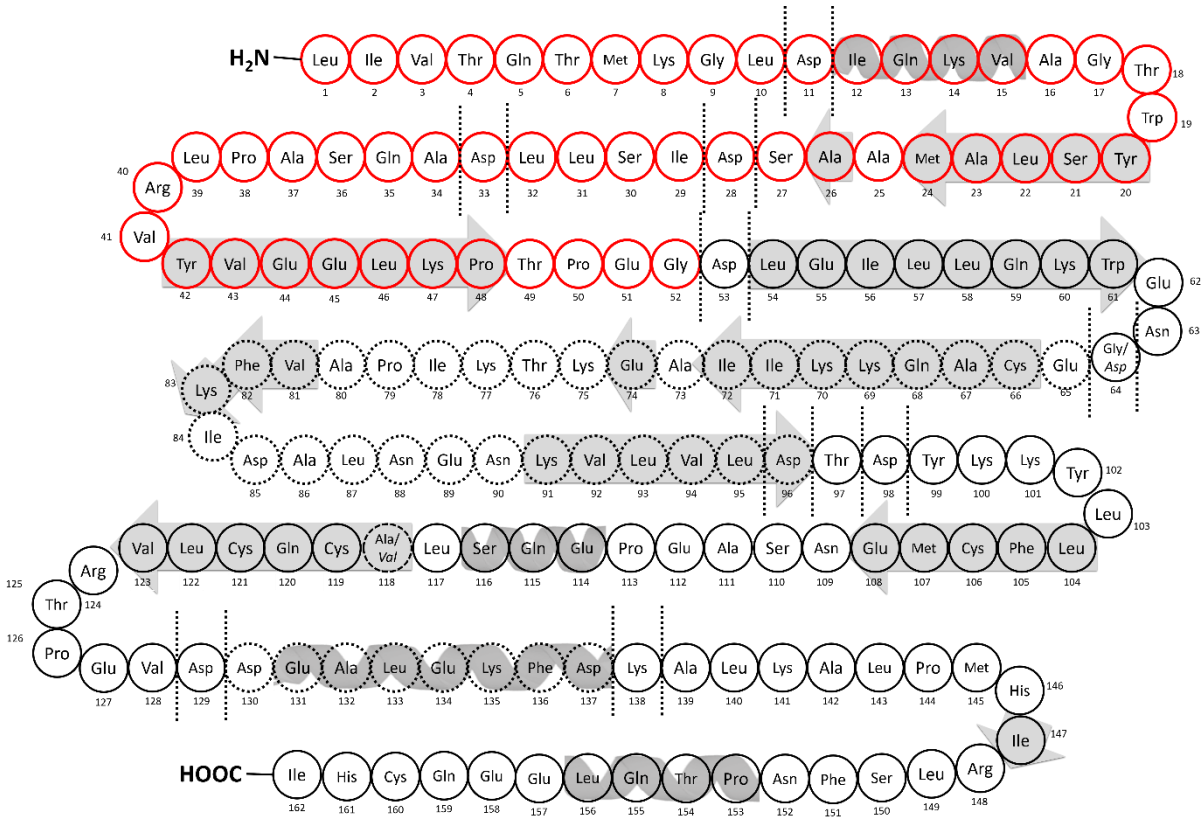

FIG 2-6 Cleavage points of BLG during acid hydrolysis according to Akkermans et al. (2008). Red: Amino acids which are built into pH 2 fibrils. Black: Amino acids which are possibly build into pH 2 fibrils. Striped black: Amino acids which were not found in pH 2 fibrils.

Ionic strength

The ionic strength of the protein solution influences the amyloid aggregation kinetics (Schokker et al. 2000; Arnaudov and Vries 2006) as well as the resulting fibril morphology (Arnaudov and Vries 2006; Loveday et al. 2010) to a high extent. The repulsion forces between the monomers, caused by the charge potential of the relatively high proton activity, lead to a slow but ordered fibril growth (Loveday et al. 2017). The addition of NaCl, $CaCl_2$ or other salts leads to an accumulation of the anions (Cl^-) and thus to a decrease of this charge potential (Loveday et al. 2010; Loveday et al. 2011). This results in a weaker repulsion and a faster, but also more chaotic arrangement of the building blocks. As a result, a low ion strength leads to long semiflexible fibrils, while accelerated growth of worm-like and flexible morphologies occurs at salt concentrations ≥ 60 mM NaCl or ≥ 33 mM $CaCl_2$ (Loveday et al. 2010; Loveday et al. 2011). Use of $CaCl_2$ shortens the lag phase as well. Loveday et al. (2010) hypothesized that Ca^{2+} might act as a nucleophilic unit between two peptides and thus accelerate nucleation. Adamcik and Mezzenga (2011) observed an adjustability of the periodic pitch of the twisted ribbons when adding > 50 mM NaCl after fibril formation.

Temperature

So far, fibrillation in independence of solvents (TFE, ethanol, methanol) has only been described at temperatures above the denaturation temperature of BLG (> 70 °C) (Cao and Mezzenga 2019; Loveday et al. 2017; Loveday 2016). During protein unfolding, the internal bonds break and previously buried residues can be hydrated (Cao and Mezzenga 2019). It was also shown that the hydrolysis rate at pH 2 in the temperature range from 353 to 383 K follows an Arrhenius relation (Kroes-Nijboer et al. 2011). In the shown temperature and pH range, the fibril growth kinetics may be limited by the hydrolysates or by the association rate of the peptide building blocks (Kroes-Nijboer et al. 2011). A higher temperature leads to a shortened lag phase and a higher aggregation kinetics (Loveday et al. 2012b; Loveday et al. 2011). As already mentioned, the temperature-dependent diffusion rate of the building blocks apparently has no influence on the association kinetics (Dave et al. 2014b). The fibril yield, i.e. the maximum amount of amyloid material per protein used, is independent of the temperature at more than 80 °C and is even decreasing from 110 °C (Loveday et al. 2012b; Loveday et al. 2011). Effects of temperature on morphology are limited to the presence of multi-stranded structures at temperatures above 100 °C and the observance of fragmented strands after prolonged heating at 120 °C (Loveday et al. 2012b).

Protein concentration

The protein concentration influences the fibril growth rate (Arnaudov and Vries 2006; Arnaudov et al. 2003; Ye et al. 2018; Schokker et al. 2000; Kroes-Nijboer et al. 2009) as well as the resulting morphology (Mudgal et al. 2011b; vandenAkker et al. 2011; Ye et al. 2018). At BLG concentrations up to ~4 wt% and a pH value of 2 semiflexible elongated fibrils can be observed, while from 7.5 wt% worm-like fibrils with a shorter contour length were described (Ye et al. 2018; vandenAkker et al. 2011). It was suggested that the morphological variance base on different nucleation mechanisms and a variation of peptide building blocks (Ye et al. 2018). Increasing the protein concentration lowers the beta-sheet structure in the aggregates, while the random and alpha-helix content increase (vandenAkker et al. 2011). The higher monomer density also leads to a faster, but also more chaotic association, similar to a higher ionic strength in the solution (Arnaudov and Vries 2006; Kroes-Nijboer et al. 2009). However, an independent protein concentration effect from the ionic strength has been demonstrated (Arnaudov and Vries 2006). A minimum concentration of 0.16 wt% BLG is required for fibril formation (Kroes-Nijboer et al. 2009).

Mechanical energy

The shearing of the protein solutions by shear rheometer, four-roller mill or magnetic stirrers leads to a shortening of the lag phase and increase of the aggregation kinetics and to an improved fibril yield (Akkermans et al. 2008a; Akkermans et al. 2006; Dunstan et al. 2009; Hill et al. 2006; Bolder et al. 2007; Sharma et al. 2014). Initially, as already described, the protein can unfold faster in the shear flow (Rahaman et al. 2015; Arosio et al. 2012), which can lead directly to accelerated aggregation (Hill et al. 2006) or increase the hydrolysis rate and thus the provision of potential fibril building blocks. Investigations with shear pulses have shown that these stimulate the rapid formation of a nucleus (primary nucleation) whose presence itself prepares the transition into the growth phase (Akkermans et al. 2006). Additionally, for the formation of BLG fibrils—as for other polymers—an improved alignment of the building blocks was described. Akkermans et al. (Akkermans et al. 2008a) explained the increase of fibril amount as a function of the shear rate by an improved assembly of the protein monomers at the fibril tips to which they are transported in the flow field. However, an excessive increase in shear stress has a negative effect on the fibril conversion, which is explained by the breaking of non-matured bonds inside the fibril (Akkermans et al. 2008a; Hill et al. 2006). This is again mentioned for the accelerated effect under stirring (Dunstan et al. 2009; Bolder et al. 2007). The destruction of protofibrillar structures leads to smaller fragments (seeds), which are available as nuclei for the assembly of further building blocks (secondary nucleation) (Dunstan

et al. 2009; Bolder et al. 2007; Arosio et al. 2012). Therefore, the higher density of potential docking sites for the monomers accelerates the formation of fibrils. Arosio et al. (2012) highlighted the fact, that the mechanical treatment of the solutions can create water-air interfaces, which itself can influence the aggregation process. *Mechanical treatment by other forms of stressing, such as torsion or impact forces have not been investigated yet. As shear affects the formation kinetics of fibrils, it is unclear if aggregation kinetics of worm-like aggregates can also be increased* **(see hypothesis 4, manuscript 3).**

Seeding

For many types of amyloid aggregates, seeding of an active amyloid nucleus accelerates fibril growth (Krebs et al. 2000; Mahul-Mellier et al. 2015; Morozova-Roche et al. 2000; Saelices et al. 2018; Scherpelz et al. 2016; Yang et al. 2019). So far, successful seeding by using freeze-dried and thus fractionated semi flexible and worm-like BLG fibrils (addition of 80 mM $CaCl_2$) has only been described by Loveday et al. (2012a). The use of intact, mature fibrils has no stimulating effect due to the low density of active areas (Bolder et al. 2007). Only the fractionation of the fibrils reveals new active areas, which is also suggested as a fibrils growth accelerating effect of stirring or shearing (Hill et al. 2006). The resulting morphologies are independent of the seed morphology (Loveday et al. 2012a). However, seeding with fractionated straight fibrils is more efficient (Loveday et al. 2012a). This is due to the increased stability of the worm-like fibrils during the drying process, and the assumption that the active nucleus of these fibrils is rather obscured (Loveday et al. 2012a).

2.3.2. Post-fibrillisation influencing factors

The use of BLG fibrils as emulsifiers for oil in water emulsions has valuable potential in terms of improved chemical and physical stability compared to the use of native BLG (Gao et al. 2017; Serfert et al. 2014; Moro et al. 2013; Mantovani et al. 2018). At the same time, the process chain of emulsion production contains a variety of factors that can influence the highly structured aggregates (Oboroceanu et al. 2011). It has already been established that, for example, the use of rotor-stator-dispersion systems and high-pressure homogenization affect not only the oil droplet size but also the aggregate size (Serfert et al. 2014; Koo et al. 2018; Rogers et al. 2005; Oboroceanu et al. 2011). When using the rotor-stator system for pre-emulsification, shearing forces are primarily used for particle size reduction (Utomo et al. 2009; Bourne and Studer 1992). In the subsequent high-pressure homogenization, cavitation and pressure gradients play a role in addition to shear forces (Gothsch et al. 2016). In addition, the oil-water interface can influence the protein (Fang and Dalgleish 1997) or the fibrils (Sluzky et

al. 1991; Macchi et al. 2011) by a certain additional force potential. *However, there is still no comparison about the single fragmentation factors such as shear by rotor-stator, cavitation and micro fluidisation or destructive influences by interfaces. Furthermore, there is no evidence about the robustness of semiflexible fibrils and worm-like aggregates against processing factors* **(see hypothesis 5, manuscript 4**).

High shear stress

During pre-emulsification in the rotor-stator system or during subsequent high-pressure homogenization, processing sometimes takes place under extreme shear stress. While cavitation can be an additional stress factor in the high-pressure system (**see section: cavitation**), particle size reduction in rotor-stator designs takes place explicitly under the use of shear. For this purpose, the particles are disrupted in the conical gap between the toothed or smooth rotor and stator (Karbstein and Schubert 1995). The fluid enters in the rotor, circulates and jets emerging from the stator slot as the fluid impinged on the leading edge of the stator teeth (Utomo et al. 2008). Here the turbulent flow is responsible for particle breaking (Karbstein and Schubert 1995), while the dissipation of the turbulent kinetic energy depends on the size of the gap (Utomo et al. 2008). The flowrate is proportional to the rotation speed and the energy dissipation rate scales with (rotation speed)^3 * (rotor diameter)^2 (Utomo et al. 2008). Gaps can have a width between 100 and 3,000 µm (Karbstein and Schubert 1995), while the peripheral speed is usually between 5 and 50 m s^{-1} (Utomo et al. 2008) creating very high shear rates of 20,000 to 100,000 s^{-1} (Paul et al. 2004). During high-pressure homogenisation shear rates might even be higher (Schultz et al. 2004). It was shown before, that BLG fibrils can disrupt already at shear rates of 8 – 107 s^{-1} (Kroes-Nijboer et al. 2010). Using a colloid mill strong breakage of the fibrils to short fragments occur (Mantovani et al. 2018; Rogers et al. 2005; Serfert et al. 2014), which are even shorter when high pressure homogenisation is used (Serfert et al. 2014; Oboroceanu et al. 2014).

Cavitation

Cavitation describes the formation of vapour-filled cavities in liquids. This happens in the course of a rapid decrease in the static pressure below the evaporation pressure of the liquid and a collapse of the vapour bubbles when the static pressure rises again. This formation and implosion of the cavitation bubbles leads to extreme local pressure (100 – 1,000 bar) and temperature peaks (1,000 – 10,000 K) (Luss et al. 1999; Gogate 2011). This rapid change in the static pressure can be caused by an extreme acceleration of the liquid and thus an increase in the dynamic pressure (e.g. in high pressure homogenisation) (Gogate 2011) or by the use of sonication (Sutariya et al. 2018): Ultrasound transmits waves of compression and rarefaction to

the medium it passes, which cause the molecules in the medium to oscillate (Sutariya et al. 2018). The acoustic pressure of rarefaction can cause a sufficiently large negative pressure to a liquid, where the distance between the molecules can exceed the critical molecular distance of an intact medium. Therefore the liquid breaks down and cavitation bubbles can occur (Mason and Peters; Sutariya et al. 2018). However, the treatment with sonication induces an extremely complex stress field in which the formation of liquid-gas interfaces/bubbles and high reactive oxygen species (e.g. $OH\cdot$, H_2O_2, O_2^-) play a role in addition to mechanical shear stress and high local temperatures (Cao and Mezzenga 2019). Acoustic cavitation by sonication was described to induce structural and physico-chemical changes of native BLG (Ma et al. 2018; Stanic-Vucinic et al. 2012; Sutariya et al. 2018) as well as hydrodynamic cavitation by high pressure micro fluidisation (Zhong et al. 2012). Ultra-sonication can induce the monomeric solution of beta2-microglobulin and alpha-synuclein to form amyloid fibrils (Adachi et al. 2015; Ohhashi et al. 2005; Patterson et al. 2019; Maity et al. 2011; Chatani et al. 2009), but also can influence globular proteins to aggregate in an amyloid-like way (Stathopulos et al. 2004). Nucleation accelerating effects of ultra-sonication were described as this treatment breaks down the preformed fibrils into fibril seeds (Chatani et al. 2009; Sneideris et al. 2015). However, so far the shortening effect of ultra-sonication on BLG fibrils has only been investigated in combination with rotor-stator treatment (Mantovani et al. 2018). The changes in the secondary structure and grade of denaturation of native BLG as well as the fragmentation of BLG fibrils by hydrodynamic cavitation as a result of high-pressure micro fluidisation were investigated by Oboroceanu et al. (2011)

Interfaces

In the course of processing the protein- or fibril solution, air can be trapped (Arosio et al. 2012) or cavitation might occur (Gogate 2011), leading to the formation of vapour bubbles and thus the formation of water-air interfaces. When mixed with a liquid lipid phase to produce an emulsion, formation of a oil-water interface with a high specific surface area depending on the particle size happens. The adsorption of a protein or polymer at the interface is associated with a change in the net Gibbs energy and leads to a deformation of the polymer (Malmsten 2003). The degree of deformation depends on the solvent conditions, the interfacial tension and the resistance of the polymer (caused by intramolecular binding forces) (Malmsten 2003). Explicitly in globular proteins such as BLG with a hydrophobic cavity, adsorption at oil or air interfaces leads to a strong change in conformation. During the formation of amyloid aggregates from peptides, hydrophobic surfaces lead to a strong acceleration of the nucleation kinetics (Campioni et al. 2014; Hamley 2010; Li et al. 2018; Morinaga et al. 2010; Malmsten 2003;

Pronchik et al. 2010b; Sluzky et al. 1991). This is due to the concentration of the monomers in the micro environment of the surface and a high contact number of the fibril building blocks in the course of a 2D diffusion at the surface (Shezad et al. 2016). No effect of interfaces or surfaces on amyloid aggregation has been described so far for globular amylogenic proteins or formed fibrils. Unfolding, hydrolysis and association of BLG could be promoted by the interfaces, but a fragmenting effect of the amyloid fibrils would also be conceivable.

Pressure

In a high pressure homogenizer, a liquid is pumped through a constriction by a high pressure positive displacement pump. This process converts the high static pressure into kinetic energy. A commonly in food industry used homogenizer is designed to operate at static pressure ranging from 50 to 300 bar (Gogate 2011). However, during the cavitation events short pressure maxima of 1,000 bar can occur. High pressure can affect protein conformation and can lead to protein denaturation and aggregation events (Messens et al. 1997). BLG has a high sensitivity to pressure, due to its cavities, exposure and solvation of hydrophobic residues, and dissociation of electrostatic bonds can lead to the decrease in volume (Messens et al. 1997; Patel et al. 2005). Already at pressures between 500 and 1,000 bar a structural rearrangement of BLG can occur which leads to the exposure of free cysteine (Stapelfeldt and Skibsted 1999). As π-π stacking interactions are prone to negative volume change, the formation of amorphous aggregates and amyloid fibrils might be caused by high pressure (van Eldik et al. 1989). However, some studies have demonstrated the dissociation of amyloid protofibrils or even mature fibrils due to the pressure sensitivity of water-excluded cavities and hydrophobic pockets in the fibril structure (Foguel et al. 2003; Shah et al. 2012; Radovan et al. 2008). Dissociation of mature lysozyme fibrils were described to occur at pressures ≥ 450 bar (Shah et al. 2012), which leads to the suggestion that these amyloid fibrils are in high-volume and high compressibility state (Cao and Mezzenga 2019)

2.4. References

A. Bos, M., & van Vliet, T. (2001). Interfacial rheological properties of adsorbed protein layers and surfactants. *Adv Colloid Interface Sci*, 91(3), 437–71. http://dx.doi.org/10.1016/S0001-8686(00)00077-4.

Adachi, M., So, M., Sakurai, K., Kardos, J., & Goto, Y. (2015). Supersaturation-limited and Unlimited Phase Transitions Compete to Produce the Pathway Complexity in Amyloid Fibrillation. *the journal of biological chemistry*, 290(29), 18134–45. http://dx.doi.org/10.1074/jbc.M115.648139.

Adamcik, J., Jung, J.-M., Flakowski, J., Los Rios, P. de, Dietler, G., & Mezzenga, R. (2010a). Understanding amyloid aggregation by statistical analysis of atomic force microscopy images. *Nat Nanotechnol*, 5(6), 423–8. http://dx.doi.org/10.1038/nnano.2010.59.

Adamcik, J., & Mezzenga, R. (2011). Adjustable twisting periodic pitch of amyloid fibrils. *Soft Matter*, 7(11), 5437. http://dx.doi.org/10.1039/c1sm05382e.

Adamcik, J., & Mezzenga, R. (2018). Amyloid Polymorphism in the Protein Folding and Aggregation Energy Landscape. *Angew Chem Int Ed Engl*, 57(28), 8370–82. http://dx.doi.org/10.1002/anie.201713416.

Akkermans, C., van der Goot, A.J., Venema, P., van der Linden, E., & Boom, R.M. (2008a). Formation of fibrillar whey protein aggregates. *Food Hydrocolloids*, 22(7), 1315–25. http://dx.doi.org/10.1016/j.foodhyd.2007.07.001.

Akkermans, C., Venema, P., Rogers, S.S., van der Goot, A.J., Boom, R.M., & van der Linden, E. (2006). Shear Pulses Nucleate Fibril Aggregation. *Food Biophysics*, 1(3), 144–50. http://dx.doi.org/10.1007/s11483-006-9012-5.

Akkermans, C., Venema, P., van der Goot, A.J., Gruppen, H., Bakx, E.J., & Boom, R.M., et al. (2008b). Peptides are building blocks of heat-induced fibrillar protein aggregates of beta-lactoglobulin formed at pH 2. *Biomacromolecules*, 9(5), 1474–9. http://dx.doi.org/10.1021/bm7014224.

Ananthanarayanan, V.S., Ahmad, F., & Bigelow, C.C. (1977). The denaturation of β-lactoglobulin-A at pH 2. *Biochimica et Biophysica Acta (BBA) - Protein Structure*, 492(1), 194–203. http://dx.doi.org/10.1016/0005-2795(77)90226-4.

Arnaudov, L.N., & Vries, R. de (2005). Thermally induced fibrillar aggregation of hen egg white lysozyme. *Biophys J*, 88(1), 515–26. http://dx.doi.org/10.1529/biophysj.104.048819.

Arnaudov, L.N., & Vries, R. de (2006). Strong impact of ionic strength on the kinetics of fibrilar aggregation of bovine beta-lactoglobulin. *Biomacromolecules*, 7(12), 3490–8. http://dx.doi.org/10.1021/bm060584i.

Arnaudov, L.N., Vries, R. de, Ippel, H., & van Mierlo, C.P.M. (2003). Multiple steps during the formation of beta-lactoglobulin fibrils. *Biomacromolecules*, 4(6), 1614–22. http://dx.doi.org/10.1021/bm034096b.

Arosio, P., Beeg, M., Nicoud, L., & Morbidelli, M. (2012). Time evolution of amyloid fibril length distribution described by a population balance model. *Chemical Engineering Science*, 78, 21–32. http://dx.doi.org/10.1016/j.ces.2012.04.031.

Astbury, W.T., Dickinson, S., & Bailey, K. (1935). The X-ray interpretation of denaturation and the structure of the seed globulins. *Biochem. J.*, 29(10), 2351-2360.1. http://dx.doi.org/10.1042/bj0292351.

Aymard, P., Durand, D., & Nicolai, T. (1996). The effect of temperature and ionic strength on the dimerisation of β-lactoglobulin. *International Journal of Biological Macromolecules*, 19(3), 213–21. http://dx.doi.org/10.1016/0141-8130(96)01130-0.

Aymard, P., Nicolai, T., Durand, D., & Clark, A. (1999). Static and Dynamic Scattering of β-Lactoglobulin Aggregates Formed after Heat-Induced Denaturation at pH 2. *Macromolecules*, 32(8), 2542–52. http://dx.doi.org/10.1021/ma981689j.

Bauer, R., Carrotta, R., Rischel, C., & Øgendal, L. (2000). Characterization and Isolation of Intermediates in β-Lactoglobulin Heat Aggregation at High pH. *Biophys J*, 79(2), 1030–8. http://dx.doi.org/10.1016/S0006-3495(00)76357-0.

Bee, J.S., Stevenson, J.L., Mehta, B., Svitel, J., Pollastrini, J., & Platz, R., et al. (2009). Response of a concentrated monoclonal antibody formulation to high shear. *Biotechnol Bioeng*, 103(5), 936–43. http://dx.doi.org/10.1002/bit.22336.

Bekard, I.B., Asimakis, P., Bertolini, J., & Dunstan, D.E. (2011). The effects of shear flow on protein structure and function. *Biopolymers*, 95(11), 733–45. http://dx.doi.org/10.1002/bip.21646.

Belloque, J., & Smith, G.M. (1998). Thermal Denaturation of β-Lactoglobulin. A 1 H NMR Study. *J Agric Food Chem*, 46(5), 1805–13. http://dx.doi.org/10.1021/jf9709313.

Bhattacharjee, C., & Das, K.P. (2000). Thermal unfolding and refolding of beta-lactoglobulin. An intrinsic andextrinsic fluorescence study. *European Journal of Biochemistry*, 267(13), 3957–64. http://dx.doi.org/10.1046/j.1432-1327.2000.01409.x.

Bhattacharjee, C., Saha, S., Biswas, A., Kundu, M., Ghosh, L., & Das, K.P. (2005). Structural Changes of ? *Protein J*, 24(1), 27–35. http://dx.doi.org/10.1007/s10930-004-0603-z.

Bolder, S.G., Sagis, L.M.C., Venema, P., & van der Linden, E. (2007a). Effect of stirring and seeding on whey protein fibril formation. *J Agric Food Chem*, 55(14), 5661–9. http://dx.doi.org/10.1021/jf063351r.

Bolisetty, S., Adamcik, J., Heier, J., & Mezzenga, R. (2012). Amyloid Directed Synthesis of Titanium Dioxide Nanowires and Their Applications in Hybrid Photovoltaic Devices. *Adv. Funct. Mater.*, 22(16), 3424–8. http://dx.doi.org/10.1002/adfm.201103054.

Bolisetty, S., Arcari, M., Adamcik, J., & Mezzenga, R. (2015). Hybrid Amyloid Membranes for Continuous Flow Catalysis. *Langmuir*, 31(51), 13867–73. http://dx.doi.org/10.1021/acs.langmuir.5b03205.

Bolisetty, S., Boddupalli, C.S., Handschin, S., Chaitanya, K., Adamcik, J., & Saito, Y., et al. (2014). Amyloid fibrils enhance transport of metal nanoparticles in living cells and induced cytotoxicity. *Biomacromolecules*, 15(7), 2793–9. http://dx.doi.org/10.1021/bm500647n.

Bolisetty, S., & Mezzenga, R. (2016). Amyloid-carbon hybrid membranes for universal water purification. *Nat Nanotechnol*, 11(4), 365–71. http://dx.doi.org/10.1038/nnano.2015.310.

Bolisetty, S., Peydayesh, M., & Mezzenga, R. (2019). Sustainable technologies for water purification from heavy metals. *Chem Soc Rev*, 48(2), 463–87. http://dx.doi.org/10.1039/c8cs00493e.

Bourne, J.R., & Studer, M. (1992). Fast reactions in rotor-stator mixers of different size. *Chemical Engineering and Processing: Process Intensification*, 31(5), 285–96. http://dx.doi.org/10.1016/0255-2701(92)87002-X.

Bouyer, E., Mekhloufi, G., Rosilio, V., Grossiord, J.-L., & Agnely, F. (2012). Proteins, polysaccharides, and their complexes used as stabilizers for emulsions. *Int J Pharm*, 436(1-2), 359–78. http://dx.doi.org/10.1016/j.ijpharm.2012.06.052.

Braunitzer, G., Chen, R., Schrank, B., & Stangl, A. (1973). Die Sequenzanalyse des β-Lactoglobulins. *Hoppe-Seyler´s Zeitschrift für physiologische Chemie*, 354(2), 867–78. http://dx.doi.org/10.1515/bchm2.1973.354.2.867.

Campioni, S., Carret, G., Jordens, S., Nicoud, L., Mezzenga, R., & Riek, R. (2014). The presence of an air-water interface affects formation and elongation of α-Synuclein fibrils. *J Am Chem Soc*, 136(7), 2866–75. http://dx.doi.org/10.1021/ja412105t.

Cao, Y., & Mezzenga, R. (2019). Food protein amyloid fibrils. *Adv Colloid Interface Sci*, 269, 334–56. http://dx.doi.org/10.1016/j.cis.2019.05.002.

Carrotta, R., Bauer, R., Waninge, R., & Rischel, C. (2001). Conformational characterization of oligomeric intermediates and aggregates in beta-lactoglobulin heat aggregation. *Protein Sci*, 10(7), 1312–8. http://dx.doi.org/10.1110/ps.42501.

Casal, H.L., Köhler, U., & Mantsch, H.H. (1988). Structural and conformational changes of β-lactoglobulin B. *Biochimica et Biophysica Acta (BBA) - Protein Structure and Molecular Enzymology*, 957(1), 11–20. http://dx.doi.org/10.1016/0167-4838(88)90152-5.

Chapman, M.R., Robinson, L.S., Pinkner, J.S., Roth, R., Heuser, J., & Hammar, M., et al. (2002). Role of Escherichia coli curli operons in directing amyloid fibre formation. *Science*, 295(5556), 851–5. http://dx.doi.org/10.1126/science.1067484.

Chatani, E., Lee, Y.-H., Yagi, H., Yoshimura, Y., Naiki, H., & Goto, Y. (2009). Ultra-sonication-dependent production and breakdown lead to minimum-sized amyloid fibrils. *Proc Natl Acad Sci U S A*, 106(27), 11119–24. http://dx.doi.org/10.1073/pnas.0901422106.

Colvin, M.T., Silvers, R., Ni, Q.Z., Can, T.V., Sergeyev, I., & Rosay, M., et al. (2016). Atomic Resolution Structure of Monomorphic Aβ42 Amyloid Fibrils. *J Am Chem Soc*, 138(30), 9663–74. http://dx.doi.org/10.1021/jacs.6b05129.

Considine T, Flanagan J, Loveday SM. Interactions between Milk Proteins and Micronutrients. In: . Milk Proteins. Elsevier; 2014. p. 421–449.

Considine, T., Patel, H.A., Anema, S.G., Singh, H., & Creamer, L.K. (2007). Interactions of milk proteins during heat and high hydrostatic pressure treatments — A Review. *Innovative Food Science & Emerging Technologies*, 8(1), 1–23. http://dx.doi.org/10.1016/j.ifset.2006.08.003.

Creamer, L.K., Bienvenue, A., Nilsson, H., Paulsson, M., van Wanroij, M., & Lowe, E.K., et al. (2004). Heat-induced redistribution of disulfide bonds in milk proteins. 1. Bovine beta-lactoglobulin. *J Agric Food Chem*, 52(25), 7660–8. http://dx.doi.org/10.1021/jf049388y.

Creamer, L.K., Parry, D.A.D., & Malcolm, G.N. (1983). Secondary structure of bovine β-lactoglobulin B. *Archives of Biochemistry and Biophysics*, 227(1), 98–105. http://dx.doi.org/10.1016/0003-9861(83)90351-X.

Dave, A.C., Loveday, S.M., Anema, S.G., Jameson, G.B., & Singh, H. (2014a). Glycation as a Tool To Probe the Mechanism of β-Lactoglobulin Nanofibril Self-Assembly. *J. Agric. Food Chem.*, 62(14), 3269–78. http://dx.doi.org/10.1021/jf405441g.

Dave, A.C., Loveday, S.M., Anema, S.G., Jameson, G.B., & Singh, H. (2014b). Modulating β-lactoglobulin nanofibril self-assembly at pH 2 using glycerol and sorbitol. *Biomacromolecules*, 15(1), 95–103. http://dx.doi.org/10.1021/bm401315s.

Dave, A.C., Loveday, S.M., Anema, S.G., Loo, T.S., Norris, G.E., & Jameson, G.B., et al. (2013). B-lactoglobulin self-assembly. *J Agric Food Chem*, 61(32), 7817–28. http://dx.doi.org/10.1021/jf401084f.

Dissanayake, M., Ramchandran, L., Donkor, O.N., & Vasiljevic, T. (2013). Denaturation of whey proteins as a function of heat, pH and protein concentration. *International Dairy Journal*, 31(2), 93–9. http://dx.doi.org/10.1016/j.idairyj.2013.02.002.

Dissanayake, M., & Vasiljevic, T. (2009). Functional properties of whey proteins affected by heat treatment and hydrodynamic high-pressure shearing. *J Dairy Sci*, 92(4), 1387–97. http://dx.doi.org/10.3168/jds.2008-1791.

Dunstan, D.E., Hamilton-Brown, P., Asimakis, P., Ducker, W., & Bertolini, J. (2009). Shear-induced structure and mechanics of β-lactoglobulin amyloid fibrils. *Soft Matter*, 5(24), 5020. http://dx.doi.org/10.1039/b914089a.

Dupont, M. (1965). Étude d'une étape réversible dans la thermodénaturation de la β-lactoglobuline bovine a. *Biochimica et Biophysica Acta (BBA) - Biophysics including Photosynthesis*, 102(2), 500–13. http://dx.doi.org/10.1016/0926-6585(65)90140-8.

Eisenberg, D.S., & Sawaya, M.R. (2017). Structural Studies of Amyloid Proteins at the Molecular Level. *Annu Rev Biochem*, 86, 69–95. http://dx.doi.org/10.1146/annurev-biochem-061516-045104.

Erabit, N., Flick, D., & Alvarez, G. (2014). Formation of β-lactoglobulin aggregates during thermomechanical treatments under controlled shear and temperature conditions. *Journal of Food Engineering*, 120, 57–68. http://dx.doi.org/10.1016/j.jfoodeng.2013.07.003.

Fang, & Dalgleish (1997). Conformation of beta-Lactoglobulin Studied by FTIR. *J Colloid Interface Sci*, 196(2), 292–8. http://dx.doi.org/10.1006/jcis.1997.5191.

Farrell, H.M., Jimenez-Flores, R., Bleck, G.T., Brown, E.M., Butler, J.E., & Creamer, L.K., et al. (2004). Nomenclature of the Proteins of Cows' Milk—Sixth Revision. *J Dairy Sci*, 87(6), 1641–74. http://dx.doi.org/10.3168/jds.S0022-0302(04)73319-6.

Foguel, D., Suarez, M.C., Ferrão-Gonzales, A.D., Porto, T.C.R., Palmieri, L., & Einsiedler, C.M., et al. (2003). Dissociation of amyloid fibrils of alpha-synuclein and transthyretin by pressure reveals their reversible nature and the formation of water-excluded cavities. *Proceedings of the National Academy of Sciences*, 100(17), 9831–6. http://dx.doi.org/10.1073/pnas.1734009100.

Fowler, D.M., Koulov, A.V., Alory-Jost, C., Marks, M.S., Balch, W.E., & Kelly, J.W. (2006). Functional amyloid formation within mammalian tissue. *PLoS Biol*, 4(1), e6. http://dx.doi.org/10.1371/journal.pbio.0040006.

Fyrberg, E., & Beall, C. (1990). Genetic approaches to myofibril form and function in Drosophila. *Trends in Genetics*, 6, 126–31. http://dx.doi.org/10.1016/0168-9525(90)90127-R.

Gaaloul, S., Corredig, M., & Turgeon, S.L. (2009). The Effect of Shear Rate on the Molecular Mass Distribution of Heat-Induced Aggregates of Mixtures Containing Whey Proteins and κ-Carrageenan. *Food Biophysics*, 4(1), 13–22. http://dx.doi.org/10.1007/s11483-008-9099-y.

Gao, Z., Zhao, J., Huang, Y., Yao, X., Zhang, K., & Fang, Y., et al. (2017). Edible Pickering emulsion stabilized by protein fibrils. Part 1. *LWT - Food Science and Technology*, 76, 1–8. http://dx.doi.org/10.1016/j.lwt.2016.10.038.

García-Hernández, E., Hernández-Arana, A., Zubillaga, R., & Rojo-Domínguez, A. (1998). Spectroscopic and thermodynamic evidence for a complex denaturation mechanism of bovine β-lactoglobulin A. *TBMB*, 45(4), 761–8. http://dx.doi.org/10.1080/15216549800203172.

Gezimati, J., Creamer, L.K., & Singh, H. (1997). Heat-Induced Interactions and Gelation of Mixtures of β-Lactoglobulin and α-Lactalbumin. *J Agric Food Chem*, 45(4), 1130–6. http://dx.doi.org/10.1021/jf960564f.

Gibbs CJ. Bovine Spongiform Encephalopathy. New York, NY: Springer New York 1996.

Goers, J., Permyakov, S.E., Permyakov, E.A., Uversky, V.N., & Fink, A.L. (2002). Conformational prerequisites for alpha-lactalbumin fibrillation. *Biochemistry*, 41(41), 12546–51. http://dx.doi.org/10.1021/bi0262698.

Gogate, P.R. (2011). Hydrodynamic Cavitation for Food and Water Processing. *Food Bioprocess Technol*, 4(6), 996–1011. http://dx.doi.org/10.1007/s11947-010-0418-1.

Goldschmidt, L., Teng, P.K., Riek, R., & Eisenberg, D. (2010). Identifying the amylome, proteins capable of forming amyloid-like fibrils. *Proc Natl Acad Sci U S A*, 107(8), 3487–92. http://dx.doi.org/10.1073/pnas.0915166107.

Gosal, W.S., Clark, A.H., & Ross-Murphy, S.B. (2004). Fibrillar beta-lactoglobulin gels. *Biomacromolecules*, 5(6), 2430–8. http://dx.doi.org/10.1021/bm0496615.

Gothsch, T., Richter, C., Beinert, S., Schilcher, C., Schilde, C., & Büttgenbach, S., et al. (2016). Effect of cavitation on dispersion and emulsification process in high-pressure microsystems (HPMS). *Chemical Engineering Science*, 144, 239–48. http://dx.doi.org/10.1016/j.ces.2016.01.034.

Gremer, L., Schölzel, D., Schenk, C., Reinartz, E., Labahn, J., & Ravelli, R.B.G., et al. (2017). Fibril structure of amyloid-β(1-42) by cryo-electron microscopy. *Science*, 358(6359), 116–9. http://dx.doi.org/10.1126/science.aao2825.

Hamada, D., Segawa, S.-i., & Goto, Y. (1996). Non-native α-helical intermediate in the refolding of β-lactoglobulin, a predominantly β-sheet protein. *Nat Struct Mol Biol*, 3(10), 868–73. http://dx.doi.org/10.1038/nsb1096-868.

Hamley, I.W. (2010). Amyloid formation. *Nat Chem*, 2(9), 707–8. http://dx.doi.org/10.1038/nchem.816.

Hansen, J., Nazarenko, L., Ruedy, R., Sato, M., Willis, J., & Del Genio, A., et al. (2005). Earth's energy imbalance. *Science*, 308(5727), 1431–5. http://dx.doi.org/10.1126/science.1110252.

Hardy, J. (1997). Amyloid, the presenilins and Alzheimer's disease. *Trends in Neurosciences*, 20(4), 154–9. http://dx.doi.org/10.1016/S0166-2236(96)01030-2.

Harwalkar, V.R. (1980). Kinetics of Thermal Denaturation of β-Lactoglobulin at pH 2.5. *J Dairy Sci*, 63(7), 1052–7. http://dx.doi.org/10.3168/jds.S0022-0302(80)83046-3.

Hettiarachchi, C.A., Melton, L.D., Gerrard, J.A., & Loveday, S.M. (2012). Formation of β-lactoglobulin nanofibrils by microwave heating gives a peptide composition different from conventional heating. *Biomacromolecules*, 13(9), 2868–80. http://dx.doi.org/10.1021/bm300896r.

Hill, E.K., Krebs, B., Goodall, D.G., Howlett, G.J., & Dunstan, D.E. (2006). Shear Flow Induces Amyloid Fibril Formation. *Biomacromolecules*, 7(1), 10–3. http://dx.doi.org/10.1021/bm0505078.

Høiberg-Nielsen, R., Fuglsang, C.C., Arleth, L., & Westh, P. (2006). Interrelationships of glycosylation and aggregation kinetics for Peniophora lycii phytase. *Biochemistry*, 45(15), 5057–66. http://dx.doi.org/10.1021/bi0522955.

Hoyer, W., Antony, T., Cherny, D., Heim, G., Jovin, T.M., & Subramaniam, V. (2002). Dependence of α-Synuclein Aggregate Morphology on Solution Conditions. *J Mol Biol*, 322(2), 383–93. http://dx.doi.org/10.1016/S0022-2836(02)00775-1.

Humblet-Hua, N.-P.K., van der Linden, E., & Sagis, L.M.C. (2013). Surface rheological properties of liquid–liquid interfaces stabilized by protein fibrillar aggregates and protein–polysaccharide complexes. *Soft Matter*, 9(7), 2154. http://dx.doi.org/10.1039/c2sm26627j.

Iametti, S., Gregori, B. de, Vecchio, G., & Bonomi, F. (1996). Modifications occur at different structural levels during the heat denaturation of beta-lactoglobulin. *European Journal of Biochemistry*, 237(1), 106–12. http://dx.doi.org/10.1111/j.1432-1033.1996.0106n.x.

Iconomidou, V.A., Vriend, G., & Hamodrakas, S.J. (2000). Amyloids protect the silkmoth oocyte and embryo. *FEBS Lett*, 479(3), 141–5. http://dx.doi.org/10.1016/s0014-5793(00)01888-3.

Iordache, M., & Jelen, P. (2003). High pressure microfluidization treatment of heat denatured whey proteins for improved functionality. *Innovative Food Science & Emerging Technologies*, 4(4), 367–76. http://dx.doi.org/10.1016/S1466-8564(03)00061-4.

Jayawardena, N., Kaur, M., Nair, S., Malmstrom, J., Goldstone, D., & Negron, L., et al. (2017). Amyloid Fibrils from Hemoglobin. *Biomolecules*, 7(2). http://dx.doi.org/10.3390/biom7020037.

Jung, J.-M., Gunes, D.Z., & Mezzenga, R. (2010). Interfacial activity and interfacial shear rheology of native β-lactoglobulin monomers and their heat-induced fibres. *Langmuir*, 26(19), 15366–75. http://dx.doi.org/10.1021/la102721m.

Jung, J.-M., & Mezzenga, R. (2010). Liquid Crystalline Phase Behavior of Protein Fibres in Water. *Langmuir*, 26(1), 504–14. http://dx.doi.org/10.1021/la9021432.

Jurado, R., Adamcik, J., López-Haro, M., González-Vera, J.A., Ruiz-Arias, Á., & Sánchez-Ferrer, A., et al. (2019). Apoferritin Protein Amyloid Fibrils with Tunable Chirality and Polymorphism. *J Am Chem Soc*, 141(4), 1606–13. http://dx.doi.org/10.1021/jacs.8b11418.

Karbstein, H., & Schubert, H. (1995). Developments in the continuous mechanical production of oil-in-water macro-emulsions. *Chemical Engineering and Processing: Process Intensification*, 34(3), 205–11. http://dx.doi.org/10.1016/0255-2701(94)04005-2.

Keppler, J.K., Martin, D., Garamus, V.M., & Schwarz, K. (2015). Differences in binding behavior of (-)-epigallocatechin gallate to β-lactoglobulin heterodimers (AB) compared to homodimers (A) and (B). *J Mol Recognit*, 28(11), 656–66. http://dx.doi.org/10.1002/jmr.2480.

Knowles, T.P.J., & Mezzenga, R. (2016). Amyloid Fibrils as Building Blocks for Natural and Artificial Functional Materials. *Adv Mater Weinheim*, 28(31), 6546–61. http://dx.doi.org/10.1002/adma.201505961.

Kockmann, A., Hesselbach, J., Zellmer, S., Kwade, A., & Garnweitner, G. (2015). Facile surface tailoring of metal oxide nanoparticles via a two-step modification approach. *RSC Adv.*, 5(75), 60993–9. http://dx.doi.org/10.1039/C5RA08932H.

Kontopidis, G., Holt, C., & Sawyer, L. (2002). The Ligand-binding Site of Bovine β-Lactoglobulin. *J Mol Biol*, 318(4), 1043–55. http://dx.doi.org/10.1016/S0022-2836(02)00017-7.

Kontopidis, G., Holt, C., & Sawyer, L. (2004). Invited Review. *J Dairy Sci*, 87(4), 785–96. http://dx.doi.org/10.3168/jds.S0022-0302(04)73222-1.

Koo, C.K.W., Chung, C., Ogren, T., Mutilangi, W., & McClements, D.J. (2018). Extending protein functionality. *Journal of Food Engineering*, 223, 189–96. http://dx.doi.org/10.1016/j.jfoodeng.2017.10.020.

Krebs, M.R., Wilkins, D.K., Chung, E.W., Pitkeathly, M.C., Chamberlain, A.K., & Zurdo, J., et al. (2000). Formation and seeding of amyloid fibrils from wild-type hen lysozyme and a peptide fragment from the beta-domain. *J Mol Biol*, 300(3), 541–9. http://dx.doi.org/10.1006/jmbi.2000.3862.

Krebs, M.R.H., Devlin, G.L., & Donald, A.M. (2009). Amyloid fibril-like structure underlies the aggregate structure across the pH range for beta-lactoglobulin. *Biophys J*, 96(12), 5013–9. http://dx.doi.org/10.1016/j.bpj.2009.03.028.

Kroes-Nijboer, A., Venema, P., Baptist, H., & van der Linden, E. (2010). Fracture of protein fibrils as induced by elongational flow. *Langmuir*, 26(16), 13097–101. http://dx.doi.org/10.1021/la1025262.

Kroes-Nijboer, A., Venema, P., Bouman, J., & van der Linden, E. (2009). The Critical Aggregation Concentration of β-Lactoglobulin-Based Fibril Formation. *Food Biophysics*, 4(2), 59–63. http://dx.doi.org/10.1007/s11483-009-9101-3.

Kroes-Nijboer, A., Venema, P., Bouman, J., & van der Linden, E. (2011). Influence of protein hydrolysis on the growth kinetics of β-lg fibrils. *Langmuir*, 27(10), 5753–61. http://dx.doi.org/10.1021/la104797u.

Ladner-Keay, C.L., Griffith, B.J., & Wishart, D.S. (2014). Shaking alone induces de novo conversion of recombinant prion proteins to β-sheet rich oligomers and fibrils. *PLoS ONE*, 9(6), e98753. http://dx.doi.org/10.1371/journal.pone.0098753.

Lara, C., Adamcik, J., Jordens, S., & Mezzenga, R. (2011). General self-assembly mechanism converting hydrolyzed globular proteins into giant multistranded amyloid ribbons. *Biomacromolecules*, 12(5), 1868–75. http://dx.doi.org/10.1021/bm200216u.

Lara, C., Handschin, S., & Mezzenga, R. (2013). Towards lysozyme nanotube and 3D hybrid self-assembly. *Nanoscale*, 5(16), 7197–201. http://dx.doi.org/10.1039/c3nr02194g.

Lassé, M., Ulluwishewa, D., Healy, J., Thompson, D., Miller, A., & Roy, N., et al. (2016). Evaluation of protease resistance and toxicity of amyloid-like food fibrils from whey, soy, kidney bean, and egg white. *Food Chem*, 192, 491–8. http://dx.doi.org/10.1016/j.foodchem.2015.07.044.

Law, A.J., & Leaver, J. (2000). Effect of pH on the thermal denaturation of whey proteins in milk. *J Agric Food Chem*, 48(3), 672–9. http://dx.doi.org/10.1021/jf981302b.

Léonil, J., Mollé, D., Gaucheron, F., Arpino, P., Guénot, P., & Maubois, J.L. (1995). Analysis of major bovine milk proteins by on-line high-performance liquid chromatography and electrospray ionization-mass spectrometry. *Lait*, 75(3), 193–210. http://dx.doi.org/10.1051/lait:1995314.

Li, C., Adamcik, J., & Mezzenga, R. (2012). Biodegradable nanocomposites of amyloid fibrils and graphene with shape-memory and enzyme-sensing properties. *Nat Nanotechnol*, 7(7), 421–7. http://dx.doi.org/10.1038/nnano.2012.62.

Li, C., Bolisetty, S., & Mezzenga, R. (2013). Hybrid nanocomposites of gold single-crystal platelets and amyloid fibrils with tunable fluorescence, conductivity, and sensing properties. *Adv Mater Weinheim*, 25(27), 3694–700. http://dx.doi.org/10.1002/adma.201300904.

Li, C., Qin, R., Liu, R., Miao, S., & Yang, P. (2018). Functional amyloid materials at surfaces/interfaces. *Biomater Sci*, 6(3), 462–72. http://dx.doi.org/10.1039/c7bm01124e.

Liberski, P.P., Kwiecinski, H., Barcikowska, M., Mirecka, B., Kulczycki, J., & Kida, E., et al. (1991). PrP amyloid plaques in Creutzfeldt-Jakob disease of short duration. *Eur J Epidemiol*, 7(5), 505–10. http://dx.doi.org/10.1007/bf00143130.

Ling, S., Li, C., Adamcik, J., Shao, Z., Chen, X., & Mezzenga, R. (2014). Modulating materials by orthogonally oriented β-strands. *Adv Mater Weinheim*, 26(26), 4569–74. http://dx.doi.org/10.1002/adma.201400730.

Liu, J., & Tang, C.-H. (2013). Heat-induced fibril assembly of vicilin at pH 2.0. *Food Research International*, 51(2), 621–32. http://dx.doi.org/10.1016/j.foodres.2012.12.049.

Loveday, S.M. (2016). β-Lactoglobulin heat denaturation. *International Dairy Journal*, 52, 92–100. http://dx.doi.org/10.1016/j.idairyj.2015.08.001.

Loveday, S.M., Anema, S.G., & Singh, H. (2017). β-Lactoglobulin nanofibrils. *International Dairy Journal*, 67, 35–45. http://dx.doi.org/10.1016/j.idairyj.2016.09.011.

Loveday, S.M., Su, J., Rao, M.A., Anema, S.G., & Singh, H. (2012a). Whey protein nanofibrils. *J Agric Food Chem*, 60(20), 5229–36. http://dx.doi.org/10.1021/jf300367k.

Loveday, S.M., Wang, X.L., Rao, M.A., Anema, S.G., Creamer, L.K., & Singh, H. (2010). Tuning the properties of β-lactoglobulin nanofibrils with pH, NaCl and CaCl2. *International Dairy Journal*, 20(9), 571–9. http://dx.doi.org/10.1016/j.idairyj.2010.02.014.

Loveday, S.M., Wang, X.L., Rao, M.A., Anema, S.G., & Singh, H. (2011). Effect of pH, NaCl, CaCl2 and temperature on self-assembly of β-lactoglobulin into nanofibrils. *J Agric Food Chem*, 59(15), 8467–74. http://dx.doi.org/10.1021/jf201870z.

Loveday, S.M., Wang, X.L., Rao, M.A., Anema, S.G., & Singh, H. (2012b). β-Lactoglobulin nanofibrils. *Food Hydrocolloids*, 27(1), 242–9. http://dx.doi.org/10.1016/j.foodhyd.2011.07.001.

Luss D, Shah YT, Pandit AB, Moholkar VS. Cavitation Reaction Engineering. Boston, MA: Springer US 1999.

Ma, S., Yang, X., Wang, C., & Guo, M. (2018). Effect of ultrasound treatment on antioxidant activity and structure of β-Lactoglobulin using the Box–Behnken design. *CyTA - Journal of Food*, 16(1), 596–606. http://dx.doi.org/10.1080/19476337.2018.1441909.

Macchi, F., Hoffmann, S.V., Carlsen, M., Vad, B., Imparato, A., & Rischel, C., et al. (2011). Mechanical stress affects glucagon fibrillation kinetics and fibril structure. *Langmuir*, 27(20), 12539–49. http://dx.doi.org/10.1021/la202125c.

Mackintosh, S.H., Meade, S.J., Healy, J.P., Sutton, K.H., Larsen, N.G., & Squires, A.M., et al. (2009). Wheat glutenin proteins assemble into a nanostructure with unusual structural features. *Journal of Cereal Science*, 49(1), 157–62. http://dx.doi.org/10.1016/j.jcs.2008.08.003.

Mahul-Mellier, A.-L., Vercruysse, F., Maco, B., Ait-Bouziad, N., Roo, M. de, & Muller, D., et al. (2015). Fibril growth and seeding capacity play key roles in α-synuclein-mediated apoptotic cell death. *Cell Death Differ*, 22(12), 2107–22. http://dx.doi.org/10.1038/cdd.2015.79.

Maity, S., Kumar, P., & Haldar, D. (2011). Sonication-induced instant amyloid-like fibril formation and organogelation by a tripeptide. *Soft Matter*, 7(11), 5239. http://dx.doi.org/10.1039/c1sm05277b.

Maji SK, Schubert D, Rivier C, Lee S, Rivier JE, Riek R. Amyloid as a depot for the formulation of long-acting drugs 2008. 13 p.

Malmsten M. Biopolymers at interfaces. 2nd ed. New York: Marcel Dekker 2003. xii, 908.

Mantovani, R.A., Figueiredo Furtado, G. de, Netto, F.M., & Cunha, R.L. (2018). Assessing the potential of whey protein fibril as emulsifier. *Journal of Food Engineering*, 223, 99–108. http://dx.doi.org/10.1016/j.jfoodeng.2017.12.006.

Mason, T., & Peters, D. (). An introduction to the uses of power ultrasound in chemistry, 1–48. http://dx.doi.org/10.1533/9781782420620.1.

McKenzie, H.A., Ralston, G.B., & Shaw, D.C. (1972). Location of sulfhydryl and disulfide groups in bovine -lactoglobulins and effects of urea. *Biochemistry*, 11(24), 4539–47. http://dx.doi.org/10.1021/bi00774a017.

Meinhardt, J., Sachse, C., Hortschansky, P., Grigorieff, N., & Fändrich, M. (2009). Abeta(1-40) fibril polymorphism implies diverse interaction patterns in amyloid fibrils. *J Mol Biol*, 386(3), 869–77. http://dx.doi.org/10.1016/j.jmb.2008.11.005.

Mercadante, D., Melton, L.D., Norris, G.E., Loo, T.S., Williams, M.A.K., & Dobson, R.C.J., et al. (2012). Bovine β-lactoglobulin is dimeric under imitative physiological conditions. *Biophys J*, 103(2), 303–12. http://dx.doi.org/10.1016/j.bpj.2012.05.041.

Messens, W., van Camp, J., & Huyghebaert, A. (1997). The use of high pressure to modify the functionality of food proteins. *Trends in Food Science & Technology*, 8(4), 107–12. http://dx.doi.org/10.1016/S0924-2244(97)01015-7.

Mills, O.E. (1976). Effect of temperature on tryptophan fluorescence of β-lactoglobulin B. *Biochimica et Biophysica Acta (BBA) - Protein Structure*, 434(2), 324–32. http://dx.doi.org/10.1016/0005-2795(76)90224-5.

Mohammadian, M., & Madadlou, A. (2016). Cold-set hydrogels made of whey protein nanofibrils with different divalent cations. *International Journal of Biological Macromolecules*, 89, 499–506. http://dx.doi.org/10.1016/j.ijbiomac.2016.05.009.

Molinari, H., Ragona, L., Varani, L., Musco, G., Consonni, R., & Zetta, L., et al. (1996). Partially folded structure of monomeric bovine β-lactoglobulin. *FEBS Lett*, 381(3), 237–43. http://dx.doi.org/10.1016/0014-5793(96)00100-7.

Morinaga, A., Hasegawa, K., Nomura, R., Ookoshi, T., Ozawa, D., & Goto, Y., et al. (2010). Critical role of interfaces and agitation on the nucleation of Abeta amyloid fibrils at low concentrations of Abeta monomers. *Biochim Biophys Acta*, 1804(4), 986–95. http://dx.doi.org/10.1016/j.bbapap.2010.01.012.

Moro, A., Báez, G.D., Ballerini, G.A., Busti, P.A., & Delorenzi, N.J. (2013). Emulsifying and foaming properties of β-lactoglobulin modified by heat treatment. *Food Research International*, 51(1), 1–7. http://dx.doi.org/10.1016/j.foodres.2012.11.011.

Morozova-Roche, L.A., Zurdo, J., Spencer, A., Noppe, W., Receveur, V., & Archer, D.B., et al. (2000). Amyloid fibril formation and seeding by wild-type human lysozyme and its disease-related mutational variants. *J Struct Biol*, 130(2-3), 339–51. http://dx.doi.org/10.1006/jsbi.2000.4264.

Mudgal, P., Daubert, C.R., Clare, D.A., & Foegeding, E.A. (2011a). Effect of disulfide interactions and hydrolysis on the thermal aggregation of β-lactoglobulin. *J Agric Food Chem*, 59(5), 1491–7. http://dx.doi.org/10.1021/jf101893v.

Mudgal, P., Daubert, C.R., & Foegeding, E.A. (2011b). Effects of protein concentration and CaCl2 on cold-set thickening mechanism of β-lactoglobulin at low pH. *International Dairy Journal*, 21(5), 319–26. http://dx.doi.org/10.1016/j.idairyj.2010.11.014.

Munialo, C.D., Martin, A.H., van der Linden, E., & Jongh, H.H.J. de (2014). Fibril formation from pea protein and subsequent gel formation. *J Agric Food Chem*, 62(11), 2418–27. http://dx.doi.org/10.1021/jf4055215.

Murzin, A.G., Brenner, S.E., Hubbard, T., & Chothia, C. (1995). SCOP. *J Mol Biol*, 247(4), 536–40. http://dx.doi.org/10.1006/jmbi.1995.0159.

Nelson, R., Sawaya, M.R., Balbirnie, M., Madsen, A.Ø., Riekel, C., & Grothe, R., et al. (2005). Structure of the cross-beta spine of amyloid-like fibrils. *Nature*, 435(7043), 773–8. http://dx.doi.org/10.1038/nature03680.

Ng, S.K., Nyam, K.L., Nehdi, I.A., Chong, G.H., Lai, O.M., & Tan, C.P. (2016). Impact of stirring speed on β-lactoglobulin fibril formation. *Food Sci Biotechnol*, 25(S1), 15–21. http://dx.doi.org/10.1007/s10068-016-0093-8.

Ngarize, S., Herman, H., Adams, A., & Howell, N. (2004). Comparison of changes in the secondary structure of unheated, heated, and high-pressure-treated beta-lactoglobulin and ovalbumin proteins using Fourier transform raman spectroscopy and self-deconvolution. *J Agric Food Chem*, 52(21), 6470–7. http://dx.doi.org/10.1021/jf030649y.

Nicolai, T., Britten, M., & Schmitt, C. (2011). β-Lactoglobulin and WPI aggregates. *Food Hydrocolloids*, 25(8), 1945–62. http://dx.doi.org/10.1016/j.foodhyd.2011.02.006.

Nicolai, T., & Durand, D. (2013). Controlled food protein aggregation for new functionality. *Current Opinion in Colloid & Interface Science*, 18(4), 249–56. http://dx.doi.org/10.1016/j.cocis.2013.03.001.

Norby, J. (2000). The origin and the meaning of the little p in pH. *Trends in Biochemical Sciences*, 25(1), 36–7. http://dx.doi.org/10.1016/S0968-0004(99)01517-0.

Oboroceanu, D., Wang, L., Kroes-Nijboer, A., Brodkorb, A., Venema, P., & Magner, E., et al. (2011). The effect of high pressure microfluidization on the structure and length distribution of whey protein fibrils. *International Dairy Journal*, 21(10), 823–30. http://dx.doi.org/10.1016/j.idairyj.2011.03.015.

Oboroceanu, D., Wang, L., Magner, E., & Auty, M.A.E. (2014). Fibrillization of whey proteins improves foaming capacity and foam stability at low protein concentrations. *Journal of Food Engineering*, 121, 102–11. http://dx.doi.org/10.1016/j.jfoodeng.2013.08.023.

Ohhashi, Y., Kihara, M., Naiki, H., & Goto, Y. (2005). Ultra-sonication-induced amyloid fibril formation of beta2-microglobulin. *the journal of biological chemistry*, 280(38), 32843–8. http://dx.doi.org/10.1074/jbc.M506501200.

Pan, K., & Zhong, Q. (2015). Amyloid-like fibrils formed from intrinsically disordered caseins. *Soft Matter*, 11(29), 5898–904. http://dx.doi.org/10.1039/c5sm01037c.

Patel, H.A., Singh, H., Havea, P., Considine, T., & Creamer, L.K. (2005). Pressure-induced unfolding and aggregation of the proteins in whey protein concentrate solutions. *J Agric Food Chem*, 53(24), 9590–601. http://dx.doi.org/10.1021/jf0508403.

Patterson, J.R., Polinski, N.K., Duffy, M.F., Kemp, C.J., Luk, K.C., & Volpicelli-Daley, L.A., et al. (2019). Generation of Alpha-Synuclein Preformed Fibrils from Monomers and Use In Vivo. *J Vis Exp*(148). http://dx.doi.org/10.3791/59758.

Paul EL, Atiemo-Obeng VA, Kresta SM. Handbook of industrial mixing. Hoboken N.J.: Wiley-Interscience 2004. lxi, 1377.

Pearce, F.G., Mackintosh, S.H., & Gerrard, J.A. (2007). Formation of amyloid-like fibrils by ovalbumin and related proteins under conditions relevant to food processing. *J Agric Food Chem*, 55(2), 318–22. http://dx.doi.org/10.1021/jf062154p.

Pedersen, J.S., Andersen, C.B., & Otzen, D.E. (2010). Amyloid structure--one but not the same. *FEBS J*, 277(22), 4591–601. http://dx.doi.org/10.1111/j.1742-4658.2010.07888.x.

Pedersen, J.S., Dikov, D., Flink, J.L., Hjuler, H.A., Christiansen, G., & Otzen, D.E. (2006). The changing face of glucagon fibrillation. *J Mol Biol*, 355(3), 501–23. http://dx.doi.org/10.1016/j.jmb.2005.09.100.

Peng, D., Yang, J., Li, J., Tang, C., & Li, B. (2017). Foams Stabilized by β-Lactoglobulin Amyloid Fibrils. *J Agric Food Chem*, 65(48), 10658–65. http://dx.doi.org/10.1021/acs.jafc.7b03669.

Pepys, M.B. (2006). Amyloidosis. *Annu Rev Med*, 57, 223–41. http://dx.doi.org/10.1146/annurev.med.57.121304.131243.

Pronchik, J., He, X., Giurleo, J.T., & Talaga, D.S. (2010). In vitro formation of amyloid from alpha-synuclein is dominated by reactions at hydrophobic interfaces. *J Am Chem Soc*, 132(28), 9797–803. http://dx.doi.org/10.1021/ja102896h.

Qi, X.L., Brownlow, S., Holt, C., & Sellers, P. (1995). Thermal denaturation of β-lactoglobulin. *Biochimica et Biophysica Acta (BBA) - Protein Structure and Molecular Enzymology*, 1248(1), 43–9. http://dx.doi.org/10.1016/0167-4838(94)00225-6.

Qi, X.L., Holt, C., McNulty, D., Clarke, D.T., Brownlow, S., & Jones, G.R. (1997). Effect of temperature on the secondary structure of beta-lactoglobulin at pH 6.7, as determined by CD and IR spectroscopy. *Biochem. J.*, 324 (Pt 1), 341–6. http://dx.doi.org/10.1042/bj3240341.

Qin, B.Y., Bewley, M.C., Creamer, L.K., Baker, H.M., Baker, E.N., & Jameson, G.B. (1998). Structural basis of the Tanford transition of bovine beta-lactoglobulin. *Biochemistry*, 37(40), 14014–23. http://dx.doi.org/10.1021/bi981016t.

Radovan, D., Smirnovas, V., & Winter, R. (2008). Effect of pressure on islet amyloid polypeptide aggregation. *Biochemistry*, 47(24), 6352–60. http://dx.doi.org/10.1021/bi800503j.

Rahaman, T., Vasiljevic, T., & Ramchandran, L. (2015). Conformational changes of β-lactoglobulin induced by shear, heat, and pH-Effects on antigenicity. *J Dairy Sci*, 98(7), 4255–65. http://dx.doi.org/10.3168/jds.2014-9010.

Renard, D., Lefebvre, J., Griffin, M.C.A., & Griffin, W.G. (1998). Effects of pH and salt environment on the association of β-lactoglobulin revealed by intrinsic fluorescence studies. *International Journal of Biological Macromolecules*, 22(1), 41–9. http://dx.doi.org/10.1016/S0141-8130(97)00086-X.

Reynolds, N.P., Adamcik, J., Berryman, J.T., Handschin, S., Zanjani, A.A.H., & Li, W., et al. (2017). Competition between crystal and fibril formation in molecular mutations of amyloidogenic peptides. *Nat Commun*, 8(1), 1338. http://dx.doi.org/10.1038/s41467-017-01424-4.

Riek, R., & Eisenberg, D.S. (2016). The activities of amyloids from a structural perspective. *Nature*, 539(7628), 227–35. http://dx.doi.org/10.1038/nature20416.

Rogers, S.S., Venema, P., Sagis, L.M.C., van der Linden, E., & Donald, A.M. (2005). Measuring the Length Distribution of a Fibril System. *Macromolecules*, 38(7), 2948–58. http://dx.doi.org/10.1021/ma0474224.

Rühs, P.A., Scheuble, N., Windhab, E.J., Mezzenga, R., & Fischer, P. (2012). Simultaneous control of pH and ionic strength during interfacial rheology of β-lactoglobulin fibrils adsorbed at liquid/liquid Interfaces. *Langmuir*, 28(34), 12536–43. http://dx.doi.org/10.1021/la3026705.

Rytkönen J. Effect of heat denaturation of bovine milk beta-lactoglobulin on its epithelial transport and allergenicity. Oulu: University of Oulu 2006. 67, [33] s.

Saelices, L., Chung, K., Lee, J.H., Cohn, W., Whitelegge, J.P., & Benson, M.D., et al. (2018). Amyloid seeding of transthyretin by ex vivo cardiac fibrils and its inhibition. *Proc Natl Acad Sci U S A*, 115(29), E6741-E6750. http://dx.doi.org/10.1073/pnas.1805131115.

Sakurai, K., & Goto, Y. (2002). Manipulating monomer-dimer equilibrium of bovine Beta - lactoglobulin by amino acid substitution. *the journal of biological chemistry*, 277(28), 25735–40. http://dx.doi.org/10.1074/jbc.M203659200.

Sakurai, K., Konuma, T., Yagi, M., & Goto, Y. (2009). Structural dynamics and folding of beta-lactoglobulin probed by heteronuclear NMR. *Biochim Biophys Acta*, 1790(6), 527–37. http://dx.doi.org/10.1016/j.bbagen.2009.04.003.

Sasso, L., Suei, S., Domigan, L., Healy, J., Nock, V., & Williams, M.A.K., et al. (2014). Versatile multi-functionalization of protein nanofibrils for biosensor applications. *Nanoscale*, 6(3), 1629–34. http://dx.doi.org/10.1039/c3nr05752f.

Sawyer, L., & Kontopidis, G. (2000). The core lipocalin, bovine β-lactoglobulin. *Biochimica et Biophysica Acta (BBA) - Protein Structure and Molecular Enzymology*, 1482(1-2), 136–48. http://dx.doi.org/10.1016/S0167-4838(00)00160-6.

Sawyer, W.H., Norton, R.S., Nichol, L.W., & McKenzie, G.H. (1971). Thermodenaturation of bovine β-lactoglobulin. *Biochimica et Biophysica Acta (BBA) - Protein Structure*, 243(1), 19–30. http://dx.doi.org/10.1016/0005-2795(71)90032-8.

Scherpelz, K.P., Lu, J.-X., Tycko, R., & Meredith, S.C. (2016). Preparation of Amyloid Fibrils Seeded from Brain and Meninges. *Methods Mol Biol*, 1345, 299–312. http://dx.doi.org/10.1007/978-1-4939-2978-8_20.

Schokker, E.P., Singh, H., Pinder, D.N., & Creamer, L.K. (2000). Heat-induced aggregation of β-lactoglobulin AB at pH 2.5 as influenced by ionic strength and protein concentration. *International Dairy Journal*, 10(4), 233–40. http://dx.doi.org/10.1016/S0958-6946(00)00047-9.

Schokker, E.P., Singh, H., Pinder, D.N., Norris, G.E., & Creamer, L.K. (1999). Characterization of intermediates formed during heat-induced aggregation of -lactoglobulin AB at neutral pH. *International Dairy Journal*, 9(11), 791–800. http://dx.doi.org/10.1016/S0958-6946(99)00148-X.

Schrader, M., Pommerehne, K., Wolf, S., Finke, B., Schilde, C., & Kampen, I., et al. (2019). Design of a CFD-DEM-based method for mechanical stress calculation and its application to glass bead-enhanced cultivations of filamentous Lentzea aerocolonigenes. *Biochemical Engineering Journal*, 148, 116–30. http://dx.doi.org/10.1016/j.bej.2019.04.014.

Schultz, S., Wagner, G., Urban, K., & Ulrich, J. (2004). High-Pressure Homogenization as a Process for Emulsion Formation. *Chem. Eng. Technol.*, 27(4), 361–8. http://dx.doi.org/10.1002/ceat.200406111.

Seo, J.-A., Hédoux, A., Guinet, Y., Paccou, L., Affouard, F., & Lerbret, A., et al. (2010). Thermal denaturation of beta-lactoglobulin and stabilization mechanism by trehalose analysed from Raman spectroscopy investigations. *J Phys Chem B*, 114(19), 6675–84. http://dx.doi.org/10.1021/jp1006022.

Serfert, Y., Lamprecht, C., Tan, C.-P., Keppler, J.K., Appel, E., & Rossier-Miranda, F.J., et al. (2014). Characterisation and use of β-lactoglobulin fibrils for microencapsulation of lipophilic ingredients and oxidative stability thereof. *Journal of Food Engineering*, 143, 53–61. http://dx.doi.org/10.1016/j.jfoodeng.2014.06.026.

Shah, B.R., Maeno, A., Matsuo, H., Tachibana, H., & Akasaka, K. (2012). Pressure-accelerated dissociation of amyloid fibrils in wild-type hen lysozyme. *Biophys J*, 102(1), 121–6. http://dx.doi.org/10.1016/j.bpj.2011.10.041.

Sharma, R.K., Furusawa, K., Fukui, A., & Sasaki, N. (2014). Effects of a flow field on amyloid fibrillogenesis in a β-lactoglobulin solution. *International Journal of Biological Macromolecules*, 70, 490–7. http://dx.doi.org/10.1016/j.ijbiomac.2014.06.034.

Shezad, K., Zhang, K., Hussain, M., Dong, H., He, C., & Gong, X., et al. (2016). Surface Roughness Modulates Diffusion and Fibrillation of Amyloid-β Peptide. *Langmuir*, 32(32), 8238–44. http://dx.doi.org/10.1021/acs.langmuir.6b01756.

Simmons, M.J.H., Jayaraman, P., & Fryer, P.J. (2007). The effect of temperature and shear rate upon the aggregation of whey protein and its implications for milk fouling. *Journal of Food Engineering*, 79(2), 517–28. http://dx.doi.org/10.1016/j.jfoodeng.2006.02.013.

Sluzky, V., Tamada, J.A., Klibanov, A.M., & Langer, R. (1991). Kinetics of insulin aggregation in aqueous solutions upon agitation in the presence of hydrophobic surfaces. *Proceedings of the National Academy of Sciences*, 88(21), 9377–81. http://dx.doi.org/10.1073/pnas.88.21.9377.

Sneideris, T., Milto, K., & Smirnovas, V. (2015). Polymorphism of amyloid-like fibrils can be defined by the concentration of seeds. *PeerJ*, 3, e1207. http://dx.doi.org/10.7717/peerj.1207.

Spiegel, T., & Huss, M. (2002). Whey protein aggregation under shear conditions - effects of pH value and removal of calcium. *Int J Food Sci Tech*, 37(5), 559–68. http://dx.doi.org/10.1046/j.1365-2621.2002.00612.x.

Stanic-Vucinic, D., Stojadinovic, M., Atanaskovic-Markovic, M., Ognjenovic, J., Grönlund, H., & van Hage, M., et al. (2012). Structural changes and allergenic properties of β-lactoglobulin upon exposure to high-intensity ultrasound. *Mol Nutr Food Res*, 56(12), 1894–905. http://dx.doi.org/10.1002/mnfr.201200179.

Stapelfeldt, H., & Skibsted, L.H. (1999). Pressure denaturation and aggregation of beta-lactoglobulin studied by intrinsic fluorescence depolarization, Rayleigh scattering, radiationless energy transfer and hydrophobic fluoroprobing. *J Dairy Res*, 66(4), 545–58. http://dx.doi.org/10.1017/s0022029999003714.

Stathopulos, P.B., Scholz, G.A., Hwang, Y.-M., Rumfeldt, J.A.O., Lepock, J.R., & Meiering, E.M. (2004). Sonication of proteins causes formation of aggregates that resemble amyloid. *Protein Sci*, 13(11), 3017–27. http://dx.doi.org/10.1110/ps.04831804.

Sunde, M., Serpell, L.C., Bartlam, M., Fraser, P.E., Pepys, M.B., & Blake, C.C. (1997). Common core structure of amyloid fibrils by synchrotron X-ray diffraction. *J Mol Biol*, 273(3), 729–39. http://dx.doi.org/10.1006/jmbi.1997.1348.

Sutariya, S., Sunkesula, V., Kumar, R., Shah, K., & Yildiz, F. (2018). Emerging applications of Ultra-sonication and cavitation in dairy industry. *Cogent Food & Agriculture*, 4(1), 1083. http://dx.doi.org/10.1080/23311932.2018.1549187.

Tanford, C. (1997). How protein chemists learned about the hydrophobic factor. *Protein Sci*, 6(6), 1358–66. http://dx.doi.org/10.1002/pro.5560060627.

Tang, C.-H., & Wang, C.-S. (2010). Formation and characterization of amyloid-like fibrils from soy β-conglycinin and glycinin. *J Agric Food Chem*, 58(20), 11058–66. http://dx.doi.org/10.1021/jf1021658.

Taulier, N., & Chalikian, T.V. (2001). Characterization of pH-induced transitions of beta-lactoglobulin. *J Mol Biol*, 314(4), 873–89. http://dx.doi.org/10.1006/jmbi.2001.5188.

Thomas, L.H., Forsyth, V.T., Sturcová, A., Kennedy, C.J., May, R.P., & Altaner, C.M., et al. (2013). Structure of cellulose microfibrils in primary cell walls from collenchyma. *Plant Physiol*, 161(1), 465–76. http://dx.doi.org/10.1104/pp.112.206359.

Thorn, D.C., Ecroyd, H., Sunde, M., Poon, S., & Carver, J.A. (2008). Amyloid fibril formation by bovine milk alpha s2-casein occurs under physiological conditions yet is prevented by its natural counterpart, alpha s1-casein. *Biochemistry*, 47(12), 3926–36. http://dx.doi.org/10.1021/bi701278c.

Thorn, D.C., Meehan, S., Sunde, M., Rekas, A., Gras, S.L., & MacPhee, C.E., et al. (2005). Amyloid fibril formation by bovine milk kappa-casein and its inhibition by the molecular chaperones alphaS- and beta-casein. *Biochemistry*, 44(51), 17027–36. http://dx.doi.org/10.1021/bi051352r.

Townend, R., Weinberger, L., & Timasheff, S.N. (1960). Molecular Interactions in β-Lactoglobulin. IV. The Dissociation of β-Lactoglobulin below pH 3.5 2. *J Am Chem Soc*, 82(12), 3175–9. http://dx.doi.org/10.1021/ja01497a047.

Tsemekhman, K., Goldschmidt, L., Eisenberg, D., & Baker, D. (2007). Cooperative hydrogen bonding in amyloid formation. *Protein Sci*, 16(4), 761–4. http://dx.doi.org/10.1110/ps.062609607.

Usov, I., Adamcik, J., & Mezzenga, R. (2013). Polymorphism complexity and handedness inversion in serum albumin amyloid fibrils. *ACS Nano*, 7(12), 10465–74. http://dx.doi.org/10.1021/nn404886k.

Usov, I., & Mezzenga, R. (2014). Correlation between nanomechanics and polymorphic conformations in amyloid fibrils. *ACS Nano*, 8(11), 11035–41. http://dx.doi.org/10.1021/nn503530a.

Utomo, A., Baker, M., & Pacek, A.W. (2009). The effect of stator geometry on the flow pattern and energy dissipation rate in a rotor–stator mixer. *Chemical Engineering Research and Design*, 87(4), 533–42. http://dx.doi.org/10.1016/j.cherd.2008.12.011.

Utomo, A.T., Baker, M., & Pacek, A.W. (2008). Flow pattern, periodicity and energy dissipation in a batch rotor–stator mixer. *Chemical Engineering Research and Design*, 86(12), 1397–409. http://dx.doi.org/10.1016/j.cherd.2008.07.012.

Valiente-Gabioud, A.A., Torres-Monserrat, V., Molina-Rubino, L., Binolfi, A., Griesinger, C., & Fernández, C.O. (2012). Structural basis behind the interaction of Zn^{2+} with the protein α-synuclein and the Aβ peptide. *J Inorg Biochem*, 117, 334–41. http://dx.doi.org/10.1016/j.jinorgbio.2012.06.011.

van der Linden, E., & Venema, P. (2007). Self-assembly and aggregation of proteins. *Current Opinion in Colloid & Interface Science*, 12(4-5), 158–65. http://dx.doi.org/10.1016/j.cocis.2007.07.010.

van Eldik, R., Asano, T., & Le Noble, W.J. (1989). Activation and reaction volumes in solution. 2. *Chem. Rev.*, 89(3), 549–688. http://dx.doi.org/10.1021/cr00093a005.

vandenAkker, C.C., Engel, M.F.M., Velikov, K.P., Bonn, M., & Koenderink, G.H. (2011). Morphology and persistence length of amyloid fibrils are correlated to peptide molecular structure. *J Am Chem Soc*, 133(45), 18030–3. http://dx.doi.org/10.1021/ja206513r.

Verheul, M., Pedersen, J.S., Roefs, S.P.F.M., & Kruif, K.G. de (1999). Association behavior of native ? *Biopolymers*, 49(1), 11–20. http://dx.doi.org/10.1002/(SICI)1097-0282(199901)49:1<11::AID-BIP2>3.0.CO;2-1.

Wada, R., Fujita, Y., & Kitabatake, N. (2006). Effects of heating at neutral and acid pH on the structure of beta-lactoglobulin A revealed by differential scanning calorimetry and circular dichroism spectroscopy. *Biochim Biophys Acta*, 1760(6), 841–7. http://dx.doi.org/10.1016/j.bbagen.2005.12.025.

Wälti, M.A., Ravotti, F., Arai, H., Glabe, C.G., Wall, J.S., & Böckmann, A., et al. (2016). Atomic-resolution structure of a disease-relevant Aβ(1-42) amyloid fibril. *Proc Natl Acad Sci U S A*, 113(34), E4976-84. http://dx.doi.org/10.1073/pnas.1600749113.

Wang, W., Nema, S., & Teagarden, D. (2010). Protein aggregation--pathways and influencing factors. *Int J Pharm*, 390(2), 89–99. http://dx.doi.org/10.1016/j.ijpharm.2010.02.025.

Wei, G., Su, Z., Reynolds, N.P., Arosio, P., Hamley, I.W., & Gazit, E., et al. (2017). Self-assembling peptide and protein amyloids. *Chem Soc Rev*, 46(15), 4661–708. http://dx.doi.org/10.1039/c6cs00542j.

Wei, Z., & Huang, Q. (2019). Assembly of iron-bound ovotransferrin amyloid fibrils. *Food Hydrocolloids*, 89, 579–89. http://dx.doi.org/10.1016/j.foodhyd.2018.11.028.

Wilde, S.C., Treitz, C., Keppler, J.K., Koudelka, T., Palani, K., & Tholey, A., et al. (2016). β-Lactoglobulin as nanotransporter--Part II. *Food Chem*, 197(Pt A), 1022–9. http://dx.doi.org/10.1016/j.foodchem.2015.11.011.

Wit, J.N. de (2009). Thermal behaviour of bovine β-lactoglobulin at temperatures up to 150°C. a review. *Trends in Food Science & Technology*, 20(1), 27–34. http://dx.doi.org/10.1016/j.tifs.2008.09.012.

Wong, D.W., Camirand, W.M., & Pavlath, A.E. (1996). Structures and functionalities of milk proteins. *Crit Rev Food Sci Nutr*, 36(8), 807–44. http://dx.doi.org/10.1080/10408399609527751.

Xiong, Y.L., Dawson, K.A., & Wan, L. (1993). Thermal Aggregation of β-Lactoglobulin. *J Dairy Sci*, 76(1), 70–7. http://dx.doi.org/10.3168/jds.S0022-0302(93)77324-5.

Yan, Y., Seeman, D., Zheng, B., Kizilay, E., Xu, Y., & Dubin, P.L. (2013). pH-Dependent aggregation and disaggregation of native β-lactoglobulin in low salt. *Langmuir*, 29(14), 4584–93. http://dx.doi.org/10.1021/la400258r.

Yang, F., Zhang, M., Zhou, B.-R., Chen, J., & Liang, Y. (2006). Oleic acid inhibits amyloid formation of the intermediate of alpha-lactalbumin at moderately acidic pH. *J Mol Biol*, 362(4), 821–34. http://dx.doi.org/10.1016/j.jmb.2006.07.059.

Yang, X., Williams, J.K., Yan, R., Mouradian, M.M., & Baum, J. (2019). Increased Dynamics of α-Synuclein Fibrils by β-Synuclein Leads to Reduced Seeding and Cytotoxicity. *Sci Rep*, 9(1), 17579. http://dx.doi.org/10.1038/s41598-019-54063-8.

Ye, X., Hedenqvist, M.S., Langton, M., & Lendel, C. (2018). On the role of peptide hydrolysis for fibrillation kinetics and amyloid fibril morphology. *RSC Adv.*, 8(13), 6915–24. http://dx.doi.org/10.1039/C7RA10981D.

Zahn, D. (2004). On the Role of Water in Amide Hydrolysis. *Eur. J. Org. Chem.*, 2004(19), 4020–3. http://dx.doi.org/10.1002/ejoc.200400316.

Zhang, Y.-H., & Huang, L.-H. (2014). Effect of heat-induced formation of rice bran protein fibrils on morphological structure and physico-chemical properties in solutions and gels. *Food Sci Biotechnol*, 23(5), 1417–23. http://dx.doi.org/10.1007/s10068-014-0194-1.

Zhong, J.Z., Liu, W., Liu, C.M., Wang, Q.H., Li, T., & Tu, Z.C., et al. (2012). Aggregation and conformational changes of bovine β-lactoglobulin subjected to dynamic high-pressure microfluidization in relation to antigenicity. *J Dairy Sci*, 95(8), 4237–45. http://dx.doi.org/10.3168/jds.2012-5333.

3. Manuscript 1 – Structure and physico-chemical properties of amyloid and amyloid-like aggregates

Influence of the polydispersity of pH 2 and pH 3.5 beta-lactoglobulin amyloid fibril solutions on analytical methods

Timon R. Heyn[1]*, Vasil M. Garamus[2], Hendrikje R. Neumann[3], Maximilian J. Uttinger[4], Tobias Guckeisen[4], Monique Heuer[1], Christine Selhuber-Unkel[3], Wolfgang Peukert[4], Julia K. Keppler[1,5]

Published previously in European Polymer Journal (2019): Heyn, Timon R.; Garamus, Vasil M.; Neumann, Hendrikje R.; Uttinger, Maximilian J.; Guckeisen, Tobias; Heuer, Monique et al. (2019): Influence of the polydispersity of pH 2 and pH 3.5 beta-lactoglobulin amyloid fibril solutions on analytical methods. DOI: 10.1016/j.eurpolymj.2019.08.038.

[1]Institute of Human Nutrition and Food Science, Division of Food Technology, Kiel University, 24118 Kiel, Germany

[2]Helmholtz-Zentrum Geesthacht, Centre for Materials and Coastal Research, 21502 Geesthacht, Germany

[3]Institute of Materials Science, Department for Biocompatible Nanomaterials, Kiel University, 24143 Kiel, Germany

[4]Institute of Particle Technology, Interdisciplinary Center for Functional Particle Systems, Friedrich-Alexander-Universität Erlangen-Nürnberg, Erlangen, Germany;

[5] Laboratory of Food Process Engineering, Wageningen University, Wageningen, The Netherlands

3.1. Abstract

It is well known that amyloid beta-lactoglobulin (BLG) fibril solutions contain a heterogeneous mixture of amyloid aggregates and non-amyloid material. However, few information are available on how strongly separated fractions of different morphologies (straight fibrils at pH 2 and worm-like aggregates at pH 3.5) vary with respect to physico-chemical properties and building blocks as most analyses are conducted with unfractionated solutions where superposition effects occur.

The pH value shift resulted in an altered degree of acid hydrolysis which led to dissimilar building blocks of the aggregates (peptides at pH 2, non-hydrolysed protein at pH 3.5). The respective separated amyloid and non-amyloid fractions showed significantly different size (SAXS, SEC, AUC) and charge properties (Zeta-potential) than the whole samples. Strong superposition effects were evident with common analyses such as FTIR, TRP fluorescence and Thioflavin-T. At the same time, structural differences of pH 2 and pH 3.5 aggregates could be presented more clearly.

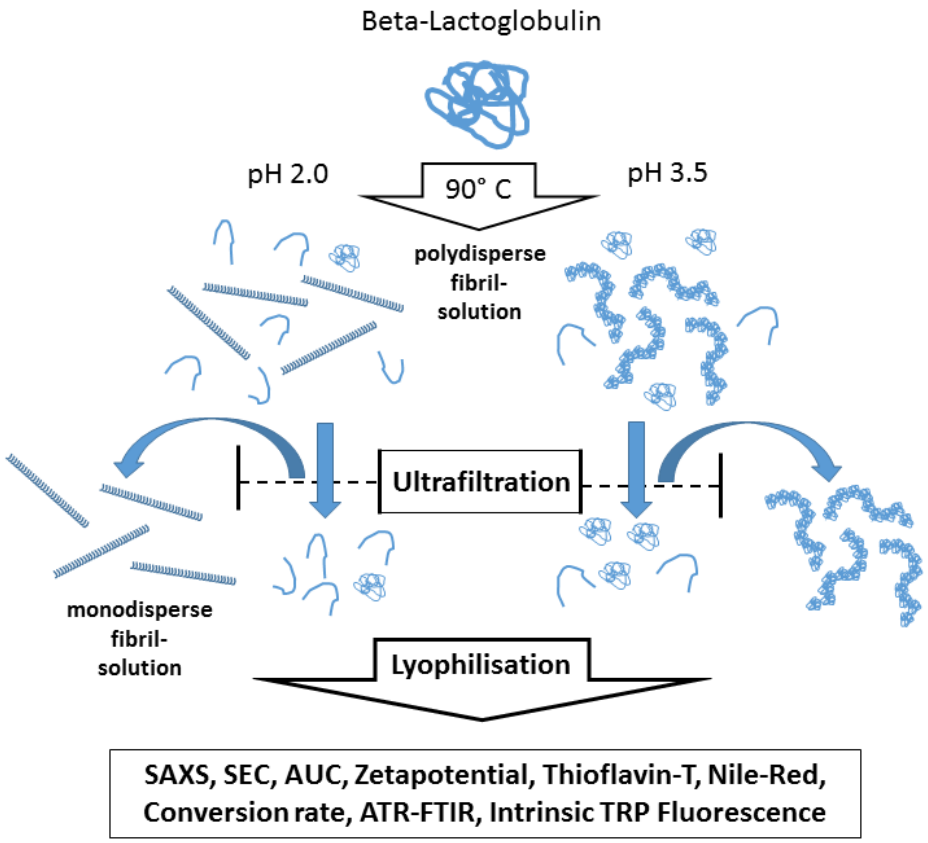

Abbreviations

BLG, beta-lactoglobulin

LBLG, lyophilised beta-lactoglobulin

HS, heated solution

LHS, lyophilised heated solution

LR, lyophilised retentate

LF, lyophilised filtrate

DBLG, dissociated beta-lactoglobulin

DLBLG, dissociated lyophilised beta-lactoglobulin

DHS, dissociated heated solution

DLHS, dissociated lyophilised heated solution

DLR, dissociated lyophilised retentate

DLF, dissociated lyophilised filtrate

DTT, dithiothreitol,

TRP, tryptophan,

3.2. Introduction

Amyloids are ordered β-sheet structures that are commonly associated with diseases such as Parkinsons's, Alzheimer's and diabetes mellitus. Some amyloid structures, however, are also non-toxic building blocks found naturally in biofilms or for hormone storage and nitrogen catabolism (Knowles and Mezzenga 2016). In the recent past, interest in the physico-chemical and functional properties of amyloid aggregates made from whey protein beta-lactoglobulin (BLG) has been growing. Apart from typical food applications, such as foaming (Oboroceanu et al. 2010), gelation (Loveday et al. 2017) and emulsification (Serfert et al. 2014), BLG fibrils were also applied as biosensors, hybrids and nanocomposites in biomaterials (Knowles and Mezzenga 2016; Humblet-Hua et al. 2012; Mohammadian and Madadlou 2018).

BLG can form long fibrillary amyloid aggregates by applying high temperature (~90 °C) at low pH values (~pH 2) and low ionic strength during an incubation time of several hours (Loveday et al. 2017; Adamcik et al. 2010). However, at pH values near to the isoelectric point (pI), amyloid worm-like aggregates occur (Jung et al. 2008; Mudgal et al. 2009; Serfert et al. 2014).

Various pathways for amyloid association have been proposed so far (Oboroceanu et al. 2010), of which the peptide model (Akkermans et al. 2008; Lara et al. 2011) is the more widely accepted way. Here, BLG is suggested to be subjected to temperature-induced denaturation and simultaneous to acid hydrolysis. The emerging peptides reassemble and form stacked beta-sheet structures (amyloids). Various methods showed that there is no complete conversion of BLG to fibrils (Jung et al. 2008; Akkermans et al. 2008; Serfert et al. 2014). Following this, not only amyloid aggregates are present in the final sample, but also non-amyloid or non-aggregated material.

While the straight fibrils, that develop at pH values below 3 are very well investigated, the worm-like amyloid aggregates at pH 3.5 are less well characterized. Worm-like structures also occurr at pH values > pI (Nicolai et al. 2011; Jung et al. 2008), but the pH value of 3.5 offers a good possibility to compare them with straight fibrils due to the similar processing factors (same ion- and protein concentration, positive zeta-potential). Some previous studies suggested that at pH 3.5, "intact" non-hydrolyzed BLG assembles instead of peptides (Nicolai and Durand 2013; Loveday et al. 2017), which indicates an altered component mixture of amyloid aggregates and non-amyloid material.

In addition, a different component mixture between the incubated samples of straight fibrils at pH 2 and of worm-like aggregates at pH 3.5 is also likely. It is yet unclear how strongly this

would affect the physico-chemical properties (zeta-potential, building-block size, hydrophobicity) of each of the separated fractions as most analyses are conducted with unfractionized solutions, where superposition effects occur.

Thus, the building blocks of pH 2 and pH 3.5 amyloids and their separated fractions (retentate: mostly amyloid and filtrate: non-amyloid) were assessed in the present study, followed by an investigation of their respective physico-chemical properties as well as how they affect various common analysis methods. The different amyloid morphologies were briefly illustrated using atomic force microscopy (AFM) and small angle X-ray scattering (SAXS) and then an analysis of the composition of the aggregates and protein solutions using size exclusion chromatography (SEC) and analytical ultracentrifugation (AUC) was performed. Afterwards, several methods (Thioflavin-T test, Nile red assay, infrared spectroscopy, tryptophan fluorescence) for the separated and unseparated solutions were applied.

The analysis of separated samples provides an even clearer picture of the structure and physico-chemical properties of amyloid aggregates and their respective non-aggregated part. The results will also give an indication on the possible functionality of the separated fractions in the aggregate solutions at pH 2 or pH 3.5 in order to elucidate their role in future applications.

3.3. Materials and Methods

3.3.1. Materials

BLG was obtained from *Davisco Foods International, Inc* (Eden Prairie, USA) with 97 % protein and 96 % BLG in dry matter. Calculated NaCl content was 0.0496 mmol/g protein. Thioflavin-T (ThT >95 %) was obtained from *EMD Chemicals Inc*. Guanidine hydrochloride (GHCl ≥99.5%) was obtained from *Carl Roth GmbH&Co. KG* and 1,4-dithiothreitol (DTT ≥ 99 %) originated from *Sigma Aldrich Inc*. All other chemicals were of analytical grade and obtained from *Sigma Aldrich Inc*. All experiments were conducted with ultra pure water (>17 MΩ; total oxidizable carbon < 5ppb).

3.3.2. Amyloid aggregate preparation and characterization

3.3.2.1. Preparation of BLG solutions and production of amyloid aggregates

BLG-fibril solutions were prepared as described by Keppler et al. (Keppler et al. 2019): Protein solutions were predissolved, adjusted to the desired pH value of 2.0 or 3.5, using 6 M and 1 M HCl and then diluted to a final protein concentration of 2.5 wt% BLG. For fibril preparation, 40 ml solutions were put into Schott glasses with closed screw caps (125 ml max volume, fill level 19 mm). The samples were heated in a water bath at 90° C for 5 h under continuous stirring at 350 rpm, using a waterproof magnetic stirrer (*2mag MIXdrive 6HT, 2mag AG, Munich, Germany*) and uniform stir bars of 3.22 ± 0.02 mm diameters. This sample is denoted as heated sample (HS). The pH-adjusted native BLG and HS were lyophilised to obtain lyophilised beta-lactoglobulin (LBLG) and lyophilised heated sample (LHS).

3.3.2.2. Purification of aggregated and non-aggregated material by ultrafiltration

20 ml of the HS obtained after 5 hours were diluted 5-fold and placed in ultrafiltration units (UF tubes) *(Vivaspin 20, PES, Sartorius AG, Germany)* with a nominal molecular weight cutoff of 300 kDa. The UF tubes were centrifuged for 30 min at 1000*g until 5ml of concentrated retentate remained. The retentate and filtrate were frozen seperately overnight at -18 °C and then lyophilised (lyophilised retentate (LR) and lyophilised filtrate (LF)). Their purity and morphology was controlled by AFM (see below).

3.3.2.3. Determination of protein concentration in amyloid aggregates

The protein solutions were diluted to 0.1 wt % using ultra-pure water set to the respective pH value and protein concentration was determined by measuring the absorbance at 278 nm in a in a Genysis 10S UV-VIS spectrometer (*ThermoFisher Scientific, United States*). Protein quantification was done by using a calibration with native BLG between 1 and 0.01 mg/ml protein (limit of detection 0.016 mg/ml; limit of quantitation 0.054mg/ml according to DIN 32645).

3.3.2.4. Characterization of the morphology

Atomic Force Microscopy (AFM)
Fibril morphology was investigated using AFM (*NanoWizard 3, JPK Instruments AG, Berlin, Deutschland*) following the preparation protocol of Serfert et al. (Serfert et al. 2014) and Adamcik et al. (Adamcik et al. 2010). For tapping mode, ACTA-Cantilevers (spring constant 40 N/m, resonance frequency 300 kHz; *Applied Nano-Structures, Inc., Mountain View, USA*) were used at a scan rate of 0.5 Hz.

Small angle X-ray scattering (SAXS)
SAXS experiments were performed at the BioSAXS Beamline P12 at PETRA III (*EMBL/DESY, Hamburg, Germany*). The energy of the X-ray beam was 10 keV and the beam size 0.1 mm (V) x 0.2 mm (H). The sample to detector distance was 3.1 m and the q-range 0.03 – 4 nm^{-1}. Scattering patterns were measured using Pilatus 2 M pixel detector. The protein samples were diluted to 0.5 and 0.25 wt%. Separated samples (retentate and filtrate) were only ultra-filtrated but not lyophilised. In order to reduce the risk of radiation damage the sample was moved slightly during the exposure. For each measurement, 20 diffraction patterns were recorded, originating from the same sample volume, using an exposure time of 0.045 s per frame. The background-corrected SAXS data were used to calculate one-dimensional scattering curves by angular averaging. The data were corrected for the transmitted beam. In order to verify that no artefacts had occurred as a result of radiation damage, all scattering curves for a recorded dataset were compared to a reference curve (typically the first exposure) before being integrated using an automated acquisition and analysis program (Franke et al. 2012). The range of the reciprocal space vector q was calibrated using diffraction patterns of silver behenate (Blanton et al. 2000). Further details regarding fitting procedure are shown in the **supplementary material chapter 3.8**.

3.3.2.5. Methods to determine amyloid building blocks

Size exclusion chromatography (SEC)

For SEC analysis, the samples BLG, LBLG, HS, LHS, LR and LF were dissociated according to a method described by (Akkermans et al. 2008). *Dissociated beta-lactoglobulin (DBLG), Dissociated lyophilised beta-lactoglobulin (DLBLG), Dissociated heated sample (DHS), Dissociated lyophilised heated sample (DLHS), Dissociated lyophilised filtrate (DLF) and Dissociated lyophilised retentate (DLR)* were obtained.

SEC was conducted using an Agilent 1100 HPLC equipped with a diode array detector set to 205 nm, 214 nm, 278 nm and 280 nm and a Superdex^{TM} 200 increase 10/300 GL column, kindly provided from *GE Healthcare* (*Bio-Sciences AB, Uppsala, Sweden*). The eluent was 0.15 M Tris-HCL buffer pH 8. The flow rate was 0.3 ml/min. Sample injection volume was 50 µl. The column was run at 25 °C. Calibration was conducted for molecular weights between 6,500 and 75,000 Da.

Analytical Ultracentrifugation (AUC)

Prior to the measurements via AUC, the samples were prepared by diluting with ultrapure water at the respective pH and a stock solution of 1 M NaCl. The final samples contained 0.5 g/L, 1.0 g/L and 1.5 g/L of protein and 100 mM NaCl in order to ensure a well-defined optical signal. The pH of the final solution was checked and if necessary adjusted to 2.0 and 3.5 by adding small amounts of 6 M HCl. Afterwards, the protein concentration was controlled by measuring the optical signal of the samples at 280 nm and 290 nm.

A modified preparative centrifuge, type Optima L-90 K, available from *Beckman Coulter* with an integrated UV/visible multiwavelength detector has been used. For sedimentation velocity (SV) experiments, the rotor speed was set to 40,000 rpm. Sedimentation data were acquired for wavelengths between 280 nm and 294 nm. The buffer solution was taken as a reference when converting intensity data to absorbance. The temperature was set to 20° C throughout the measurements. Titanium centerpieces with an optical path length of 12 mm were used for all experiments. Further details of the applied multiwavelength can be found in literature (Walter and Peukert 2016). Data analysis of SV experiments was performed using the c(s) method implemented in SEDFIT (Version 15.01b) (Schuck and Rossmanith 2000).

3.3.2.6. Characterization and phyisco-chemical properties

Characterization of the surface charge by zeta-potential

Zeta-potential was measured via an electrophoretic mobility measurement (*Zetasizer Nano-ZS, Malvern Instruments GmbH,* Herrenberg, Germany) using the Smoluchowski model. The analysis was performed after protein solutions were diluted to 0.1 wt% protein with pH-adjusted water, using disposable capillary cells (*DTS1070*). Every measurement was repeated three times with 14 – 42 runs at 25° C after temperature equilibration for 60 sec. The refractive index of 1.45 for proteins was taken. The viscosity of the samples was assumed to be 0.88 cP (Keppler et al. 2015).

Colorimetric assays: Thioflavin-T and Nile-Red

The ThT assay was conducted as described by Serfert et al. (2014) and in the supplemental material.

Nile red assay was performed following a modified protocol of (Mishra et al. 2007): 2,7 ml of Nile red solution (50 µM Nile red dissolved in 25 mM HCl) was incubated with 300 µl sample containing 2,5 wt% protein or fibrils for one hour at room temperature. Afterwards the samples were measured in a fluorescence spectrometer (*Cary Eclipse, Varian GmbH Darmstadt, Germany*) by excitation of 530 nm and emission of 615 nm against a blank sample containing water instead of protein or fibrils.

Determination of the conversion rate by ultrafiltration

Conversion of BLG into amyloid aggregates was investigated by a modified protocol of the centrifugal filtration method described by Serfert et al. (Serfert et al. 2014). The unheated and the HS were diluted to 0.1 wt% protein with pH-adjusted water. 1 ml of the diluted protein solution was then centrifuged with centrifugal filter devices (*Vivaspin 2, PES, Sartorius AG, Germany*) at 193 *g for 15 min. Protein quantity from permeate of the heated samples was compared with the protein of the unfiltered samples and with the protein in permeate from unheated samples. Loss of protein was then declared as yield. In addition, the retentate and filtrate were tested by Thioflavin-T assay and AFM for remaining amyloid material.

Protein conformation by attenuated-total-reflection infrared-spectroscopy (ATR-FTIR)

Changes of the protein beta-sheet conformation were investigated with the Confocheck^{TM} , a specialized protein in solution FTIR System, using a Tensor 2 from *Bruker Optik GmbH, Ettlingen, Germany* fitted with a thermally controlled BioATR II Cell. Protein samples at pH 2 or pH 3.5 were diluted to 0.5 % protein concentration and 20 µl of the sample volume was pipetted onto the ATR crystal. The sample was equilibrated for several minutes to adapt to the target temperature which was set to 25 °C.

The spectra were acquired and averaged over 120 scans at a resolution of 0.7 cm^{-1}. After atmospheric correction for absorbance of CO_2 and H_2O as vapour and solute, respectively, the protein spectra from 4000 cm^{-1} to 900 cm^{-1} were vector-normalized. The amid I band (1590 – 1700 cm^{-1}) was cut out from the whole spectra. For 2nd derivation spectra the second derivation was calculated with 9 smoothing points.

Intrinsic tryptophan fluorescence
The protein solutions (samples taken during fibril production) were diluted to 0.01 wt% final protein concentration and the intrinsic tryptophan fluorescence was followed in a fluorescence spectrometer (*Cary Eclipse, Varian GmbH Darmstadt, Germany*) by excitation at 294 nm. An emission scan between 300 nm and 500 nm was taken to follow blue/red and intensity shifts.

3.3.3. Statistical analysis

Statistical analysis of the collected data was conducted by GraphPad PRISM (*version 6.07, GraphPad Software, San Diego, USA*). SAXS data were fitted with SAXSview (Doucet et al. 2017) SasView Version 4.1, Zenodo.

3.4. Results

3.4.1. Different Morphologies at pH 2 and pH 3.5 (AFM and SAXS)

The morphology of amyloid aggregates prepared at pH values 2 and 3.5 was analysed with AFM after 0.5, 1, 3 and 5 hours incubation. With increasing incubation time, increasing numbers of aggregates were evident **(FIG 3-1)** until the formation of a dense fibril network can be observed. The thickness of the pH 2 fibrils after 5 h was approximately 3 – 4 nm, the length was approximately 7 to >10 µm (no statistical determination of the fibril dimensions). The typical twisting periodic pitch along their contour length was observed for most of the strains (Adamcik and Mezzenga 2011; Serfert et al. 2014). Incubation at pH 3.5 for 0.5 h resulted in small point-like structures, which accumulate to worm-like morphologies within 3 h. The average height of the worm-like aggregates prepared at pH 3.5 after 5 h was approximately 1 – 3 nm and their length was 0.05 – 0.20 µm. Their shape was heterogenic, due to unsteady height and width variance along the contour length. Compared to pH 2 fibrils, these worm-like aggregates were rather isolated.

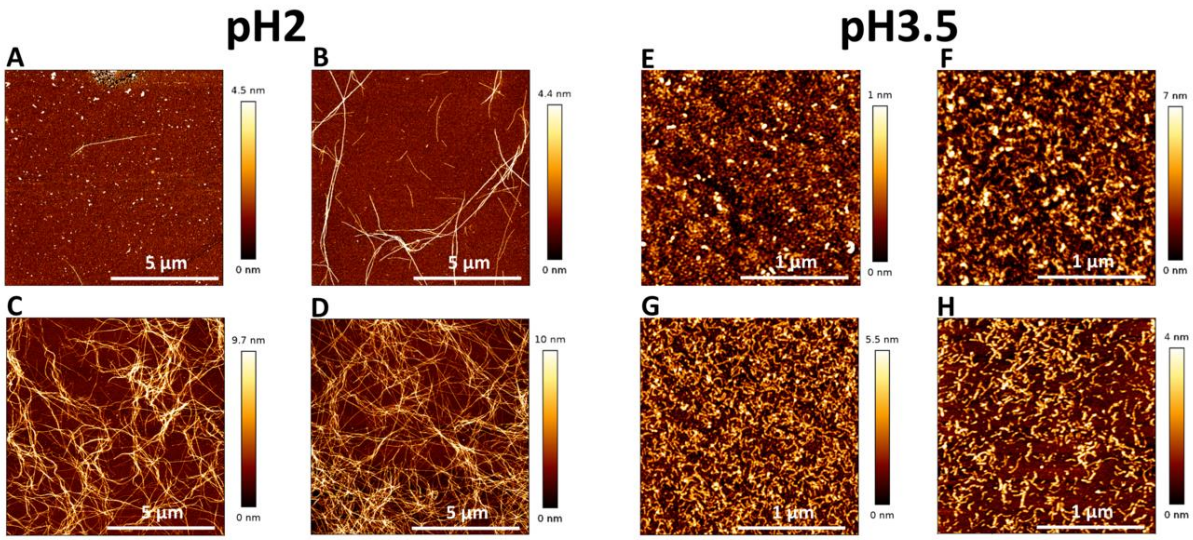

FIG 3-1 AFM images of pH 2 and pH 3.5 amyloid aggregates during the formation process after 0.5 (A+E), 1 (B+F), 3 (C+G) and 5 hours (D+H) at 90°C. In order to get a better impression of the morphology, the scale of the pH 2 AFM images was set to 5 µm, wheras it was 1 µm for the pH 3.5 aggregates.

SAXS model parameters determined at different time intervals of amyloid aggregation at pH 2 or 3.5 are given in **TAB 3-1**. They result from the analysis of the slopes of SAXS curves of pH 2 and pH 3.5 samples and also point towards the formation of fibrils *i.e.*, rod-like objects, which can be different in length, cross section parameters and flexibility. Details of the modelling are given in the **supplementary material chapter 3.8**

In agreement with the previous results, the obtained parameters in **TAB 3-1** indicate a different growth character for pH 2 and pH 3.5 amyloids. For a separated fibril fraction at pH 2, a flexible model gives the best fit and the observed structures consist of more than 2000 monomers, a length of more than 2000 nm, a cross section of 1.4 nm and a persistence length (Kuhn length, *i.e.*, measure of flexibility) of 81 nm. This structure could well describe the semi-flexible amyloid fibrils formed by BLG at pH 2, although the building blocks are no monomers but peptides. The filtrate contains small objects in the size range of dimers, possibly also small aggregates formed by peptides. Likewise, the mean length of 4 nm and the cross section of 1.7 nm confirm the successful removal of fibrils from the solution by filtration.

TAB 3-1 SAXS model parameters determined at different time intervals of amyloid aggregation at pH 2 or 3.5. Model: Two different models of rod-like fibrils of elliptical cross section were chosen: "Stiff" and "Flexible with polydispersity in length" (lognormal distribution); number of monomers: The mean number of monomers per fibrils; , <L> : The mean length of the amyloid aggregates in nm; B: the statistical segment length (Kuhn length) which is a measure of the flexibility of the chain in nm; Elliptical cross-section and value of the minor semiaxis of cross section (A) and axis ratio ( ). No results are listed for 5 h, as no fit for pH 3.5 was possible. "Retentate" and Filtrate were prepared with a 300 kDa membrane without prior lyophilisation.

Incubation time [h] and pH value		*Model*	*Number of monomers*	*<L> [nm]*	*B [nm]*	*Small semiaxis A [nm] and axis ratio γ [nm]*
0 h	pH 2	Stiff	1.3	4.0±0.2		1.7±0.1, 1
	pH 3.5	Stiff	3.2	7.8±0.3		1.9±0.1, 1
4 h	pH 2	Stiff	130	550±50		1.45±0.1, 1
	pH 3.5	Stiff	> 2000	> 1000		1.75±0.1, 4.1±0.1
Retentate (not lyophilised)	pH 2	Flexible	> 2000	> 2000	81±1	1.4±0.1, 1.2±0.1
	pH 3.5	Flexible	> 2000	> 2000	9.8±0.1	2.2±0.1, 3.4±0.1
Filtrate (not lyophilised)	pH 2	Stiff	2.1	4.4±0.4		1.7±0.1, 1
	pH 3.5	Stiff	> 1000	900±100	7.8±0.1	2.2±0.1, 3.4±0.1

At pH 3.5, already at the beginning the mean number of monomers observed is 3.2 and a length of ~7 nm is evident. This means that dimers or trimers are in solution, as expected for this pH value and as described later on. The pH 3.5 retentate (*i.e.*, the separated amyloid aggregates) contains long flexible fibrils with a contour length of more than 2000 nm and an elliptical cross section of an axis ratio of 3.4 nm. The Kuhn length of the worm-like aggregates is ~10 nm and therefore the aggregate is intrinsically more flexible than the pH 2 fibrils. The pH 3.5 filtrate seems to contain large amyloid aggregates, which shows an insufficient filtering process here in contrast to the pH 2 fibrils.

3.4.2. Fibril building block determination (SEC and AUC)

To assess the different building blocks, two methods were used: SEC was conducted under dissociative conditions, while the unmanipulated small-size-fraction of the fibril solution was determined by AUC-SV analyses.

The amyloid aggregate solutions were either dissociated completely (DHS), or separated by centrifugal ultrafiltration, lyophilised and then diccociated (DLR and DLF). The DHS and

DLHS (mixture of all compounds), the DLR (large aggregates >300 kDa fibrils and some other aggregates) and the DLF (peptides, intact protein and small aggregates) were only used for SEC **(FIG 3-2)**. For analysis with AUC (**FIG 3-3**) non-disscoiated conditions were used.

It is apparent that amyloid aggregates prepared at pH 2 or pH 3.5 not only have a different morphology **(FIG 3-1 and TAB 3-1)** but also different building blocks **(FIG 3-2).** Initially (t0), at pH 2 and pH 3.5, most of the protein present in the sample had a molecular weight of approximately 22.3 kDa (~unfolded monomeric BLG). With increasing incubation time, the monomeric protein intensity decreased, whereupon smaller molecular weight fractions occur. These peaks show a strong overlay, but main fractions of 11.7 kDa, 6.6 kDa and 4.3 kDa were identified at both pH values **(FIG 3-2)**. However, the kinetics of BLG degradation was significantly different between pH 2 and pH 3.5.

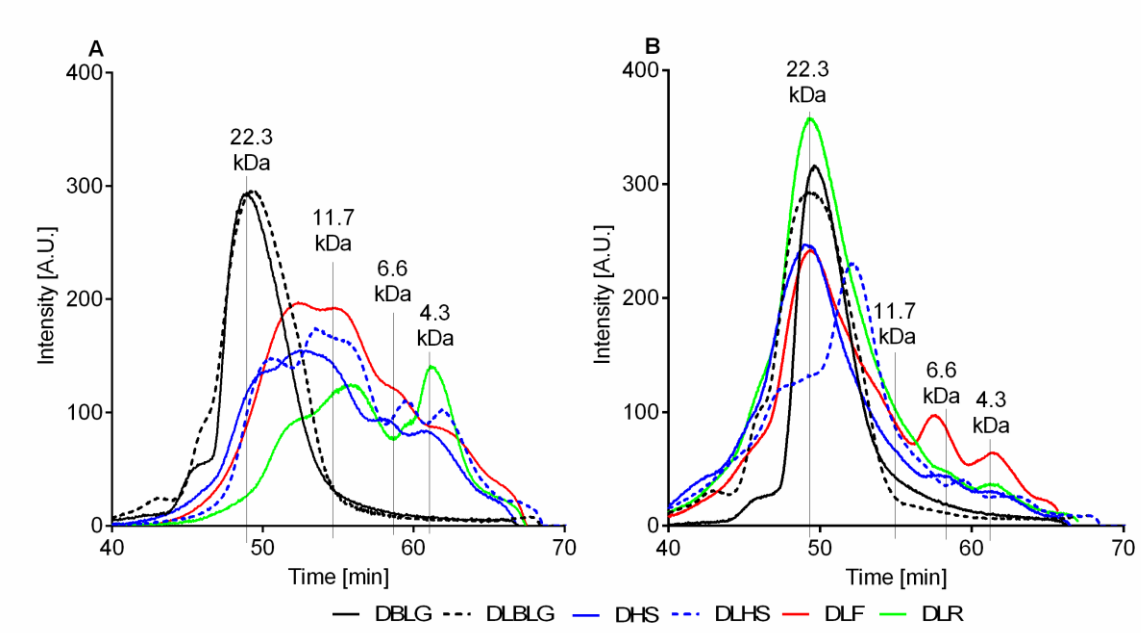

FIG 3-2 Size exclusion chromatograms of in Tris-HCl eluent dissociated samples before (DBLG* and DLBLG) and after (DHS*, DLHS, DLF and DLR) the 5 h heating at 90° C at pH 2 A) and at pH 3.5 B). The corresponding molecular weight fractions are listed for each peak and prominent peaks were highlighted by vertical lines. *Shown before by Keppler et al. (2019).

SEC gives evidence about the building blocks, which are associated to amyloid aggregates. After removing of non-aggregated material, a clear conception about the building blocks from pH 2 and pH 3.5 fibrils could be reached: after 5 hours, pH 2 fibrils seem to be a mix of different size fractions which superimpose, especially from the 4.3 kDa size fraction. It is noticeable, that this fraction not only has a high concentration in the retentate, but is also lacking in the filtrate, while here the 6.6 kDa fraction dominates.

When considering dissociated pure fibril fractions (DLR) and pure non-fibril fractions (DLF), it is evident that at pH 2 the fibril building blocks are composed of smaller peptides, whereas the non-fibril building blocks tend towards the larger peptides. However, a clear distinction is not possible, given that several peptide fractions co-elute and overlay. In contrast to pH 2, however, the aggregate building blocks are significantly altered at pH 3.5: here, they seem to consist predominantly of "intact" BLG, whereas the filtrate material contains all size fractions, but also whole protein **(FIG 3-2 B).**

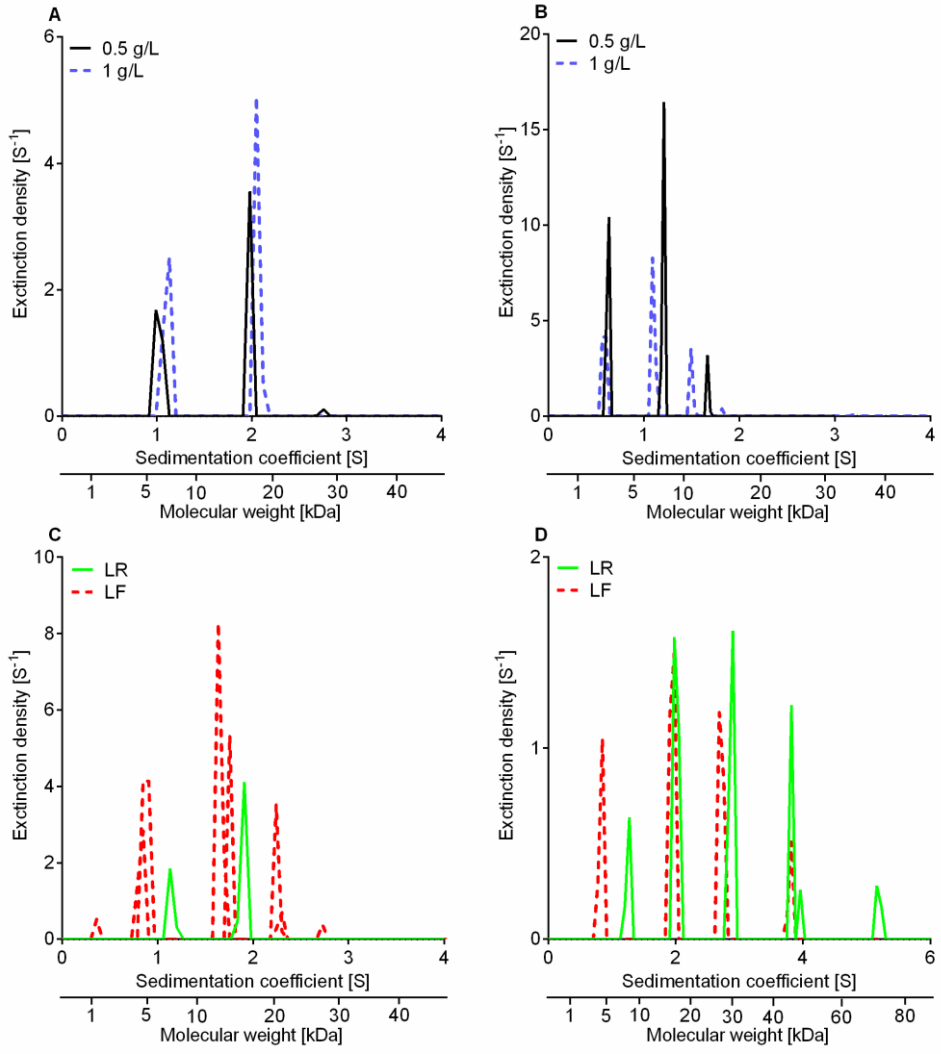

FIG 3-3 Sedimentation coefficient distributions from AUC-SV experiments for the 5 h fibril solutions at pH 2 (A) and pH 3.5 (B), respectively after dilution to two different concentrations (0.5/1 g/L). Molar masses are calculated from the c(s)-method in SEDFIT. Adsorption was adjusted by variation of the wavelength. Sedimentation coefficient distributions as obtained from c(s)-method in SEDFIT for filtrated samples at pH 2 (C) and pH 3.5 (D). The lyophilised retentate (LR) as well as the lyophilised (LF) was analysed for both pH values with 1 g/L at 280 nm.

AUC experiments are performed in order to reliably determine sedimentation and diffusion properties of fibrils and other macromolecules (Arosio et al. 2016; Le Pham et al. 2011) for biological applications. This is the first time that amyloid-like material from BLG are analysed by AUC. The fine fraction of the samples (*i.e.*, material < 100 kDa) was investigated via AUC-sedimentation velocity (SV), whereas large aggregates (*i.e.*, fibrils) gave scattered results (data not shown), due to tangling, deformation and self-association. **FIG 3-3** shows the obtained sedimentation coefficient distributions, along with the molar masses of the individual species in the pH 2 and pH 3.5 samples after 5 h incubation, as obtained from the c(s)-method in SEDFIT. Notably, no regularization was applied throughout the analysis (Schuck 2000).

One critical parameter in the analysis procedure is the partial specific volume of the proteins. The partial specific volume of monomeric BLG was assumed for all size fractions of the analysis, since it is not possible to determine the partial specific volume for samples which exhibit a large molar mass range as well as polydispersity in shape. The applied model is in good agreement with measured data. This can be seen in the differences of the calculated data from the c(s) data in SEDFIT and measured data (**see supplementary material chapter 3.8**).

Clearly, several species were detected via AUC-SV in the mass range up to 100 kDa for all samples. The observed small differences between the measurements at different concentrations and constant pH for the untreated samples (**see FIG 3-3 A**), indicate slight hydrodynamic and thermodynamic non-idealities. Similar effects were also described previously by (Mercadante et al. 2012). Also complex formation, tangling or network formation may influence the data.

FIG 3-3 A illustrates molar masses of ~32 kDa, ~19 kDa and ~7 kDa, which were observed at pH 2 after 5 h incubation. These findings reflect the presence of BLG monomers, dimers (or dimer-sized aggregates), and also some peptides in the solution at pH 2. At pH 3.5 **(see FIG 3-3 B),** the amount of peptide material <15 kDa seems to be higher compared to bigger size fractions (~15 kDa and ~17 kDa) and oligomer compounds (48 kDa).

In order to test the stability and purity of the LR and LF (which was previously used for SEC in dissociated condition), AUC was conducted and the fine fractions (*i.e.*, <100 kDa) were analysed. **FIG 3-3 C and D** illustrate the results for the filtered samples separated into fibril material and non-fibril fraction for pH 2 and pH 3.5. For both pH values, it is clearly evident that the LR contains still size fractions in the <100 kDa region. At pH 2, a ~7 kDa and a ~15 kDa fraction remain in the LR **(FIG 3-3 C)**, while the LF contains sizes from ~1 kDa to ~22 kDa. At pH 3.5, only the ~10 kDa fraction remains similar in the whole sample **(FIG 3-3 B)** and

in the LF sample **(FIG 3-3 D)**, while at pH 3.5 LR several oligomeric fractions (~35 to ~84 kDa) were detected.

3.4.3. Influence of polydispersity of fibrils solutions on different kind of analyses

The colorimetric-assays ThT and Nile red are used to detect amyloid structures. During heating of BLG there is an expected increase in ThT FL intensity at both pH values, with an even higher value at pH 3.5 (102.4 ± 5.4 a.u.) **(FIG 3-4 A).** Lyophilisation of BLG and HS had no significant effect on ThT-fluorescence. At pH 2, the ThT FL of the LR shows an significant increase to 296.3 ± 9.3. At pH 3.5, the increase is only moderate compared to HS with a fluorescence intensity of 115.0 ± 1.9 a.u.

As shown in **FIG 3-4 B,** the stronger increase in fluorescence intensity of the protein solution during 5 h heating can also be detected using the Nile-red assay (e.g. 105.5 ± 5.2 a.u. (pH 2) or 150.3 ± 4.0 a.u. (pH 3.5). However, lyophilisation of samples had a strong effect on LBLG and LHS at both pH values: At pH 2 the LBLG fluorescence increased about +37 % to 21.4 ± 0.6 a.u. and the HS fluorescence about +112 % to 224.3 ± 6.7 a.u.. At pH 3.5, an increase of the BLG fluorescence of about +28 % to 23.4 ± 2.0 a.u. were observed. Lyophilisation of the pH 3.5 HS had a significant effect as evident by a fluorescence increase of +183 % to 425.1 ± 3.4 a.u. Like the ThT, the Nile red reacts very strongly to the LR. However, the retentate at pH 3.5 shows a higher value (545.6 ± 3.6 a.u.) than at pH 2 (401.6 ± 1.3 a.u). In contrast to the ThT-assay, with Nile red quite high fluorescence of 144.8 ± 5.6 a.u. (pH 2) or 166.7 ± 6.7 a.u. (pH 3.5) are obtained for the LF.

The zeta-potential describes the electro kinetic potential at the shear plane. It is an important indicator of the stability of colloidal dispersions. During 5 h heating of BLG the zeta-potential increases. After lyophilisation, a reduction of the zeta-potential was observed for the pH 2 fibrils of about -33 to -39 %. However, no decrease was evident for the pH 3.5 samples. The LF with 56.0 ± 1.0 mV (pH 2) or 60.0 ± 1.6 mV (pH 3.5) had a higher zeta-potential than the LR with 40.9 ± 2.0 mV (pH 2) or 33.4 ± 1.9 mV (pH 3.5) **(FIG 3-4 C).**

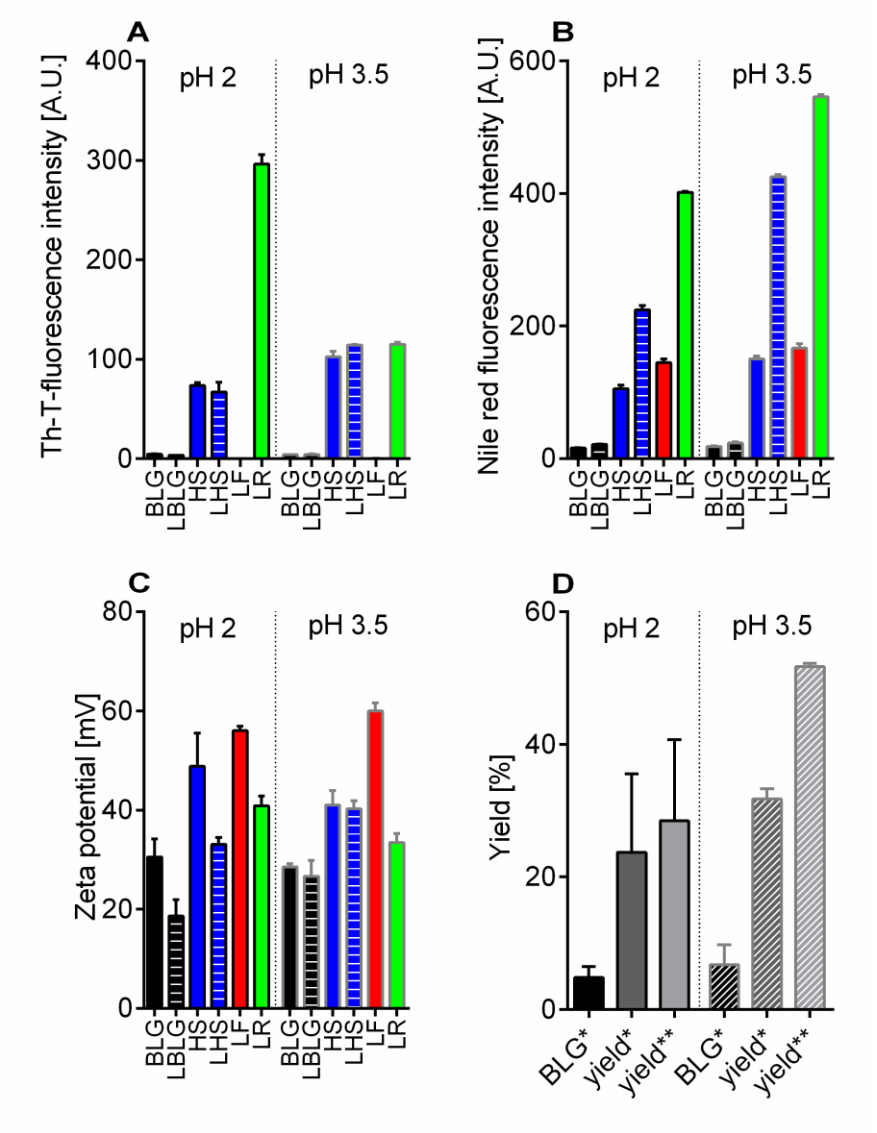

FIG 3-4 A) Thioflavin-T flouresence (a.u.) **B**) Nile-red fluorescence (a.u) and **C)** Zeta-potential (mV) of beta-lactoglobulin (BLG: black), lyophilised beta-lactoglobulin (LBLG: striped black), 5 h at 90 °C heated solution (HS: blue), lyophilised heated solution (LHS: striped blue), lyophilised filtrate (LF: red) and lyophilised retentate (LR: green) at pH 2 (black border) and pH 3.5 (grey border). **D**) Loss of protein during ultra-filtration of BLG (black) and 5 h HS calculated with Absorbance of BLG (yield* : dark grey) and filtrate (yield** : bright grey) formed at pH 2 (plane and black border) and pH 3.5 (striped and grey border). All measurement were conducted in triplicate and are listed as mean and standard deviation.

Ultrafiltration was used to determine how much BLG was converted to amyloid aggregates. As illustrated in **FIG 3-4 D,** the ultrafiltration of native BLG by using 300 kDa filters resulted in a loss of 6.8 ± 3.0 % (pH 2) and 4.8 ± 1.7 % (pH 3.5) or protein in the filtrate. This loss is taken into account in the calculation of the yield* achieved after 5 hours of heating and results in an additional loss of 23.7 ± 11.9 % (pH 2) or 31.8 ± 1.5 % (pH 3.5) or protein calculated with the extinction coefficient of native BLG. Since the extinction coefficient of the freeze-dried filtrate is changed, this was also taken into account for the calculation of the yield**, resulting in higher yields of 28.49 ± 11.9 % (pH 2) and 51.8 ± 0.5 % (pH 3.5).

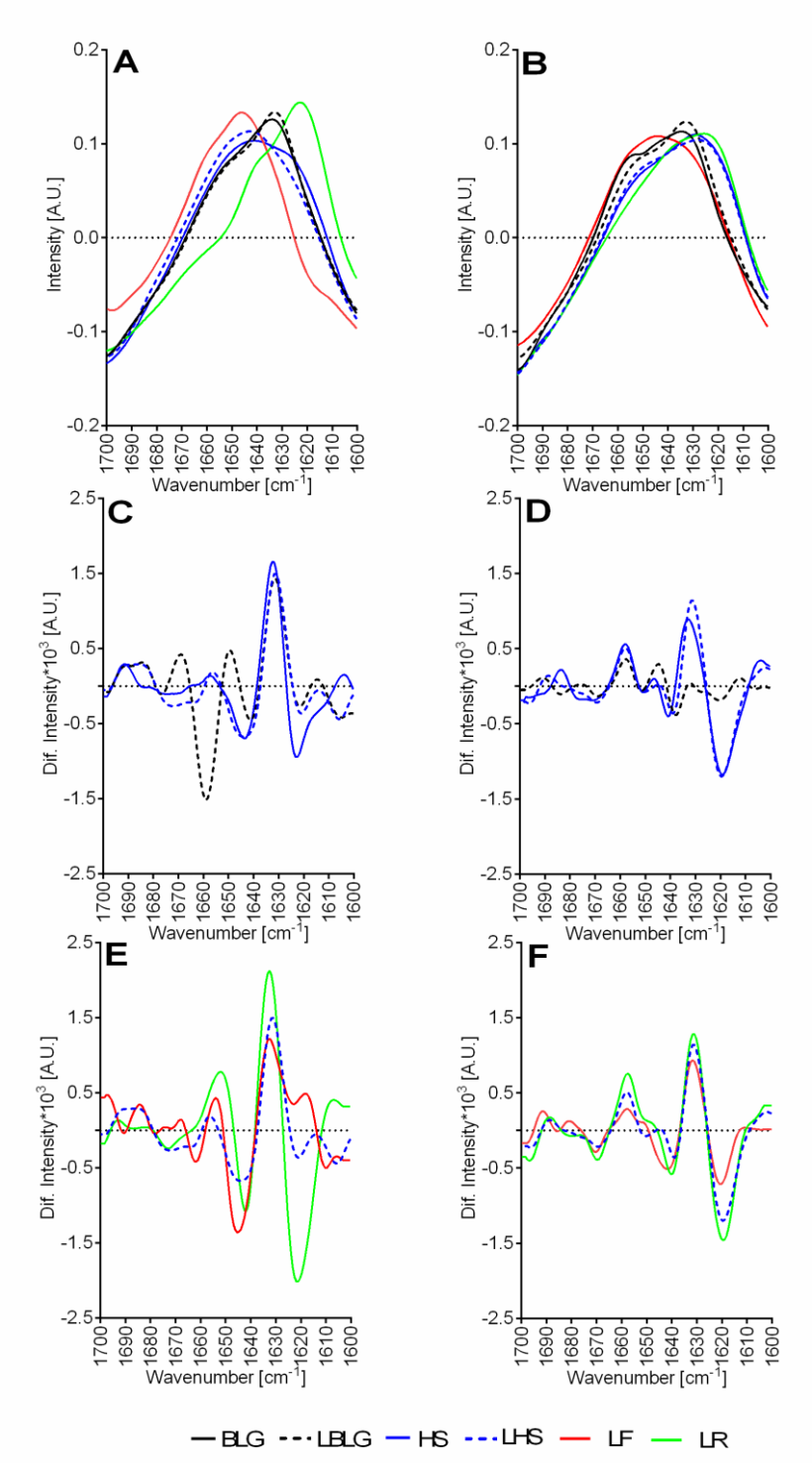

FIG 3-5 Amid I band (1600 – 1700 cm-1) spectra measured with ATR-FTIR of beta-lactoglobulin (BLG)*, lyophilised beta-lactoglobulin (LBLG), 5 h at 90°C heated solution (HS)*, lyophilised heated solution (LHS), lyophilised filtrate (LF) and lyophilised retentate (LR). Normalized spectra of samples pH 2 (A) and pH 3.5 (B) before (BLG, LBLG: black) and after (HS, LHS, LF, LR: blue, red and green) the fibril-formation process. C - F show 2nd derivation difference spectra of A and B respectively. All measurement were conducted in three replicates. *Shown before by Keppler et al. (2019).

ATR-FTIR was used to analyse the secondary structure of the (amyloid aggregated) protein. FTIR absorbance of the amide I spectra (1700 - 1600 cm^{-1}) of native BLG at pH 2 and pH 3.5 and during the production of fibrils are shown in **FIG 3-5 A and B**, whereas the corresponding difference spectra of the 2nd derivation are shown in **FIG 3-5 C to F**. Native BLG at pH 2 exhibited band maxima at 1632 cm^{-1} (intense) and 1691 cm^{-1} (weak) for intramolecular beta-sheets. Band maxima at 1655 cm^{-1} are indicative for alpha-helix conformation, while the weaker bands at 1666 and 1683 cm^{-1} can be assigned to beta-turns (Keppler et al. 2017; Baldassarre et al. 2016; Kavanagh et al. 2000).

During incubation at pH 2, the 1622 cm^{-1} band increases at the expense of the 1632 cm^{-1} band until saturation was reached after approximately 5 h incubation (**FIG 3-5 E and F)**. The strong difference between LR and LF is significantly recognizable in **FIG 3-5 A.** This is more pronounced in the 2nd derivative difference spectra **(FIG 3-5 E)**: Here, it is also evident that random coil (1645 cm^{-1}) structures increase during HS incubation and helix structures decrease (1655 cm^{-1}). In the 2nd derivation difference spectrum of LR **(FIG 3-5 G)**, the maximum at 1622 cm^{-1} has a twofold higher intensity compared to unfiltered HS material, confirming the strong presence of intermolecular beta-sheets in LR. By comparison, bands described for alpha-helix (1655 cm^{-1}) and intramolecular beta-sheets (1632 cm^{-1}) are strongly decreased. The main difference between LR and LF at pH 2 is the strong 1622 cm^{-1} band in LR. Lyophilisation of pH 2 samples only had an effect on native BLG **(FIG 3-5 C)**. Here an increase of the band (1660 cm^{-1}) and a reduction of the intramolecular beta-sheets were observed in the lyophilised BLG.

A similar effect, albeit less intense, was observed at pH 3.5, which is shown in **FIG 3-5 B, D and F**: During incubation, the 2nd derivative difference spectra give evidence that the intermolecular beta-sheet band maximum (1619 cm^{-1} , pH 3.5) is decreased at the expense of the intramolecular beta-sheets (1629 cm^{-1} , pH 3.5) **(FIG 3-5 H)**. Similar to the results at pH 2, the alpha-helix concentration decreases (at 1657 cm^{-1}), while turns and random coil structures increase (at 1671 cm^{-1} and 1641 cm^{-1}, respectively). Interestingly, the difference spectrum of LR at pH 3.5 is similar to that of the LHS after 5 h, while LF shows a less pronounced intermolecular aggregation band (1619 cm^{-1}) and higher values for alpha-helix and random coil elements, compared to HS and LR. Lyophilisation of pH 3.5 BLG and HS had no effect on the amid I spectra **(FIG 3-5 D).**

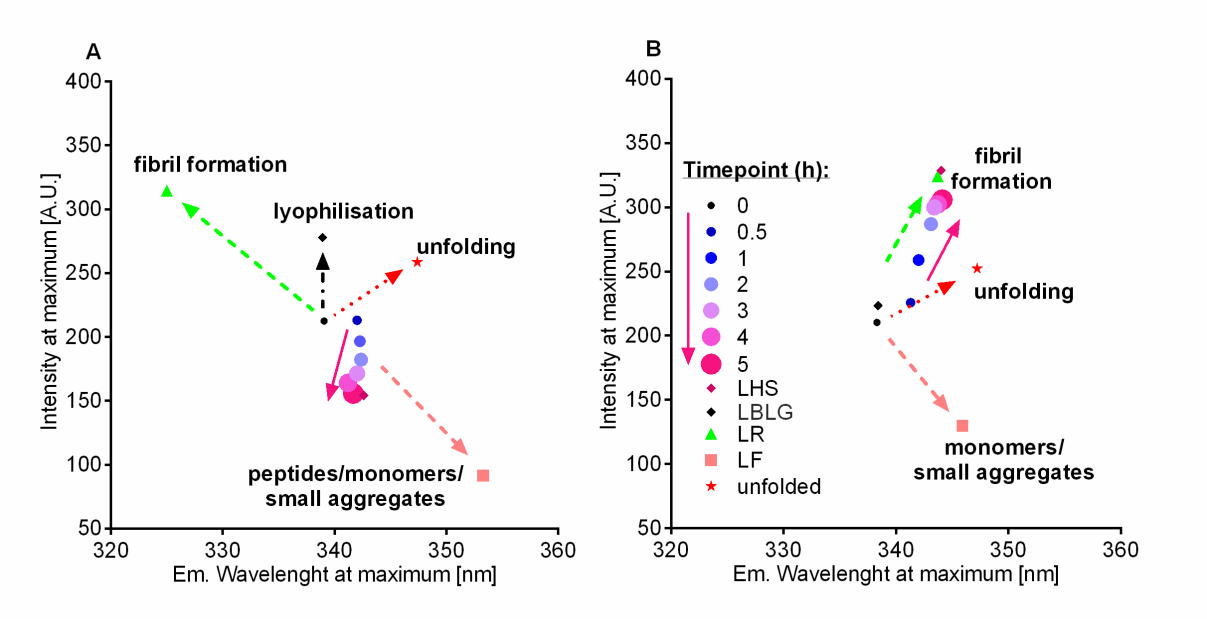

FIG 3-6 Tryptophan fluorescence intensity and emission followed during 5 h fibril production process of BLG at pH 2 (A) and pH 3.5 (B). All measurements were conducted in triplicate. Dots represent means of measurements.

The intrinsic tryptophan fluorescence is often used as a sensitive indicator of protein unfolding and refolding, since its fluorescence intensity and its emission maximum is strongly dependent on the neighbouring amino acids (such as quenching effects by adjacent disulphide bridges) or TRP solvent accessibility (Ali et al. 2018; Hettiarachchi et al. 2012). **FIG 3-6** shows the fluorescence emission spectra of BLG during the fibril production process at pH 2 and 3.5. For comparison, the TRP fluorescence of lyophilised samples LBLG, LHS, LR and LF were measured. As reference, BLG was unfolded by incubation with guanidine-HCl at pH 2 and 3.5 in order to assess the influence of protein unfolding itself.

During fibril-formation, different observations for pH 2 and pH 3.5 fibrils were made: At pH 2, the fluorescence intensity decreases from 212.5 ± 1.4 (t0) to 143.2 ± 0.5 a.u. during 9 h incubation **(FIG 3-6 A).** In addition, the emission maximum red shifts from 339 nm to 341 nm in the first 0.5 h. Lyophilisation of BLG (LBLG) resulted in an increase of the maximum fluorescence intensity by +31 % (+67.6 ± 1.9 a.u.), but no shift was evident. However, no alteration of the fluorescence intensity was observed for the LHS compared to the 5 h HS, but a slight redshift of about one wavelength was evident. Separation of aggregated and non-aggregated material exhibits a strong blue shift of TRP-fluorescence in the LR fraction paired with an increase of intensity maximum, while a decrease of the intensity maximum occurs at the monomer and hydrolysed material (LF). In contrast, the emission intensity of the tryptophan fluorescence in the pH 3.5 sample increased during 9 h from 210.3 ± 1.4 a.u. (t0) to 302.2 ± 1.8

a.u. **(FIG 3-6 B)** during the production process, while the emission maximum is continuously red shifted from 334 nm to approximately 344 nm. A similar spectral shift was observed for LR and also for unfolded BLG, while the TRP-fluorescence intensity of LF decreased. Lyophilisation of 5 h incubated samples had only minor effects on LBLG and LHS at pH 3.5 of about +6 % (+13.1 ± 1.6 a.u.) and +7 % (+22.7 ± 1.8 a.u.), respectively.

3.5. Discussion

3.5.1. Morphology of amyloid aggregates (AFM & SAXS)

AFM **(FIG 3-1)** illustrates the straight morphology of pH 2 fibrils and the irregular worm-like shape of the pH 3.5 amyloid aggregates.

The quality of the AFM images does not allow a comprehensive qualitative description of the aggregates as they are mostly used to confirm the presence of fibrils and worm-like aggregates: The shape and dimensions of the pH 2 fibrils are in agreement with the observed straight, semiflexible fibrils already described in detail elsewhere (Loveday et al. 2010; Adamcik et al. 2010; Serfert et al. 2014) and likewise, the worm-like structures are in agreement with other amyloids produced at pH 3.5 (Keppler et al. 2019; Serfert et al. 2014) and differ only marginally from other worm-like amyloid aggregates, which were produced at other factor combinations (protein or salt concentration) (Ye et al. 2018; vandenAkker et al. 2016; Gosal et al. 2004). A more detailed descriptions of these morphologies by AFM and electron microscopy have been made in the past by various working groups (Adamcik et al. 2010; Adamcik and Mezzenga 2011; Jung et al. 2008; Mudgal et al. 2009; Serfert et al. 2014).

The results shown here by AFM (**FIG 3-1)** and SAXS **(TAB 3-1)** are consistent with previous analyses regarding the cross-section and contour lenghts of straight (vandenAkker et al. 2016) and worm-like (Jung et al. 2008) amyloid aggregates. According to the present findings, the pH value determines if stiff (pH 2) or worm-like (pH 3.5) morphologies occur while incubating BLG for 5 h at 90 °C and low ionic strength **(FIG 3-1)**. The contour length and cross-section observed by SAXS for the concenrated pH 2 fibrils (retentate) in **TAB 3-1** are only slighty lower than observed with AFM **(FIG 3-1A - D).** The investigations confirm the amyloidogenic nature of both aggregates. This is in accordance with previous findings, stating that amyloid morphologies can be altered in general by using different pH values (Kavanagh et al. 2000; Serfert et al. 2014; Jung et al. 2008).

The different morphology of the amyloid aggregates at pH 3.5 is based on the increase in pH above pH 3.35 (Mudgal et al. 2011; Loveday et al. 2010). While linear fibrillary structures

occur at pH values ≤pH 3.0 (Lee et al. 2012; Adamcik et al. 2010; Loveday et al. 2010), a further increase of the pH value (≥pH3.35) next to the isoelectric point of the protein (pI = 4.7 (Lee et al. 2012)) first leads to worm-like (Serfert et al. 2014; Mudgal et al. 2009) and then to spherical aggregated structures (Jung et al. 2008; Serfert et al. 2014), as far as a low protein (2.5 wt%) and ion concentration is considered. This change in fibril morphology (Lee et al. 2015) is suggested to be primarily due to pH-dependent electrostatic interactions between the aggregates, which decrease near the isoelectric point (Lee et al. 2012).

Furthermore, it can be stated that a fractionation of the HS into retentate and filtrate by means of ultrafiltration leads to a mostly successful separation of large aggregates and small aggregates or BLG and peptide monomers. However, with some limitations for the pH 3.5 filtrate.

3.5.2. Building blocks analysis (SEC & AUC)

The present results confirm that the building blocks of amyloid aggregates at pH 2 and pH 3.5 differ significantly (i.e. peptides at pH 2 and whole BLG at pH 3.5).

The pH value determines the acid hydrolysis rate (Loveday et al. 2017). Acid hydrolysation was described as an essential step in the formation of straight as well as worm-like fibrils that occur at pH 2 (vandenAkker et al. 2016). Terminal segments with amino acid sequence location 1 – 32 (3437.7 Da) or 1 – 53 (5737 Da) were found in pH 2 fibrils (Ye et al. 2018; Akkermans et al. 2008), which would also fit in the variation range of the SEC detected 4.3 kDa fraction **(FIG 3-2 A)**. Moreover, C-terminal fragments with > 6 kDa were only listed for DLF and DHS (Akkermans et al. 2008). In general, AUC findings also confirm that at pH 2 most of the protein is associated to aggregates > 100 kDa, leaving intact protein (~19 kDa) and large peptides in the non-amyloid material **(FIG 3-3 A).** However, the present AUC findings suggest that during processing (*i.e.,* filtration and lyophilization), also smaller aggregates remain in the LR, while new fractions (probably fractures of fibrils) occur in the LF **(FIG 3-3 C)**. Similar observations regarding lyophilization were made previously (Loveday et al. 2012).

At pH 3.5, non-hydrolysed BLG are the building blocks in the worm-like aggregates **(FIG 3-2),** as it was assumed for amyloids prepared at the pH value of pH 3.35 (Mudgal et al. 2011). However, the question whether this is also a reason for the worm-like morphology cannot be answered unequivocally, since straight fibrils formed by intact BLG are also possible under certain conditions (Hamada and Dobson 2002; Hettiarachchi et al. 2012). Although SEC analysis has already been conducted for pH 2 fibrils, so far, it has not been discribed for pH 3.5

BLG amyloid aggregates. Here an increased proportion of peptides of the size fraction < 6.6 kDa can be observed in the DLR- and DHS- compared to the DLF sample **(FIG 3-2 B).** In general, however, the proportion of small peptide fractions is reduced by a weaker acid hydrolysis at pH 3.5. The peptide fractions observed with AUC give evidence that also at this pH value, acid hydrolysis occurs. However, it is unclear why the intensities are more distinct than at pH 2, where hydrolysis is more pronounced. The peptide size fractions could either be different peptides, or aggregates of smaller peptides **(FIG 3-3 B).** Here, small variations might be caused by inaccuracies of the method, as discussed before. It is interesting to note that at pH 3.5 several oligomeric fractions occur **(FIG 3-3 D)**, that were not observed in the whole sample, but fit to sizes of dimer, trimer and pentamer of BLG (Uhrínová et al. 2000). Similar to observations at pH 2, these might be detachments from the original, intact aggregates, which are linked to the processing stress by ultrafiltration and freeze-drying (Loveday et al. 2012). The AUC gives indications that most of the intact BLG seems to be in the > 100kDa aggregates (either in the amyloid aggregates, or as pentameric and higher order aggregates), leaving the peptides in the fine fraction **(FIG 3-3 B**).

3.5.3. Physico-chemical properties of the amyloid and non-amyloid fractions

The zeta-potential **(FIG 3-4 A)** increases in the course of amyloid aggregation at both pH values**,** which has already been shown in previous studies (Serfert et al. 2014). However, the investigation of the different fractions reveals that the amyloid aggregates have a lower zeta-potential as compared to the non-amyloid material in the filtrate. One explanation could be an increased occurrence of acidic amino acid residues in the course of hydrolysis and unfolding of the protein, which are hidden again in the course of amyloid aggregation or an over proportional presence of hydrophobic amino acid residues in the aggregates. It is unclear why the zeta-potential of the freeze-dried unfiltered pH 2 samples decreased this much. It can therefore be assumed that further acid concentration through drying influences the protein. The HCL concentration in the pH 2 samples was higher than in the pH 3.5 samples, which could explain the effects observed for pH 2 fibrils. Additionally, a stronger effect of lyophilisation on pH 2 fibrils has been described before (Loveday et al. 2012). Further analyses (see below) also showed an effect on the biophysical properties of the protein, which could also have influenced the zeta-potential.

Comparing the amyloid aggregation of HS with the ThT **(FIG 3-4 B)** and Nile red fluorescence **(Figure 4 C)** of separated amyloids (LR), some similarities at pH 2, but also some inconsistencies at pH 3.5 can be found: The strong ThT FL increase of the pH 2 LR fraction

shows that the purification of the fibrils by ultrafiltration and freeze-drying works without a loss of the intrinsic beta-sheet structure (Krebs et al. 2005), even if other structural and chemical changes can occur in the course of lyophilisation (Loveday et al. 2012). LR shows significantly lower ThT FL at pH 3.5 than at pH 2, which leads to the assumption that the proportion of amyloid material in LR is reduced after lyophilisation. The comparison of lower ThT FL and higher aggregate yield at pH 3.5 **(FIG 3-4 D)** to pH 2, leads to the assumption that worm-like aggregates compensate their lower amyloid content in the HS by a higher degree of aggregation. The lacking fluorescence increase of the pH 3.5 LR sample is probably not due to destructive effects of the freeze-drying process, as the lyophilisation of the unfiltered samples does not lead to an increase of the ThT FL.

However, Nile red analysis confirms significant influences of freeze-drying on fibrils and worm-like aggregates. The high Nile red fluorescence of LHS, LR—especially at pH 3.5—shows that the dried samples have a higher hydrophobic surface than the original samples (Sackett and Wolff 1987). This could also indicate destabilization of the amyloids by the purification process (as also indicated by AUC), which for example leads to an increased surface availability and thus to increased binding sites for Nile red. This would also explain the comparatively high increase in fluorescence of the LF. Investigations by AFM have shown that the worm-like aggregates at pH 3.5 are strongly degraded by the freeze-drying step **(see Supplementary Material chapter 3.8).**

The results confirm a more pronounced intermolecular aggregation in HS as well as in LR at pH 2 compared to pH 3.5, which indicates the stronger presence of amyloid material here. It also confirms the previous observation, that LF does not contain any amyloid protein, which is clearly concentrated in LR at pH 2 and which is in affirmation with ThT **(FIG 3-4 A)** and TRP fluorescence **(FIG 3-6).** At pH 3.5, similar to the results for ThT, the beta-sheet concentration of LR is very close to the one observed in 5 h HS. As previously discussed, this could indicate the loss of amyloid character in pH 3.5 LR, since otherwise the conversion rate **(FIG 3-3)** would have to be higher.

Observations by FTIR **(FIG 3-5)** indicate a decrease of intramolecular (native) beta-sheets during heat denaturation of BLG as well as a shoulder in the FTIR spectrum between 1623 cm^{-1} and 1618 cm^{-1}, which is indicative for intermolecular beta-sheets. These intermolecular sheets correlate generally with protein aggregation (Baldassarre et al. 2016; Kavanagh et al. 2000). For different kinds of fibrils from various proteins, intense absorption bands between 1615 and below 1630 cm^{-1} are well described by FTIR (Gosal et al. 2004). Moran and Zanni (2014)

explained, that the low frequency range of amyloid beta-sheets with their extended and extremely well-ordered structure results in vibrational motions that extend along large sections of the amyloid backbone. In contrast to the present results, higher contents of alpha-helical and random coil elements in worm-like aggregates compared to straight fibrils from BLG prepared with high protein concentration were described previously (Ye et al. 2018). Suggestions were made, that this new alpha-helix structure is an indication of an altered "building block", which may account for the morphological differences (Gosal et al. 2004). When worm-like fibrils were formed in dependence of the pH value, a decrease of helical structures was observed **(FIG 3-5 D),** however the pH 3.5 samples show a generally higher intensity of alpha helix elements compared to pH 2. This indicates that the present worm-like aggregates behave similar to worm-like aggregates prepared at pH 2 at high protein concentration (Ye et al. 2018). This results also show the significant difference in the protein conformation of the isolated amyloids (LR) and the non-amyloid material (LF) in the 1622cm^{-1} waveband at pH 2 but not at pH 3.5. Since the HS is a superposition of LR and LF, the different polydispersity of pH 2 and pH 3.5 samples become evident.

As shown in **FIG 3-6,** TRP fluorescence emission in pH 2 and pH 3.5 samples is exposed to significant changes during production of amyloid aggregates which indicates reorganization of the protein tertiary structures during the amyloid aggregation process. These changes are completely different for pH 2 and pH 3.5 amyloid aggregates as well as their respective non-amyloid fractions, which again confirms the previous results.

The emission red shift at pH 2 fibril formation in the first 0.5 h incubation **(FIG 3-5 A)** suggests an increasing polarity next to the TRP, which is associated with unfolding of the protein (Hettiarachchi et al. 2012; Stănciuc et al. 2012; Al-Shabib et al. 2019). It was proposed, that the amyloid protein aggregation process might only start after this first unfolding rearrangement (Vetri and Militello 2005). The further development of intrinsic TRP fluorescence of HS is increasingly influenced by an overlay of different effects: unfolding, acid hydrolysis, amyloid aggregation and altered proportions of non-amyloid material. To separate these effects, LR, LF and denatured BLG were measured as reference: The blue shift of LR at pH 2 indicates the presence of solvent inaccessible apolaric sites in the vicinity of TRP (Gasymov et al. 2000) and could be a sign of amyloid aggregation. In addition, BLG contains only two TRP residues (at position 19 and position 61). In native BLG, TRP^{61} is present at the surface (Al-Shabib et al. 2018) and almost totally quenched by water exposition (Stănciuc et al. 2012) and its location near to a disulphide bond (CYS^{66} – CYS^{160}) (Cho et al. 1994). Protein unfolding und the

cleavage of disulphide bonds enhances the TRP fluorescence since TRP^{61} now also contributes to the fluorescence yield. In addition, the fluorescence intensity increase of LR might also be explained by a disparate distribution of TRP in fibril and non-fibril material: Akkermans et al. (2008) demonstrated a high probability of peptide 1 – 32 or 1-53 in the amyloid fraction of BLG which contains TRP^{19}. Furthermore, this would also explain the drop of fluorescence in the LF fraction at pH 2, in case peptides with TRP^{19} (and maybe TRP^{61}) are mainly building blocks of fibrils. The present results support these observations and indicate that aromatic pi-pi stacking (Greenwald and Riek 2010) may have an important role in the distribution of TRP to filtrate and retentate. This is supported by the observation that the filtrate has a lower absorption than the retentate at the wavelength of 278 nm specific for aromatic amino acids **(see Supplementary material FIG-S 3-12**). In contrast to LR, the LF at pH 2 was strongly red shifted which also hints at increased solvent exposure of TRP, typical for hydrolysates. Additionally, TRP quenching effects during protein denaturation could be caused by specific amino acid residues (e.g. lysine) (Bhattacharjee and Das 2000). Also the role of oxidation on TRP fluorescence during the heating process should be considered. However, lyophilisation might also have an impact, as fluorescence of LBLG is strongly increased compared to BLG.

In contrast to pH 2, the fluorescence evolution at pH 3.5 during the aggregation-process mainly follows an unfolding characteristics comparable to chemical protein unfolding, as indicated by **FIG 3-6 B**. This also confirms that these worm-like aggregates consist of intact denatured protein, which is probably less densely packed than the amyloid beta-sheet stacks of the pH 2 fibrils. This would explain the strong red shift of the worm-like amyloids (*i.e.,* increased TRP solvent exposure) compared to the blue shifted pH 2 fibrils (*i.e.*, inaccessible apolar TRP environment). In addition, the LF and LR fractions are less different than at pH 2, which was also observed in FTIR. That means that the change in tertiary structure during pH 3.5 amyloid aggregation is dominated by protein unfolding and exposure of the TRP^{19} to water. Similar to pH 2, however, the TRP in LF at pH 3.5 decreases. This observation could suggest that there is no redistribution of the aromatic amino acids involved in the aggregation, as discussed for pH 2 - since at pH 3.5 BLG units with probably unchanged primary structure aggregate for the most part. However, other factors could also have an impact here, e.g. increased grade of oxidation, increased solvent accessibility of TRP^{19} and TRP^{61} (Stănciuc et al. 2012), or disulphide formation in the non-amyloid material.

In general, TRP fluorescence showed significant differences in the tertiary structure of BLG-amyloid aggregates formed at pH 2 and at pH 3.5.

3.6. Conclusion

The present experiments revealed that the evaluation of amyloid aggregates at different pH values must be considered with more caution than previously assumed:

SAXS and AFM results showed the occurrence of straight fibrils at pH 2 and worm-like aggregates at pH 3.5. SEC and AUC confirmed, that the building-blocks of amyloid aggregates are peptides in the straight fibrils at pH 2, while non-hydrolyzed BLG occurred in the worm-like amyloid aggregates formed at pH 3.5. Thus, a polydisperse mixture of amyloid aggregated and non-aggregated material is formed to a different degree at pH 2 and pH 3.5. The ThT FL confirmed an adequate separation of amyloid and non amyloid by ultrafiltration. The TRP fluorescence of these separated fractions demonstrates a more dense packed and apolar microenvironment with low zeta-potential in purified fibrils, while the non-amyloid fraction had a higher zeta-potential and hydrophilic environment. An over proportional incorporation of aromatic amino acids was assumed in pH 2 fibrils, depleting the non-amyloid fraction of these amino acids. Also, a strong hydrophobic character of the separated pH 3.5 aggregates was detected and the pH 3.5 non-amyloid filtrate shows a higher zeta-potential compared to its retentate and even compared to pH 2 fractions. However, it has to be considered that the lyophilisation step also has a high impact on some physico-chemical properties of the native and amyloid aggregated BLG, since the pH 3.5 worm-like aggregates seemed to be less stable during processing than the pH 2 fibrils.

Investigations of the structure and conformation analysed with FTIR and the intrinsic TRP fluorescence show the extent of the superposition effects on the results in HS when they are compared to the respective amyloid and non-amyloid fractions. In addition, the sample heterogeneity was more pronounced for pH 2 than for pH 3.5 samples due to the stronger heterogeneity of building blocks caused by acid hydrolysis at pH 2. In order to clarify the structure of different amyloid aggregates, the heterogeneity of the different fractions should be considered.

Acknowledgement
This project was funded by the German research foundation (DFG) priority programme SPP 1934 DiSPBiotech (Project no. 315456892 and 315396049). We are grateful to Jörg R. Knipp, Phillip M. Meissner, Monica Gamba and Jil J. Kayser of the Food Technology Division, Kiel University and Simon Wawra of the Institute of Particle Technology, TU Erlangen for skilful help. We gratefully acknowledge technical support from Clement Blanchet (EMBL) at the P12 BioSAXS beamline (EMBL/DESY, PETRA III) and the beamtime allocation for proposal 718. SAXS analysis It also benefited from the use of the SasView application, originally developed under National Science Foundation (NSF, US) Award DMR-0520547. SasView also contains code developed with funding from the EU Horizon 2020 programme under the SINE2020 project grant no 654000.

3.7. References

Adamcik, J., Jung, J.-M., Flakowski, J., Los Rios, P. de, Dietler, G., & Mezzenga, R. (2010). Understanding amyloid aggregation by statistical analysis of atomic force microscopy images. *Nat Nanotechnol*, 5(6), 423–8. http://dx.doi.org/10.1038/nnano.2010.59.

Adamcik, J., & Mezzenga, R. (2011). Adjustable twisting periodic pitch of amyloid fibrils. *Soft Matter*, 7(11), 5437. http://dx.doi.org/10.1039/c1sm05382e.

Akkermans, C., Venema, P., van der Goot, A.J., Gruppen, H., Bakx, E.J., & Boom, R.M., et al. (2008). Peptides are building blocks of heat-induced fibrillar protein aggregates of beta-lactoglobulin formed at pH 2. *Biomacromolecules*, 9(5), 1474–9. http://dx.doi.org/10.1021/bm7014224.

Ali, M., Keppler, J.K., Coenye, T., & Schwarz, K. (2018). Covalent Whey Protein-Rosmarinic Acid Interactions. *J Food Sci*, 83(8), 2092–100. http://dx.doi.org/10.1111/1750-3841.14222.

Al-Shabib, N.A., Khan, J.M., Malik, A., Alsenaidy, M.A., Rehman, M.T., & AlAjmi, M.F., et al. (2018). Molecular insight into binding behavior of polyphenol (rutin) with beta lactoglobulin. *Journal of Molecular Liquids*, 269, 511–20. http://dx.doi.org/10.1016/j.molliq.2018.07.122.

Al-Shabib, N.A., Khan, J.M., Malik, A., Sen, P., Alsenaidy, M.A., & Husain, F.M., et al. (2019). A quercetin-based flavanoid (rutin) reverses amyloid fibrillation in β-lactoglobulin at pH 2.0 and 358 K. *Spectrochim Acta A Mol Biomol Spectrosc*, 214, 40–8. http://dx.doi.org/10.1016/j.saa.2019.02.004.

Arosio, P., Cedervall, T., Knowles, T.P.J., & Linse, S. (2016). Analysis of the length distribution of amyloid fibrils by centrifugal sedimentation. *Analytical Biochemistry*, 504, 7–13. http://dx.doi.org/10.1016/j.ab.2016.03.015.

Baldassarre, M., Bennett, M., & Barth, A. (2016). Simultaneous acquisition of infrared, fluorescence and light scattering spectra of proteins. *Analyst*, 141(3), 963–73. http://dx.doi.org/10.1039/c5an02283e.

Bhattacharjee, C., & Das, K.P. (2000). Thermal unfolding and refolding of β-lactoglobulin. *European Journal of Biochemistry*, 267(13), 3957–64. http://dx.doi.org/10.1046/j.1432-1327.2000.01409.x.

Blanton, T.N., Barnes, C.L., & Lelental, M. (2000). Preparation of silver behenate coatings to provide low- to mid-angle diffraction calibration. *J Appl Crystallogr*, 33(1), 172–3. http://dx.doi.org/10.1107/S0021889899012388.

Brautigam, C.A. (2015). Calculations and Publication-Quality Illustrations for Analytical Ultracentrifugation Data. *Meth Enzymol*, 562, 109–33. http://dx.doi.org/10.1016/bs.mie.2015.05.001.

Chen, W.-R., Butler, P.D., & Magid, L.J. (2006). Incorporating intermicellar interactions in the fitting of SANS data from cationic worm-like micelles. *Langmuir*, 22(15), 6539–48. http://dx.doi.org/10.1021/la0530440.

Chen, Y., & Barkley, M.D. (1998). Toward understanding tryptophan fluorescence in proteins. *Biochemistry*, 37(28), 9976–82. http://dx.doi.org/10.1021/bi980274n.

Cho, Y., Batt, C.A., & Sawyer, L. (1994). Probing the retinol-binding site of bovine beta-lactoglobulin. *the journal of biological chemistry*, 269(15), 11102–7.

Doucet M, Cho JH, Alina G, Bakker J, Bouwman W, Butler P, et al. Sasview Version 4.1. Zenodo 2017.

Feigin LA, Svergun DI, Taylor GW. Structure Analysis by Small-Angle X-Ray and Neutron Scattering. Boston, MA, s.l.: Springer US 1987. 335 p.

Franke, D., Kikhney, A.G., & Svergun, D.I. (2012). Automated acquisition and analysis of small angle X-ray scattering data. *Nuclear Instruments and Methods in Physics Research Section A: Accelerators, Spectrometers, Detectors and Associated Equipment*, 689, 52–9. http://dx.doi.org/10.1016/j.nima.2012.06.008.

Gasymov, O.K., Abduragimov, A.R., Yusifov, T.N., & Glasgow, B.J. (2000). Resolution of ligand positions by site-directed tryptophan fluorescence in tear lipocalin. *Protein Sci*, 9(2), 325–31. http://dx.doi.org/10.1110/ps.9.2.325.

Gosal, W.S., Clark, A.H., & Ross-Murphy, S.B. (2004). Fibrillar beta-lactoglobulin gels. *Biomacromolecules*, 5(6), 2408–19. http://dx.doi.org/10.1021/bm049659d.

Greenwald, J., & Riek, R. (2010). Biology of amyloid. *Structure*, 18(10), 1244–60. http://dx.doi.org/10.1016/j.str.2010.08.009.

Hamada, D., & Dobson, C.M. (2002). A kinetic study of beta-lactoglobulin amyloid fibril formation promoted by urea. *Protein Sci*, 11(10), 2417–26. http://dx.doi.org/10.1110/ps.0217702.

Hettiarachchi, C.A., Melton, L.D., Gerrard, J.A., & Loveday, S.M. (2012). Formation of β-lactoglobulin nanofibrils by microwave heating gives a peptide composition different from conventional heating. *Biomacromolecules*, 13(9), 2868–80. http://dx.doi.org/10.1021/bm300896r.

Humblet-Hua, N.-P.K., van der Linden, E., & Sagis, L.M.C. (2012). Microcapsules with protein fibril reinforced shells. *J Agric Food Chem*, 60(37), 9502–11. http://dx.doi.org/10.1021/jf3024529.

Jerke, G., Pedersen, J.S., Egelhaaf, S.U., & Schurtenberger, P. (1997). Static structure factor of polymerlike micelles. *Phys. Rev. E*, 56(5), 5772–88. http://dx.doi.org/10.1103/PhysRevE.56.5772.

Jung, J.-M., Savin, G., Pouzot, M., Schmitt, C., & Mezzenga, R. (2008). Structure of heat-induced beta-lactoglobulin aggregates and their complexes with sodium-dodecyl sulfate. *Biomacromolecules*, 9(9), 2477–86. http://dx.doi.org/10.1021/bm800502j.

Kavanagh, G.M., Clark, A.H., & Ross-Murphy, S.B. (2000). Heat-induced gelation of globular proteins. *International Journal of Biological Macromolecules*, 28(1), 41–50. http://dx.doi.org/10.1016/S0141-8130(00)00144-6.

Keppler, J.K., Heyn, T.R., Meissner, P.M., Schrader, K., & Schwarz, K. (2019). Protein oxidation during temperature-induced amyloid aggregation of beta-lactoglobulin. *Food Chem*, 289, 223–31. http://dx.doi.org/10.1016/j.foodchem.2019.02.114.

Keppler, J.K., Martin, D., Garamus, V.M., Berton-Carabin, C., Nipoti, E., & Coenye, T., et al. (2017). Functionality of whey proteins covalently modified by allyl isothiocyanate. Part 1

physico-chemical and antibacterial properties of native and modified whey proteins at pH 2 to 7. *Food Hydrocolloids*, 65, 130–43. http://dx.doi.org/10.1016/j.foodhyd.2016.11.016.

Keppler, J.K., Martin, D., Garamus, V.M., & Schwarz, K. (2015). Differences in binding behavior of (-)-epigallocatechin gallate to β-lactoglobulin heterodimers (AB) compared to homodimers (A) and (B). *J Mol Recognit*, 28(11), 656–66. http://dx.doi.org/10.1002/jmr.2480.

Knowles, T.P.J., & Mezzenga, R. (2016). Amyloid Fibrils as Building Blocks for Natural and Artificial Functional Materials. *Adv Mater Weinheim*, 28(31), 6546–61. http://dx.doi.org/10.1002/adma.201505961.

Krebs, M.R.H., Bromley, E.H.C., & Donald, A.M. (2005). The binding of thioflavin-T to amyloid fibrils. *J Struct Biol*, 149(1), 30–7. http://dx.doi.org/10.1016/j.jsb.2004.08.002.

Lara, C., Adamcik, J., Jordens, S., & Mezzenga, R. (2011). General self-assembly mechanism converting hydrolyzed globular proteins into giant multistranded amyloid ribbons. *Biomacromolecules*, 12(5), 1868–75. http://dx.doi.org/10.1021/bm200216u.

Le Pham, C.L., Mok, Y.-F., & Howlett, G.J. (2011). Sedimentation velocity analysis of amyloid fibrils. *Methods Mol Biol*, 752, 179–96. http://dx.doi.org/10.1007/978-1-60327-223-0_12.

Lee, G., Lee, W., Lee, H., Lee, C.Y., Eom, K., & Kwon, T. (2015). Self-assembled amyloid fibrils with controllable conformational heterogeneity. *Sci Rep*, 5, 16220. http://dx.doi.org/10.1038/srep16220.

Lee, G., Lee, W., Lee, H., Woo Lee, S., Sung Yoon, D., & Eom, K., et al. (2012). Mapping the surface charge distribution of amyloid fibril. *Appl. Phys. Lett.*, 101(4), 43703. http://dx.doi.org/10.1063/1.4739494.

Loveday, S.M., Anema, S.G., & Singh, H. (2017). β-Lactoglobulin nanofibrils. *International Dairy Journal*, 67, 35–45. http://dx.doi.org/10.1016/j.idairyj.2016.09.011.

Loveday, S.M., Su, J., Rao, M.A., Anema, S.G., & Singh, H. (2012). Whey protein nanofibrils. *J Agric Food Chem*, 60(20), 5229–36. http://dx.doi.org/10.1021/jf300367k.

Loveday, S.M., Wang, X.L., Rao, M.A., Anema, S.G., Creamer, L.K., & Singh, H. (2010). Tuning the properties of β-lactoglobulin nanofibrils with pH, NaCl and CaCl2. *International Dairy Journal*, 20(9), 571–9. http://dx.doi.org/10.1016/j.idairyj.2010.02.014.

Mercadante, D., Melton, L.D., Norris, G.E., Loo, T.S., Williams, M.A.K., & Dobson, R.C.J., et al. (2012). Bovine β-lactoglobulin is dimeric under imitative physiological conditions. *Biophys J*, 103(2), 303–12. http://dx.doi.org/10.1016/j.bpj.2012.05.041.

Mishra, R., Sörgjerd, K., Nyström, S., Nordigården, A., Yu, Y.-C., & Hammarström, P. (2007). Lysozyme amyloidogenesis is accelerated by specific nicking and fragmentation but decelerated by intact protein binding and conversion. *J Mol Biol*, 366(3), 1029–44. http://dx.doi.org/10.1016/j.jmb.2006.11.084.

Mohammadian, M., & Madadlou, A. (2018). Technological functionality and biological properties of food protein nanofibrils formed by heating at acidic condition. *Trends in Food Science & Technology*, 75, 115–28. http://dx.doi.org/10.1016/j.tifs.2018.03.013.

Moran, S.D., & Zanni, M.T. (2014). How to Get Insight into Amyloid Structure and Formation from Infrared Spectroscopy. *J Phys Chem Lett*, 5(11), 1984–93. http://dx.doi.org/10.1021/jz500794d.

Mudgal, P., Daubert, C.R., & Foegeding, E.A. (2009). Cold-set thickening mechanism of β-lactoglobulin at low pH. *Food Hydrocolloids*, 23(7), 1762–70. http://dx.doi.org/10.1016/j.foodhyd.2009.03.009.

Mudgal, P., Daubert, C.R., & Foegeding, E.A. (2011). Effects of protein concentration and CaCl2 on cold-set thickening mechanism of β-lactoglobulin at low pH. *International Dairy Journal*, 21(5), 319–26. http://dx.doi.org/10.1016/j.idairyj.2010.11.014.

Nicolai, T., Britten, M., & Schmitt, C. (2011). β-Lactoglobulin and WPI aggregates. *Food Hydrocolloids*, 25(8), 1945–62. http://dx.doi.org/10.1016/j.foodhyd.2011.02.006.

Nicolai, T., & Durand, D. (2013). Controlled food protein aggregation for new functionality. *Current Opinion in Colloid & Interface Science*, 18(4), 249–56. http://dx.doi.org/10.1016/j.cocis.2013.03.001.

Oboroceanu, D., Wang, L., Brodkorb, A., Magner, E., & Auty, M.A.E. (2010). Characterization of beta-lactoglobulin fibrillar assembly using atomic force microscopy, polyacrylamide gel electrophoresis, and in situ Fourier transform infrared spectroscopy. *J Agric Food Chem*, 58(6), 3667–73. http://dx.doi.org/10.1021/jf9042908.

Pedersen, J.S., & Schurtenberger, P. (1996). Scattering Functions of Semiflexible Polymers with and without Excluded Volume Effects. *Macromolecules*, 29(23), 7602–12. http://dx.doi.org/10.1021/ma9607630.

Sackett, D.L., & Wolff, J. (1987). Nile red as a polarity-sensitive fluorescent probe of hydrophobic protein surfaces. *Analytical Biochemistry*, 167(2), 228–34. http://dx.doi.org/10.1016/0003-2697(87)90157-6.

Schuck, P. (2000). Size-Distribution Analysis of Macromolecules by Sedimentation Velocity Ultracentrifugation and Lamm Equation Modeling. *Biophys J*, 78(3), 1606–19. http://dx.doi.org/10.1016/S0006-3495(00)76713-0.

Schuck, P., & Rossmanith, P. (2000). Determination of the sedimentation coefficient distribution by least-squares boundary modeling. *Biopolymers*, 54(5), 328–41. http://dx.doi.org/10.1002/1097-0282(20001015)54:5<328::AID-BIP40>3.0.CO;2-P.

Serfert, Y., Lamprecht, C., Tan, C.-P., Keppler, J.K., Appel, E., & Rossier-Miranda, F.J., et al. (2014). Characterisation and use of β-lactoglobulin fibrils for microencapsulation of lipophilic ingredients and oxidative stability thereof. *Journal of Food Engineering*, 143, 53–61. http://dx.doi.org/10.1016/j.jfoodeng.2014.06.026.

Stănciuc, N., Aprodu, I., Râpeanu, G., & Bahrim, G. (2012). Fluorescence spectroscopy and molecular modeling investigations on the thermally induced structural changes of bovine β-lactoglobulin. *Innovative Food Science & Emerging Technologies*, 15, 50–6. http://dx.doi.org/10.1016/j.ifset.2012.03.001.

Uhrínová, S., Smith, M.H., Jameson, G.B., Uhrín, D., Sawyer, L., & Barlow, P.N. (2000). Structural Changes Accompanying pH-Induced Dissociation of the β-Lactoglobulin Dimer †,‡. *Biochemistry*, 39(13), 3565–74. http://dx.doi.org/10.1021/bi992629o.

vandenAkker, C.C., Schleeger, M., Bruinen, A.L., Deckert-Gaudig, T., Velikov, K.P., & Heeren, R.M.A., et al. (2016). Multimodal Spectroscopic Study of Amyloid Fibril Polymorphism. *J Phys Chem B*, 120(34), 8809–17. http://dx.doi.org/10.1021/acs.jpcb.6b05339.

Verheul, M., Pedersen, J.S., Roefs, S.P.F.M., & Kruif, K.G. de (1999). Association behavior of native ? *Biopolymers*, 49(1), 11–20. http://dx.doi.org/10.1002/(SICI)1097-0282(199901)49:1<11::AID-BIP2>3.0.CO;2-1.

Vetri, V., & Militello, V. (2005). Thermal induced conformational changes involved in the aggregation pathways of beta-lactoglobulin. *Biophys Chem*, 113(1), 83–91. http://dx.doi.org/10.1016/j.bpc.2004.07.042.

Walter, J., & Peukert, W. (2016). Dynamic range multiwavelength particle characterization using analytical ultracentrifugation. *Nanoscale*, 8(14), 7484–95. http://dx.doi.org/10.1039/c5nr08547k.

Ye, X., Hedenqvist, M.S., Langton, M., & Lendel, C. (2018). On the role of peptide hydrolysis for fibrillation kinetics and amyloid fibril morphology. *RSC Adv.*, 8(13), 6915–24. http://dx.doi.org/10.1039/C7RA10981D.

3.8. Supplementary Material

Supporting information regarding AFM

Additional description of the morphology

The morphology of amyloid aggregates prepared at pH values 2 and 3.5 was analysed with AFM after 0.5, 1, 3 and 5 hours incubation . With increasing incubation time, increasing numbers of aggregates were evident. The thickness of the pH 2 fibrils after 5 h was approximately 3 - 4 nm, the length was 7 to >10 µm. The typical twisting periodic pitch along their contour length was observed for most of the strains. The average height of the worm-like aggregates prepared at pH 3.5 after 5 h was approximately 1 – 3 nm and their length was 0.05 – 0.20 µm. Their shape was heterogenic, due to unsteady height and width variance along the contour length.

Retentate and filtrate controlled by AFM before and after lyophilisation process.

Straight fibrils produced at pH 2.0 and ultra filtrated and lyophilized

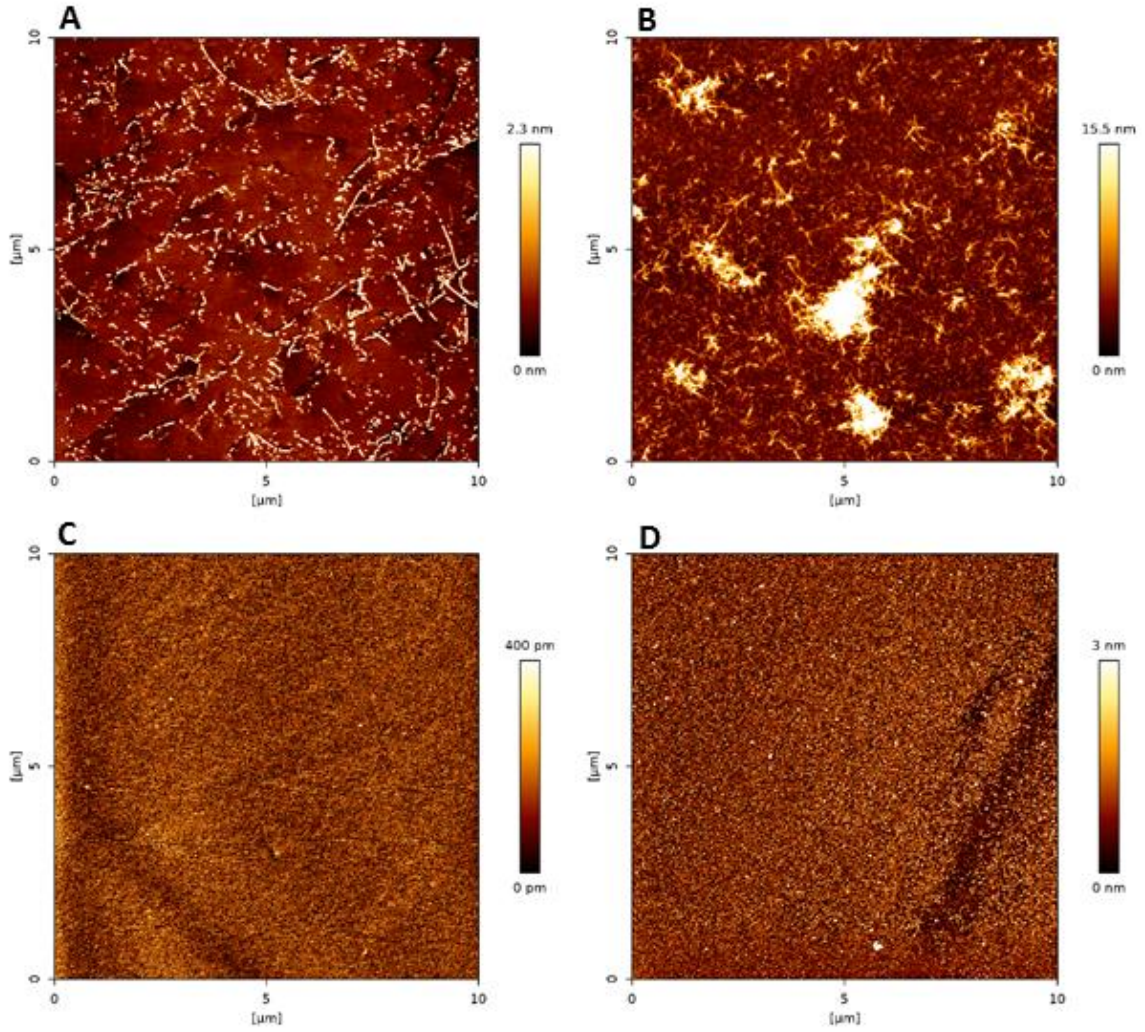

FIG-S 3-7 Fibrils formed at pH 2 and 5 hours at 90°C and low ion concentration processed by ultrafiltration (300 kDa cut off and 1000g*) and lyophilisation. Retentate without (A) and with lyophilisation step (B). Filtrate without (C) and with lyophilisation step (D). Ultrafiltration and lyophilisation process has high impact on morphology of straight fibrils (A + B). No fibrils were found in filtrate (C +D).

Worm-like amyloid aggregates produced at pH 3.5 and ultra filtrated and lyophilized

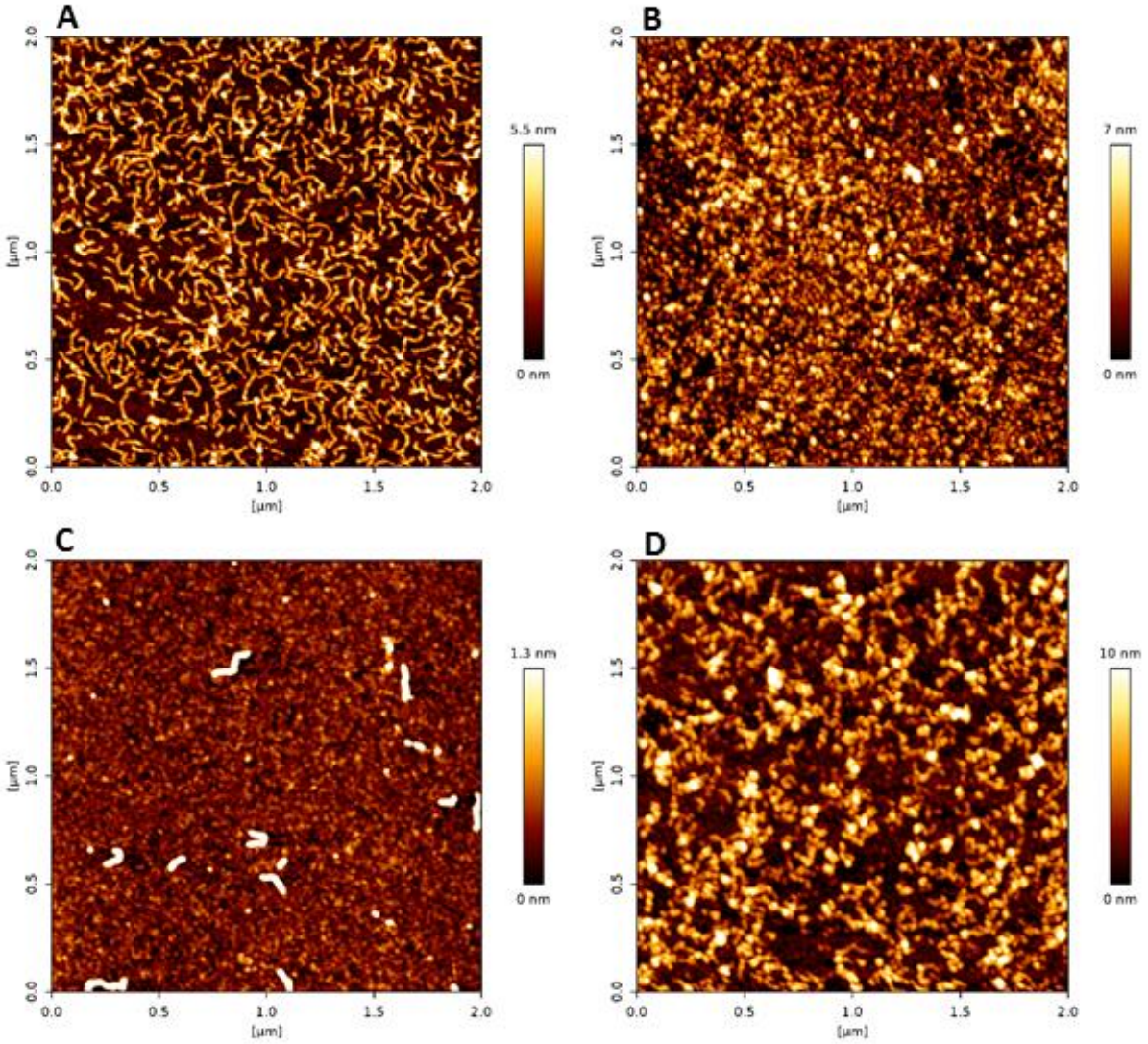

FIG-S 3-8 Worm-like amyloids formed at pH 3.5 and 5 hours at 90°C and low ion concentration processed by ultrafiltration (300 kDa cut off and 1000g*) and lyophilisation. Retentate without (A) and with lyophilisation step (B). Filtrate without (C) and with lyophilisation step (D). Lyophilisation step has high impact on morphology of straight fibrils (B). Worm-like fibrils were found in filtrate (C +D).

Supporting Information regarding analysis of SAXS data

SAXS data were fitted with SAXSview (Doucet et al. 2017) SasView Version 4.1, Zenodo, http://doi.org/10.5281/zenodo.438138). SAXS data have been modelled by scattering function of stiff cylinders of length L and elliptical cross section a and γa (Feigin et al. 1987) Polydispersity of fibrils length has been taken into account as log normal distribution. π

EQU-S 3-1 Scattering function (SAXS) of length distribution

$$I(q) = I(0)\frac{2}{\pi}\int_0^{\pi/2}\int\left[\frac{2J_1\left(qr(\mathrm{a},\gamma\mathrm{a},\phi,\alpha)\right)}{qr(\mathrm{a},\gamma\mathrm{a},\phi,\alpha)}\frac{sin(qLcosa/2)}{qLcosa/2}\right]^2 d\phi \sin\alpha d\alpha$$

where J_1 is the first-order Bessel function and $r(a,\gamma\mathrm{a},\phi,\alpha) = [\mathrm{a}^2 sin^2\phi + (\gamma\mathrm{a})^2 cos^2\phi]^{1/2} sin\alpha$.

The flexibility of the fibrils can be obtained by fitting the full range of scattering curves with function

$I(q) \sim S_{WC}(q,L,b)S_{CS}(q,\mathrm{a},\gamma\mathrm{a})$,

where $S_{wc}(q,L,b)$ is the single chain scattering function for a semi-flexible chain with excluded-volume effects of the contour length *L* and the Kuhn length *b*. A detailed expression for $S(q,L,b)$ can be found in Ref. (Pedersen and Schurtenberger 1996; Chen and Barkley 1998; Chen et al. 2006). $S_{CS}(q,\ \mathrm{a},\ \gamma\mathrm{a})$ represents the scattering of the elliptical cross section of semi-flexible aggregates. It was assumed that there is polydispersity of fibril length as lognormal distribution

EQU-S 3-2 Scattering function (SAXS) of fibril flexibility

$$S_{CS}(q,\mathrm{a},\gamma\mathrm{a}) = \frac{2}{\pi}\int_0^{\pi/2}\left(\frac{2J_1\left(qr(\mathrm{a},\gamma\mathrm{a},\theta)\right)}{r(\mathrm{a},\gamma\mathrm{a},\theta)}\right)^2 d\theta$$

with $r(\mathrm{a},\gamma\mathrm{a},\theta) = [\mathrm{a}^2 sin^2\theta + \gamma\mathrm{a}^2 cos^2\theta]^{1/2}$.

The fitting parameters of the should be taken with caution: the studied q range from 0.02 nm^{-1} allows only to observe objects with a size below 300 nm. In most cases studied here, no Guinier´s region at the lowest q range was visible because the amyloid aggregates were larger

than 300 nm. Therefore, only a rough estimation of the overall mean size of objects in the heterogenous heated sample was possible and solid information can only be obtained on the cross section parameter (circular or elliptical) and the level of flexibility (stiff or with some flexibility). In addition, all different objects in the sample contribute to the SAXS signal, which is strongly influenced by the sample heterogeinity so the results give only a mean scattering profile of these objects. That is why the models of stiff cylinders with elliptical cross section (called "Stiff") or for semiflexible chains (called "Flexible") have been fitted to the scattering curves. The stiff cylinder model applied in present analysis only reflects the local stiffness of random coils in length scale of SAXS observation windows ~ 1-100 nm.

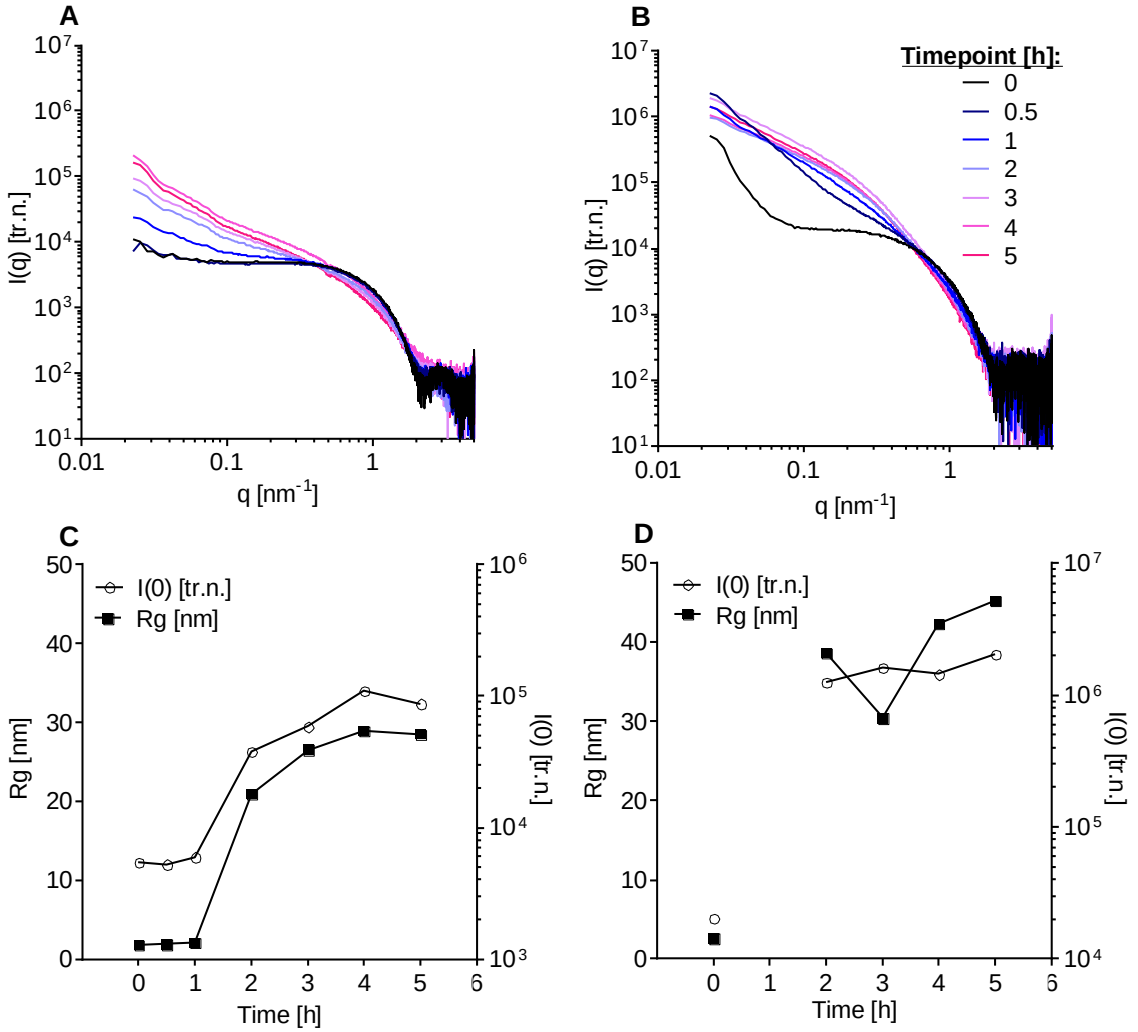

FIG-S 3-9 The SAXS scattering intensities of BLG solutions during 5 h of amyloid aggregation at pH 2 and a sample dilution to 0.25% protein (A) and at pH 3.5 and a sample dilution to 0.5 % protein (B). The SAXS-S-form dependence of the radius of gyration (Rg) (filled symbols) and the scattering at zero angle (I(0)) for different time points of amyloid aggregation are given in (C) and (D) for pH 2 and pH 3.5, respectively. Due to differences in the protein concentration, the scattering intensities are not

comparable between the different pH values. All curves show the merged data of three independent replicates. In Figure D, time points 0.5 and 1 have missing values because the Guinier fitting was not possible.

FIG-S 3-9 The SAXS scattering intensities of BLG solutions during 5 h of amyloid aggregation at pH 2 and a sample dilution to 0.25% protein (A) and at pH 3.5 and a sample dilution to 0.5 % protein (B). The SAXS-S-form dependence of the radius of gyration (Rg) (filled symbols) and the scattering at zero angle (I(0)) for different time points of amyloid aggregation are given in (C) and (D) for pH 2 and pH 3.5, respectively. Due to differences in the protein concentration, the scattering intensities are not comparable between the different pH values. All curves show the merged data of three independent replicates. In Figure**A and B** show the I(q) curves on the log-log scale for different time points of the amyloid aggregation of BLG. The comparison the scattering intensities collected at different fibril concentration is allowed while test measurements perfomed at concentration interval from 0.1 to 2.5% have shown that there is no concentration dependent inter-particle fibril association and interaction for concentration up to 0.5%. At pH 2 **(FIG-S 3-9** The SAXS scattering intensities of BLG solutions during 5 h of amyloid aggregation at pH 2 and a sample dilution to 0.25% protein (A) and at pH 3.5 and a sample dilution to 0.5 % protein (B). The SAXS-S-form dependence of the radius of gyration (Rg) (filled symbols) and the scattering at zero angle (I(0)) for different time points of amyloid aggregation are given in (C) and (D) for pH 2 and pH 3.5, respectively. Due to differences in the protein concentration, the scattering intensities are not comparable between the different pH values. All curves show the merged data of three independent replicates. In Figure**A)**, no growth of fibrils in the first 0.5 h of incubation is evident, as those scattering curves superimpose. The nearly constant scattering intensity in the q-interval 0.1 to 0.7 nm^{-1} for the native and the 0.5 h incubation samples indicates that the mean aggregates are in the order of a few nanometres in size *i.e.*, probably monomers of proteins. An increase in the scattering intensity at low q (<0.1 nm^{-1}) reflects the increasing aggregation process of the samples between 0.5 and 5 h. Simultaneously, the scattering intensity follows the power law behaviour of $I(q) \sim q^{-1}$ in the intermediate q range, which supports the occurrence of larger and rod-like objects as expected for BLG fibrils (Feigin et al. 1987). The determination of the integral parameters of the system, such as radius of gyration (Rg) and scattering at "zero angle" (I(0)) vs time points (Figure 2 C) have been performed using q range intervals which was changing 0.3-0.7 nm^{-1} for initial time points (monomers) and 0.03-0.1 nm^{-1} for later time points (fibrils). Obtained Rg values represent some correlation length in fibrils system. Rg and I(0) follows a well know S-form and allows to determine the different phases in the formation of amyloid fibrils (*i.e.*, lag phase, steep elongation phase and depletion of building blocks). The mean Rg of the whole sample derived from the Guinier analysis starts at 1.8 nm, which is slightly higher than that determined in previous SAXS analyses of BLG monomers at pH 2 (*i.e.*, 1.69 nm (Keppler et al. 2017) 1.52 nm (Verheul et al. 1999)) and hints at some dimer structures. A further increase to 2.0 nm is evident after 1 h incubation. A significant growth can only be observed between 1 and 2 h incubation where the mean Rg increases to ~21 nm. Further incubation has only a minor effect on the Rg and saturation is observed with an Rg of approximately 28 nm after 4 h.

The behaviour of the scattering intensity at pH 3.5 (concentration 0.5%) **(FIG-S 3-9 B)** is more complicated than at pH 2. Initially, at time 0 h, there is constant scattering at an intermediate and a high part of q, which reflects the low and almost constant scattering of few nanometer sized object (*i.e.*, BLG). However, the lowest part of the scattering curve shows some very large objects in micrometer length scale, probably artifacts due to non-proper positioning of sample in capillary. The scattering intensity dramatically increases already after 0.5 h of incubation and in the scattering curve one can observe scattering from rod-like objects ($I(q)\sim q^{-1}$) at an intermediate q, which shows even higher slope $\sim q^{-(1.5\text{-}2)}$ at lower q interval. This is a sign of flexibility of the rod-like shaped aggregates at larger length scale (Jerke et al. 1997; Pedersen and Schurtenberger 1996). Some sign of flexibility is still visible after 1 h incubation. For further incubation, however, $I(q)\sim q^{-1}$ is evident at low and intermediate q, which means that the rod-like objects are rather stiff in the studied length scale. The determination of the S-curve **(FIG-S 3-9 D)** is impaired at pH 3.5, because it is not possible to get a proper interval for time points 0.5 and 1 h for the determination of Rg and I(0). However, an S-shaped curve can be deduced, starting with a Rg of 2.6 nm (consistent with previous findings by SAXS for BLG dimers (Keppler et al. 2015), as expected at pH 3.5). According to the scattering curves **(FIG-S 3-9 B),** a steep increase of the mean Rg is expected already after 0.5 h, until an Rg of ~38 nm is reached after 2 h. Further incubation increases the mean Rg to 42 nm after 4 h and 45 nm after 5 h incubation, revealing a higher aggregation kinetics and higher yield than observed at pH 2.

TAB-S 3-2 SAXS model parameters determined at different time intervals of amyloid aggregation at pH 2 or 3.5. Model: Two different models of rod-like fibrils of elliptical cross section were chosen: "Stiff" and "Flexible with polydispersity in length" (lognormal distribution); number of monomers: The mean number of monomers per fibrils; , <L> : The mean length of the amyloid aggregates in nm; B: the statistical segment length (Kuhn length) which is a measure of the flexibility of the chain in nm; Elliptical cross-section and value of the minor semiaxis of cross section (A) and axis ratio ( ). For pH 3.5 no results are listed for 5 h, as no fit was possible.

Incubation time [h] and pH value		*Model*	*Number of monomers*	*<L> [nm]*	*B [nm]*	*Small semiaxis A [nm] and axis ratio γ [nm]*
0.5 h	pH 2	Stiff	1.4	4.3±0.3		1.7±0.1, 1
	pH 3.5	Flexible	>2000	>1000	15.5±0.1	1.4±0.1, 1.8±0.1
1 h	pH 2	Stiff	1.4	4.8±0.4		1.6±0.1, 1
	pH 3.5	Flexible	>2000	>1000	4.4±0.1	1.3±0.1, 2.0±0.1

2 h	pH 2	Stiff	2.7	12±1		1.4±0.1, 1
	pH 3.5	Stiff	~1000	~1000		1.4±0.1,4.9±0.1
3 h	pH 2	Stiff	15	77±5		1.3±0.1,1
	pH 3.5	Stiff	>2000	>1000		1.7±0.1, 4.7±0.1
5 h	pH 2	-	-	-	-	-
	pH 3.5	Stiff	>2000	>1000		2.0±0.1, 3.9±0.1

At pH 2, there is quite a long lag phase up to 1 h where the average species in the sample has a mean size of 1.3 BLG monomers with a contour length of 4 nm and a cross-section of 1.7 nm. These monomers slowly grow to short cylinders with a length of 12 nm and slightly decreasing cross sections to 1.4 nm after 2 h incubation and a further growth is evident to long and stiff cylinders of 550 nm length and no further change of the cross section after 4 h.

After 0.5 and 1 h incubation at pH 3.5, the amyloids grow in length (already much larger than the observation window of SAXS experiments) and flexible objects with cross sections of only one monomer (1.7 nm) occur. The Kuhn length decreases from 15 nm at 0.5 h to 4 nm after 1 h incubation, which reflects an increasing flexibility of the observed aggregates.

At pH 3.5, already at the beginning the mean number of monomers observed is 3.2 and a length of ~7 nm is evident. This means that dimers or trimers are in solution, as expected for this pH value and as observed in **FIG 3-2**. After 0.5 and 1 h incubation at pH 3.5, the amyloids grow in length (already much larger than the observation window of SAXS experiments) and flexible objects with cross sections of only one monomer (1.7 nm) occur. The Kuhn length decreases from 15 nm at 0.5 h to 4 nm after 1 h incubation, which reflects an increasing flexibility of the observed aggregates. After further incubation (*i.e.*, 2 to 5 h) the aggregates transform to stiff rod-like objects with larger elliptical cross-section of 4 monomers. The large cross-section indicates the intertwining of up to 4 aggregates. The fibril retentate (*i.e.*, the purified amyloid aggregates) contains long flexible fibrils, a contour length of more than 2000 nm and an elliptical cross section of an axis ratio of 3.4 nm. The Kuhn length of the worm-like aggregates is ~10 nm and therefore the aggregate is intrinsically more flexible than the pH 2 fibrils. The filtrate seems to contain large amyloid aggregates, which shows an insufficient filtering process here in contrast to the pH 2 fibrils. It is unclear why the observed aggregates in the filtrate seem to be larger than those in the retentate or why the purified aggregates have a smaller size than

the samples during production of fibrils after 3, 4 or 5 h incubation. One can speculate that an interaction between the amyloid and the non-amyloid material occurs here.

Supporting information regarding AUC

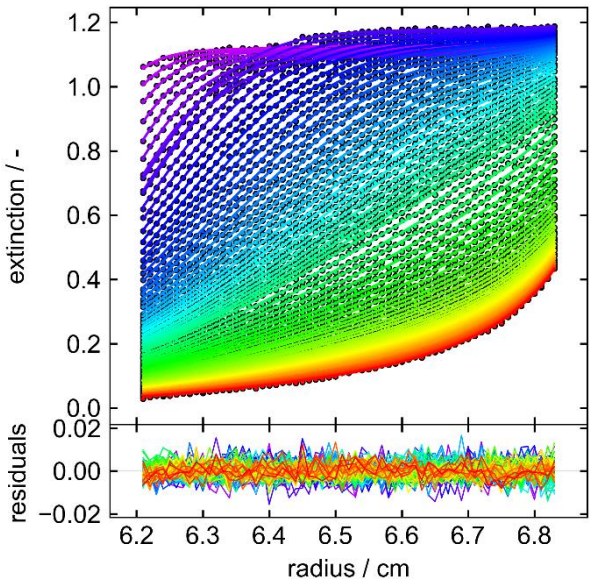

FIG-S 3-10 Measured sedimentation data (open circles) at a wavelength of 280 nm and fitted model (straight lines). The residuals are ploted underneath. No systematics can be observed. The Plot was created using GUSSI (Brautigam 2015).

Molar masses of the individual species in the pH 2 and pH 3.5 samples after 5 h incubation were obtained from the c(s)-method in SEDFIT.

The sedimentation and diffusion coefficient are obtained from fitting Lamm's equation. In a sector shaped centrifuge cell, Lamm's equation describes the evolution of concentration c, which is dependent on the time t and the radial-position r:

EQU-S 3-3 Lamm's equation (AUC)

$$\frac{\partial c}{\partial t} = \frac{1}{r}\frac{\partial}{\partial r}\left[r \cdot D\frac{\partial c}{\partial r} - s \cdot \omega^2 \cdot r^2 \cdot c\right]$$

However, s and D are linked via this expression:

EQU-S 3-4 calculation of the aggregate diameter (AUC).

$$D = k_B T\left(2\left(\frac{1}{\bar{v}} - \rho_S\right)\right)^{0.5} \cdot \left(18\pi s^{0.5}\left(\eta\frac{f}{f_0}\right)^{\frac{3}{2}}\right)^{-1}$$

T is the temperature, kB denotes Boltzmann's constant, η and ρ_S are the solvent viscosity and density, respectively. In the expression above, an important parameter is the frictional ratio f/f0,

which includes the change of the frictional coefficient f with respect to the frictional ratio of an equivalent sphere f_0. The frictional ratio is highly dependent on the structure

The molar mass M of the particles is then calculated from the Svedberg Equation (see below) from the fitted values for s and D, taking into account that the partial specific volume and the frictional ratio are constant for all species:

EQU-S 3-5 Svedberg Equation (AUC)

$$M = \frac{s \cdot R \cdot T}{D(1 - \bar{v} \cdot \rho_S)}$$

In this expression, N_A denotes Avogadro's constant and R is the universal gas constant.

Supporting information regarding zeta-potential

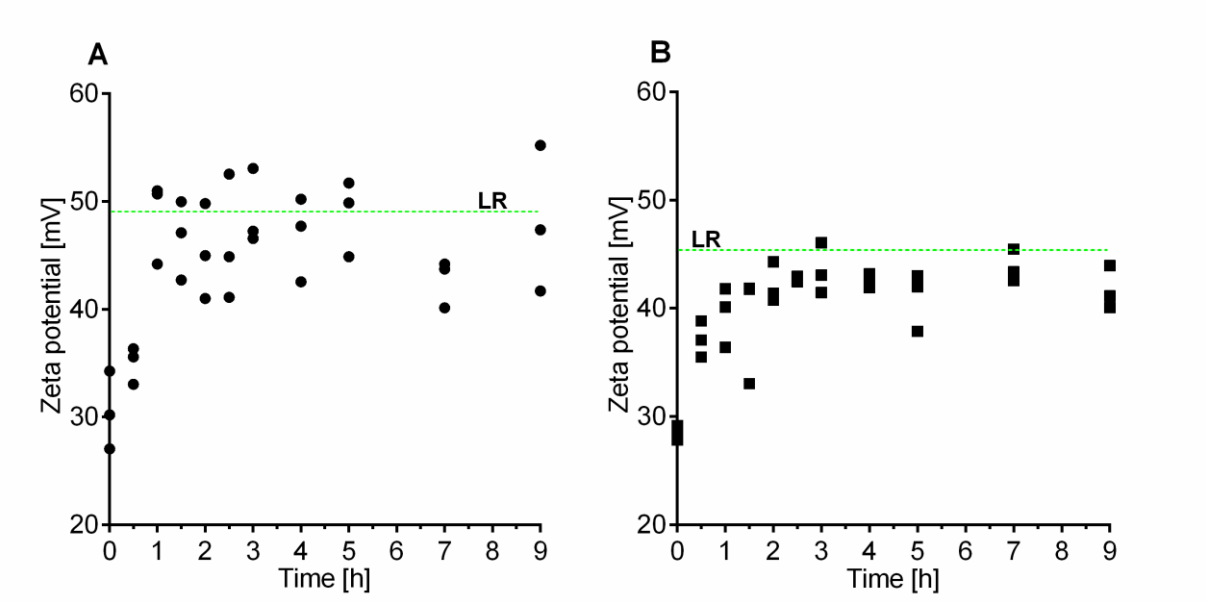

FIG-S 3-11 Change in zeta-potential (mV) during fibril formation of BLG at pH 2 (A) and pH 3.5 (B) measured with Zeta-sizer at 0.1 wt% protein concentration. All measurements were conducted in three individually prepared samples and each measurement point is given. The dotted line indicates the zeta-potential determined for purified lyophilized retentate (LR).

As illustrated in **FIG-S 3-11 A**, the initial zeta-potential at pH 2 was 30.5±3.7 mV. During fibril formation, the zeta-potential increased sharply for the first 1 h to 48.6±3.8 mV, until saturation was reached after 3 h at approximately 48 mV. The mean of LR was only slighty higher at 49.3 ±3.0 mV. At pH 3.5 zeta-potential increased from 28.5±0.7 mV (native BLG) to 39.4 ± 2.8 mV (amyloid aggregates) **(FIG-S 3-11 B).** Similarly to pH 2 fibril formation, the plateau was reached

after 3 h at 43 mV, with a subsequent slight drop. For LR, a mean of 45.6 ± 1.3mV was observed.

Supporting information regarding filtration of heated samples

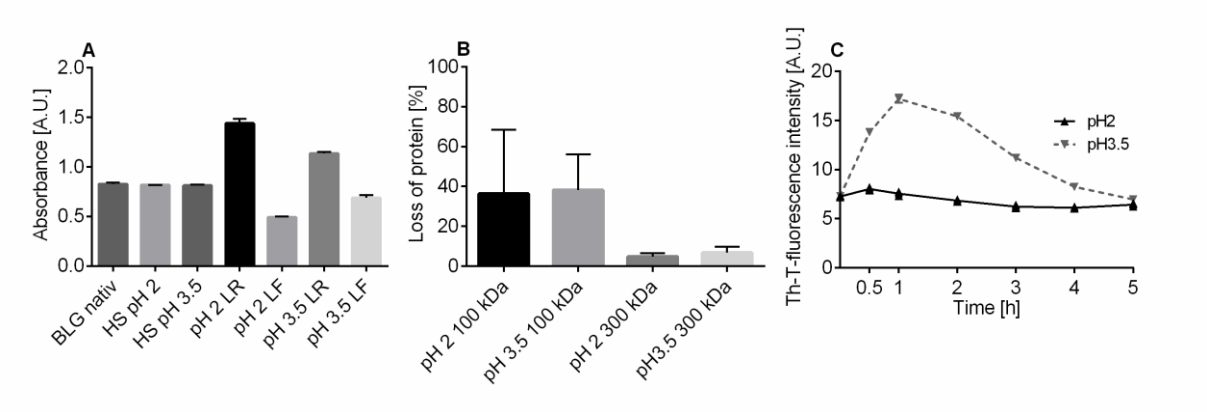

FIG-S 3-12 Measurement of absorbance of native beta-lactoglobulin (BLG native), of heated sample (HS) at pH 2 and pH 3.5, of isolated lyophilised retentate (LR) and isolated lyophilised filtrate (LF) prepared at pH 2 and pH 3.5. All samples contain 0.1 wt% protein. B) Determination of native protein loss (at 278 nm wavelength) during centrifugal ultrafiltration with 100kDa or 300 kDa membranes. C) Analysis of pH 2 and pH 3.5 filtrate after centrifugal ultrafiltration with 300 kDa of HS determined by ThT-assay. All measurements were conducted in triplicate and are listed as mean and standard deviation.

The following experiments were conducted to define the optimal method for the determination of conversion rates and protein concentration. The methodology for investigating the yield by mechanical separation of the heated sample solution (HS) into amyloid (LR) and non-amyloid material (LF) by ultrafiltration contains three critical steps: 1. Protein determination by UV vis at 278 nm **(FIG-S 3-12 A)**; 2. Comparison of different ultrafiltration cut-offs (*i.e.,* 100 kDa and 300 kDa) **(FIG-S 3-12 B);** 3. ensuring that no amyloid material passes through the membrane **(FIG-S 3-12 C).**

For protein determination, the results confirm that during the fibrillation process there is no change in the absorption at 278 nm wavelength of HS during the 5 h fibrillation process: The absorption before and after heating is ~0.8 a.u. at 0.1 wt% protein in the solution. However, it is interesting that the absorption measurements of the respective isolated fractions (LR and LF) differ significantly at both pH values (*i.e.,* $A_{278\,nm} = 1.439 \pm 0.046$ for LR and 0.493 ± 0.009 for LF at pH 2). The difference between LR and LF at pH 3.5 is not as pronounced as at pH 2 (*i.e.,* $A_{278\,nm} = 1.136 \pm 0.016$ for LR and 0.688 ± 0.029 for LF). The comparison of different filter cut-off demonstrates that the use of the 100 kDa cut-off filters led to a considerable loss of native protein at both pH values (up to 71 and 51 wt% BLG at pH 2 and pH 3.5, respectively) **(FIG-S 3-12 B)**. In contrast, the maximum loss of native protein in the 300 kDa filters was at 6.2 wt% (pH 2) or 9.9 % (pH 3.5). When using the filter with 300 kDa cut-off, however, it was evident that immature amyloid aggregates formed at pH 3.5 in the first 5 h diffused through the

filter membrane as analysed by ThT. The maximum leakage of the filtrate was reached after 1 h with 17 a.u. No leakage was observed after 5 h incubation, which indicates that all amyloid aggregates in the sample are considerably bigger than monomers or dimers.

Supporting information regarding conversionrate

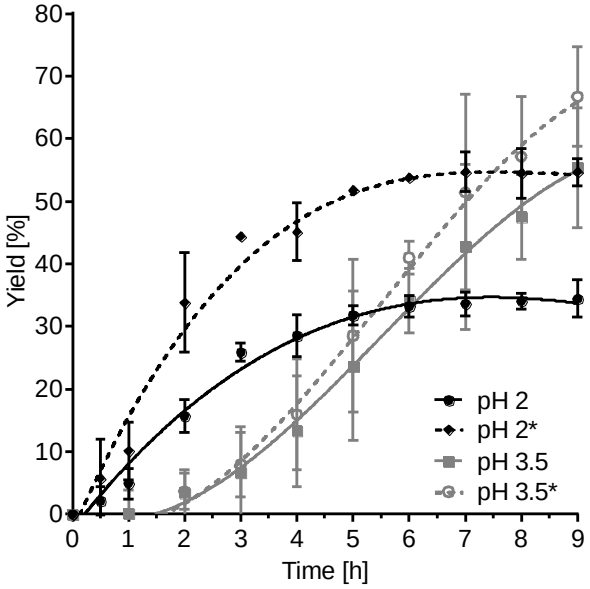

FIG-S 3-13 Determination of conversion rate (yield in %) by centrifugal ultrafiltration with 300 kDa filters and analysis of protein concentration by UV-VIS spectroscopy at 278 nm during 9 h of fibril formation at pH 2 (black) and pH 3.5 (grey). The protein concentration of pH 2 and pH 3.5 filtrate was determined by either calibrated with beta-lactoglobulin (solid line) or with LF (dotted line). These curves follow a third-degree polynomial and are only used for a better illustration of the approximately course over time. All measurement were conducted in three replicates and are listed as mean and standard deviation.

The yield determination is based on the measurement of the protein loss in the filtrate. Since the absorption at 278 nm for the isolated lyophilised filtrate (LF) differs from the absorption of the native BLG **(FIG-S 3-12 A)**, but the LF is only formed during the process, the following method was calibrated with both materials (native BLG and LF). The fibril yield by filtration gave evidence that the formation of pH 2 and pH 3.5 fibrils follows a different kinetics: As illustrated in **FIG-S 3-13** at pH 2, a short lag-phase of 1 hour was observed in the beginning. Then the amount of LR increased to 30 – 44% and reached a plateau at 32 - 52 % after 5 h. Further incubation had only a minor effect of additional 4 to 11 % amyloid material. At pH 3.5, a longer lag phase than observed for the pH 2 fibrils is evident by centrifugal filtration (**FIG-S 3-13)**, but then a strong increase of aggregates up to 23 – 28 % after 5 h and to 55 - 67 % after 9 h incubation is evident. After 9 h incubation, still no plateau of the aggregate formation

occurred. During the observed lag phase of the pH 3.5 amyloid formation by filtration, a leakage of small LR occurred in the first 3 h **(FIG-S 3-12 C)**.

Supporting information regarding colorimetric assays

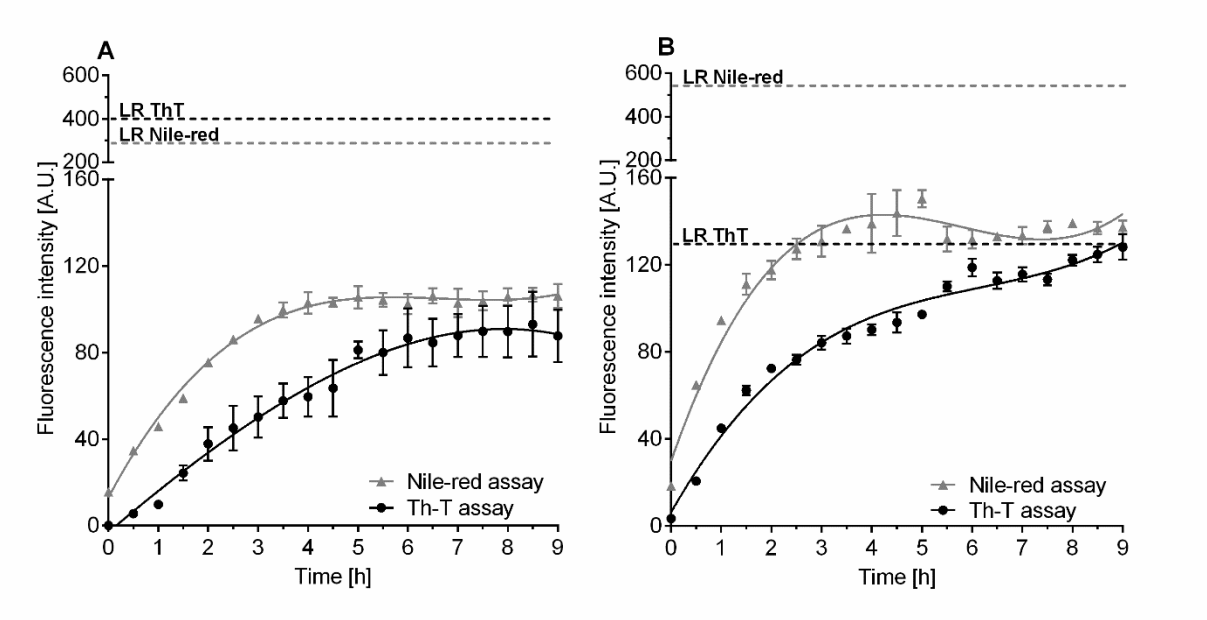

FIG-S 3-14 Monitoring of amyloid material in the protein sample by Thioflavin-T-assay and Nile-red-assay during the formation process of pH 2 fibrils (A) and pH 3.5 amyloid aggregates (B) during 9 hours at 1 wt% (ThT) and 2.5 wt% (Nile-red) protein. The lines follow a third-degree polynomial and are only used for a better illustration of the approximately course over time. All measurements were conducted in triplicate and are listed as mean and standard deviation.

In order to verify the yield measurements, colometric assays were conducted in the following to the whole sample (HS) as well as to the respective isolated purified fractions (LR). Similar to the yield determination, the ThT-assay for fibrils prepared at pH 2 shows a short lag phase in the first 2 h followed by an increase of the ThT-fluorescence until it reaches a plateau at 88 ± 10 a.u. after 5-7 h incubation **(FIG-S 3-14 A)**. In contrast, at pH 3.5, the samples show a steep increase in ThT FL uorescence during the first 2 h and a further more slight and linear increase for the next 7 hours to 128 ± 5.8 a.u. of maximum intensity. Similar to the yield determination, no plateau was observed after 9 h incubation.

The Nile-red assay at pH 2 and pH 3.5 follows roughly the trend of the ThT assays at both pH values, albeit no plateau was evident and the equilibrium phase was reached after ~4 h incubation for both pH values (**FIG-S 3-14 A and B)**. At pH 2, a plateau was reached at 105 ±

5 a.u., whereas at pH 3.5 the Nile red fluorescence intensity reached a maximum at 150 ± 4.0 a.u. after 5 h, revealing a higher hydrophobicity for pH 3.5 aggregates.

The analysis of the pure pH 2 fibril fraction (LR) shows a ThT FL uorescence of 402 ± 1.3 a.u. and a Nile red fluorescence of 296 ±9.3 a.u. for a 1% protein solution. For the purified amyloid aggregates at pH 3.5, a low ThT FL uorescence of only 115 ± 1.9 a.u. is evident, but an extremely high increase of the Nile red fluorescence to 545.6 ± 3.6 a.u.

Supporting information regarding ATR-FTIR

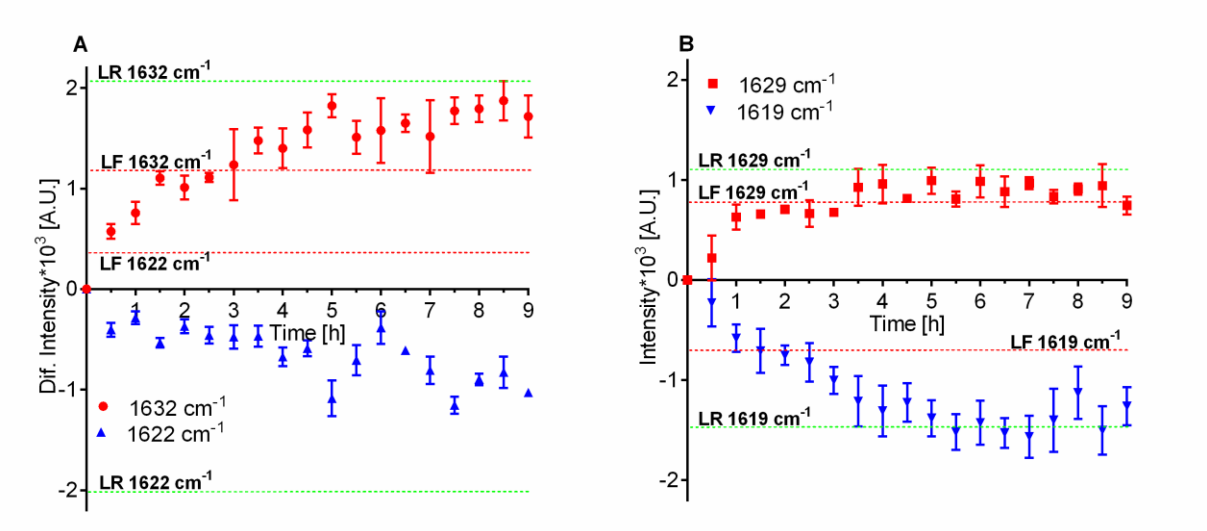

FIG-S 3-15 Intensity of intramolecular and intermolecular beta-sheets from 2nd derivation difference spectra of the Amid I band (1600 to 1700cm-1) measured with ATR-FTIR are provided in graphic A and B for pH 2 and pH 3.5 samples respectively. All measurement were conducted in triplicate and listed as mean and in graphic E and F with standard deviation.

In order to further visualize the kinetics of the pH 2 and pH 3.5 beta-sheet changes, the native beta-sheet band intensity as well as the intermolecular beta-sheets in the 2nd derivation spectra were plotted as a function of the protein incubation time.

In **FIG-S 3-15 A,** the upper curve illustrates that the reduction (which corresponds to a signal increase in the 2nd derivation) of intramolecular beta-sheets (1632 cm^{-1}) follows saturation kinetics at pH 2. A strong loss of native beta-sheets is evident in the first 1 to 1.5 h of incubation, while saturation is reached after ~4 to 5 h incubation. The increase (which corresponds to a signal decrease in the 2nd derivation) of intermolecular beta-sheets (1622 cm^{-1}) is illustrated by the lower curve in **FIG-S 3-15 A** and similarly reaches equilibrium after ~4-5 h incubation. It is also evident that LR has almost the double signal intensity compared to the HS at saturation, which could hint at a conversion rate of ~40-50 %. The pH 3.5 worm-like aggregates exhibited the strongest decrease of intramolecular beta-sheet band at 1629 cm^{-1} in the first 60 min of the process and saturation was reached between 3 to 4 h incubation. The intermolecular beta sheets

(1619 cm^{-1}) increased strongly up to saturation after 5 h **(FIG-S 3-15 B).** When comparing HS after 5 to 9 h incubation at pH 2 or pH 3.5, it is apparent that the intermolecular beta-sheets are less pronounced at pH 2 in equilibrium. Conversely, LR at pH 2 has more intense amyloid character than at pH 3.5.

References

[1] M. Doucet, J.H. Cho, G. Alina, J. Bakker, W. Bouwman, P. Butler, K. Campbell, M. Gonzales, R. Heenan, A. Jackson, P. Juhas, S. King, P. Kienzle, J. Krzywon, A. Markvardsen, T. Nielsen, L. O'Driscoll, W. Potrzebowski, R. Ferraz Leal, T. Richter, P. Rozycko, A. Washington, Sasview Version 4.1, Zenodo, 2017.

[2] L.A. Feigin, D.I. Svergun, G.W. Taylor (Eds.), Structure Analysis by Small-Angle X-Ray and Neutron Scattering, Springer US, Boston, MA, s.l., 1987.

[3] J.S. Pedersen, P. Schurtenberger, Scattering Functions of Semiflexible Polymers with and without Excluded Volume Effects, Macromolecules 29 (23) (1996) 7602–7612. https://doi.org/10.1021/ma9607630.

[4] Y. Chen, M.D. Barkley, Toward understanding tryptophan fluorescence in proteins, Biochemistry 37 (28) (1998) 9976–9982. https://doi.org/10.1021/bi980274n.

[5] W.-R. Chen, P.D. Butler, L.J. Magid, Incorporating intermicellar interactions in the fitting of SANS data from cationic worm-like micelles, Langmuir 22 (15) (2006) 6539–6548. https://doi.org/10.1021/la0530440.

[6] J.K. Keppler, D. Martin, V.M. Garamus, C. Berton-Carabin, E. Nipoti, T. Coenye, K. Schwarz, Functionality of whey proteins covalently modified by allyl isothiocyanate. Part 1 physico-chemical and antibacterial properties of native and modified whey proteins at pH 2 to 7, Food Hydrocolloids 65 (2017) 130–143. https://doi.org/10.1016/j.foodhyd.2016.11.016.

[7] M. Verheul, J.S. Pedersen, S.P.F.M. Roefs, K.G. de Kruif, Association behavior of native ?: -lactoglobulin, Biopolymers 49 (1) (1999) 11–20. https://doi.org/10.1002/(SICI)1097-0282(199901)49:1<11:AID-BIP2>3.0.CO;2-1.

[8] G. Jerke, J.S. Pedersen, S.U. Egelhaaf, P. Schurtenberger, Static structure factor of polymerlike micelles: Overall dimension, flexibility, and local properties of lecithin reverse micelles in deuterated isooctane, Phys. Rev. E 56 (5) (1997) 5772–5788. https://doi.org/10.1103/PhysRevE.56.5772.

[9] J.K. Keppler, D. Martin, V.M. Garamus, K. Schwarz, Differences in binding behavior of (-)-epigallocatechin gallate to β-lactoglobulin heterodimers (AB) compared to homodimers (A) and (B), J. Mol. Recognit. 28 (11) (2015) 656–666. https://doi.org/10.1002/jmr.2480.

[10] C.A. Brautigam, Calculations and Publication-Quality Illustrations for Analytical Ultracentrifugation Data, Meth. Enzymol. 562 (2015) 109–133. https://doi.org/10.1016/bs.mie.2015.05.001.

4. Manuscript 2 – Aggregation kinetics of amyloid aggregates in aqueous systems

The threshold of amyloid aggregation of beta-lactoglobulin: Relevant factor combinations

Timon R. Heyn[a], Julian Mayer[b], Hendrikje R. Neumann[c], Christine Selhuber-Unkel[c], Arno Kwade[b], Karin Schwarz[a], Julia K. Keppler[a, d,]

Published previously in Journal of Food Engineering (2020): Heyn, Timon R.; Mayer, Julian; Neumann, Hendrikje R.; Selhuber-Unkel, Christine; Kwade, Arno; Schwarz, Karin; Keppler, Julia K. (2020): The threshold of amyloid aggregation of beta-lactoglobulin. Relevant factor combinations. DOI: 10.1016/j.jfoodeng.2020.110005.

[a] Institute of Human Nutrition and Food Science, Division of Food Technology, Kiel University, 24118 Kiel, Germany

[b] Institute of Particle Technology, Technical University Braunschweig, 38106 Braunschweig, Germany

[c] Institute of Materials Science, Department for Biocompatible Nanomaterials, Kiel University, 24143 Kiel, Germany

[d] Laboratory of Food Process Engineering, Wageningen University, 6708 PB Wageningen, The Netherlands

4.1. Abstract

This study identifies critical factor combinations of pH, temperature, stirring speed, protein and ion concentration that specifically affect the lag-, and growth phase of beta-lactoglobulin amyloid aggregation and provides information on how, when and why certain factor combinations affect the onset of amyloid aggregation.

Conditions at the threshold of amyloid formation were chosen to prolong the lag and growth phase for several hours. Temperature was the most important factor in all aggregation stages. Interactions between low pH and temperature in the growth phase were caused by elevated protein denaturation at low pH (DSC). Interactions between stirring speed and temperature in the lag phase were caused by viscosity-dependent shear stress (CFD-simulation).

Even if none of the factor combinations could shift the onset of amyloid aggregation, important factor combinations were identified that favour the onset of amyloid aggregation. Therefore, the results of this study could be relevant for industrial production.

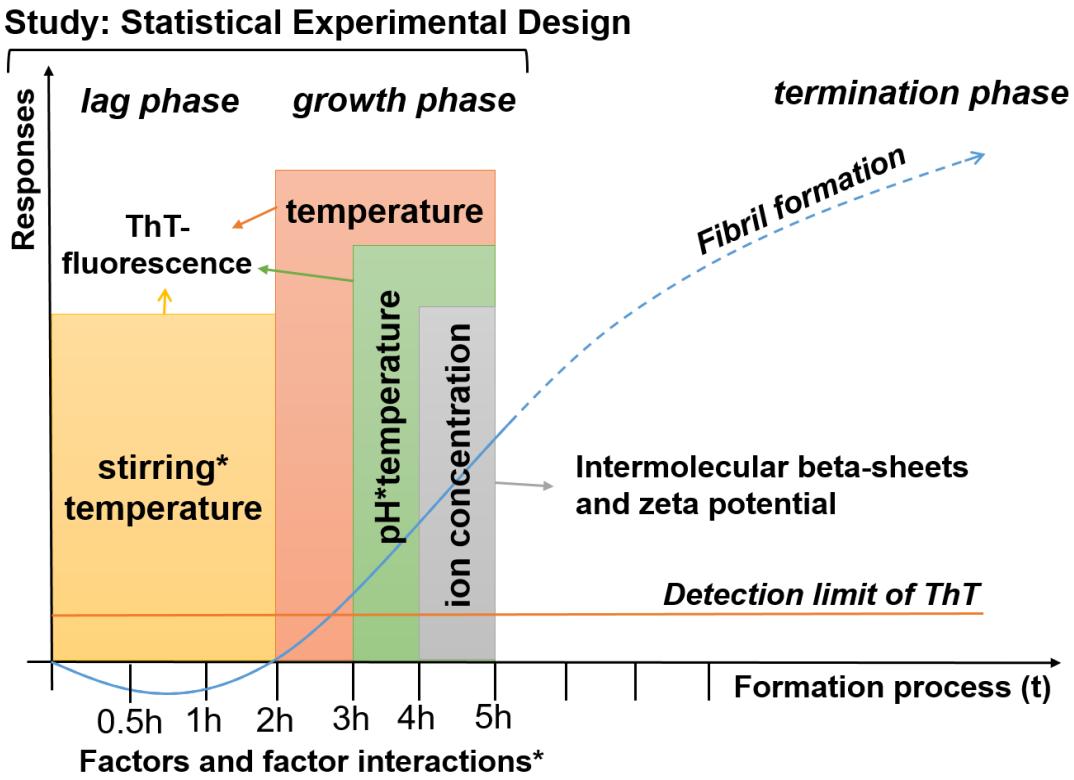

Abbreviations

BLG, beta-lactoglobulin;

ThT, Thioflavin-T

AFM, atomic force microscopy

ATR-FTIR, attenuated total reflection Fourier transform infrared spectroscopy

DSC, differential scanning calorimetry

CFD, computational fluid dynamics

VOF, volume of fluid

DOE; design of experiments

4.2. Introduction

One of the most frequently studied fibril forming proteins in whey is beta-lactoglobulin (BLG), which forms several micrometre long fibres at low pH values and high temperatures after several hours of incubation (Jung et al. 2008; Loveday et al. 2010; Nicolai and Durand 2013). BLG-fibrils are of industrial interest because of their improved functional properties to form gels (Mohammadian and Madadlou 2016), stabilise foams (Peng et al. 2017) and emulsions (Gao et al. 2017), as well as for microencapsulation (Serfert et al. 2014). Additionally, their potential for nano- and biomaterial applications are of increasing interest (Knowles and Mezzenga 2016).

In order to use the entire functional potential of the aggregates, the formation of temperature-induced BLG fibrils should be investigated in detail. In recent years, this has led to the intensive study of various influencing factors.

The pH value is the primary influencing factor for acid hydrolysis, providing peptide building blocks for the semiflexible fibrils at pH values < 3.0 (Akkermans et al. 2008b; Ye et al. 2018), while unhydrolysed proteins aggregate at pH values ≥ 3.5 (Keppler et al. 2019). Simultaneously, pH-related electrostatic repulsion affects the ordered aggregation—and thus the different fibril morphologies—observed with increasing pH value (Loveday et al. 2010).

Since incubation temperature significantly affects protein denaturation and acid hydrolysis, it is a key factor for the aggregation kinetics (Loveday et al. 2012b; Loveday 2016). Also the molecular motion (Ciuciu et al. 2016; Dvorsky et al. 2000; Einstein 1905) and dielectric constant (Havinga 1961; Pitera et al. 2001; Zhu et al. 2015) of the protein solution are influenced by the incubation temperature. Both factors in turn influence protein interactions.

Likewise, protein concentration is related to interaction effects between particles in the solution (Arnaudov and Vries 2006) and thus influences the aggregation kinetics (Pellarin and Caflisch 2006) and morphology (Ye et al. 2018).

Moreover, the ion concentration reduces the charge of the particles and thus the electrostatic repulsion effects (Loveday et al. 2017) which results in different morphologies and aggregation kinetics (Loveday et al. 2010).

Stirring speed provides additional energy to the protein solution and leads to a turbulent shear flow, which influences the particle motion with respect to particle collision while exerting a certain level of shear stress on the protein (Bliatsiou et al. 2018; Ng et al. 2016). Therefore,

moderate stirring enhances the amyloid aggregation (Bolder et al. 2007; Ng et al. 2016) by shortening the lag phase (Dunstan et al. 2009).

Notably, the incubation time can be viewed as an amplifier of the previous factors. Amyloid aggregation can be divided into the time-dependent lag, growth and termination phase (Loveday et al. 2017). The lag phase is characterised by providing the fibril building blocks and can be skipped or shortened by adding so-called "seeds" (Loveday et al. 2012). Fibril growth begins with nucleation, whereby the proteins/peptides are first reversibly and then tightly bound together (Pellarin and Caflisch 2006). The termination phase is purported to be caused by the depletion of available building blocks (Loveday et al. 2017).

However, to date the influence of factor combination on the lag and growth phases were only investigated under optimal conditions (temperature >80 °C, pH value <2.5) for fibril formation (Loveday et al. 2011). It can be hypothesised that a combination of the necessary factors (discovered by screening) with other optional factors might also affect fibril formation and that during the lag phase other factor combinations than in the growth or stationary phase are relevant. In addition to identifying these factor combinations, the present study also aims to elucidate their underlying mechanisms in further experiments.

The investigation of this critical point provides information on how strongly, when and why certain factor combinations are capable of shifting the threshold of amyloid aggregation. Since a major challenge is the detection of minimal fibrillation, several independent methods were used, including mechanical separation (ultrafiltration), structure characterisation (Fourier transform infrared spectroscopy (FTIR)), fluorescence spectroscopy (Thioflavin-T (ThT)-assay), and the imaging of aggregates (atomic force microscopy (AFM)). To obtain a mechanistic understanding of the factor combinations, additional experiments were conducted with differential scanning calorimetry (DSC) and computational fluid dynamics (CFD) modelling.

4.3. Materials and Methods

4.3.1. Materials

BLG was obtained from *Davisco Foods International Inc.* (Eden Prairie, US) with 97 % protein and 96 % BLG in dry matter. Calculated NaCl content was 49.6 µmol g^{-1} protein. ThT (> 95 %) acid was obtained from *EMD Chemicals Inc.*, while all additional chemicals were obtained from *Sigma Aldrich Inc* were analytical grade. All experiments were conducted with ultra-pure water (>17 MΩ; total oxidizable carbon <5ppb).

4.3.2. Methods

4.3.2.1. Preparation of BLG solutions and production of BLG fibrils

For screening BLG fibril solutions were prepared as described by (Heyn et al. 2019).

To screen the effects of protein concentration, pH value, temperature, stirring velocity and NaCl concentration, only one of these parameters was changed at a time (**TAB 4-1**). The pH values of the solutions were adjusted with 6 M HCl and experiments were conducted in 100 ml Schott bottles with a 8.5 x 2 mm cylindric stirring bar.

TAB 4-1 Parameters used for the screening.

Parameters	*Basic parameters*	*Additional parameters*
Temperature [°C]	90	40, 55, 70, 75, 85, 95
pH value	2	1*, 3, 4, 5, 6, 7, 8, 9, 10*, 11*, 12*
Protein concentration. [wt%]	2.5	0.1, 0.25, 0.5, 1, 1.5, 5
NaCl concentration [mM]	0	5, 15
Stirring velocity [RPM]	350	0, 700, 1300

**no data available for Fourier transform infrared spectroscopy*

For the Design of Experiments (**DOE**) the parameters used are provided in **TAB 4-2**. Water bath temperature was controlled and protocolled using an EBI 2 temperature logger (*Ebro Elektronic GmbH*, Germany).

TAB 4-2 Parameters used for the design of experiments.

Parameters	*Level-1-factors*	*Center-point-factors*	*Level-2-factors*
Temperature [°C]	70	72.5	75
pH value	2.5	2.75	3
Protein concentration [wt%]	1	1.25	1.5
NaCl concentration [mM]	0	5	10
Stirring velocity [RPM]	200	250	300

After 0.5, 1, 2, 3, 4 and 5 h, samples were taken and cooled in an ice-water bath for 30 min and stored at 4 °C until further use. For all following dilution processes, pH-adjusted Milli-Q-Water was used.

4.3.2.2. Physico-chemical characterization of native and fibrillar BLG

To monitor fibril growth during incubation, the development of amyloid beta sheets was followed by the intensity of Thioflavin-T-fluorescence (ThT FL) and the conversion rate was analysed by centrifugal ultrafiltration. The secondary structure was analysed using ATR-FTIR and fibril morphology by AFM. The concentrations of monomer and peptide material were analysed via size exclusion chromatography (SEC) from dissociated samples and the level of hydrolysis was calculated from the loss of monomeric BLG. All these experiments were performed following the protocol of (Heyn et al. 2019).

To obtain numerical values for the relative changes in beta-sheets, respective changes in the intensities of the second derivative of FTIR wavenumber 1632 cm^{-1} (intramolecular beta-sheets) and FTIR band wavenumber 1622 cm^{-1} (intermolecular beta-sheets) were determined. From the numerical intensity values at the respective wavenumbers at time t_i, the intensity values of the same wavenumber at time t_0 of the respective measurement series were subtracted. Mean and standard deviation were calculated from triplicate measurements.

4.3.2.3. Differential scanning calorimetry (DSC)

DSC was performed using the DSC250 (*TA Instruments, New Castle, USA*). BLG solution with 1 wt% was prepared as described by Heyn et al. (2019) and adjusted to the respective pH values of 2.0, 2.5 and 3.0.

The temperature was increased by 5 °C min^{-1} to a final temperature of 110 °C, followed by an isothermal phase for 1 min. The temperature was then decreased by 20 °C min^{-1} to a final temperature of 20 °C, followed by an isothermal phase of 1 min. Temperature-ramps to 110 °C and 20 °C were then repeated without isothermal phases. The enthalpy, as well as the onset and peak of denaturation temperature, were then calculated.

4.3.2.4. Statistical analysis of screening, DOE and fitting of values

Statistical analysis of the collected data was conducted by GraphPad PRISM (*version 6.07, GraphPad Software, San Diego, USA*). A significant increase of the ThT-values was verified

by two-way ANOVA with Tukey's multiple comparison test at the 0.05- significance level. The increase of ThT-values as a function of time was fitted by the sigmoidal equation

EQU 4-1 Increase of amyloid structures in dependence of time **.**

$$f_t = \alpha + \ ((\beta - \ \alpha))/(1 + \ exp((\gamma - \ t)/k) \ )$$

in where f_t is fluorescence at time *t*, *k* is the slope and α, β and γ are arbitrary constants.

Level of hydrolysis was fitted by an exponential plateau equation:

EQU 4-2 Increase of hydrolysed material in dependence of time.

$$h_t = h_0 - (h_0 - \ h_m \ ) * \ exp((-k * t))$$

in where h_t is the level of hydrolysis at time *t*, *k* is the rate constant, h_0 is the amount of hydrolysed material at t_0 and h_m is the maximum amount of hydrolysed material.

For the DOE, the means of the responses "ThT-intensity" and "fibril yield" were calculated. The DOE was planned and evaluated by Stat-Ease Design-Expert (*version 10.0.7.0 Stat-Ease Inc.*, Minneapolis, USA). A fractional 2level 5factorial design type with three centre points and one replicate was created.

4.3.2.5. Computational fluid dynamics (CFD)

CFD were used to obtain additional information regarding the influence of flow and stress parameters during amyloid fibril formation of BLG. The exact shape of the Schott bottle was provided by the manufacturer and the dimensions of the stirring bar were measured manually. The geometries used in the simulation were created using SolidEdge ST9 in stereolithography (STL) format. The simulations were conducted with open-source software OpenFOAM-5.0. The solver interDyMFoam was chosen for isothermal non-miscible incompressible fluids and multiphase flow with the volume of fluid (VOF) method, which includes mesh motions, optional topology changes and adaptive re-meshing. The mesh generation was performed with the tools "blockMesh" for the basic mesh (60 cells in x, y, and z direction each) and "snappyHexMesh" for the implementation of the STL geometries as well as the detailing and refinement of the mesh. The refined mesh has a total cell number of 299,212. A section through the created mesh can be seen in **FIG 4-1 A**. A finer mesh was created in the area of the glass walls and the stirring bar to account for zones of high velocities and stressing. As evident in **FIG 4-1 B**, a rotational zone with the OpenFOAM method of arbitrary mesh interfaces (AMI) was generated to perform the rotation of the stirring bar. The stirring bar velocity was set to 20.944 (200 RPM) and 31.416 rad s^{-1} (300 RPM), respectively. The regions of suspension and

air were generated with "setFields" in such a way that the glass was filled with suspension up to a height of 19 mm. The standard k-ε model was used to deal with turbulent flow in the stirred fluid. The basic governing equations (conservation of mass and momentum) were calculated using the basic Navier-Stokes and Reynolds-Averaged equations. The equations of continuity and motion were solved to attain velocities and velocity profiles, eddy energy (k) and eddy dissipation (ε). Thereafter, shear rates and shear stresses were calculated, with images of the setup and flow pattern being generated using ParaView 5.4.0. For the initial conditions at the walls, a zero flux was imposed to computational domains and gravity was set to 9.81 m s^{-2} in the negative vertical direction. The viscosity of the fluid was modelled as Newtonian in the relevant shear rate range above 1 s^{-1}. The viscosity parameters were determined by a shear rate ramp (10^{-4} to 10^{3} s^{-1}) at 70 °C and 75 °C of 1.25 wt% BLG and fibril solutions with a Bohlin Gemini rheometer (*Rotometic drive 2, Malvern Instruments,* UK) equipped with double gap geometry.

The shear-thinning behaviour of the fibrils and the specific viscosities, which are passed through between the start and end time, were not taken into account. The surface tension of the suspension was set to the constant 72.75E-03 kg s^{-2}.

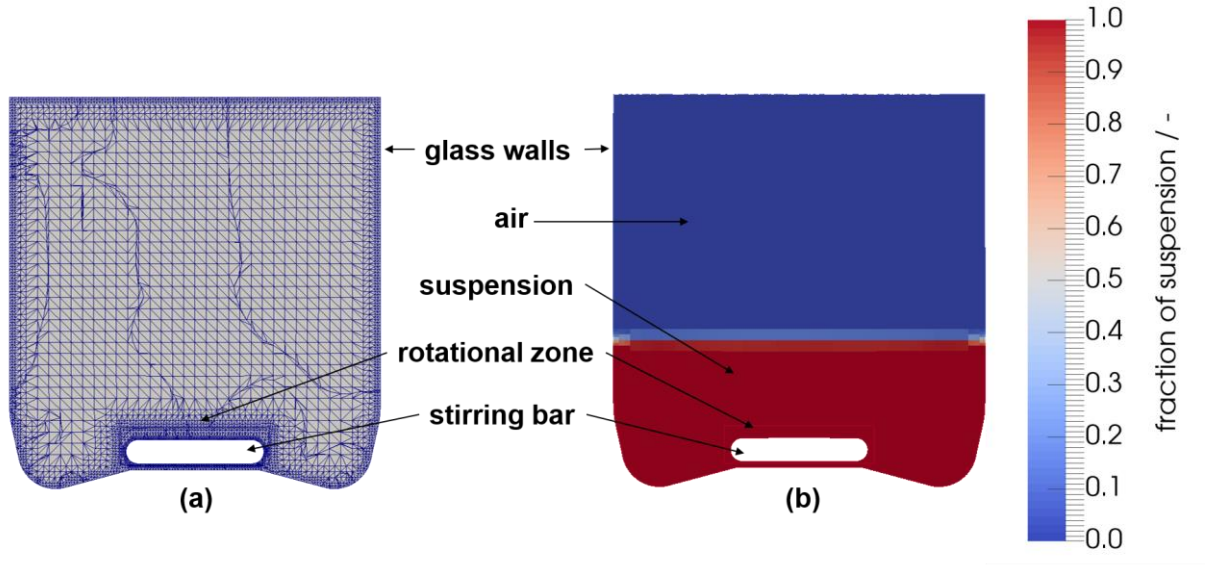

FIG 4-1 Meshing (A) and general geometrical setup of the CFD simulation (B).

4.4. Results & Discussion

4.4.1. Screening for the threshold of amyloid aggregation

The influence of acidic pH values (i.e., pH 1–4), temperature (i.e., 55–95 °C), protein concentration (0.1–5 wt%), stirring speed (0–1300 RPM) and ion concentration (0–15 mM NaCl) on fibril formation were screened during a period of 5 h using the ThT-assay and FTIR. The influence of the pH value on morphology was also investigated by AFM.

The observed threshold parameters were observed to be in a temperature range between 70 and 75 °C (**FIG 4-2 C and D**) since no significant aggregation was observed below 70 °C during 5 h incubation at pH 2. At 90 °C, the threshold pH value range was between pH 2.5 to 3 (**FIG 4-2 A and B**) since evidence for the first occurrence of worm-like aggregates together with fibrils was observed at pH 3. This indicates an altered amyloid-like morphology and aggregation behaviour from straight fibrils to worm-like aggregates (Keppler et al. 2019), while only straight fibrils were evident in representative AFM images at pH 2 (Heyn et al. 2019). While higher protein concentrations resulted in higher ThT FL intensities (**FIG 4-2 E and F**), the proportion of intermolecular beta-sheets did not differ significantly. Therefore, a range between 1 and 1.5 wt% protein concentration was chosen at pH 2 and 90 °C. Low protein concentration also excludes effects caused by the viscoelasticity of more concentrated protein solutions. Concentrations lower than 1 wt% were not possible due to the detection limit of the utilised methods.

Moreover, the addition of NaCl up to 15 mM showed no effect on amyloid aggregation; therefore the chosen threshold was between 0 and 10 mM. Higher stirring speed (between 350 and 1300 RPM) increased the aggregation kinetics—especially at the beginning of the process at pH 2 and 90 °C (**FIG 4-2 G and H**). The stirring speed range of 200 to 300 RPM was chosen since stirring speeds greater than 300 RPM resulted in increasing air intake (**FIG 4-6**) while stirring speed lower than 200 RPM did not result in a continuous circulation.

The described screening results are mostly in agreement with other observations on pH value (Jung et al. 2008; Krebs et al. 2009; Loveday et al. 2011; Serfert et al. 2014), ion concentration, temperature (Loveday et al. 2011), protein concentration (Schleeger et al. 2013) and stirring speed (Ng et al. 2016).

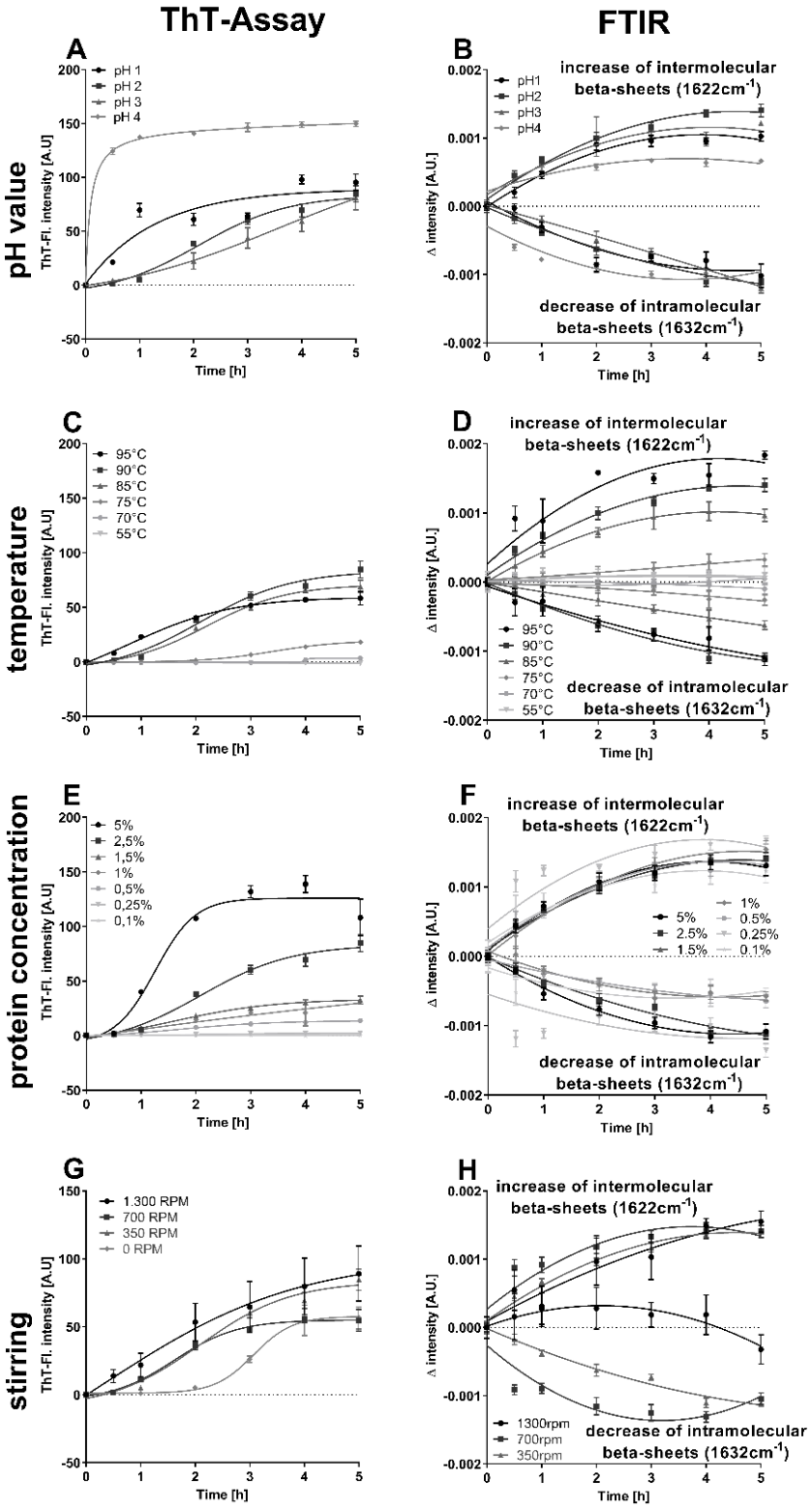

FIG 4-2 Influence of pH values (A and B), temperature (C and D), protein concentration (E and F) and stirring velocity (G and H) on Thioflavin-T-fluorescence (ThT FL) and beta-sheet alteration (FTIR) during the first 5 h of fibril production. For improved visibility, a sigmoidal (ThT FL) or a second-order polynomial (FTIR) fitting of measurement points was conducted. Standard process parameters were pH 2, 90 °C heating temperature, 2.5 wt% protein concentration, 350 RPM stirring and 0 mM NaCl.

4.4.2. Statistical experimental design

The 2^5 factorial design was conducted via 35 randomised experiments using the threshold parameters determined in the screening experiments (**TAB 4-2**). The amyloid aggregation was measured by several different methods, called "responses": ThT-assay (responses "*ThT FL t0.5" – t5*), centrifugal ultrafiltration (response "*fibril yield*"), FTIR (response "*Delta 1632 cm^{-1}*" and "*Delta 1622 cm^{-1}*") and zeta-potential (response "*zeta-potential*"). In addition, the ThT FL data from six time points over 5 h of incubation were fitted by non-linear regression and the correlation coefficient (R^2) was taken (response "*regression fitting*").

The limit of quantification for the ThT-assay was 1.58 a.u., while 0.73 a.u. was the limit of detection. As illustrated in **FIG 4-2**, the level of ThT FL —even just above the detection limit—was a suitable value to describe the formation of fibrils. Analysis with centrifugal ultrafiltration and FTIR did not reach detection limits in most of the cases and were only listed as supportive results for ThT-assay. Nevertheless, the observed secondary structural responses correlated well with the ThT FL results: Intramolecular beta sheets (*Delta 1632 cm^{-1}*) decreased (correlation factor (cf): -0.332) and intermolecular beta sheets (*Delta 1622 cm^{-1}*) increased (cf: 0.301) when the *ThT FL t5* increased. In addition, the fibril yield was also positively correlated with *ThT FL . t5* (cf: $\leq$0.603).

TAB 4-3 Coefficient table of the statistical experimental design of significant factor-response combinations.

Responses	**Intercept**	***Factors***					***Factor interactions***	
		A	**b**	**C**	**D**	**e**	**Ab**	**be**
ThT FL int. t0.5	*-0.198*		*-0.057[c]*			*0.065[c]*		0.219[b]
ThT FL int. t1	*-0.178*		*-0.069[c]*			*0.068[c]*		0.222[b]
ThT FL int. t2	*-0.087*		*0.071[c]*			*0.125[c]*		0.238[b]
ThT FL int. t3	*0.293*		**0.393[a]**			*0.119[c]*		*0.216[c]*
ThT FL int. t4	*1.598*	-0.107[b]	**0.391[a]**			*0.044[c]*	**-0.159[a]**	*0.024[c]*
ThT FL int. t5	*1.866*	*-0.111[c]*	**0.622[a]**			*0.087[c]*	**-0.196[a]**	*-0.0115[c]*
Regression fitting	*0.579*	**-0.071[a]**	**0.253[a]**			*0.034[c]*		*-0.058[c]*
fibril yield	*5.235*		**1.695[a]**			*0.367[c]*		*0.281[c]*
Delta 1632 cm-1	*4.037*	0.432[b]	**-0.603[a]**	*0.003[c]*	*-0.095[c]*	*-0.158[c]*		*0.049[c]*
Delta 1622 cm-1	*3.108*		*1.203c*		**2.589[a]**	*1.386[c]*		*0.566[c]*
Zeta-potential	*24.008*				-1.383[b]			

Significance level of calculated coefficient: [a] **$p < 0.05$**, [b]:$p < 0.10$, [c] *$p >= .10$*
Factors: pH value (A), temperature (b), protein concentration (C), NaCl concentration (D), stirring velocity (e)
ThT FL int.: Thioflavin-T fluorescence intensity

Consideration of the time factor during the process (only ThT-assay) showed an initial decrease in ThT FL for all experiments, followed by an increase after 3 h and a maximum average value of 2.69 ± 2.66 a.u. after 5 h. If only runs with a high temperature (75 °C) were considered, the initial ThT FL decrease was even lower and the first significant increase was already reached after 2 h (instead of 3 h), while a maximum ThT FL of 5.07 ± 2.02 a.u. occurred after 5 h. When only runs with a low temperature factor (70 °C) were considered, only weak significant differences were observed after 5 h processing.

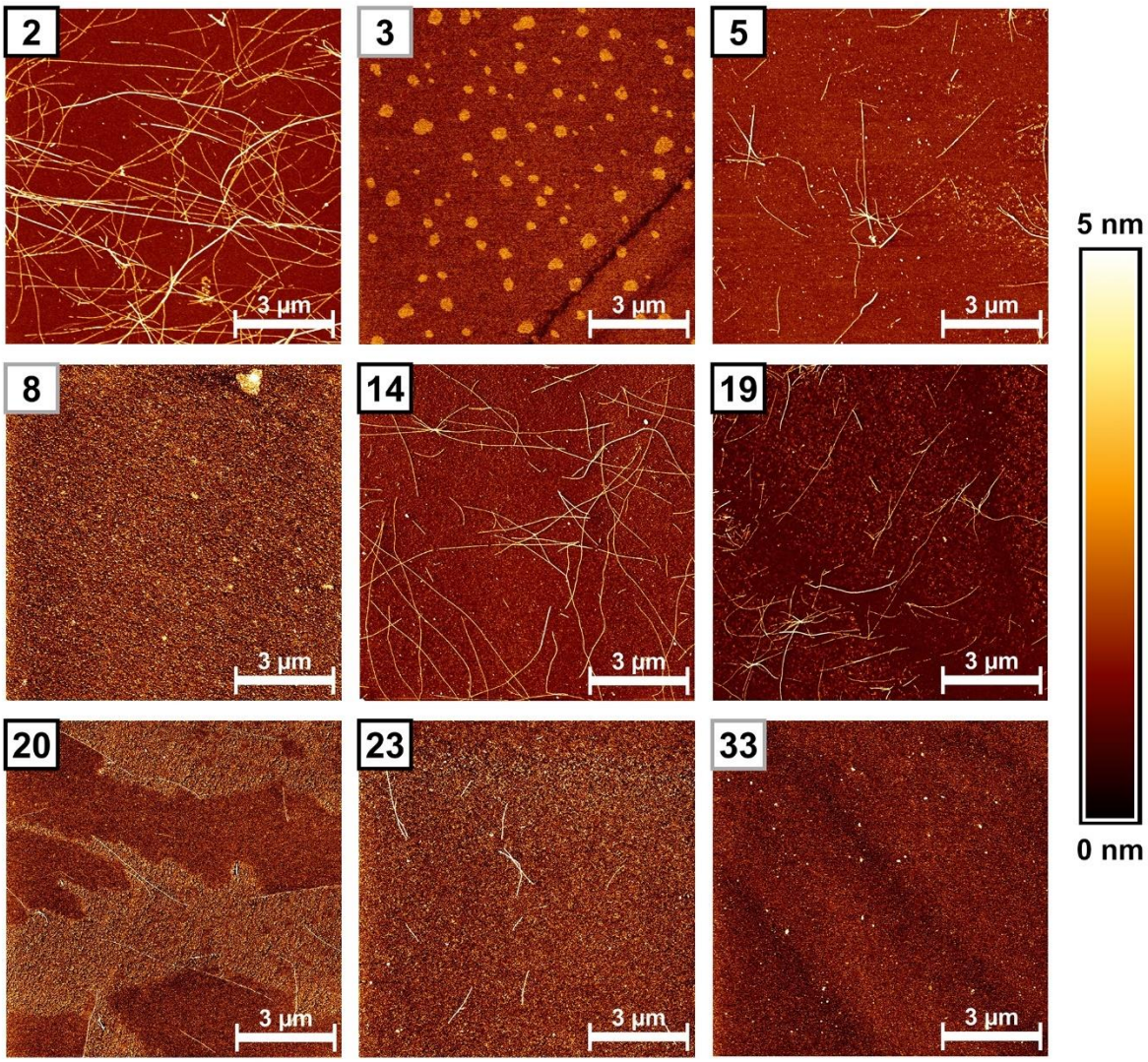

FIG 4-3 Atomic force microscopy images of samples with 0.01 wt% protein. Factor combinations leading to fibril formation (black border): Run2 (ThT FL : 8.899 a.u.); Run5 (ThT FL : 2.841 a.u.); Run14 (ThT FL : 6.74 a.u.); Run19 (ThT FL : 2.84 a.u.); Run23 (ThT FL : 1.633 a.u.); Centre point Run20 (ThT FL : 1.419 a.u.); Runs without fibril formation (grey border): Run3 (ThT FL : 0.229 a.u.); Run8 (ThT FL : 0.578 a.u.); Run33 (ThT FL : 0.350 a.u.).

The pH value (**factor A**) influenced the *regression fitting* in a negative manner (calculated coefficient (cc): -0.071) (**FIG 4-3**). Furthermore, the intramolecular beta sheets (*Delta 1632 cm*$^{-1}$) seemed to increase at higher pH values (cc: 0.432).

The temperature (**factor b**) showed the strongest influence on most responses (**TAB 4-3**). A significant positive temperature-dependent effect was evident for the ThT FL after 3, 4 and 5 h incubation (cc: 0.393 to 0.622) (e.g. Run2 (ThT FL : 8.9 ± 0.62 a.u.), Run7 (ThT FL : 7.9 ± 0.61 a.u.), Run31 (ThT FL : 7.3 ± 0.61 a.u.) and Run17 (ThT FL : 7.1 ± 0.62 a.u.)): all of these runs were at a high temperature level (75 °C). All runs with a temperature equal to or above 75 °C were quantifiable. It has to be assumed that some of the runs at 70 °C also produced fibrils (for example run 23) (**FIG 4-3**). Also, the *regression fitting* (cc: 0.253), *fibril yield* (cc: 1.695), as well as the decrease of intramolecular beta sheets (*Delta 1632 cm^{-1}*) (cc: -0.603) were influenced by temperature (**FIG 4-3 A to C**).

The **ion concentration** (**Factor D**) affected the increase of intermolecular beta sheets (*Delta 1622 cm^{-1}*) (cc: 2.589), while the *zeta-potential* was negatively (cc: -1.383) influenced (**TAB 4-3**).

No significant effects on any response were detected for the **protein concentration (Factor C**) or the **stirring speed (Factor E)**.

The pH value showed no effect on the threshold of fibril formation as a single factor, however the response of *ThT FL t5* was influenced by the pH value in combination with the temperature (cc: -0.196) (**Interaction Factor Ab**) (**TAB 4-3**). This interaction occurred at high temperature levels (75 °C) and led to higher ThT values at lower pH value levels (pH 2.5) (**FIG 4-4 G**).

Another interaction was observed between the stirring speed and the temperature (**Interaction Factor be**), which influenced the ThT FL in the first 2 h (cc: 0.219 to 0.238) (**TAB 4-3**). At low stirring speed (200 RPM) ThT FL was negatively affected with increasing temperature, while exhibited a positive effect at high stirring speed (300 RPM) (**FIG 4-4 D to F**). Since amyloid aggregation and the associated ThT FL increase were related to a shift from the intramolecular to the intermolecular beta-sheets (Heyn et al. 2019), the correlation effect between fibril yield, ThT-assays and FTIR results is explainable.Observation of the ThT FL during the incubation period showed a decrease in the first 2 h compared to the initial sample (t0 = native BLG). Notably, a detectable amyloid aggregation did not occur until the third hour of the process. This indicates conformational changes of the native BLG being accompanied by a lower binding capacity of the ThT molecule at the beginning of the process (Krebs et al. 2005).

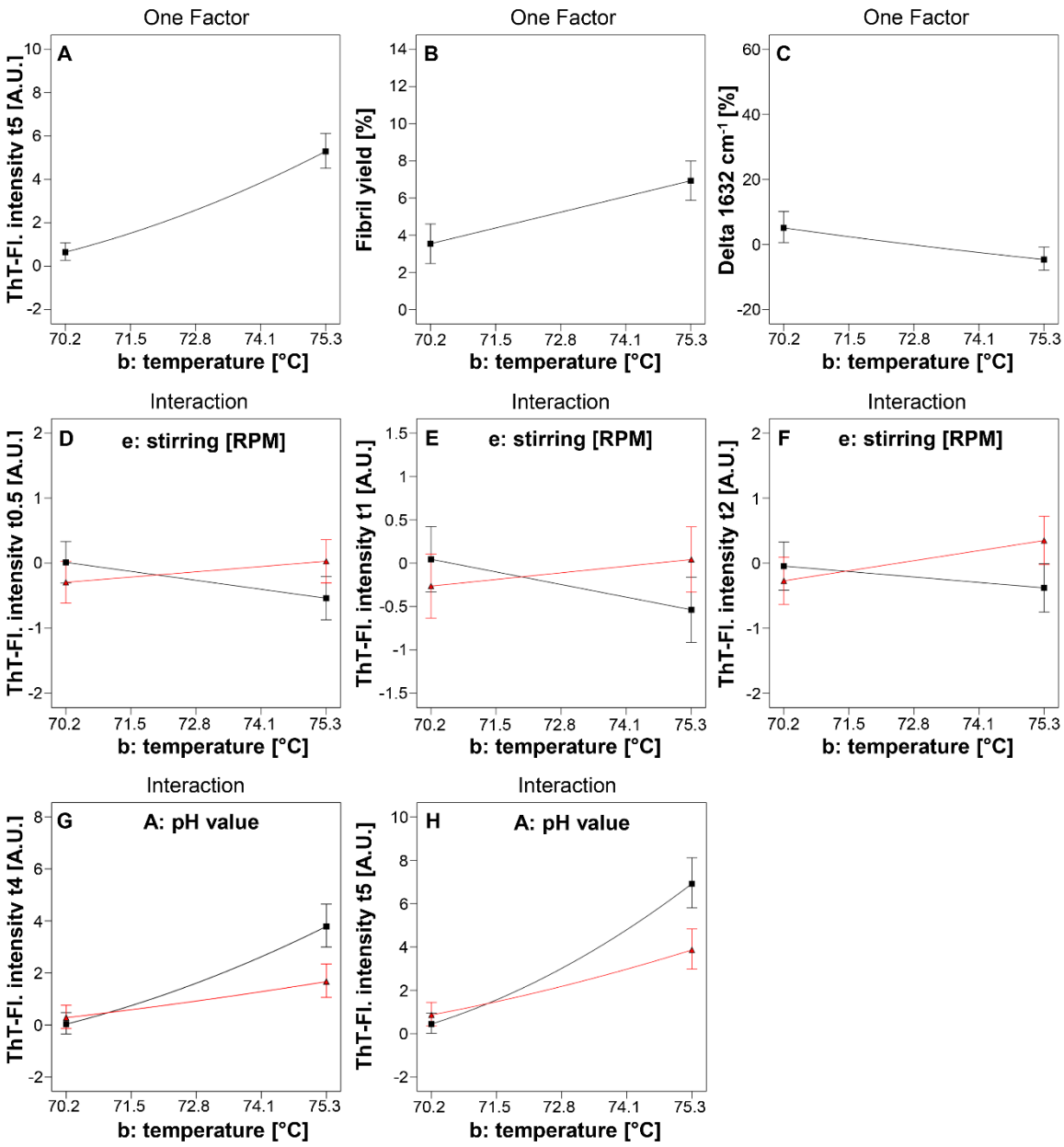

FIG 4-4 Influence of temperature on Thioflavin-T-fluorescence (ThT FL) after 5 h (A), fibril yield (B) and intramolecular beta sheets (C) at pH 2.75, 1.25 wt% protein concentration, 5 mMol NaCl and 250 RPM stirring. Interaction of stirring*temperature as an influencing factor on ThT FL t0.5 (D), t1 (E) and t2 (F). Stirring at 300 RPM (Δ) and 200 RPM (□) (Other parameters are pH 2.75, 1.25 wt% protein concentration and 5 mMol NaCl). Interaction of pH value*temperature (Ab) to influence ThT FL t4 (G) and t5 (H). pH 3 (Δ) and pH 2.5 (□) (Other parameters are 1.25 wt% protein concentration, 5 mMol NaCl concentration and 250 RPM stirring velocity). The curve between Level 1 and Level 2 values is hypothetical and the respective curvature was calculated using the position of the centre points.

This can include the unfolding as well as the accompanying hydrolysis of the protein (Mishra et al. 2007). Therefore, the first 2 h of the present experiment can be considered the preparatory lag phase of the process. The process then enters into the growth phase, in which the nucleus begins to grow above a detectable size (Loveday et al. 2017). That these phases can be reached slower or faster, depending on the temperature, has already been described (Loveday et al.

2012). The initiation phase is considerably extended due to the selected low factor values. Therefore, the present experimental setup at the threshold to amyloid aggregation can be regarded as a closer look into the lag and initial stages of the growing phase of amyloid aggregation. Notably, that the observed factor combinations at different time points are either strong effects that influence the aggregation process in a timely manner—and can thus be directly assigned to the different phases of amyloid aggregation—or weak effects that accumulate slowly and reach a significant intensity with delay.

First and primarily, an effect of temperature on fibril formation was observed during the growing phase (≥3 h). This is a confirmation of the hypothesis that temperature might be an important factor for the denaturation of BLG, its hydrolysis rate and/or the aggregation kinetics of the building blocks. This question is investigated and discussed in greater detail in **chapter 4.4.3**.

After 4 h, an interaction between the pH value and temperature was observed, with a stronger amyloid aggregation at lower pH values. This effect opposes the increased electrostatic repulsion at lower pH values (Bhattacharjee 2016; Gilbert et al. 2014; Krebs et al. 2009). The lower pH value had a decreasing effect on the required denaturing temperature of the protein and thus accelerated the amyloid aggregation. This question is investigated in **chapter 4.4.4** with the help of a DSC investigation. A similar interaction at higher temperatures and more acidic pH values (between pH 1.5 and 2.5) than applied in the present experiments was described by (Loveday et al. 2011). The observed interaction could be explained by the temperature and pH-dependent kinetics of hydrolysis and the associated supply of fibril building blocks (Kroes-Nijboer et al. 2011). However, no pH-dependent threshold shift can be derived from this since the effect only occurs at higher temperatures.

Another effect that influences the ThT FL during the lag phase (i.e. below 3 h incubation here) was stirring speed in the incubation glass vessel in combination with temperature. Notably, both factors influence particle movement in the solution. In addition to the temperature-dependent effect, a shear-dependent effect may also play a role in protein conformation (Rahaman et al. 2015). These effects are investigated in greater detail in **chapter 4.4.5** via CFD simulation.

As expected, zeta-potential decreased due to increased ion concentration (Bhattacharjee 2016). The increase of intermolecular beta-sheets (~1622 cm^{-1}) is described in the literature in the course of amyloid aggregation (Baldassarre et al. 2016; Kavanagh et al. 2000). The positive effect of NaCl concentration on the intensity increase of this secondary structure can be

attributed to the neutralisation of repulsive electrostatic interactions by Na^+ ions (Bryant and McClements 2000).

4.4.3. Influence of temperature on amyloid aggregation

To determine whether the temperature is only crucial in the first stage but not in the later stages of fibril growth, the standard heating protocol was changed after a defined period of time. Therefore, the temperature was lowered from 90 °C to either 30 °C or 60 °C after 2 and 3 h, while all other parameters were maintained.

As presented in **FIG 4-5**, the ThT FL in the process of fibril formation at 90 °C reached an intensity of 38.2 ± 7.1 a.u. after 2 h and 53.9 ± 1.3 a.u. after 3 h (**FIG 4-5**). If the temperature was lowered to 30 or 60 °C at the respective time points, the ThT FL increase ($k_{ThT)}$ was significantly lower with $\Delta \ln k_{ThT} = -3.7$ (30 °C) and $\Delta \ln k_{ThT} = -2.1$ (60 °C) compared to 90° C in the two scenarios. Furthermore, SEC analysis illustrates that the loss of BLG through hydrolysis was followed by a decreasing exponential function, as previously described by (Kroes-Nijboer et al. 2011). The level of hydrolysis reached ~30 % after 2 h and ~41 % after 3 h. Moreover, the temperature reduction to 30 °C led to a decrease in the hydrolysis rate by $\Delta \ln k_h = -6.63$ compared to 90 °C, while at 60 °C a hydrolysis rate of $\Delta \ln k_h = -2.89$ was calculated by the Arrhenius equation described by (Kroes-Nijboer et al. 2011).

The results indicate that the fibril formation process was interrupted by a temperature drop regardless of the incubation time. The strong influence of temperature on amyloid aggregation during the initiation phase was highlighted by the fact that protein denaturation—and thus acid hydrolysis—was induced. However, the irreversible denaturation of BLG at 90 °C might be completed in the first few hours of the process (Keppler et al. 2014; Loveday 2016), so that the reduced fibril formation after temperature reduction was not likely caused by reduced denaturation. However, temperature strongly affects the hydrolysis rate and thus the availability of fibril building blocks (hydrolysed/peptide material) (Kroes-Nijboer et al. 2011; Ye et al. 2018). According to the measured hydrolysis level (i.e. after 2 h = ~30 %, after 3 h = ~41 %) (**FIG 4-5**), as well as our previous studies on the amount of peptides that are incorporated into the fibrils (i.e. after 2 h = ~13 %, after 3 h = ~19 %) (Heyn et al. 2019) and the amount of peptides required for fibril formation (i.e. after 2 h = ~26 %, after 3 h = ~38 %) (Keppler et al. 2019) at pH 2 and 90 °C, there seems to be sufficient surplus fibril building blocks available (i.e. after 2 h = ~4 %, after 3 h = ~3 %) to ensure a further fibril formation of approximately 10 a.u. ThT FL after each temperature drop.

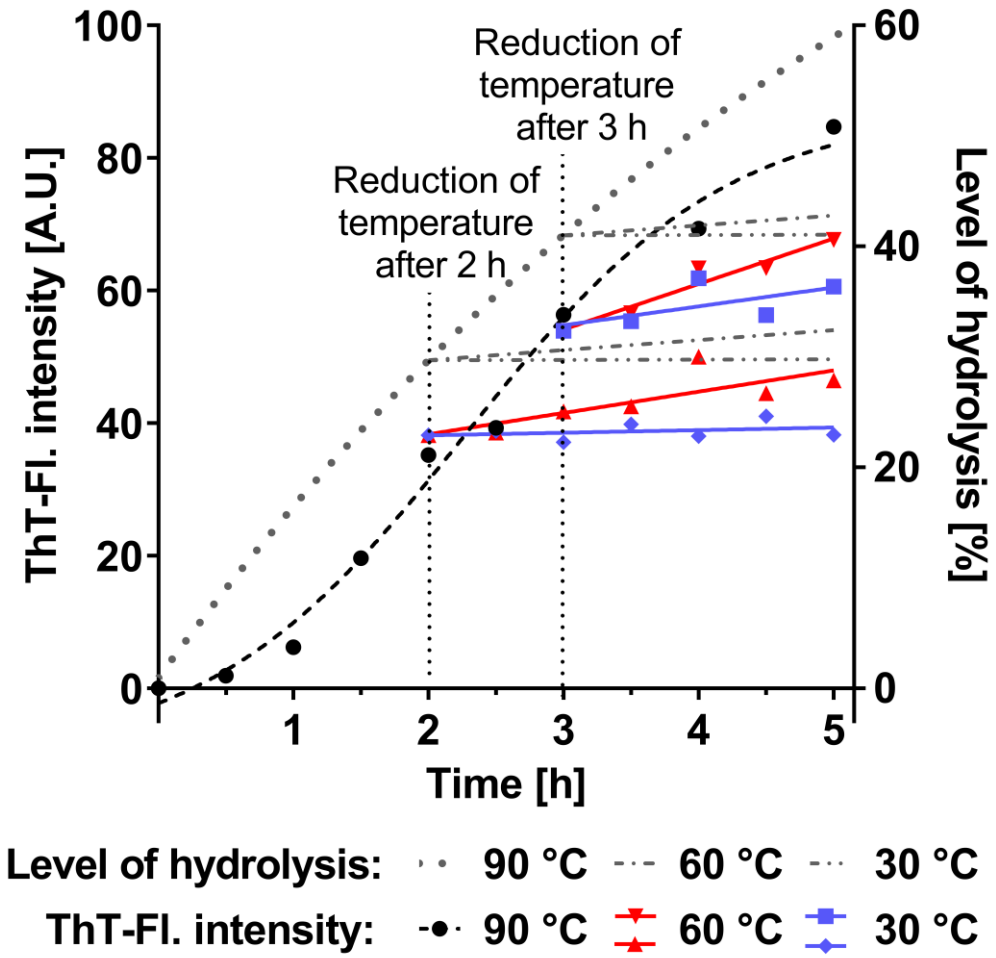

FIG 4-5 ThT-assays of fibril formation (90 °C, pH 2, 350 RPM) with a temperature drop after 2 h or 3 h and continuation of the process at 30 °C or 60 °C (pH 2, 350 RPM) until a total of 5 hours was reached. For improved visualization the ThT FL at 90 °C was fitted with a sigmoidal logarithmic equation, while ThT FL at 30 °C and 60 °C were fitted with a linear equation. The level of hydrolysis was measured by size exclusion chromatography and fitted with an exponential plateau equation. Hydrolysis rates were calculated using the Arrhenius equation given by Kroes-Nijboer et al. (2011).

Therefore, it is hypothesised that this instant temperature-dependent decrease is primarily related to the aggregation kinetics and less dependent on the hydrolysis rate**.** In fact, there was an instant drop in the aggregation kinetics ($\Delta \ln k_{ThT}$ = -3.7 (30 °C) and $\Delta \ln k_{ThT}$ = -2.1 (60 °C)) as soon as the solutions cooled down (**FIG 4-5**). Additionally, the amyloid-like aggregation of BLG is also possible without hydrolysation (for example at pH 3.5 and 90 °C) where the depletion of building blocks is independent of the peptide concentration (Heyn et al. 2019). A further effect of temperature on the entire progression of amyloid aggregation might also include other mechanisms. For example, it is possible that reversible protein conformations are

induced by higher temperatures, that lead to amyloid aggregation (Bhattacharjee and Das 2000). Another possible mechanism could be the dependence of the diffusion coefficient of the protein on temperature (Macchioni et al. 2008), which increases the frequency of molecular collisions and leads to the accelerated formation of aggregates (Wang et al. 2010); however, this would be affected by the turbulence in the system (**chapter 3.3.3**). Another factor is that the dielectric constant of the medium decreases with increasing temperature, which favours interactions between proteins—and thereby amyloid aggregation (Kayser et al. 2020).

However, since the observed acid hydrolysis rate at 30 °C and 60 ° C decreased compared to 90 °C ($\Delta \ln k_h$ = -6.63 (30 °C), $\Delta \ln k_h$ = -2.89 (60 °C) (**FIG 4-5**), the limiting factor in the long run of the fibril aggregation process will ultimately be a depletion of building blocks, when all available protein is finally hydrolysed, as previously mentioned before by Kroes-Nijboer et al. (2011).

Ultimately, several overlapping mechanisms seem to explain the observed strong positive influence of temperature on amyloid aggregation (**TAB 4-3**).

4.4.4. Interaction of temperature and pH value

The investigation of a pH-dependent denaturation effect was performed by DSC. The 1 wt% BLG samples were adjusted to pH values of 2.0, 2.5 and 3.0 to achieve parameters similar to those in the statistical experiment.

Samples were heated to 110 °C at 5 °C min^{-1} and cooled to 20 °C at 20 °C min^{-1}. Notably decreasing energy absorption of the BLG solution at increasing pH values (below the isoelectric point: pI = 4.7) during heat development was observed: At pH 2.0, the denaturation enthalpy was 448.13 ± 8.37 kJ mol^{-1}, while at pH 2.5 it was 288.68 ± 29.44 kJ mol^{-1} and at pH 3.0 it was 226.58 ± 31.63 kJ mol^{-1} (**TAB 4-4**).

TAB 4-4 Differential scanning calorimetry (DSC) of beta-lactoglobulin (1 wt%) at pH 2.0, 2.5 and 3.0.

pH value	*Enthalpy [kJ mol^{-1}]*	*Onset [°C]*	*Peak [°C]*
pH 2.0	448.13 ± 8.37	71.95 ± 0.10	84.32 ± 0.80
pH 2.5	288.68 ± 29.44	79.89 ± 0.41	86.01 ± 0.16
pH 3.0	226.58 ± 31.63	82.14 ± 0.17	90.24 ± 0.57

Simultaneously, the threshold of BLG denaturation increased with increasing pH value. At pH 2, the onset temperature was ~72 °C, while at pH 2.5 it was ~80 °C and at pH 3.0 it was ~82 °C (**TAB 4-4**). The maximum denaturation for BLG was reached at a pH value of 2.0 at ~84 °C, while this was observed at pH 2.5 at ~86 °C and at pH 3.0 at ~90 °C (**TAB 4-4**).

The results indicate that the denaturation of BLG depended on pH values being below the isoelectric point. As previously described by (Haug et al. 2009), the temperature at which BLG begins to denature increases with increasing pH value in an acidic environment. Variations in the literature (Griko and Privalov 1992; Kella and Kinsella 1988; Wada et al. 2006; Wit and Swinkels 1980) can be explained by the utilised methods and the the dependence of denaturation enthalpy and temperature on other factors such as protein and ion concentration (Dissanayake et al. 2013). In combination with the pH value, protein and ion concentrations influence the BLG monomer/dimer equilibrium, while dimers or multimers were subsequently found to stabilise the native structure of BLG and thus affect the denaturation temperature (Haug et al. 2009; Renard et al. 1998).

The present results prove that a pH value shift from pH 3.0 to pH 2.5 already leads to a reduction in temperature, which is required for the protein to unfold. It could be speculated that increased reversible conformational changes (Bhattacharjee and Das 2000) can influence the rate of aggregation, as fibrillisation prone peptide segments become accessible (van der Linden and Venema 2007). Thus, if the pH makes the protein more prone to denaturation and the aggregation kinetics depend directly on the protein conformation, this effect would shift the threshold of amyloid aggregation. However, the lower thermal stability of BLG at lower pH values not only increases the unfolding of the protein, but acid hydrolysis at lower pH values is also favoured, which is an additional factor that amplifies together with temperature (**Chapter 3.3.1**). Since this effect only led to increased ThT-values at high temperature (**FIG 4-4 G and H**), and no shift of the amyloid aggregation threshold occurred, a direct effect of denaturation on aggregation kinetics is less conceivable.

4.4.5. Influence of fluid dynamics on amyloid aggregation

In **FIG 4-6,** it can be observed that the region with the highest velocities—and thus the highest strain on the proteins—was located at the tips of the stirring bar. The energy input of the stirring bar drove the suspension outwards along the bottom of the glass container, where it finally flowed upwards at the outer edge of the glass container and then back towards the stirrer in the middle of the glass container due to the conservation of mass (**FIG 4-6 A**).

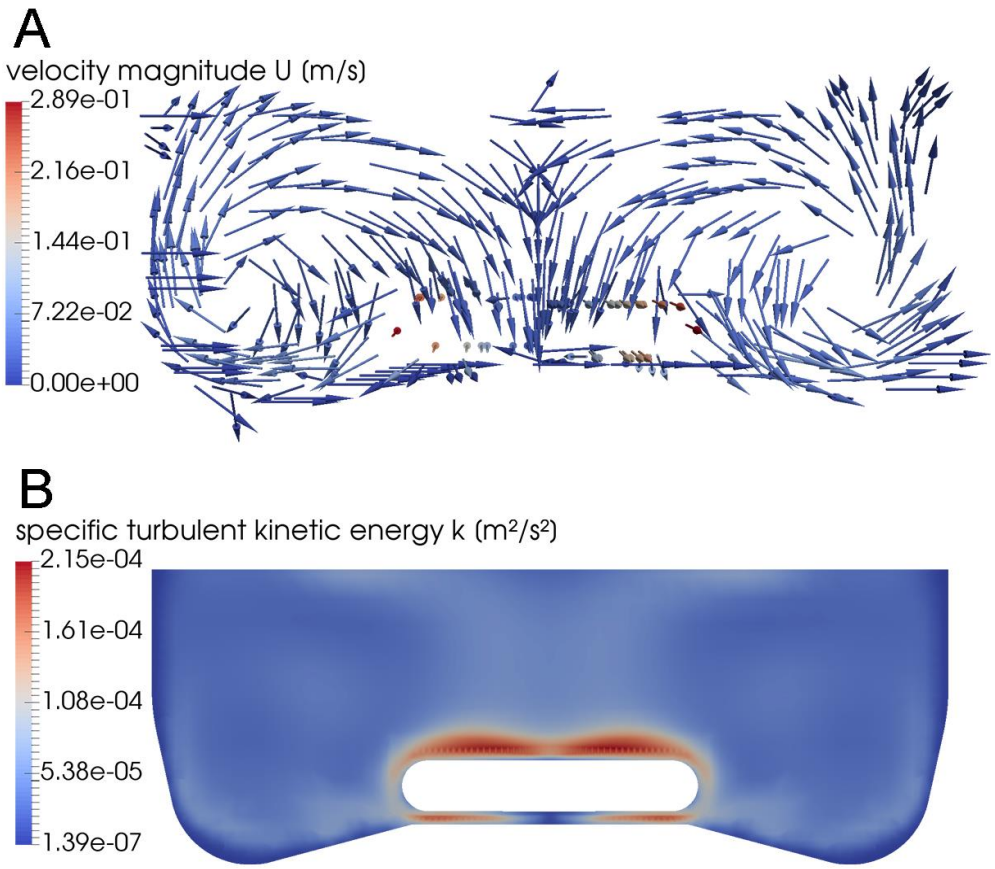

FIG 4-6 The resulting flow pattern (A) and specific turbulent kinetic energy (B) for the simulation of 300 RPM at 70 °C and t0 in the section of the suspension domain in the y-direction after 1.90 s of simulation time.

This results in large flow vortices in which the proportion of turbulence also varies (**FIG 4-6 B**), thereby resulting in variance in both turbulent and laminar flow. This results in small areas with high shear and large areas with low shear, which can lead to uneven stress distribution of the suspension—and thus of the proteins as well. The distribution of the shear stress in the system may have the same effect of causing short time impulses in a small volume, thereby interrupting the laminar flow. Thus, the intense but short mechanical stress impulses over the small area around the stirrer (**FIG 4-6**) can lead to the obligatory unfolding of the protein (Dunstan et al. 2009) or to a fracture of protofibrils to seeds (Hill et al. 2006), whereby a primary or secondary nucleation of the building blocks can occur in the large areas with low laminar stress (Akkermans et al. 2008a). The aggregation-accelerating effect of 30 s shear pulses has been previously described (Akkermans et al. 2006). This simulation clearly presents fibril growth

accelerating (**FIG 4-2 G**) shear heterogeneity in the chosen parameter range in a stirred glass container (Bolder et al. 2007).

As shown in **TAB 4-3**, significant interactions between temperature and stirring speed occurred, which positively influence amyloid aggregation (i.e. ThT FL increase). The CFD model used here calculates the averaged mean and maximum shear stresses during the simulated stirring time, shear rate, turbulence eddy dissipation (ε) and energy (k) in the turbulence model, depending on temperature, viscosity and stirring speed. The viscosity depends on the degree of aggregation, protein concentration and temperature, and was specifically determined for time points t0 and t5 using a shear rheometer at a protein concentration of 1.25 wt%.

TAB 4-5 Viscosity data used for computational fluid dynamics (CFD) simulations.

	Kinematic viscosity [m^2 s^{-1}]	***Density [kg m^{-3}]***	***Dynamic viscosity [mPas]***
t0, 70°C:	0.80E-06	1001.33	0.80
t0, 75°C:	1.50E-06	998.44	1.50
t5, 70°C:	1.10E-06	1001.33	1.10
t5, 75°C:	1.20E-06	998.44	1.12
Air	15.35E-06	1.188	0.02

The consideration of all flow-dependent parameters show an increase as a function of stirring speed; for example, a mean shear stress of t0 at 70 °C increase from 0.040 ± 0.001 Pa to 0.064 ± 0.002 (**FIG 4-7 A**), the mean shear rate from 50.1 ± 1.6 s^{-1} to 79.7 ± 2.4 s^{-1} (**FIG 4-7 C**) and the mean turbulence eddy dissipation from 0.0008 ± 0.0002 to 0.0019 ± 0.0016 (**FIG 4-7 E**). Stirring speed-dependent increases in shear stress, shear rate and turbulence were also observed for the maximum values (**FIG 4-7 B, D and F**).

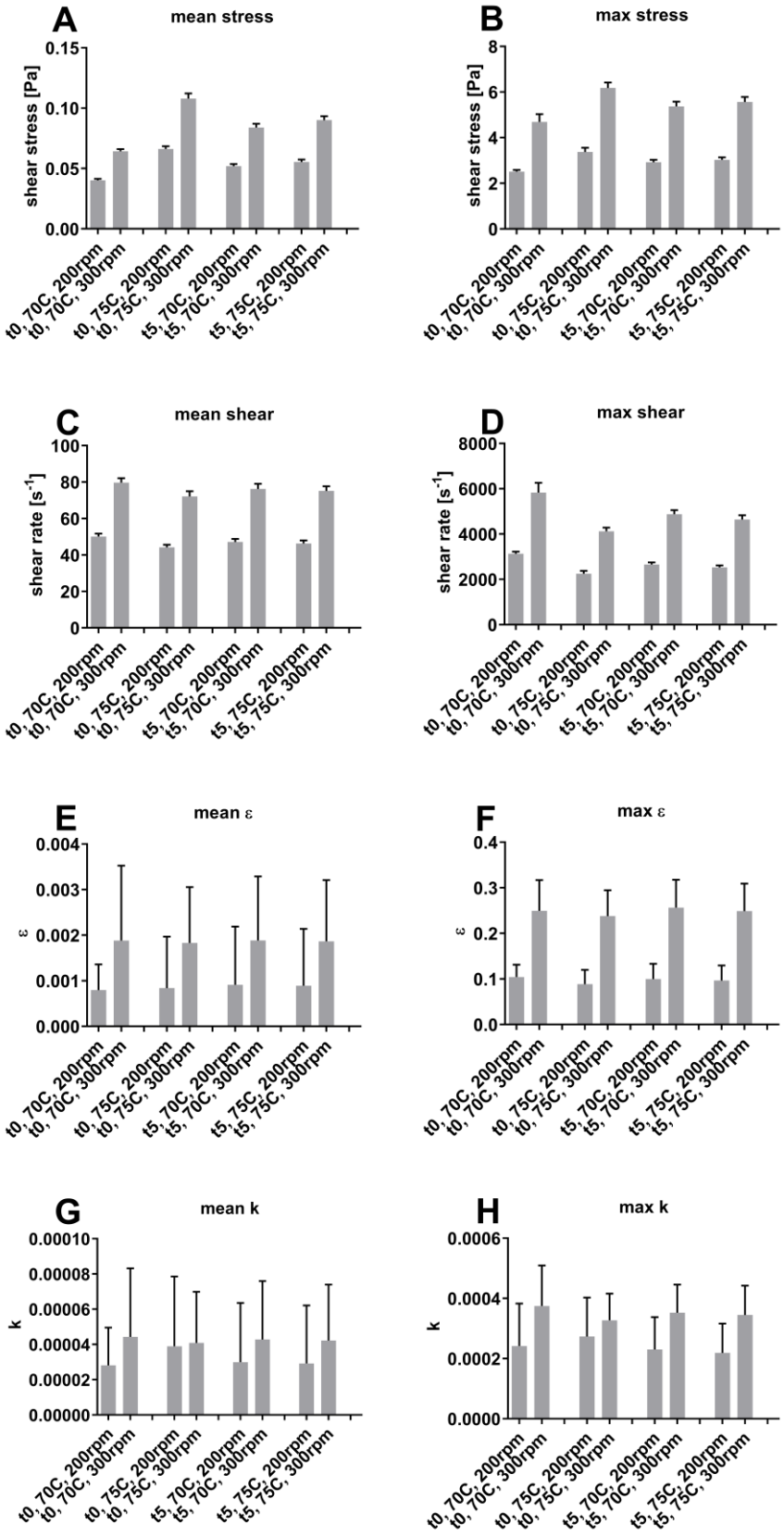

FIG 4-7 Stress factors in the stirring container during 5 h of fibril formation calculated via CFD simulation. Sample viscosity was determined at each time point using a shear rheometer. k describes the turbulence kinetic energy. ε describes the rate of dissipation of turbulence energy.

Although, significant Pearson correlations between the stress factors (shear stress, shear rate, epsilon and k) and the measured ThT FL t0.5 to t5 were not observed, relatively high r-values were evident between shear stress and ThT FL from time t2. Additionally, a temperature-dependent increase was only achieved with rising shear stress. At t0, 200 RPM and 75 °C the mean shear stress increased to 0.067 ± 0.002 Pa, while it increased to 0.108 ± 0.004 Pa at 300 RPM. A similar increase was also observed at the maximum values. However, it should be noted that this temperature-dependent increase was lost after 5 h. The reason for this is the dependency of the shear stress on the respective viscosity:

$$\tau = \eta \cdot \dot{\gamma}$$

where $\dot{\gamma}$ is the shear rate and η is the dynamic viscosity. As listed in **TAB 4-5**, the t0 sample had a dynamic viscosity of 0.8 mPas s at 70 °C and rose to 1.5 mPas s at 75 °C. For the t5 sample, the viscosity at 70 °C increased only slightly from 1.1 mPas s to 1.2 mPas s. The lower viscosity of the sample (although heated for 5 hours) can be explained by the shear-thinning behaviour of the fibrillary component in the t5 sample.

Effects being detected mainly during the lag phase of the process could be an indication that the shear stress exerts an effect on the conformation of the unhydrolysed BLG. (Rahaman et al. 2015) already described a shear-dependent reduction of the hydrophobicity of BLG at pH3 and a resulting increased polymerisation and compactness to which the ThT could react.

The shear-induced effect on protein conformation would thus have the potential to influence the threshold of amyloid aggregation. However, the ThT FL values during the growth phase showed no further stirring-dependent effects. Perhaps the shear difference between the two levels was insufficient for the detection of further effects. Another reason could be that the increasing viscosity counteracts protein aggregation: either by lower particle diffusion or because the associated increased shear stress disrupts the forming nucleus again (Akkermans et al. 2006; Dunstan et al. 2009). However, as described in **Chapter 4.4.4**, an irreversible change in protein conformation or denaturation may not be responsible for amyloid aggregation alone.

4.5. Conclusion

The present experimental parameters were chosen to prolong the lag and growth phase of the amyloid aggregation and thus give evidence for important processing parameters at the onset of amyloid aggregation. The experiments presented indicate that, at the threshold of fibril formation, partly different interaction effects can occur than at the optimum: however, the most important factor is the temperature in every stage of amyloid aggregation, which could be due

to manifold effects that superpose each other. This is also confirmed by further interactions between stirring speed and temperature during the lag phase and between pH and temperature during the growth phase.

With the help of a CFD simulation of the stirring process, higher shear stress at higher stirring speeds and temperatures could be identified as the reason for the interaction, which likely negatively affects the protein nativity and thus reduces the lag phase. The increased viscosity of the protein solution at higher temperatures likely plays a major role in this interaction.

The effect of pH value and temperature in the growth phase could be explained by DSC experiments, which revealed that BLG was more likely to denature at pH 2.5 than at pH 3.0 for the selected factor combinations.

Thus, each of the chosen process parameters affects the underlying forces of amyloid aggregation in multiple and sometimes opposing ways, while only the sum of the effects can be observed here at a certain point in the amyloid aggregation phase.

Due to the very slow aggregation kinetics of the selected parameters, the investigations provide a more detailed view of the most important factors and when they come into effect. Meanwhile, new interactions could also be described. These do not seem to shift the threshold; however, it is conceivable that other and more extreme factor combinations might decrease the necessary temperature under 70 °C.

Acknowledgement
This project was funded by the German Research Foundation (DFG) priority programme SPP 1934 DiSPBiotech (Project no. 273937032 and 315456892). We are grateful to Monique Heuer and Jil J. Kayser of the Food Technology Division, Kiel University and to Maurice Strubel of the Department of Agrotechnology and Food Sciences, Wageningen University for their skilful help.

4.6. References

Akkermans, C., van der Goot, A.J., Venema, P., van der Linden, E., & Boom, R.M. (2008a). Formation of fibrillar whey protein aggregates. *Food Hydrocolloids*, 22(7), 1315–25. http://dx.doi.org/10.1016/j.foodhyd.2007.07.001.

Akkermans, C., Venema, P., Rogers, S.S., van der Goot, A.J., Boom, R.M., & van der Linden, E. (2006). Shear Pulses Nucleate Fibril Aggregation. *Food Biophysics*, 1(3), 144–50. http://dx.doi.org/10.1007/s11483-006-9012-5.

Akkermans, C., Venema, P., van der Goot, A.J., Gruppen, H., Bakx, E.J., & Boom, R.M., et al. (2008b). Peptides are building blocks of heat-induced fibrillar protein aggregates of beta-lactoglobulin formed at pH 2. *Biomacromolecules*, 9(5), 1474–9. http://dx.doi.org/10.1021/bm7014224.

Arnaudov, L.N., & Vries, R. de (2006). Strong impact of ionic strength on the kinetics of fibrilar aggregation of bovine beta-lactoglobulin. *Biomacromolecules*, 7(12), 3490–8. http://dx.doi.org/10.1021/bm060584i.

Baldassarre, M., Bennett, M., & Barth, A. (2016). Simultaneous acquisition of infrared, fluorescence and light scattering spectra of proteins. *Analyst*, 141(3), 963–73. http://dx.doi.org/10.1039/c5an02283e.

Bhattacharjee, C., & Das, K.P. (2000). Thermal unfolding and refolding of beta-lactoglobulin. An intrinsic andextrinsic fluorescence study. *European Journal of Biochemistry*, 267(13), 3957–64. http://dx.doi.org/10.1046/j.1432-1327.2000.01409.x.

Bhattacharjee, S. (2016). DLS and zeta-potential - What they are and what they are not? *J Control Release*, 235, 337–51. http://dx.doi.org/10.1016/j.jconrel.2016.06.017.

Bliatsiou, C., Malik, A., Böhm, L., & Kraume, M. (2018). Influence of Impeller Geometry on Hydromechanical Stress in Stirred Liquid/Liquid Dispersions. *Ind. Eng. Chem. Res.*, 58(7), 2537–50. http://dx.doi.org/10.1021/acs.iecr.8b03654.

Bolder, S.G., Sagis, L.M.C., Venema, P., & van der Linden, E. (2007). Effect of stirring and seeding on whey protein fibril formation. *J Agric Food Chem*, 55(14), 5661–9. http://dx.doi.org/10.1021/jf063351r.

Bryant, C.M., & McClements, D.J. (2000). Influence of NaCl and CaCl2 on Cold-Set Gelation of Heat-denatured Whey Protein. *J Food Sci*, 65(5), 801–4. http://dx.doi.org/10.1111/j.1365-2621.2000.tb13590.x.

Ciuciu, A.-M.S., Aprodu, I., Alexe, P., & Stănciuc, N. (2016). Thermally driven interactions between β-lactoglobulin and retinol acetate investigated by fluorescence spectroscopy and molecular modeling methods. *Dairy Sci. & Technol.*, 96(3), 405–23. http://dx.doi.org/10.1007/s13594-015-0277-7.

Dissanayake, M., Ramchandran, L., Donkor, O.N., & Vasiljevic, T. (2013). Denaturation of whey proteins as a function of heat, pH and protein concentration. *International Dairy Journal*, 31(2), 93–9. http://dx.doi.org/10.1016/j.idairyj.2013.02.002.

Dunstan, D.E., Hamilton-Brown, P., Asimakis, P., Ducker, W., & Bertolini, J. (2009). Shear-induced structure and mechanics of β-lactoglobulin amyloid fibrils. *Soft Matter*, 5(24), 5020. http://dx.doi.org/10.1039/b914089a.

Dvorsky, R., Sevcik, J., Caves, L.S.D., Hubbard, R.E., & Verma, C.S. (2000). Temperature Effects on Protein Motions. *J. Phys. Chem. B*, 104(44), 10387–97. http://dx.doi.org/10.1021/jp001933k.

Einstein, A. (1905). Über die von der molekularkinetischen Theorie der Wärme geforderte Bewegung von in ruhenden Flüssigkeiten suspendierten Teilchen. *Ann. Phys.*, 322(8), 549–60. http://dx.doi.org/10.1002/andp.19053220806.

Gao, Z., Zhao, J., Huang, Y., Yao, X., Zhang, K., & Fang, Y., et al. (2017). Edible Pickering emulsion stabilized by protein fibrils. Part 1. *LWT - Food Science and Technology*, 76, 1–8. http://dx.doi.org/10.1016/j.lwt.2016.10.038.

Gilbert, J., Campanella, O., & Jones, O.G. (2014). Electrostatic stabilization of β-lactoglobulin fibrils at increased pH with cationic polymers. *Biomacromolecules*, 15(8), 3119–27. http://dx.doi.org/10.1021/bm500762u.

Griko, Y.V., & Privalov, P.L. (1992). Calorimetric study of the heat and cold denaturation of beta-lactoglobulin. *Biochemistry*, 31(37), 8810–5. http://dx.doi.org/10.1021/bi00152a017.

Haug, I.J., Skar, H.M., Vegarud, G.E., Langsrud, T., & Draget, K.I. (2009). Electrostatic effects on β-lactoglobulin transitions during heat denaturation as studied by differential scanning calorimetry. *Food Hydrocolloids*, 23(8), 2287–93. http://dx.doi.org/10.1016/j.foodhyd.2009.06.006.

Havinga, E.E. (1961). The temperature dependence of dielectric constants. *Journal of Physics and Chemistry of Solids*, 18(2-3), 253–5. http://dx.doi.org/10.1016/0022-3697(61)90169-X.

Heyn, T.R., Garamus, V.M., Neumann, H.R., Uttinger, M.J., Guckeisen, T., & Heuer, M., et al. (2019). Influence of the polydispersity of pH 2 and pH 3.5 beta-lactoglobulin amyloid fibril solutions on analytical methods. *European Polymer Journal*(120), 109211. http://dx.doi.org/10.1016/j.eurpolymj.2019.08.038.

Hill, E.K., Krebs, B., Goodall, D.G., Howlett, G.J., & Dunstan, D.E. (2006). Shear Flow Induces Amyloid Fibril Formation. *Biomacromolecules*, 7(1), 10–3. http://dx.doi.org/10.1021/bm0505078.

Jung, J.-M., Savin, G., Pouzot, M., Schmitt, C., & Mezzenga, R. (2008). Structure of heat-induced beta-lactoglobulin aggregates and their complexes with sodium-dodecyl sulfate. *Biomacromolecules*, 9(9), 2477–86. http://dx.doi.org/10.1021/bm800502j.

Kavanagh, G.M., Clark, A.H., & Ross-Murphy, S.B. (2000). Heat-Induced Gelation of Globular Proteins. *Langmuir*, 16(24), 9584–94. http://dx.doi.org/10.1021/la0004698.

Kayser, J.J., Arnold, P., Steffen-Heins, A., Schwarz, K., & Keppler, J.K. (2020). Functional ethanol-induced fibrils. *Journal of Food Engineering*(270), 109764. http://dx.doi.org/10.1016/j.jfoodeng.2019.109764.

Kella, N.K., & Kinsella, J.E. (1988). Enhanced thermodynamic stability of beta-lactoglobulin at low pH. A possible mechanism. *Biochem. J.*, 255(1), 113–8. http://dx.doi.org/10.1042/bj2550113.

Keppler, J.K., Heyn, T.R., Meissner, P.M., Schrader, K., & Schwarz, K. (2019). Protein oxidation during temperature-induced amyloid aggregation of beta-lactoglobulin. *Food Chem*, 289, 223–31. http://dx.doi.org/10.1016/j.foodchem.2019.02.114.

Keppler, J.K., Sönnichsen, F.D., Lorenzen, P.-C., & Schwarz, K. (2014). Differences in heat stability and ligand binding among β-lactoglobulin genetic variants A, B and C using (1)H NMR and fluorescence quenching. *Biochim Biophys Acta*, 1844(6), 1083–93. http://dx.doi.org/10.1016/j.bbapap.2014.02.007.

Knowles, T.P.J., & Mezzenga, R. (2016). Amyloid Fibrils as Building Blocks for Natural and Artificial Functional Materials. *Adv Mater Weinheim*, 28(31), 6546–61. http://dx.doi.org/10.1002/adma.201505961.

Krebs, M.R.H., Bromley, E.H.C., & Donald, A.M. (2005). The binding of thioflavin-T to amyloid fibrils. *J Struct Biol*, 149(1), 30–7. http://dx.doi.org/10.1016/j.jsb.2004.08.002.

Krebs, M.R.H., Devlin, G.L., & Donald, A.M. (2009). Amyloid fibril-like structure underlies the aggregate structure across the pH range for beta-lactoglobulin. *Biophys J*, 96(12), 5013–9. http://dx.doi.org/10.1016/j.bpj.2009.03.028.

Kroes-Nijboer, A., Venema, P., Bouman, J., & van der Linden, E. (2011). Influence of protein hydrolysis on the growth kinetics of β-lg fibrils. *Langmuir*, 27(10), 5753–61. http://dx.doi.org/10.1021/la104797u.

Loveday, S.M. (2016). β-Lactoglobulin heat denaturation. *International Dairy Journal*, 52, 92–100. http://dx.doi.org/10.1016/j.idairyj.2015.08.001.

Loveday, S.M., Anema, S.G., & Singh, H. (2017). β-Lactoglobulin nanofibrils. *International Dairy Journal*, 67, 35–45. http://dx.doi.org/10.1016/j.idairyj.2016.09.011.

Loveday, S.M., Su, J., Rao, M.A., Anema, S.G., & Singh, H. (2012a). Whey protein nanofibrils. *J Agric Food Chem*, 60(20), 5229–36. http://dx.doi.org/10.1021/jf300367k.

Loveday, S.M., Wang, X.L., Rao, M.A., Anema, S.G., Creamer, L.K., & Singh, H. (2010). Tuning the properties of β-lactoglobulin nanofibrils with pH, NaCl and CaCl2. *International Dairy Journal*, 20(9), 571–9. http://dx.doi.org/10.1016/j.idairyj.2010.02.014.

Loveday, S.M., Wang, X.L., Rao, M.A., Anema, S.G., & Singh, H. (2011). Effect of pH, NaCl, CaCl2 and temperature on self-assembly of β-lactoglobulin into nanofibrils. *J Agric Food Chem*, 59(15), 8467–74. http://dx.doi.org/10.1021/jf201870z.

Loveday, S.M., Wang, X.L., Rao, M.A., Anema, S.G., & Singh, H. (2012b). β-Lactoglobulin nanofibrils. *Food Hydrocolloids*, 27(1), 242–9. http://dx.doi.org/10.1016/j.foodhyd.2011.07.001.

Macchioni, A., Ciancaleoni, G., Zuccaccia, C., & Zuccaccia, D. (2008). Determining accurate molecular sizes in solution through NMR diffusion spectroscopy. *Chem Soc Rev*, 37(3), 479–89. http://dx.doi.org/10.1039/b615067p.

Mishra, R., Sörgjerd, K., Nyström, S., Nordigården, A., Yu, Y.-C., & Hammarström, P. (2007). Lysozyme amyloidogenesis is accelerated by specific nicking and fragmentation but decelerated by intact protein binding and conversion. *J Mol Biol*, 366(3), 1029–44. http://dx.doi.org/10.1016/j.jmb.2006.11.084.

Mohammadian, M., & Madadlou, A. (2016). Cold-set hydrogels made of whey protein nanofibrils with different divalent cations. *International Journal of Biological Macromolecules*, 89, 499–506. http://dx.doi.org/10.1016/j.ijbiomac.2016.05.009.

Ng, S.K., Nyam, K.L., Nehdi, I.A., Chong, G.H., Lai, O.M., & Tan, C.P. (2016). Impact of stirring speed on β-lactoglobulin fibril formation. *Food Sci Biotechnol*, 25(S1), 15–21. http://dx.doi.org/10.1007/s10068-016-0093-8.

Nicolai, T., & Durand, D. (2013). Controlled food protein aggregation for new functionality. *Current Opinion in Colloid & Interface Science*, 18(4), 249–56. http://dx.doi.org/10.1016/j.cocis.2013.03.001.

Pellarin, R., & Caflisch, A. (2006). Interpreting the aggregation kinetics of amyloid peptides. *J Mol Biol*, 360(4), 882–92. http://dx.doi.org/10.1016/j.jmb.2006.05.033.

Peng, D., Yang, J., Li, J., Tang, C., & Li, B. (2017). Foams Stabilized by β-Lactoglobulin Amyloid Fibrils. *J Agric Food Chem*, 65(48), 10658–65. http://dx.doi.org/10.1021/acs.jafc.7b03669.

Pitera, J.W., Falta, M., & van Gunsteren, W.F. (2001). Dielectric Properties of Proteins from Simulation. *Biophys J*, 80(6), 2546–55. http://dx.doi.org/10.1016/S0006-3495(01)76226-1.

Rahaman, T., Vasiljevic, T., & Ramchandran, L. (2015). Conformational changes of β-lactoglobulin induced by shear, heat, and pH-Effects on antigenicity. *J Dairy Sci*, 98(7), 4255–65. http://dx.doi.org/10.3168/jds.2014-9010.

Renard, D., Lefebvre, J., Griffin, M.C.A., & Griffin, W.G. (1998). Effects of pH and salt environment on the association of β-lactoglobulin revealed by intrinsic fluorescence studies. *International Journal of Biological Macromolecules*, 22(1), 41–9. http://dx.doi.org/10.1016/S0141-8130(97)00086-X.

Schleeger, M., vandenAkker, C.C., Deckert-Gaudig, T., Deckert, V., Velikov, K.P., & Koenderink, G., et al. (2013). Amyloids. *Polymer*, 54(10), 2473–88. http://dx.doi.org/10.1016/j.polymer.2013.02.029.

Serfert, Y., Lamprecht, C., Tan, C.-P., Keppler, J.K., Appel, E., & Rossier-Miranda, F.J., et al. (2014). Characterisation and use of β-lactoglobulin fibrils for microencapsulation of lipophilic ingredients and oxidative stability thereof. *Journal of Food Engineering*, 143, 53–61. http://dx.doi.org/10.1016/j.jfoodeng.2014.06.026.

van der Linden, E., & Venema, P. (2007). Self-assembly and aggregation of proteins. *Current Opinion in Colloid & Interface Science*, 12(4-5), 158–65. http://dx.doi.org/10.1016/j.cocis.2007.07.010.

Wada, R., Fujita, Y., & Kitabatake, N. (2006). Effects of heating at neutral and acid pH on the structure of beta-lactoglobulin A revealed by differential scanning calorimetry and circular dichroism spectroscopy. *Biochim Biophys Acta*, 1760(6), 841–7. http://dx.doi.org/10.1016/j.bbagen.2005.12.025.

Wang, W., Nema, S., & Teagarden, D. (2010). Protein aggregation--pathways and influencing factors. *Int J Pharm*, 390(2), 89–99. http://dx.doi.org/10.1016/j.ijpharm.2010.02.025.

Wit, J.N. de, & Swinkels, G.A.M. (1980). A differential scanning calorimetric study of the thermal denaturation of bovine β-lactoglobulin Thermal behaviour at temperatures up to

100°C. *Biochimica et Biophysica Acta (BBA) - Protein Structure*, 624(1), 40–50. http://dx.doi.org/10.1016/0005-2795(80)90223-8.

Ye, X., Hedenqvist, M.S., Langton, M., & Lendel, C. (2018). On the role of peptide hydrolysis for fibrillation kinetics and amyloid fibril morphology. *RSC Adv.*, 8(13), 6915–24. http://dx.doi.org/10.1039/C7RA10981D.

Zhu, X., Guo, W., Jia, Y., & Kang, F. (2015). Dielectric Properties of Raw Milk as Functions of Protein Content and Temperature. *Food Bioprocess Technol*, 8(3), 670–80. http://dx.doi.org/10.1007/s11947-014-1440-5.

4.7. Supplementary material

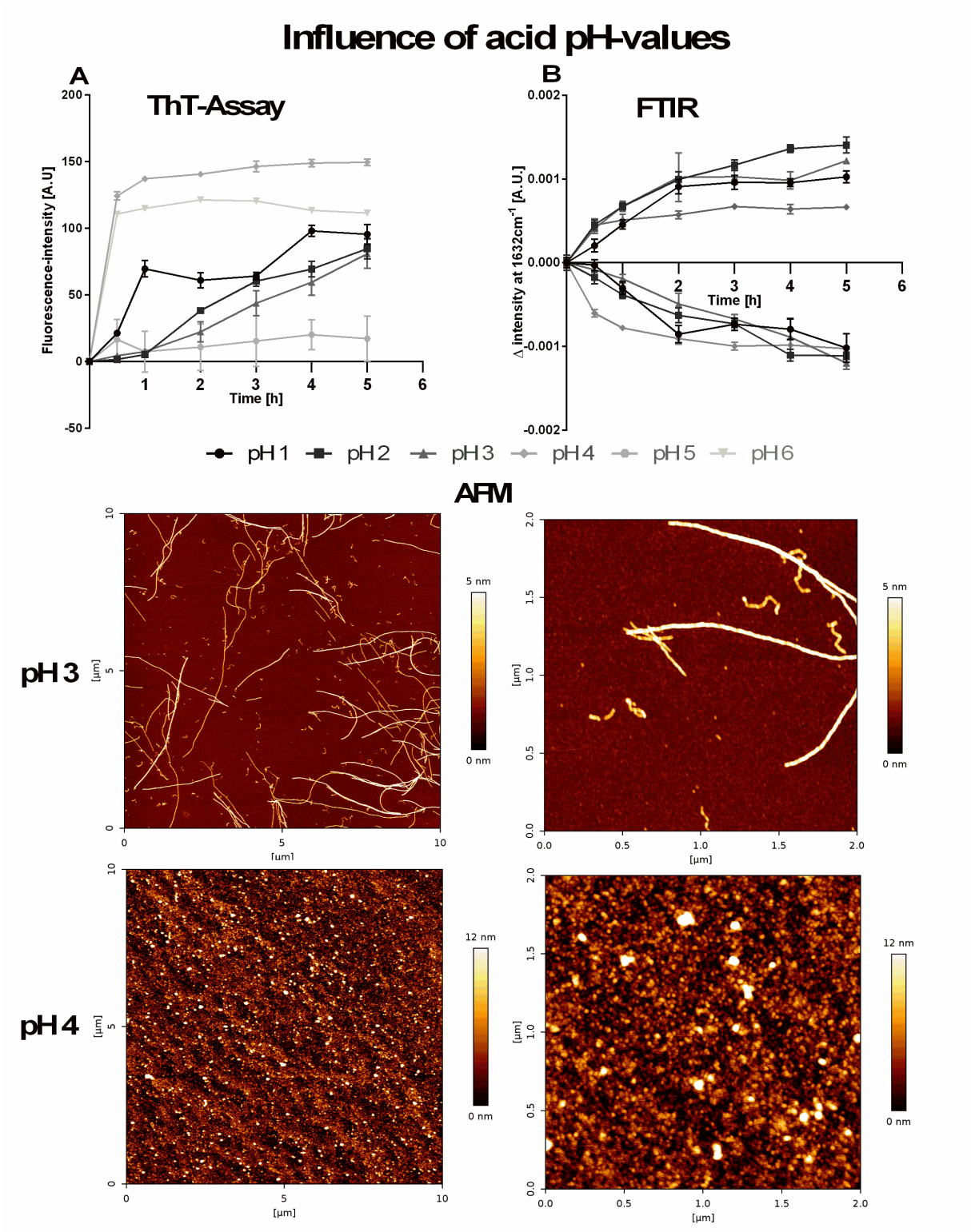

FIG-S 4-8 Influence of acid pH values on ThT-fluorescence assays, on absorbance at amid band with wavenumber 1622 cm-1 and 1632 cm-1 analysed with Fourier- transform infrared spectroscopy (FTIR) and morphology analysed with Atomic Force Microscopy (AFM).

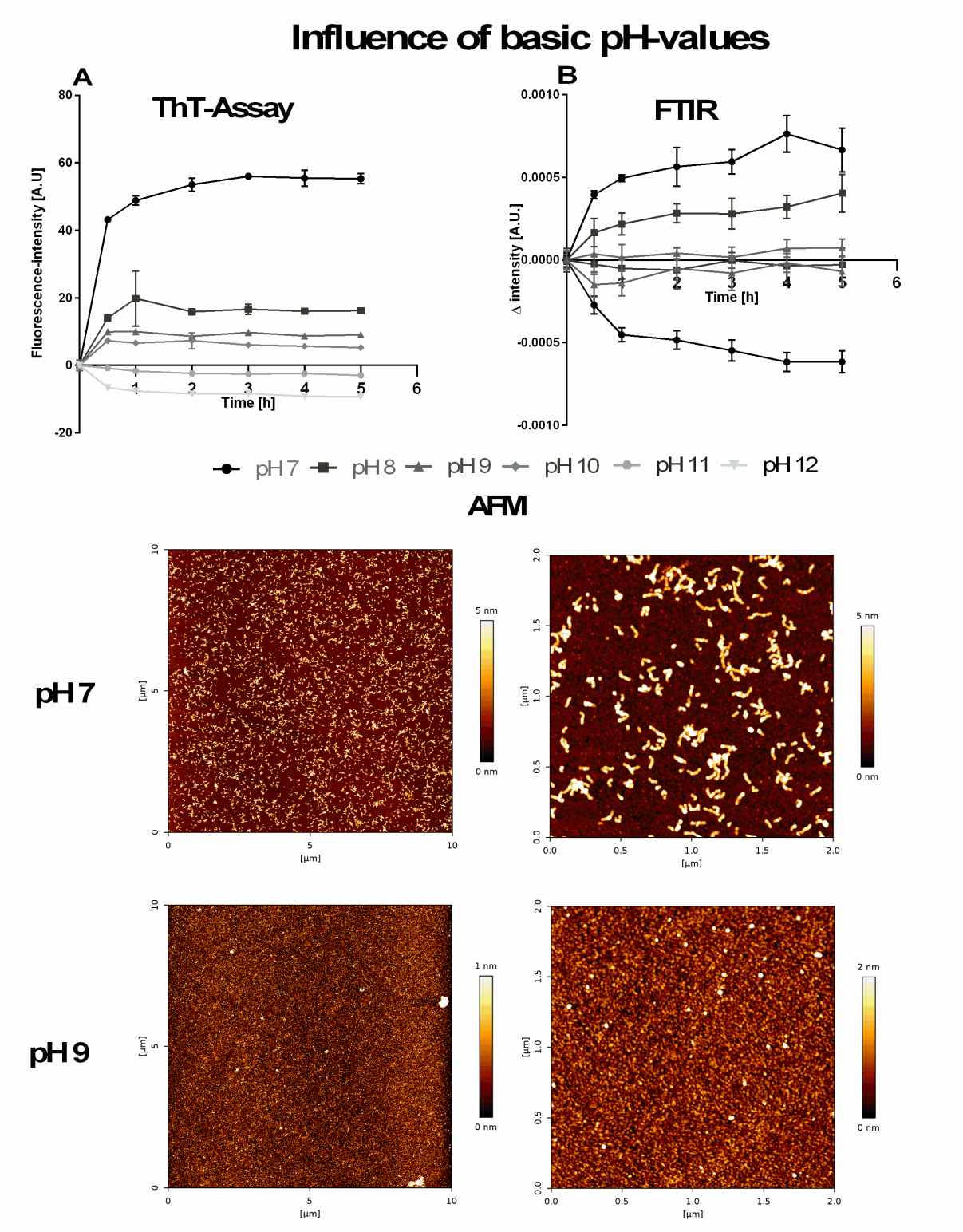

FIG-S 4-9 Influence of basic pH values on ThT-fluorescence-assays (A), on absorbance at amid band with wavenumber 1622 cm-1 and 1632 cm-1 Fourier- transform infrared spectroscopy (FTIR) and morphology analysed with Atomic Force Microscopy (AFM).

TAB-S 4-6 Sample table of the DOE with tested factors and resulted responses. T0.5 to t5 describes hours of heating. Δ 1632cm^{-1} and Δ 1622cm^{-1} are the relative alteration of absorption at these bands. At 1632cm-1 native beta-sheets are located, at 1622cm-1 amyloid beta-sheets. Temperature was protocolled and variation was -+ 0.3406. Protein concentration was verify by UV-Vis spectroscopy. NaCl-concentration is exclusive salt residues in the protein isolate. Zeta-potential was obtained from the unheated protein solution.

	Factor 1	*Factor 2*	*Factor 3*	*Factor 4*	*Factor 5*	***Response 1 - 7****							***Response 8***	***Response 9 + 10***		***Response 11***
Run	A:pH value	b:Temp.	C:Protein-conc.	D:NaCl-conc.	e:Stirring velocity	ThT FL int. t0.5	ThT FL int. t1	ThT FL int. t2	ThT FL int. t3	ThT FL int. t4	ThT FL int. t5	*Regression fitting*	fibril yield	Δ 1632cm^{-1}	Δ 1622cm^{-1}	Zeta-potential
		°C	wt%	mMol	RPM	a.u.	a.u.	a.u.	a.u.	a.u.	a.u.	*R*	%	%	%	mV
1	3	75	1.5	10	300	-0.18	-0.25	0.00	0.60	1.79	4.32	0.82	1.47	3.35	5.27	21.00
2	2.5	75	1.5	0	300	-0.09	-0.14	0.39	0.99	5.01	8.90	*0.98*	6.37	-16.70	9.91	24.77
3	3	70	1.5	10	200	0.36	0.24	0.34	0.33	0.59	0.23	*0.02*	0.00	5.00	4.22	21.90
4	2.5	70	1.5	10	300	0.13	0.16	-0.15	0.49	0.59	1.55	*0.71*	4.20	2.95	9.08	17.70
5	3	75	1	0	300	-0.03	0.33	0.21	0.32	0.84	2.84	*0.80*	9.13	-5.39	6.27	27.13
6	2.5	75	1	10	300	-0.37	-0.47	-0.22	0.15	1.57	5.82	*0.88*	3.22	-9.14	4.93	21.97
7	2.5	75	1.5	10	200	0.15	-0.02	0.12	1.61	4.25	7.91	*0.99*	8.89	-13.57	13.41	24.63
8	3	70	1	10	300	0.53	0.24	0.29	0.41	0.14	0.58	*0.09*	1.40	1.31	8.26	24.23
9	3	70	1	10	300	-1.23	-1.03	-1.02	-0.74	-0.23	1.11	*0.83*	3.57	-8.78	7.83	24.23
10	2.5	70	1.5	10	300	-0.33	-0.44	-0.57	-0.48	0.13	1.05	*0.61*	3.12	21.91	0.61	19.50
11	3	70	1	0	200	-0.25	-0.16	-0.37	-0.30	-0.50	-0.04	*0.22*	3.41	10.63	-1.37	27.13
12	2.5	70	1	10	200	-0.31	-0.52	-1.10	-1.17	-1.29	-0.93	*0.74*	3.15	3.77	11.22	21.33
13	2.5	70	1.5	0	200	0.04	-0.04	-0.13	-0.05	-0.09	0.38	*0.35*	4.34	0.34	1.41	27.00
14	2.5	75	1.5	0	300	0.08	-0.07	0.25	2.07	4.24	6.74	*0.90*	5.54	-8.93	7.61	30.97
15	2.5	70	1.5	0	200	-0.83	-0.95	-0.93	-0.73	-0.11	0.12	*0.51*	3.15	-15.34	0.04	18.83
16	2.5	70	1	0	300	-0.27	-0.52	-0.29	-0.37	0.01	1.08	*0.64*	1.15	-0.09	-3.74	29.03
17	3	75	1.5	10	300	1.24	1.33	1.59	2.42	4.99	7.05	0.89	11.74	-8.93	7.61	21.53
18	2.5	70	1	0	300	-0.75	-0.90	-0.77	-1.09	-0.56	-0.80	*0.02*	4.59	-4.20	2.07	25.50
19	3	75	1	0	300	-0.26	-0.26	0.17	0.02	1.07	2.84	*0.75*	7.18	-0.41	3.97	6.63
20	2.75	72.5	1.25	5	250	-0.02	-0.11	-0.34	-0.30	0.03	1.42	*0.77*	4.04	-2.58	4.09	24.10
21	2.5	75	1	10	300	-0.55	-0.64	-0.23	0.68	3.47	5.10	*0.88*	13.11	1.64	1.70	16.33
22	2.5	75	1	0	200	-0.26	-0.14	-0.01	0.79	2.36	4.93	*0.95*	7.38	-7.50	1.44	29.10
23	3	70	1.5	0	300	0.29	0.33	0.41	0.28	0.45	1.63	*0.75*	4.38	14.74	-4.21	25.67
24	3	75	1	10	200	-0.13	-0.21	0.23	0.07	1.04	3.35	*0.63*	6.95	-4.70	6.21	26.37
25	3	75	1.5	0	200	0.53	0.34	0.21	0.45	1.29	3.69	*0.92*	6.11	-5.66	-5.90	23.33
26	2.75	72.5	1.25	5	250	0.42	0.39	0.38	0.50	0.66	1.73	*0.69*	3.63	-4.49	9.48	24.60
27	2.5	75	1	0	200	-1.66	-1.29	-1.59	-0.98	1.35	4.57	*0.94*	3.88	1.63	-3.68	26.83
28	2.75	72.5	1.25	5	250	-0.06	0.05	-0.05	-0.09	-0.34	0.39	*0.25*	2.94	-5.09	-0.81	24.47
29	3	70	1.5	10	200	1.15	1.34	1.13	1.02	1.21	1.90	*0.10*	6.18	21.91	0.61	28.80
30	3	75	1	10	200	-1.42	-1.37	-0.63	0.08	1.29	2.02	*0.80*	6.33	-16.19	-1.09	23.17
31	2.5	75	1.5	10	200	-0.27	-0.40	0.00	1.80	6.16	7.28	*0.93*	6.52	-1.82	0.97	24.73
32	2.5	70	1	10	200	0.23	0.23	0.20	0.43	0.41	0.77	*0.46*	3.92	-5.39	6.27	26.30
33	3	70	1	0	200	-0.32	-0.11	-0.05	0.00	0.12	0.35	*0.33*	4.24	55.04	-15.14	27.13
34	3	70	1.5	0	300	-1.07	-0.41	-0.53	-0.38	0.03	0.53	*0.52*	5.53	-3.74	-0.32	28.00
35	3	75	1.5	0	200	-1.19	-1.02	-0.91	-0.77	1.42	3.86	*0.90*	4.14	24.24	5.88	31.30

TAB 4-7 Correlation between process parameters and responses. Positive correlations are marked in red and negative in blue.

	A:pH value	b:temperature	C:proteinconc.	D:NaCl-Conc.	e:Stirring	ThT FL t0.5	ThT FL t1	ThT FL t2	ThT FL t3	ThT FL t4	ThT FL t5	Regression fitting	fibril yield	Delta 1632 cm-	Delta 1622 cm-	Zetapotential
A:pH value	1.000	0.000	0.000	0.000	0.000	0.147	0.277	0.301	-0.011	-0.202	-0.208	-0.215	-0.008	0.291	-0.188	0.020
b:temperature	0.000	1.000	0.000	-0.000	0.000	-0.084	-0.088	0.154	0.449	0.698	0.818	0.720	0.563	-0.369	0.202	-0.082
C:proteinconc.	0.000	0.000	1.000	-0.000	0.000	0.336	0.341	0.315	0.402	0.353	0.269	0.094	-0.010	0.016	0.113	0.047
D:NaCl-Conc.	0.000	-0.000	-0.000	1.000	0.000	0.239	0.161	0.193	0.265	0.155	0.085	-0.008	0.036	-0.099	0.443	-0.291
e:Stirring	0.000	0.000	0.000	0.000	1.000	0.062	0.068	0.148	0.099	0.069	0.114	0.131	0.078	-0.160	0.226	-0.285
ThT FL t0.5	0.147	-0.084	0.336	0.239	0.062	1.000	0.952	0.887	0.629	0.203	0.114	-0.216	0.130	0.055	0.209	-0.027
ThT FL t1	0.277	-0.088	0.341	0.161	0.068	0.952	1.000	0.899	0.614	0.177	0.098	-0.217	0.201	0.123	0.140	0.055
ThT FL t2	0.301	0.154	0.315	0.193	0.148	0.887	0.899	1.000	0.790	0.432	0.331	-0.089	0.349	-0.011	0.153	-0.008
ThT FL t3	-0.011	0.449	0.402	0.265	0.099	0.629	0.614	0.790	1.000	0.823	0.706	0.292	0.510	-0.210	0.265	0.036
ThT FL t4	-0.202	0.698	0.353	0.155	0.069	0.203	0.177	0.432	0.823	1.000	0.934	0.577	0.603	-0.287	0.258	0.005
ThT FL t5	-0.208	0.818	0.269	0.085	0.114	0.114	0.098	0.331	0.706	0.934	1.000	0.723	0.562	-0.332	0.301	0.021
Regression fitting	-0.215	0.720	0.094	-0.008	0.131	-0.216	-0.217	-0.089	0.292	0.577	0.723	1.000	0.458	-0.339	0.240	-0.100
fibril yield	-0.008	0.563	-0.010	0.036	0.078	0.130	0.201	0.349	0.510	0.603	0.562	0.458	1.000	-0.217	0.125	-0.149
Delta 1632 cm-1	0.291	-0.369	0.016	-0.099	-0.160	0.055	0.123	-0.011	-0.210	-0.287	-0.332	-0.339	-0.217	1.000	-0.525	0.140
Delta 1622 cm-1	-0.188	0.202	0.113	0.443	0.226	0.209	0.140	0.153	0.265	0.258	0.301	0.240	0.125	-0.525	1.000	-0.153
Zetapotential	0.020	-0.082	0.047	-0.291	-0.285	-0.027	0.055	-0.008	0.036	0.005	0.021	-0.100	-0.149	0.140	-0.153	1.000

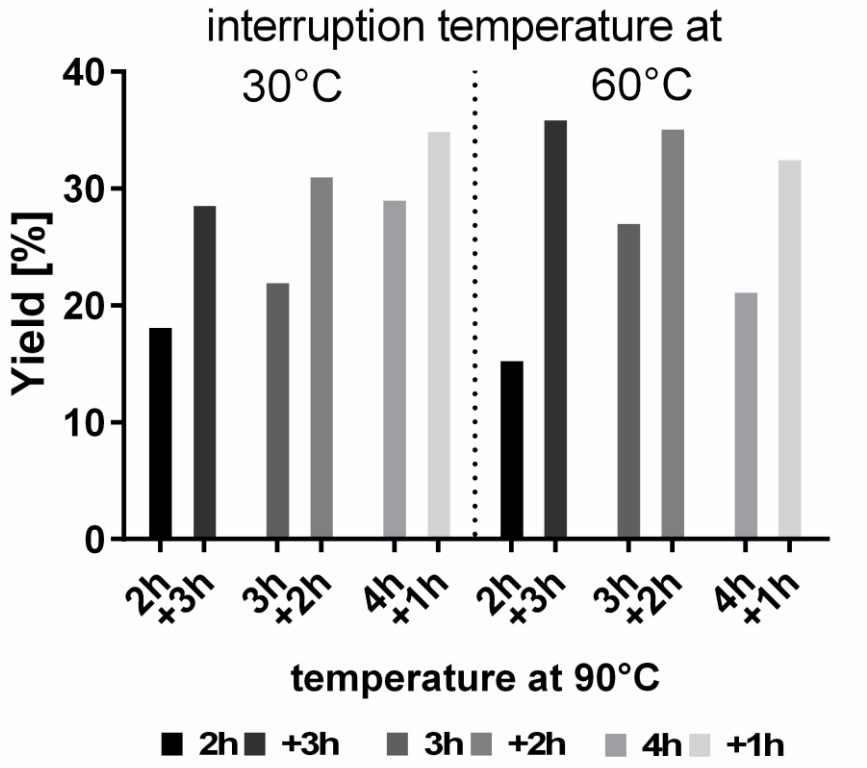

FIG-S 4-10 yield of fibrils (%) after heating at 90 °C, at pH 2, 350 RPM and 2.5 wt% protein concentration. Temperature was lowered after 2, 3 and 4 hours to 30 °C or 60 °C.

TAB-S 4-8 protocolled temperature of samples in water bath. 90 °C started from room temperature. 60 °C and 30 °C were used to cooldown samples, which came from the 90 °C water bath.

Time [min]	***90 °C***	***60 °C***	***30 °C***
0	*24.4*	*69.8*	*68.4*
10	*82.6*	*62.6*	*42.2*
20	*87.4*	*59.9*	*32.3*
30	*88.7*	*58.7*	*31.5*
40	*89.9*	*59*	*31.7*
50	*89.4*	*59.7*	*31*
60	*89.5*	*58.9*	*31.2*

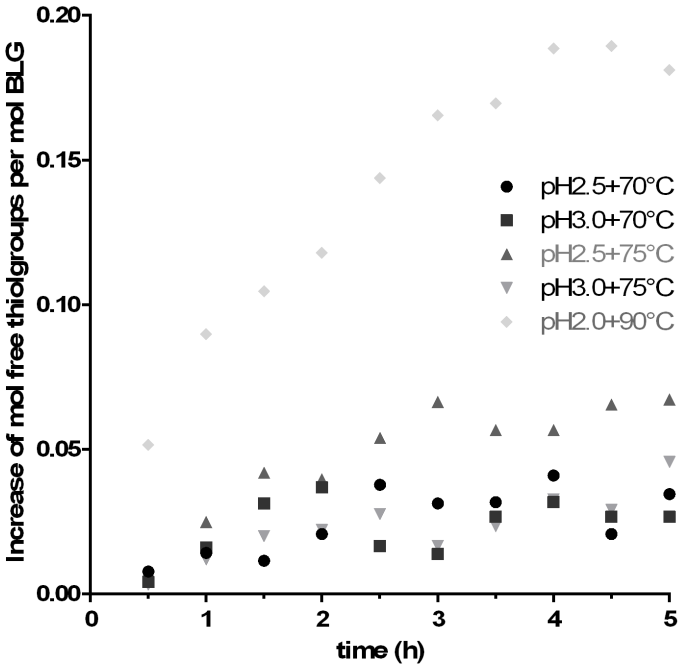

FIG-S 4-11 increasing of free thiolgroups per mol beta-lactoglobulin in dependency of different process parameters with significant stronger unfolding of the protein at pH 2.5 at 75 °C and pH 2 at 90 °C. Evaluation of the protein unfolding at the DOE parameters (70 and 75 °C; pH 2.5 and pH 3) was done by determination of free thiol groups (RSH) using Ellman's assay according to (Wilde et al. 2016). 500 µl of 1 wt% processed protein solution were added to 3500 µl 50mM Tris-glycine buffer (pH 8). 80 µl of 5,5'-Dithiobis(2-nitrobenzoic acid) (DTNB) were added and incubated for 10 min. If DTNB reacts with thiol groups the yellow dianion of the 5-thio-2-nitrobenzoate is formed. The absorbance of the samples was measured at 412 nm using the Genysis 10S UV-VIS spectrometer. Free thiolgroups per mol BLG were calculated by calibration with free L-cystein.

TAB-S 4-9 Pearson r-values of correlation between CFD simulated stress factors in stirring container and ThT FL values t0.5 - t5 at specific.

	t0.5	***t1***	***t2***	***t3***	***t4***	***t5***
max. stress	0.1746482	0.1835896	0.5224116	0.4378982	0.3461084	0.3798785
mean stress	0.1424433	0.1482802	0.5964267	0.6286556	0.5569878	0.5810636
max. shear	0.1505442	0.1626778	0.1532774	-0.1292245	-0.2200836	-0.1772388
mean shear	0.1970264	0.2087627	0.3155995	0.06985268	-0.03658118	0.004276891
max. ε	0.1978246	0.2092528	0.3612502	0.1404416	0.03433202	0.07454865
mean ε	0.1631074	0.1743609	0.362192	0.1763986	0.08234452	0.1238902
max. k	0.03667433	0.04818029	0.2010868	0.05421729	0.002668917	0.05029681
mean k	-0.1357394	-0.1257481	0.154462	0.1701421	0.1810456	0.2318975

TAB-S 4-10 p-values of correlation between CFD simulated stress factors in stirring container and ThT FL values t0.5 - t5

	t0.5	***t1***	***t2***	***t3***	***t4***	***t5***
max. stress	0.6791327	0.6634263	0.1841036	0.2778643	0.4010101	0.3532855
mean stress	0.7365096	0.726023	0.1186027	0.09501184	0.1515416	0.1309001
max. shear	0.7219654	0.7003177	0.7170745	0.760388	0.6004748	0.6745713
mean shear	0.6400247	0.6197941	0.4463702	0.8694516	0.9314715	0.9919809
max. ε	0.6386426	0.6189537	0.3792785	0.740114	0.9356781	0.8607383
mean ε	0.6995544	0.6796389	0.3779444	0.6760497	0.8463005	0.7700719
max. k	0.9312972	0.9098017	0.6330029	0.8985416	0.9949958	0.9058524
mean k	0.7485977	0.7666961	0.7149572	0.6870867	0.6678843	0.580529

TAB-S 4-11 Limit of decision, detection und quantitation of intensities of the second derivation [a.u] analysed by ATR-FTIR, ThT-fluorescence [a.u] by ThT-assay and conversion rate [%] analysed by ultrafiltration calculated by DINtest (DIN 32645). The increase of the zeta-potential as a function of the fibril content showed no linear trend. Therefore, it was not possible to calculate the limits by DINtest.

	FTIR [a.u.]		***ThT [a.u.]***	***conversionrate [%]***	***zeta [mV]***
	1622 cm-1	1632 cm-1			
Decision Limit	8.2E-05	5.0E-04	0.13	7.27	non linear
Detection Limit 2	2.2E-04	1.0E-03	0.73	9.20	
Quantitation Limit	3.8E-04	1.9E-03	1.58	11.99	

5. Manuscript 3 – Aggregation kinetics of amyloid and amyloid-like aggregates under glass bead assisted agitation

Glass beads increase the formation kinetics of beta-lactoglobulin amyloid fibrils

Timon R. Heyn[a], Marcel Schrader[b], Ingo Kampen[b], Arno Kwade[b], Karin Schwarz[a], Julia K. Keppler[a,c]

[a] Institute of Human Nutrition and Food Science, Department of Food Technology, Kiel University, 24118 Kiel, Germany

[b] Institute for Particle Technology, Technical University Braunschweig, 38104 Braunschweig, Germany

[c] Laboratory of Food Process Engineering, Wageningen University, Bornse Weilanden 9, 6708WG, Wageningen, P.O. Box 17, 6700 AA, Wageningen, the Netherlands

5.1. Abstract

In this study beta-lactoglobulin solutions were agitated with glass beads at high temperatures and low pH value to identify the effect of mechanical stressing and surfaces on amyloid aggregation kinetics. The information will provide a better understanding on how specific mechanical factors provide nucleation supporting effect on the assembling of buildings blocks for a more efficient production of functional amyloid aggregates. As aggregate morphologies vary at pH 2 (semiflexible) or pH 3.5 (worm-like), examination at both pH values gives information about their specific formation and stability characteristics. Different diameters of glass beads (20 - 1000 µm), and different shaking frequencies (0 - 280 RPM) were used to vary mechanical stress energy, which was quantified by CFD-DEM simulations. To investigate surface effects, the hydrophobicity and surface roughness of glass beads was altered by modification with stearic acid. Amyloid aggregates and bead surfaces were analysed by ThT-assay, AFM and ATR-FTIR.

Hydrophobic beads with high surface roughness affected the aggregation negatively. The use of non-hydrophobic beads increased the aggregation kinetics of fibrils but not of worm-like aggregates, although, both morphologies had a reduced mean length.

Abbreviations

AFM, atomic force microscopy

APTES, Aminopropyltriethoxysilane

ATR-FTIR, attenuated total reflection Fourier transform infrared spectroscopy

BLG, beta-lactoglobulin

CFD, Computational Fluid Dynamics

DEM, Discrete Element Method

DIC, N,N-Diisopropylcarbodimid

MS, mass spectrometry

RPM, rounds per minute

ThT, Thioflavin-T

UV/VIS; ultraviolet-visible spectroscopy

5.2. Introduction

The whey protein beta-lactoglobulin (BLG) can form amyloid fibrils (i.e., stacked beta sheet formations with a high aspect ratio) at high temperatures and low pH values (Loveday et al. 2017; Cao und Mezzenga 2019). Different amyloid (like) morphologies occur in dependence of the process parameters, for example straight fibrils from hydrolysed peptides at pH 2 or worm-like aggregates from intact BLG at pH 3.5 (vandenAkker et al. 2016; Ye et al. 2018; Heyn et al. 2019). All together, these structures extend the functional potential of the whey protein as a hydrocolloid with regard to gels (Kavanagh et al. 2000b; Gosal et al. 2004; Mudgal et al. 2011a), emulsions (Mantovani et al. 2017; Gao et al. 2017; Serfert et al. 2014), and foams (Peng et al. 2017; Oboroceanu et al. 2014). In addition to that, fibrils can be used for the development of nanocomposites and hybrid materials for biosensors and medical applications (Sasso et al. 2014; Li et al. 2012; Li et al. 2013; Bolisetty et al. 2014), photovoltaics (Bolisetty et al. 2012), catalytic purposes (Bolisetty et al. 2015) or for water purification (Bolisetty et al. 2015). New possible applications of these functional amyloid fibrils are currently being researched globally.

However, the procurement of fibrils as the starting material for all these applications has so far required a great expenditure of energy and production time: Protein solutions (2 and 5 wt%) at pH values < 3.5 are heated at > 80 °C for up to 24 h to achieve 30 to 50 % yield (Loveday et al. 2017; Cao und Mezzenga 2019; Keppler et al. 2019; Heyn et al. 2019). Protein oxidation (i.e., pathogenic carbonyl formation) was found to strongly increase during that time (Keppler et al. 2019). However, a temperature > 80 °C is necessary to induce protein denaturation, acid hydrolysis and self-association during every stage of the amyloid aggregation process otherwise the aggregation rate decreases significantly (Heyn et al. 2020). However, stirring and shearing reduces the required production time of fibrils at > 80 °C to only 5 h (Akkermans et al. 2006; Ng et al. 2016; Bolder et al. 2007; Dunstan et al. 2009). Energy intake by agitation of the protein solution was described earlier to enhance (amyloid) aggregation for different kinds of proteins (Macchi et al. 2011; Sluzky et al. 1991; Ladner-Keay et al. 2014). The addition of beads into the agitation vessel has led to an increase in the formation kinetics of pathogenic amyloid structures from alpha-synuclein (Pronchik et al. 2010). The higher mechanical stress as well as the effect of the particle surface were described as influencing factors (Macchi et al. 2011; Pronchik et al. 2010). It is not yet known whether functional amyloids can also be induced by the presence of beads similarly to natural fibrils. If this were possible such aggregates could be produced more efficiently in the future.

To investigate the effects of mechanical energy input and particle surface on amyloid aggregation of BLG at pH 2 (fibrils) and pH 3.5 (worm-like aggregates) at the threshold temperature of amyloid aggregation of 70 °C (Heyn et al. 2020), glass beads of different size classes (0 - 20, 100 - 200, 400 - 600 and 750 - 1000 µm), and thus different particle mass and surface areas were used. As the kinetic energy transferred to stressing of the protein not only depends on particle mass but also on velocity, agitation between 60 and 280 RPM was conducted. The influence of agitation speed on the stress energy and stress type was simulated with CFD-DEM. The effect of the particle surface (hydrophobicity and roughness) on the amyloid aggregation was examined, by modifying the beads with hydrophobic stearic acid. These experiments will provide a better understanding on the formation of straight fibrils and worm-like amyloid(-like) aggregates. Additionally, new ways for a faster production of fibrils can be achieved. This may help to reduce process expenses such as time and energy input. Furthermore, the oxidation of the protein might be lower than in a high temperature process.

These experiments will provide a better understanding on the formation of straight fibrils and wormlike amyloid(-like) aggregates. Additionally, new ways for a faster production of fibrils can be achieved. This may help to reduce process expenses such as time and energy input.

5.3. Materials and Methods

5.3.1. Materials

Beta-Lactoglobulin (BLG) was obtained from *Davisco Foods International, Inc* (*Eden Prairie, USA*) with 97 % protein and 96 % BLG in dry matter. Calculated NaCl content was 0.0496 mmol/g protein. The glass beads SiLibeads type S and SiLibeads SOLID Micro Glass Beads of different size classes were kindly made available by *Sigmund Lindner GmbH (Germany)*. The calculated mean diameters were ~870, ~520, ~170 and ~6.6 µm, respectively (**TAB 5-1**). Thioflavin-T (ThT > 95 %) was obtained from *EMD Millipore Corp. (USA).* 3-aminopropyltriethoxysilane (APTES ≥ 98.0 %) and N,N-diisopropylcarbodimid (DIC ≥99 %) were obtained from *Sigma Aldrich Inc*. All other chemicals were of analytical grade and obtained from *Sigma Aldrich Inc*. The experiments were conducted with ultrapure water (> 17 MΩcm; total oxidizable carbon < 5ppb).

5.3.2. Preparation of materials

5.3.2.1. Preparation of BLG solutions

BLG was predissolved in ultrapure water, adjusted to the desired pH value of 2.0 or 3.5, using 6 M and 1 M HCl and then diluted to a final protein concentration of 2.5 wt% BLG.

5.3.2.2. Preparation of stearic acid modified glass beads

TAB 5-1 Glass bead characterization. Mean and standard deviation (SD) of the diameter and spec. surface was measured by static light scattering and calculated by application software. Measurement was conducted in triplicate. The surface of 5 g glass beads was calculated using a material density of 2.5 g/cm³. The bound stearic acid was calculated with a surface coverage of 1 molecule per nm².

	Typ S 750 – 1000 µm	***Typ S 400 – 600 µm***	***Solid 100 – 200 µm***	***Solid 0 – 20 µm***
Diameter ± SD [µm]	870.72 ± 110.03	519.68 ± 84.10	171.87 ± 44.25	6.62 ± 2.34
Spec. surface [cm²/cm³]	70.04	118.68	368.85	10 344.13
Surface of 5 g glass beads [cm²]	140.08	237.37	737.71	20 688.27
Bound stearic acid on 5 g glass beads [nMol]	46.5	78.8	245.0	6870.9
Ratio beta-lactoglobulin: stearic acid	1476.3	871.2	280.3	9.996

Glass beads were modified as described by Kockmann et al. (2015): with 4 Mol NaOH treated glass beads were boiled in aminopropyltriethoxysilane (APTES)-ethanol solution for 15 h at 78 °C in a reflux cooling system. After washing for 6 times with ethanol, APTES modified glass beads were dried at 80 °C. 50 ml of a 33 mM stearic acid-ethanol solution was prepared and agitated with N,N-diisopropylcarbodimid (DIC) in a molar ratio of 1:1.5 for 30 min. Glass beads were added and covalent binding of stearic acid on APTES molecules was performed for > 15h under agitation at 150 RPM. Afterwards glass beads were washed 6 times with ethanol and dried under vacuum (50 mbar) before usage. Modification was controlled with attenuated total reflection Fourier-transform infrared spectroscopy (ATR-FTIR) (see **5.3.4.3** for more details). Concentration of free APTES, DIC and stearic acid after each washing step was controlled using mass spectrometry (MS) (results not shown). The exact particle size distribution was controlled by static light scattering (see **5.3.4.4** for more details).

5.3.3. Processing of native BLG and fibril solutions

For investigations of the mechanical stress and influence of the glass bead surface on fibril formation, modified and unmodified glass beads were agitated in a thermo-controlled shaking incubator (*KS 4000 ic, IKA-Werke GmbH & CO. KG, Staufen, Germany*). Native BLG-solutions of pH 2 or pH 3.5 were added to the glass beads into 250 ml shaking flasks with four chicanes and fixed on the agitation plate of the incubator. The temperature was set to 80 °C and monitored by sensors next to the samples. Protocolled temperatures in the solution were between 67 °C and 71 °C. Agitation velocity was 180 or 280 RPM. Agitation radius was 1 cm. For sampling after 0.5, 1, 2, 3 and 4 h agitation was interrupted for 1 min, respectively. Concentration of free stearic acid during the process was controlled using the MS (results not shown). Absorbance of the samples was analysed by UV/VIS (ultraviolet–visible) spectroscopy at 278 nm (*Helios-Gamma, ThermoFisher Scientific, Waltham, USA*) to control the protein concentration and extent of adsorption of protein material to the beads.

5.3.4. Analytical methods

5.3.4.1. Amyloid formation by Thioflavin-T (ThT) assay

The ThT assay was conducted as described by (Keppler et al. 2019). 48µl of the to 1 % diluted sample were mixed with 4 ml phosphate buffered ThT-solution. After 60 s of incubation ThT-fluorescence was measured in a fluorescence spectrophotometer (*Cary Eclipse, Varian GmbH Darmstadt,Germany*) at 440 nm excitation and 482 nm emission wavelength.

5.3.4.2. Fibril morphology and glass bead surface by atomic force microscopy (AFM)

Fibril morphology was investigated using AFM (*NanoWizard 3, JPK Instruments AG (today Bruker Nano GmbH), Berlin, Germany*) following the preparation protocol of Serfert et al. (2014) and Adamcik et al. (2010). For tapping mode, a SHR300 probe were used (force constant 40 N/m, resonance frequency 300 kHz; *BudgetSensors, Innovative Solutions Bulgaria Ltd., Sofia, Bulgaria*) were used at a scan rate of 0.6 Hz. For investigation of the glass bead surfaces the beads were attached to an object slide by superglue and measured with a SHR75 probe (force constant 3 N/m, resonance frequency 75 kHz, *BudgetSensors, Innovative Solutions Bulgaria Ltd., Sofia, Bulgaria*) at a scan rate of 0.6 Hz.

The statistical tools of *Gwyddion 2.53* were used for calculation of maximum peak high and mean roughness (σ) of the AFM scanned particle surfaces. Statistical values were calculated from height irregularities ($z_n - z$) with z as average high value (**EQU 5-1**).

EQU 5-1 calculation of surface-roughness from high irregularities.

$$\sigma = \frac{1}{N}\sum_{n=1}^{N}(z_n - z)$$

5.3.4.3. Glass bead characterisation by static light scattering

Particle size distribution of the glass beads was analysed using static light scattering (refractive index of 1.51, *Horiba LA-950V2, Retsch Technology, today Microtrac Retsch GmbH, Haan, Germany*) at dry mode. Mean and standard deviation (SD) of the diameter and spec. surface was calculated by the application software (*Horiba LA-950 V.7.02, Horiba Jobin Yvon GmbH, Beinsheim, Germany*). The surface of 5 g glass beads was calculated using a material density of 2.5 g/cm³. The bound stearic acid was calculated with a surface coverage of 1 molecule per nm².

5.3.4.4. Glass bead surfaces by ATR-FT infrared spectroscopy

Infrared spectra of glass bead surfaces were analysed using a Tensor 2 System from *Bruker Optik GmbH, Ettlingen, Germany* fitted with a at 25 °C thermally controlled BioATR Cell 2. The ~6.6 µm glass beads were applied to the ATR crystal before or after modification, or after use in the fibril formation process. The spectra were acquired and averaged over 120 scans at a resolution of 0.7 cm^{-1}. After atmospheric correction for absorbance of CO_2 and H_2O as vapour, the protein spectra from 4000 cm^{-1} to 900 cm^{-1} were baseline corrected.

5.3.5. Quantification of the mechanical stress via CFD-Dem simulations

To quantify the mechanical stress caused by the addition of glass spheres, computational fluid dynamics (CFD) simulations were used in combination with the discrete element method (DEM) to investigate the three phase flow. The basic simulation set-up was adopted from Schrader et al. (2019) and only the material properties of the fluid were adapted. Slight modifications in bead size [520 – 870 µm], bead number [27 000 – 5 800], agitation speed [60 – 280 RPM] and rotation radius [1 cm] were applied. The values of the surface tension, the dyn. viscosity and the density were adjusted to 57.05 x 10^{-3} N s^{-1}, 0.8 mPas and 1001.33 kg m^{-3}, respectively (Heyn et al. 2020). By the specific evaluation of the bead bead and bead wall collisions according to Beinert et al. (2015), coupled CFD DEM simulations provide quantitative data on the magnitude of the stress energy and frequency for different experimental

test parameters. For a deeper understanding of the dominant stress mechanism, the stress energies were subdivided into normal and shear contacts.

5.3.6. Statistical analysis

Statistical analysis of the collected data was conducted by GraphPad PRISM (*version 9.0.2, GraphPad Software, San Diego, USA*). Significance of the results was tested by 2way ANOVA with an alpha of 0.05. Multiple comparisons were corrected with the Tukey post hoc test.

5.4. Results

5.4.1. Characterisation of glass bead surfaces

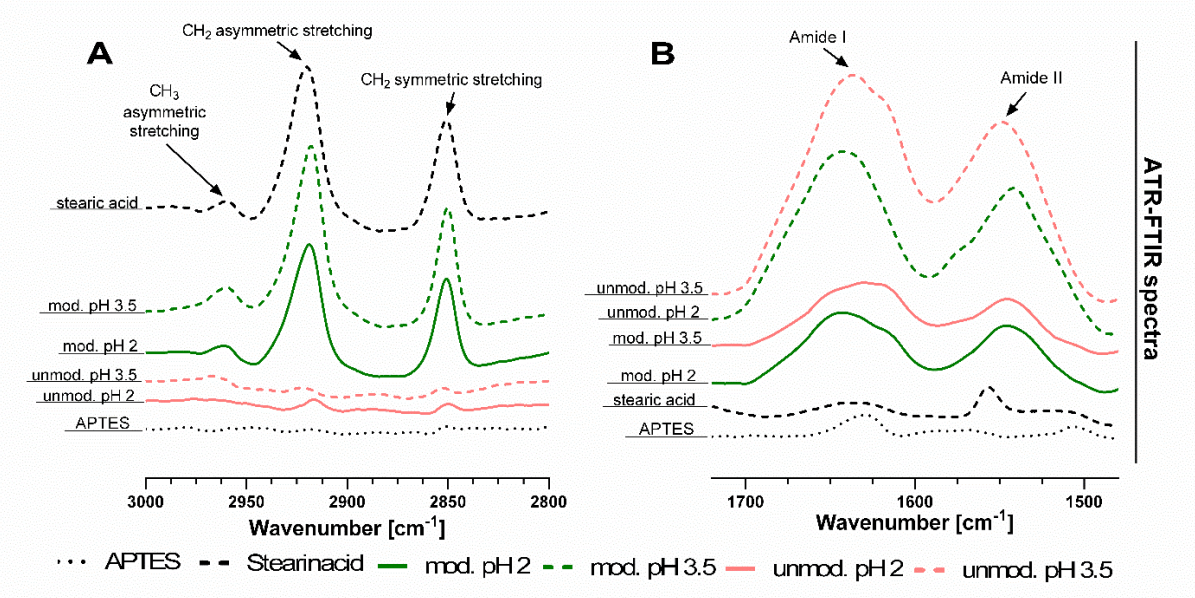

FIG 5-1 ATR-FTIR spectra of modified and unmodified glass beads. For better visibility an intensity transmission on the Y axis was conducted. Lipid relevant CH_3 asymmetric (2950 – 2960 cm^{-1}), CH_2 asymmetric (2915 – 2930 cm^{-1}) and CH_2 symmetric stretch region (2852 – 2800 cm^{-1}) **(A)** and protein relevant Amid I (1700 – 1600 cm^{-1}) and Amid II band (1555 – 1535cm^{-1}) **(B)** of ATR-FTIR analysed modified and unmodified ~6.6 µm glass beads. APTES: with 3-Aminopropyltriethoxysilan modified glass beads. Stearic acid: with stearic acid modified glass beads (after APTES modification). Mod. pH 2/pH 3.5: stearic acid modified glass beads which were agitated at 80 °C in pH 2 / pH 3.5 BLG solution. Unmod. pH 2 / pH 3.5: unmodified glass beads which were agitated at 80 °C in pH 2 / pH 3.5 BLG solution.

The surface chemistry of the smallest particle size (~6.6 µm) could be investigated by ATR-FTIR. Larger beads did not provide enough contact area to the surface of the ATR-crystal for a sufficient signal-to-noise ratio. The absorption of wavenumbers in the asymmetric and symmetric stretching area of CH3 and CH2 compounds (2960 - 2800 cm^{-1}) reflects the surface coating with a lipid (here stearic acid). Absorptions in the wavenumber of amide I (1700 - 1600 cm^{-1}) and amide II (1555 - 1535 cm^{-1}) region show the occupation of the surface with proteinogenic compounds. It has been shown that the 2-step modification of the surface first with APTES and then with stearic acid leads to absorption in the CH stretching area (**FIG 5-1 A**). As visible in **FIG 5-1 B B** the adsorption of proteinogenic material to the surfaces of unmodified beads were higher compared to stearic acid modified beads. Furthermore, the amide I band of stearic acid modified beads incubated in pH 2 and pH 3.5 BLG solution, as well as unmodified beads incubated in pH 3.5 solution, showed a slight "shoulder" at 1620 cm^{-1}.

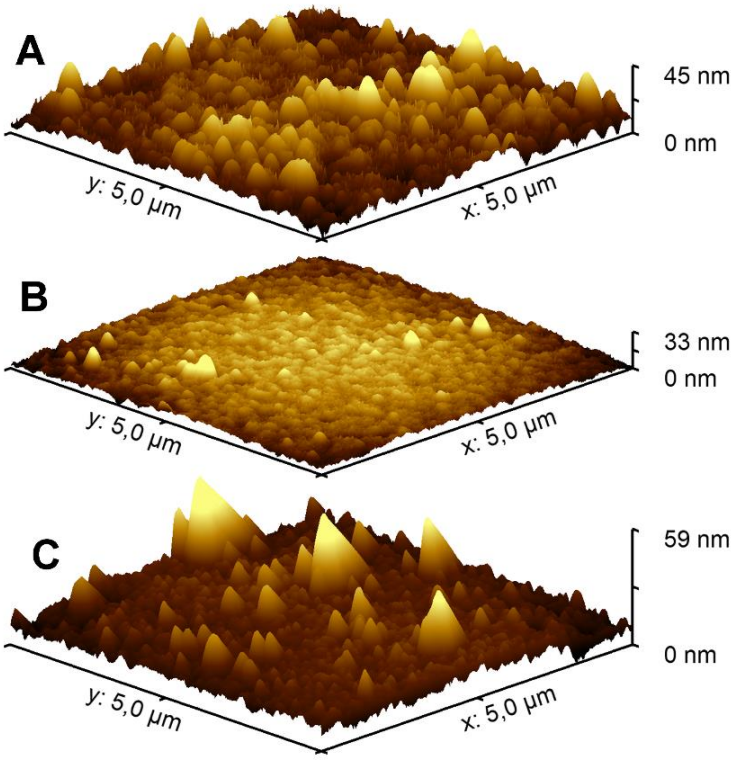

FIG 5-2 Atomic Force Microscopy scanned surfaces of unmodified (**A**), 4 molar sodium hydroxide treated (**B**) or covalently bonded stearic acid modified (**C**) glass beads with a diameter of ~520 µm.

The analysis of the physical surface properties with the help of AFM gave evidence that by treating the glass surfaces of glass beads with 4 Mol NaOH, the surface relief was removed (**FIG 5-2 A compared to B**). The calculated mean roughness (deviation from the statistical mean height value) decreases about 30 - 35 %. The modification of the spherical surfaces with

stearic acid led to the presence of punctual elevations with a maximum peak height (difference from the average height relief) of ~40 nm (**FIG 5-2 C**).

5.4.2. Influence of particle size and agitation speed on amyloid aggregation

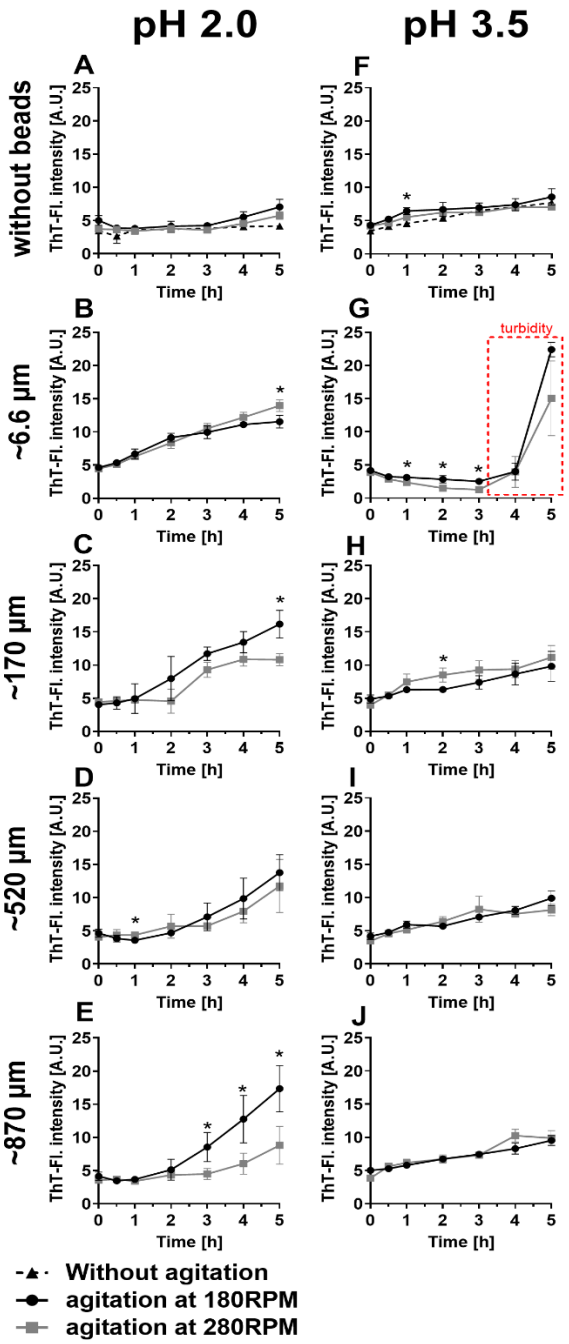

FIG 5-3 Influence of glass beads with different diameters in the shaking flasks on the amyloid aggregation kinetics of beta-lactoglobulin at ~70 °C solution temperature measured with ThT-fluorescence assay (ThT-Fl. intensity) over 5 hours. Protein solutions were adjusted to pH 2.0 or 3.5 and agitated at 0 RPM, 180 RPM or 280 RPM. Significant differences in THT-Fl. between shaking frequencies were marked with *.

The use of unmodified glass beads in the agitation incubator at pH 2 and >70 °C generally produced a greater increase in ThT-fluorescence (ThT-Fl) over time than agitating without glass beads (**FIG 5-3 A vs. B - E**). By agitating without glass beads, the ThT-Fl. rose from 5.0 a.u. to 7.1 within 5 h incubation. Increasing the bead size roughly resulted in a minor increase of the ThT-Fl during the 5 h: By using glass beads at 180 RPM, a maximum ThT-Fl. of 11.6 a.u. (~6.6 µm beads), 16.2. (~170 µm beads), 13.8 a.u. (~520 µm beads), and 17.4 a.u. (~870 µm beads) was reached (**TAB 5-2**).

The use of small beads (~6.6 µm) in combination with a faster agitation speed of 280 RPM increased the maximum ThT-Fl. after 5 hours from 5 to 14.0 a.u. (FIG 4 A). However, at 280 RPM the use of middle sized (~170 µm), or big sized (~870 µm) beads significantly decreased the yield as compared to 180 RPM to a maximum ThT-Fl. of 10.8 a.u (**FIG 5-3 C**) and 8.8 a.u (**FIG 5-3 E)** after 5 hours, respectively.

The same experiment at pH 3.5 led only to a slightly higher increase in ThT-Fl. compared with pH 2 when glass beads were used (**FIG 5-3 F - J**).). Shaking at 180 RPM without beads led to a ThT-Fl. increase of 4.3 ± 0.3 a.u. to 8.6 ± 1.2, while after 5 hours with beads ThT-Fl. of 9.8 a.u. (~170 µm), 9.9 a.u. (~520 µm) or 9.5 a.u. (~870 µm) were achieved (**TAB 5-2**). The use of ~6.6 µm beads led to protein precipitation after ~4 h. In the course of incubation, the solution got turbid, which made an adequate measurement of the sample after 5 hours impossible (**FIG 5-3 G**). This kind of observation was not made for the pH 2 solutions.

An increase of the shaking speed to 280 RPM led with the BLG solutions at pH 3.5 to few changes in the ThT-Fl.: After 5 hours: 7.1 a.u. (without beads), 11.2 a.u. (~170 µm), 8.1 a.u. (~520 µm), 9.9 a.u. (~870 µm) (**FIG 5-3 F and H - J**). Again, the ~6.6 µm beads caused precipitation of the protein, and thus turbidity of the solution (**FIG 5-3 G**). Different particle sizes and different agitation velocities led to a different stress energy. **FIG 5-4** illustrates the dependence of ThT-Fl. on the respective stress energy at pH 2 and ~70 °C protein.

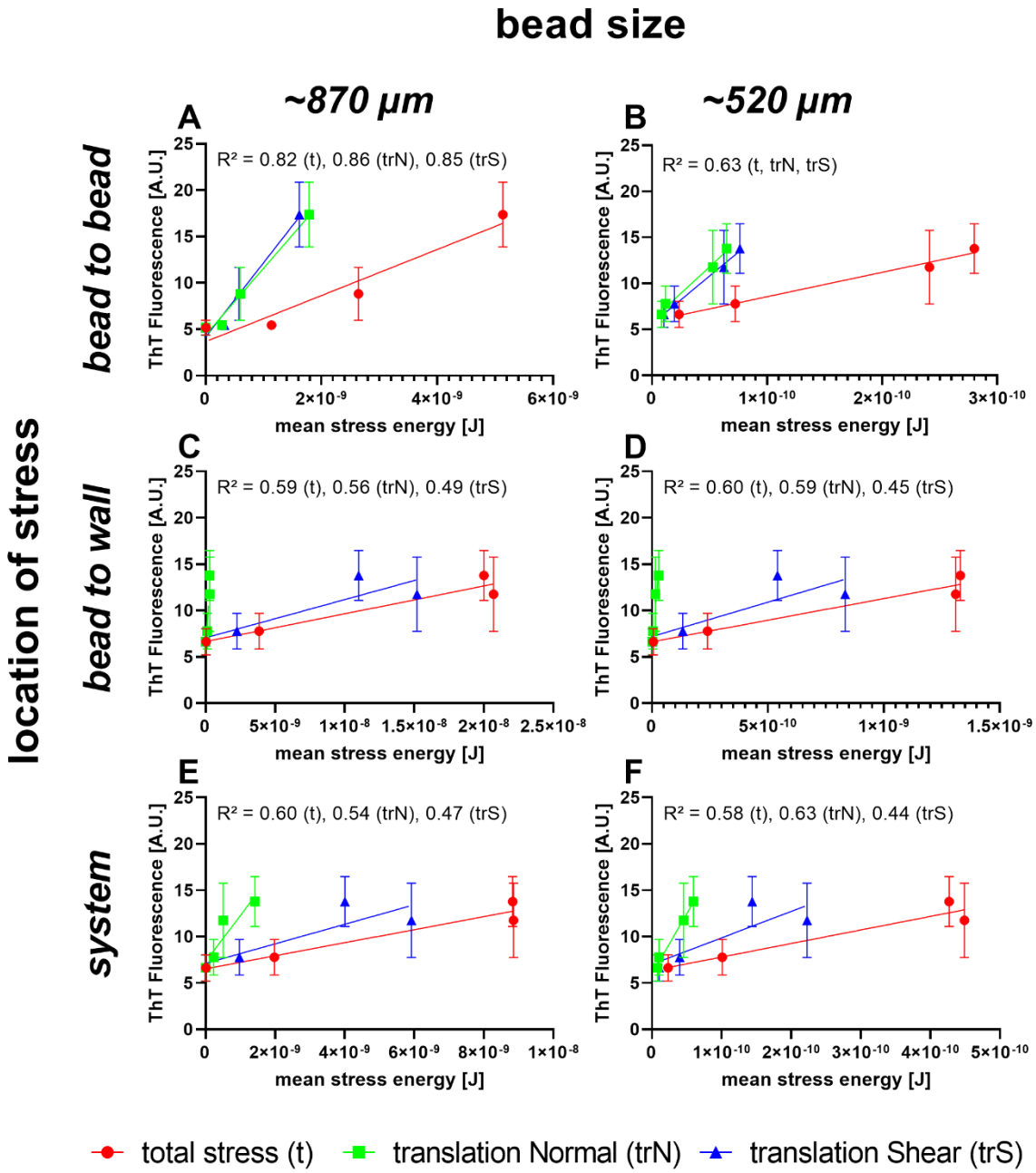

FIG 5-4 Increase of ThT-Fl. in pH 2 solutions after 5 hours depending on the stress energy in the presence of unmodified glass beads with diameter of ~870 µm vs. 520 µm. Stress energy was calculated by CFD-DEM simulation. The total stress energy was differentiated according to the type of stress movement (translational normal/ translational shear) and the locality of the stress (bead to bead / bead to wall). The stress energy calculated in the whole system represents an average of the bead to bead and bead to wall stress energy. Plotted values were linearly fitted and corresponding adjusted R-squared values are shown.

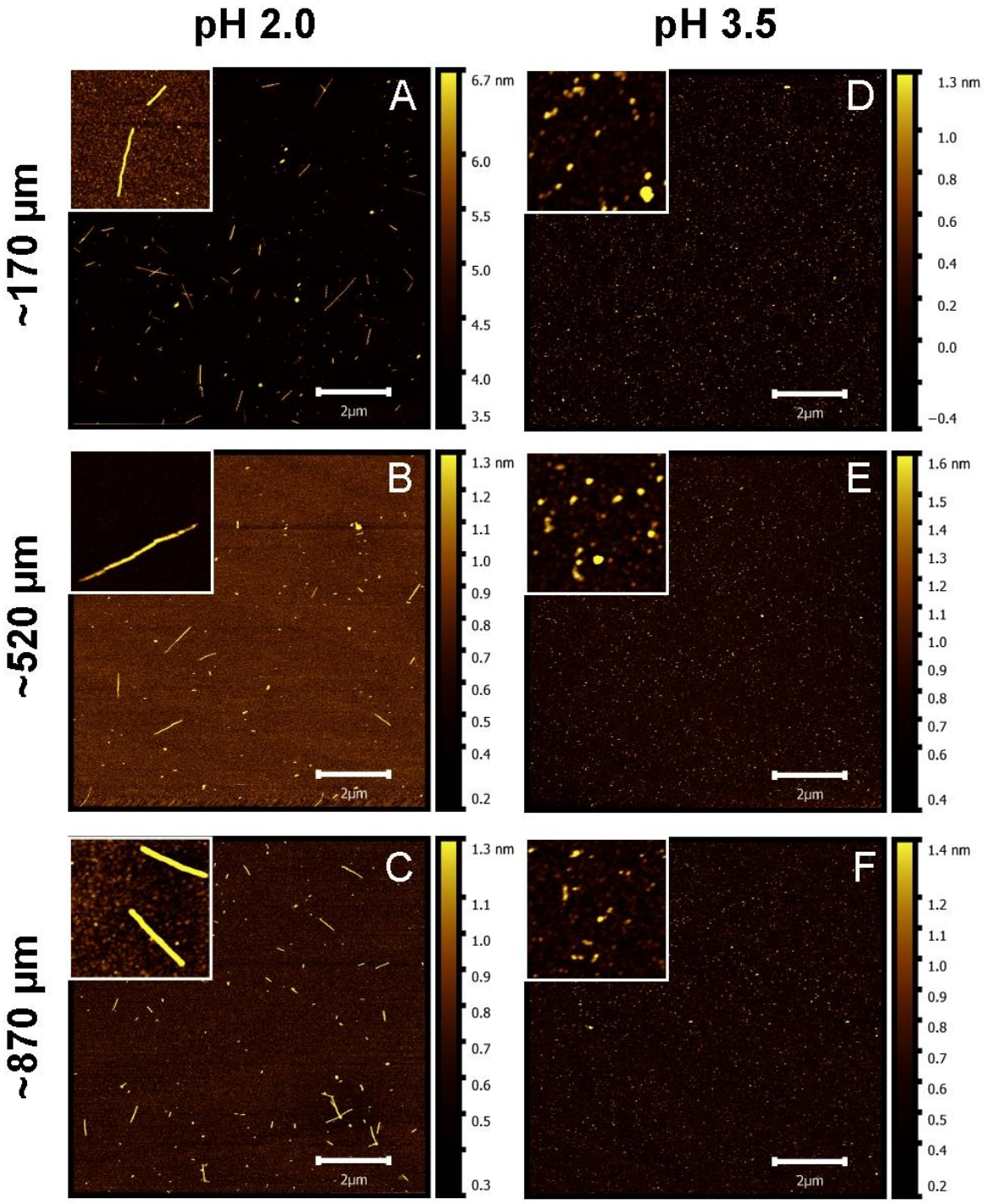

FIG 5-5 Atomic force microscopy images of samples with 0.01 wt% beta-lactoglobulin after 5 h at ~70 °C. Samples were agitated at 180 RPM with unmodified glass beads of different diameter and at different pH values. (**A**) Diameter of ~170 µm and pH 2. (**B**) Diameter of ~520 µm and pH 2. (**C**) Diameter of ~870 µm and pH 2. (**D**) Diameter of ~170 µm and pH 3.5. (**E**) Diameter of ~520 µm and pH 3.5. (**F**) Diameter of ~870 µm and pH 3.5. Edge length of the white squares is 0.5 to 1 µm.

Higher agitation velocities (280 RPM) led to lower ThT-Fl. (8.8 a.u. [~870 µm]; 11.8 a.u. [~520 µm] than lower agitation velocities (180 RPM) (ThT-Fl. 17.4 a.u. [~870 µm]; 13.8 a.u. . [~520 µm]). The stress energy introduced by the bead to bead (BB) collision or the stress energy which is generated by the movement of the beads over the bottle bottom or the bottle wall (BW), is higher for the agitated systems with larger glass beads [~870 µm] than for smaller glass beads [~520 µm] (8.9×10^{-9} J vs 4.5×10^{-10} J). Focusing on the type of stress, it was found, that the shear stress strongly dominates over the normal stress by the factor of 20 – 50 and has a higher value at an agitation velocity of 240 RPM (5.92x10-9 [~870 µm]; 2.23x10-10 [~520 µm]), compared to 180 RPM (4.01x10-9 [~870 µm]; 1.44x10-10 [~520 µm]). Interestingly, the energy mean intake generated by translational normal stress of, has the highest value of 1.79 $x10^{-9}$ J at an agitation velocity of 180 RPM.

The investigation of the aggregate morphology confirmed a formation of strand-like fibrils at pH 2 when beads larger than 100 µm were added (**FIG 5-5 A - C**). In all experiments, the very short contour length of 1 µm maximum at an average length of ~370 ± 220 nm was evident, as was the presence of many very short protein particles < 100 nm . At a pH value of 3.5, barely completed worm-like aggregates were found (**FIG 5-5 D – F**). The present aggregates had an average length of ~42 ± 17 nm. In addition, numerous protein particles of < 10 nm were observed.

5.4.3. Influence of particle surface on amyloid aggregation

To investigate the influence of the particle surface on amyloid aggregation, the surface chemistry of the glass beads was modified using covalently bound stearic acid. It was found that the hydrophobic modified surfaces inhibited the amyloid aggregation **(FIG 5-6)**. **)**. Thus, at pH 2, the ThT-Fl. increased after 5 hours to a maximum of 6.7 ± 1.3 a.u.(~6.6 µm), 8.9 ± 0.9 a.u. (~170 µm), 7.6 ± 1.0 a.u. (~520 µm) and 7.8 ± 1.8 a.u. (~870 µm), which were all significantly lower than for unmodified glass beads (**FIG 5-7 A - D**). At pH 3.5 the application of modified beads led only to small differences for the ~520 µm beads (**FIG 5-7 G**), which had a ThT-Fl. of 7.5 ± 0.5 a.u. instead of 8.1 a.u.. The analysis of the free protein concentration in solution by UV/VIS (see supporting information **TAB S5-2**) revealed a strong protein adsorption at pH 3.5 to the unmodified ~6.6 µm beads and increased occurrence of turbidity in the protein solution after 4 hours (**FIG 5-6 E**). Interestingly, using of ~6.6 µm modified beads seem to adsorb protein but avoid this turbidity in the solution.

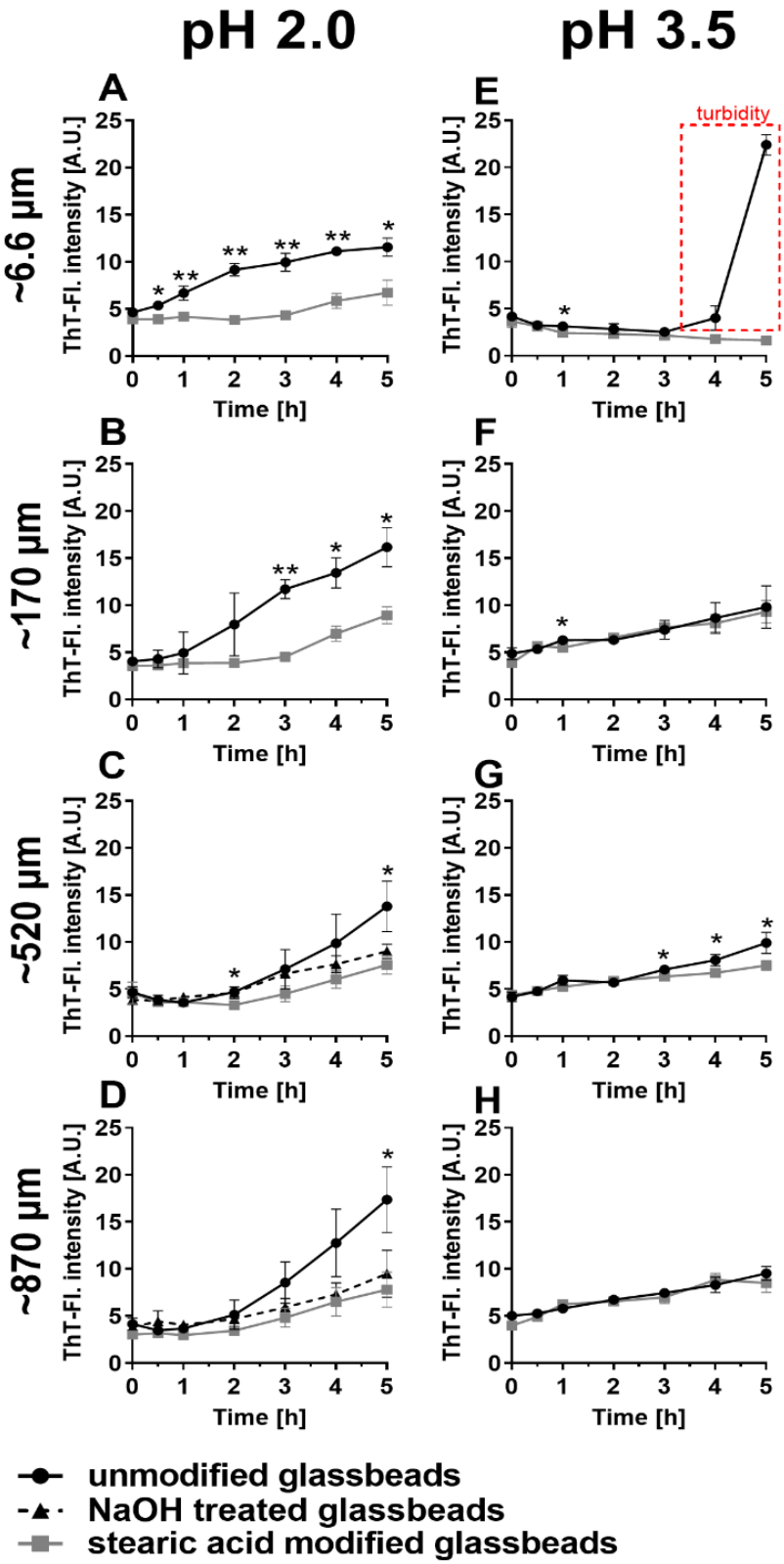

FIG 5-6 Influence of stearic acid surface modified glass beads with different diameters on the amyloid aggregation of beta-lactoglobulin at 80 °C measured with ThT FL assay over 5 h. Protein solutions were adjusted to pH 2.0 or pH 3.5 and agitated at 180 RPM. The results for unmodified glass beads correspond to the data in **FIG 5-3**. Significant differences in THT-Fl. between different treated glass beads were marked with *.

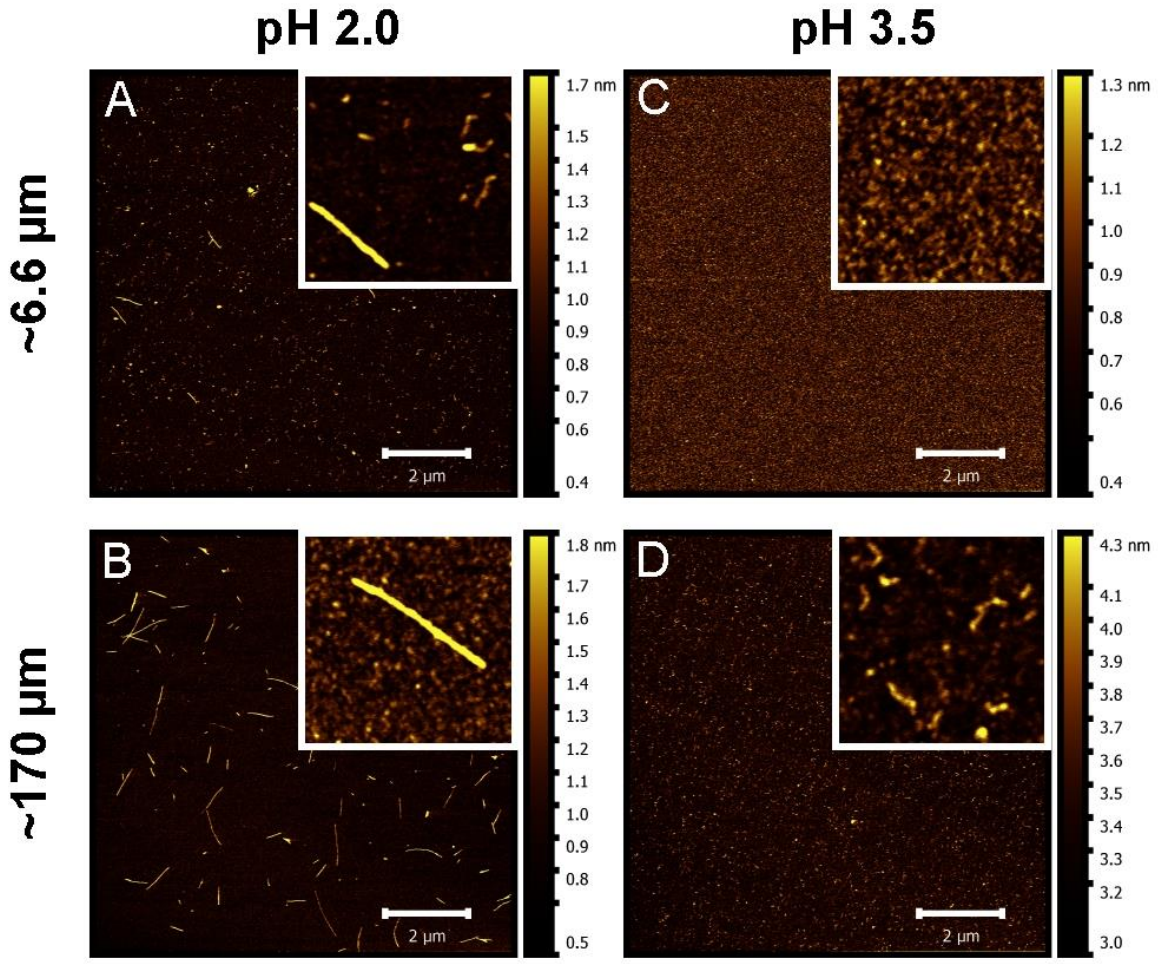

FIG 5-7 Atomic force microscopy images of samples with 0.01 wt% beta-lactoglobulin samples after 5 h at ~70 °C. Samples were agitated at 180 RPM with stearic modified glass beads of different diameter and at different pH values. (A) Diameter of ~6.6 µm and pH 2. (B) Diameter of ~170 µm and pH 2. (C) Diameter of ~6.6 µm and pH 3.5. (D) Diameter of ~170 µm and pH 3.5.

If the modified beads ~6.6 µm are used at pH 2, the AFM analysis (**FIG 5-7 A)** illustrated not only the sporadic presence of strand-like fibrils with a length of ~400 ± 130 nm, but also a large number of worm-like aggregations with a length of ~55 ± 17 nm. Modified beads with a diameter of ~170 µm did not cause worm-like structures at pH 2, but led to strand-like fibrils of ~500 ± 250 nm length (**FIG 5-7 B**). The high adsorption of protein at pH 3.5 to the ~6.6 µm beads led to a high loss of protein in the solution, which was also shown by the fact that no protein aggregates were detected by AFM (**FIG 5-7 C**). At pH 3.5 no significant adsorption to the ~170 µm beads was measured and worm-like morphologies of ~60 ± 21 nm contour length could be observed (**FIG 5-7 D**).

TAB 5-2 Influence of unmodified and modified glass beads on fibril yield (ThT-Fl.), aggregation kinetics (lag-phase), morphology (contour length) and adsorption to the particle surface in agitated (180 RPM) pH 2 or pH 3.5 protein solution at ~70 °C.

pH value of protein solution		***pH 2***			***pH 3.5***	
Surface of glass beads		unmodified	Stearic acid modified	NaOH treated	unmodified	Stearic acid modified
Maximal ThT FL [A.U.]*		17.4	8.9	9.4	9.9	9.3
Lag-phase	***~6.6 µm***	-	++		-	o
	~170 µm	+	++		-	-
	~520 µm	++	++		-	-
	~870 µm	++	++	++	-	-
contour-length [nm]	***~6.6 µm***	o	~400 ± 130	o	o	~55 ± 17
	~170 µm	~335 ± 230	~500 ± 250	o	~42 ± 17	~60 ± 21
	~520 µm	~460 ± 280	o	o	~38 ± 15	o
	~870 µm	~310 ± 170	o	o	~37 ± 15	o
Adsorption*	***aggregates***	-	+	o	++	++
	monomers/dimers	++	+	o	++	+

Legend: (-)non-existent/low; (+) existent/increased: (++) highly visible/high; (o) no results available
****~870 µm beads were used at 180 RPM***
*****~6.6 µm beads were used at 180 RPM***

5.5. Discussion

5.5.1. Effect of glass bead size and agitation on amyloid aggregation

To test the effect of glass beads on the aggregation kinetics and morphology, different bead sizes and agitation velocities were tested. When glass beads of ~870 µm diameter were used, the fibril formation yield after 5 h was higher than those observed in standard experiments, where a magnetic stirrer is used at comparable conditions (Heyn et al. (2020). The BLG solution processed by agitation with beads at a mean temperature of 69.2 °C had a ThT-Fl. of approx. 17. a.u. (**TAB 5-2**), while stirring reached only approx. 3 a.u.. Similar high values of approx. 18. a.u. were achieved with stirring at a higher temperature of 75 °C. Accordingly, the use of beads during agitation (stirring, shearing) can increase the aggregation kinetics in the lower temperature range, and allows a process temperature reduction of 5 K. AFM analyses confirm the presence of fibrils in the bead system at 70 °C. However, the AFM analyses also gave evidence of a fragmentation of the bead-induced fibrils, so that a short contour length of ~0.5 µm (**FIG 5-5 A to C/ TAB 5-2**) was achieved compared with conventional fibrils of >7 µm

(Heyn et al. 2019). Previous results have shown, that the ThT-Fl. is independent to the fibril length distribution (Heyn et al. 2021).

Despite acceleration effect on fibril formation at pH 2, the aggregation of worm-like amyloid aggregates at pH 3.5 seems to be independent of the addition of glass beads and agitation velocity.

Processing of the protein solutions at pH 3.5 with glass beads led to direct increase of the ThT-Fl within minutes. Therefore, no lag phase was evident (**FIG 5-3 F - J**), in contrast to pH 2 systems, where an increase of ThT-Fl. occurred with a lag time when no bead, or beads > 400µm were used (**FIG 5-3 C to E** This pH 2 lag phase is based on the provision of the self-assembling peptide building blocks for the fibrils by acid hydrolysis of BLG, and represents the initial nucleus phase of the amyloid aggregates (Dave et al. 2013; Akkermans et al. 2006). A different aggregation mechanism of amyloid-like aggregates at pH values ≥3.35, where intact BLG forms the self-associating building blocks due to reduced acid hydrolysis, has already been discussed previously (Mudgal et al. 2011b; Serfert et al. 2014; Heyn et al. 2019). A comparison with unpublished data, indicate a slightly higher aggregation kinetics for these agitated samples compared to stirred protein solutions. The AFM analysis demonstrated that in the agitation vessel with beads only fragments of worm-like aggregates were formed (**FIG 5-5 D - F**)), which contrasts to the formation of worm-like aggregates (50 – 200 nm) induced by magnetic stirring at similar conditions but higher temperature (Heyn et al. 2019; Serfert et al. 2014). This indicates a lower mechanical stability of the worm-like aggregates, as reported previously (Heyn et al. 2019).

The increased fibril formation occurring at larger bead sizes (> 400 µm) at pH 2 are possibly based on the physical energy input of the beads to the protein by shear, impact and rolling movement (Schrader et al. 2019). According to the literature, the input of shear forces accelerates fibril formation by carrying building blocks to the fibril tips (Akkermans et al. 2008), or by fragmentation of already formed protofibrils into seeds and a subsequent secondary nucleation (Dunstan et al. 2009). That this effect is of great relevance here could be deduced from the high apparent degree of fragmentation of fibrils at pH 2 and amyloid-like aggregates at pH 3.5 (**FIG 5-6**). At the same time, this finding confirms once again that the formation of amyloid like aggregates at pH 3.5 is independent of nucleation, since despite visible fragments no acceleration of aggregation kinetics is apparent (**FIG 5-3 H - J**).). Akkermans et al. (2008) have already shown that there is a parabolic relationship between fibril formation kinetics and shear input. The CFD-DEM results shown in **FIG 5-4** can further differentiate this dependence

into the different types of stress acting on the aggregates. Too high agitation velocities had an adverse effect on the fibril formation. The CFD-DEM simulation found an increased energy intake, due to shear stress, but a decreasing energy intake due to normal translational stress in high agitating (240 RPM) systems. Therefore, two explanations can be suggested. Firstly, at higher agitation velocities the shear stress becomes too high resulting in a parabolic relationship between shear and fibril formation. Secondly, the translation normal stress is decisive for the fibril formation, and its drop at higher agitation velocities is possibly because of "out of phase" phenomenon (Büchs, Lotter and Milbradt, 2000)). This may lead to decreased ThT-Fl. Since the increase in shear stress is disproportionally small compared to the "loss" of ThT-Fl., the second explanation is better evidenced. Further investigations show that the ThT-Fl. of mature fibrils were not affected by high stress (~74 J ml-1) (Heyn et al. 2021).

In the case of smaller beads, the lag phase at pH 2 is minimized (**TAB 5-2**). This observation may be attributed to the specific surface area at this particle size, which is large enough to enable "surface-assisted nucleation" effects (Linse et al. 2007; Pronchik et al. 2010). Known effects related to amyloid aggregation are the concentration of the protein on the particle surfaces and their subsequent assembling by diffusion in a two dimensional area (Shezad et al. 2016). Further effects may be destabilization (Perriman et al. 2007), or unfolding (Marengo et al. 2016) of the protein at the interfaces, which can increase the hydrolysis kinetics by exposing acid cleavable asparagine-linked peptides (van der Linden und Venema 2007). Although significant protein (or fibril) adsorption on the glass beads was not evident with FTIR (**FIG 5-1 B**), these effects could also be relevant in case of temporary adsorption, as it was described for the formation of alpha-synuclein fibrils (Pronchik et al. 2010; Shezad et al. 2016).

5.5.2. Effect of glass particle surface on amyloid aggregation

5.5.2.1. Adsorption effects

To test the effect of the chemical nature of interfaces on fibril formation, the particle surfaces were chemically modified with stearic acid. Analysis by ATR-FTIR showed the successful binding of stearic acid to the bead surface (**FIG 5-1**). The FTIR analysis of the protein-specific amide bands also revealed BLG adsorption to the glass bead surface after the beads were incubated for 5 h in the pH 2, or pH 3.5 protein solution: Aggregates formed at pH 3.5 showed a typical amide I shoulder at 1620 cm^{-1}, indicating the presence of aggregates on the bead surface irrespective of the surface modification (Kavanagh et al. 2000a). However, at pH 2 this shoulder only occurred when modified hydrophobic beads were used, suggesting that fibrillar

BLG does not adhere to the unmodified glass surface, but to the hydrophobic stearic acid surface. Additionally, due to their high stiffness and aspect-ratio (Adamcik et al. 2010), fibrillar aggregates may offer large targets for the shear flow and are thus easily removed from a solid, rough particle surface by shear forces. The stearic acid modified bead surfaces (**FIG 5-1 A**)) in turn provide hydrophobic anchor points, from which larger fibrils cannot be removed by the shear flow this easily. Whereas the worm-like and much smaller structures at pH 3.5 probably remained on the smooth unmodified glass surfaces due to their flexibility, small surface area and lower surface charge than the fibrils at pH 2 (Mudgal et al. 2011b; Heyn et al. 2019; Serfert et al. 2014). This adsorption phenomenon could also indicate a potential of the pH 3.5 aggregates for interface specific functionalities.

5.5.2.2. Aggregation kinetics

The use of stearic acid modified glass beads lowered the fibrillation rate in pH 2 solution compared with the use of unmodified glass beads. For the smallest particle sizes < 200 µm, the presence of the lag phase was evident again (**FIG 5-6 A / TAB 5-2**).). As shown exemplarily for the ~870 µm beads, also the initial treatment with NaOH led to a decrease of the aggregation kinetics. Possibly the modification causes several effects, which inhibit the nucleation enhancing properties. In addition to the chemical alteration, the beads also changed their physical surface properties in the course of particle modification. The 15 min activation step using 4 M NaOH solution resulted in the removal of the surface relief on the glass beads (**FIG 5-2**). Alteration of the glass particle surfaces by NaOH treatment was described before (Ozmen et al. 2009). Furthermore, too high positive surface charge after the NaOH treatment, can strongly reduce the particle contact by electrostatic repulsion forces. The change in physical surface properties can alter the friction, shear or impact forces acting between the beads and thus has an influence on the mechanical energy input. Modification with stearic acid led to an altered particle surface, with different characteristics for different particle sizes (**FIG 5-2 C**). In addition, a change in surface Youngs modulus, hardness and charge could be possible, but has not been tested here.

The increase in particle hydrophobicity in the course of stearic acid bonding might also have altered the described adsorption behaviour of BLG (Pronchik et al. 2010) or 2D diffusion at the surface (Shezad et al. 2016), which would explain the reoccurrence of a lag phase for the smallest beads (**FIG 5-6 B / TAB 5-2**).). Non-covalent interactions between the particle surface bound fatty acid residues with the BLG, especially with the cavity of BLG, are also conceivable

(Loch et al. 2012). Although BLGs affinity to saturated fatty acids is very low at pH values < 4.5 (Frapin et al. 1993), the affinity of BLG to fatty acids can be different in denatured, aggregated or hydrolysed state (Le Maux et al. 2014). In fact, the ATR-FTIR investigations revealed a lower intensity at pH 2 and at pH 3.5 for protein material at the modified glass bead surface in general (**FIG 5-1 B**), compared to the unmodified surface. However, at the modified surface, the presence of aggregated material was evident at pH 2, indicating that fibrils are more likely to attach to hydrophobic surfaces, which corresponds to the surface active character of the fibrils to oil- and air-water interfaces (Gao et al. 2017; Serfert et al. 2014; Moro et al. 2013).

5.6. Conclusion

The investigations performed in this study primarily show that the addition of glass beads in an agitation process positively supported the fibril formation of BLG at pH 2 while the aggregates formed at pH 3.5 were not affected in the aggregation kinetics. The way the fibril formation is influenced by the glass beads can be different for varying glass bead size: Larger beads primarily affected the fibril formation by additional mechanical energy input and in turn the kinetics was accelerated by secondary nucleation. However, this effect resulted in the formation of shorter fibrils and aggregate lengths than in a stirring process, probably because fibrils were fragmented during or after their formation. Based on CFD-DEM simulation, the translational normal stress, due to bead-to-bead collision, could be the decisive factor for the increased fibril formation in systems agitated with glass beads. Overall, the application of glass beads in a shaken system could accelerate fibril formation compared to a stirred system, opens up the possibility of carrying out fibril formation at lower temperatures. Especially collision loads seem to have a promoting effect. It is therefore conceivable that fibril formation could be enhanced by transforming the motion vectors from a two-dimensional circular motion to a one-dimensional plane (back and forth). As a disadvantage, the fragmentation of the fibrils in the process can be considered, whereby specific functions based on the high aspect ratio are lost. The smallest glass beads used offered a sufficiently large surface area to support the nucleation of fibrils during the lag phase by interface effects. The covalent bonding of stearic acid led to a strong reduction of these supportive effects. The reason for this might be the chemical and physical alteration of the particle surface in the course of the modification process. Based on these findings, smooth and more hydrophilic surfaces are more advantageous for particle / fibril formation. However, it can also be deduced from the results that different aggregate forms have different affinities for varying surfaces. This insight can be used to derive areas of application

for specific aggregate morphologies or to separate specific morphologies from a heterogenous system. More detailed knowledge should be gained in the future on the influence of different surface types (polymers, carboxylic acids of different lengths, etc.) and heterogeneous particle mixtures.

Acknowledgement
This project was funded by DFG SPP 1934 DiSPBiotech (Project no. 315456892 and 315460011). We are grateful to Lisiane Petersen and Jesco Reimers of the Food Technology Division Kiel for skilful help in the lab, as well as to Stephanie Michel from the Institute for Particle Technology for conducting the AFM measurements and Kathrin Schrinner from the Institute of Biochemical Engineering in Braunschweig for providing the agitation flask. The authors would like to acknowledge Wolfgang Voit from Sigmund Lindner GmbH for the kind provision of the glass beads.

5.7. References

Adamcik, Jozef; Jung, Jin-Mi; Flakowski, Jérôme; Los Rios, Paolo de; Dietler, Giovanni; Mezzenga, Raffaele (2010): Understanding amyloid aggregation by statistical analysis of atomic force microscopy images. In: *Nature nanotechnology* 5 (6), S. 423–428. DOI: 10.1038/nnano.2010.59.

Akkermans, Cynthia; van der Goot, Atze Jan; Venema, Paul; van der Linden, Erik; Boom, Remko M. (2008): Formation of fibrillar whey protein aggregates. Influence of heat and shear treatment, and resulting rheology. In: *Food Hydrocolloids* 22 (7), S. 1315–1325. DOI: 10.1016/j.foodhyd.2007.07.001.

Akkermans, Cynthia; Venema, Paul; Rogers, Salman S.; van der Goot, Atze Jan; Boom, Remko M.; van der Linden, Erik (2006): Shear Pulses Nucleate Fibril Aggregation. In: *Food Biophysics* 1 (3), S. 144–150. DOI: 10.1007/s11483-006-9012-5.

Beinert, S.; Fragnière, G.; Schilde, C.; Kwade, A. (2015): Analysis and modelling of bead contacts in wet-operating stirred media and planetary ball mills with CFD–DEM simulations. In: Chemical Engineering Science 134 (5), S. 648–662. DOI: 10.1016/j.ces.2015.05.063.

Bolder, Suzanne G.; Sagis, Leonard M. C.; Venema, Paul; van der Linden, Erik (2007): Effect of stirring and seeding on whey protein fibril formation. In: *Journal of agricultural and food chemistry* 55 (14), S. 5661–5669. DOI: 10.1021/jf063351r.

Bolisetty, Sreenath; Adamcik, Jozef; Heier, Jakob; Mezzenga, Raffaele (2012): Amyloid Directed Synthesis of Titanium Dioxide Nanowires and Their Applications in Hybrid Photovoltaic Devices. In: *Adv. Funct. Mater.* 22 (16), S. 3424–3428. DOI: 10.1002/adfm.201103054.

Bolisetty, Sreenath; Arcari, Mario; Adamcik, Jozef; Mezzenga, Raffaele (2015): Hybrid Amyloid Membranes for Continuous Flow Catalysis. In: *Langmuir : the ACS journal of surfaces and colloids* 31 (51), S. 13867–13873. DOI: 10.1021/acs.langmuir.5b03205.

Bolisetty, Sreenath; Boddupalli, Chandra Sekhar; Handschin, Stephan; Chaitanya, Krishna; Adamcik, Jozef; Saito, Yasuyuki et al. (2014): Amyloid fibrils enhance transport of metal nanoparticles in living cells and induced cytotoxicity. In: *Biomacromolecules* 15 (7), S. 2793–2799. DOI: 10.1021/bm500647n.

Büchs, Jochen; Lotter, Stefan; Milbradt, Claudia (2001): Out-of-phase operating conditions, a hitherto unknown phenomenon in shaking bioreactors. In: *Biochemical Engineering Journal* 7 (2), S. 135–141. DOI: 10.1016/S1369-703X(00)00113-3.

Cao, Yiping; Mezzenga, Raffaele (2019): Food protein amyloid fibrils. Origin, structure, formation, characterization, applications and health implications. In: *Advances in colloid and interface science* 269, S. 334–356. DOI: 10.1016/j.cis.2019.05.002.

Dave, Anant C.; Loveday, Simon M.; Anema, Skelte G.; Loo, Trevor S.; Norris, Gillian E.; Jameson, Geoffrey B.; Singh, Harjinder (2013): B-lactoglobulin self-assembly. Structural changes in early stages and disulfide bonding in fibrils. In: *Journal of agricultural and food chemistry* 61 (32), S. 7817–7828. DOI: 10.1021/jf401084f.

Doucet, Mathieu; Cho, Jae Hie; Alina, Gervaise; Bakker, Jurrian; Bouwman, Wim; Butler, Paul et al. (2017): Sasview Version 4.1. Version : Zenodo.

Dunstan, Dave E.; Hamilton-Brown, Paul; Asimakis, Peter; Ducker, William; Bertolini, Joseph (2009): Shear-induced structure and mechanics of β-lactoglobulin amyloid fibrils. In: *Soft Matter* 5 (24), S. 5020. DOI: 10.1039/b914089a.

Frapin, D.; Dufour, E.; Haertle, T. (1993): Probing the fatty acid binding site of beta-lactoglobulins. In: *Journal of protein chemistry* 12 (4), S. 443–449. DOI: 10.1007/BF01025044.

Gao, Zhiming; Zhao, Junjun; Huang, Ying; Yao, Xiaolin; Zhang, Ke; Fang, Yapeng et al. (2017): Edible Pickering emulsion stabilized by protein fibrils. Part 1. Effects of pH and fibrils concentration. In: *LWT - Food Science and Technology* 76, S. 1–8. DOI: 10.1016/j.lwt.2016.10.038.

Gosal, Walraj S.; Clark, Allan H.; Ross-Murphy, Simon B. (2004): Fibrillar beta-lactoglobulin gels. Part 3. Dynamic mechanical characterization of solvent-induced systems. In: *Biomacromolecules* 5 (6), S. 2430–2438. DOI: 10.1021/bm0496615.

Heyn, Timon R.; Garamus, Vasil M.; Neumann, Hendrikje R.; Uttinger, Maximilian J.; Guckeisen, Tobias; Heuer, Monique et al. (2019): Influence of the polydispersity of pH 2 and pH 3.5 beta-lactoglobulin amyloid fibril solutions on analytical methods. In: *European Polymer Journal. DOI:* 10.1016/j.eurpolymj.2019.08.038.

Heyn, Timon R.; Mayer, Julian; Neumann, Hendrikje R.; Selhuber-Unkel, Christine; Kwade, Arno; Schwarz, Karin; Keppler, Julia K. (2020): The threshold of amyloid aggregation of beta-lactoglobulin. Relevant factor combinations. In: *Journal of Food Engineering* 283, S. 110005. DOI: 10.1016/j.jfoodeng.2020.110005.

Kavanagh, Gaynor M.; Clark, Allan H.; Ross-Murphy, Simon B. (2000a): Heat-induced gelation of globular proteins. Part 3. Molecular studies on low pH β-lactoglobulin gels. In: *International Journal of Biological Macromolecules* 28 (1), S. 41–50. DOI: 10.1016/S0141-8130(00)00144-6.

Kavanagh, Gaynor M.; Clark, Allan H.; Ross-Murphy, Simon B. (2000b): Heat-Induced Gelation of Globular Proteins. 4. Gelation Kinetics of Low pH β-Lactoglobulin Gels. In: *Langmuir* 16 (24), S. 9584–9594. DOI: 10.1021/la0004698.

Kayser, Jil J.; Arnold, Philipp; Steffen-Heins, Anja; Schwarz, Karin; Keppler, Julia K. (2019): Functional ethanol-induced fibrils. Influence of solvents and temperature changes on amyloid-like aggregation of beta-lactoglobulin. In: *Journal of Food Engineering*, S. 109764. DOI: 10.1016/j.jfoodeng.2019.109764.

Keppler, Julia K.; Heyn, Timon R.; Meissner, Philipp M.; Schrader, Katrin; Schwarz, Karin (2019): Protein oxidation during temperature-induced amyloid aggregation of beta-lactoglobulin. In: *Food chemistry* 289, S. 223–231. DOI: 10.1016/j.foodchem.2019.02.114.

Kockmann, A.; Hesselbach, J.; Zellmer, S.; Kwade, A.; Garnweitner, G. (2015): Facile surface tailoring of metal oxide nanoparticles via a two-step modification approach. In: *RSC Adv.* 5 (75), S. 60993–60999. DOI: 10.1039/C5RA08932H.

Ladner-Keay, Carol L.; Griffith, Bethany J.; Wishart, David S. (2014): Shaking alone induces de novo conversion of recombinant prion proteins to β-sheet rich oligomers and fibrils. In: *PloS one* 9 (6), e98753. DOI: 10.1371/journal.pone.0098753.

Le Maux, Solène; Bouhallab, Saïd; Giblin, Linda; Brodkorb, André; Croguennec, Thomas (2014): Bovine β-lactoglobulin/fatty acid complexes. Binding, structural, and biological properties. In: *Dairy science & technology* 94, S. 409–426. DOI: 10.1007/s13594-014-0160-y.

Li, Chaoxu; Adamcik, Jozef; Mezzenga, Raffaele (2012): Biodegradable nanocomposites of amyloid fibrils and graphene with shape-memory and enzyme-sensing properties. In: *Nature nanotechnology* 7 (7), S. 421–427. DOI: 10.1038/nnano.2012.62.

Li, Chaoxu; Bolisetty, Sreenath; Mezzenga, Raffaele (2013): Hybrid nanocomposites of gold single-crystal platelets and amyloid fibrils with tunable fluorescence, conductivity, and sensing properties. In: *Advanced materials (Deerfield Beach, Fla.)* 25 (27), S. 3694–3700. DOI: 10.1002/adma.201300904.

Linse, Sara; Cabaleiro-Lago, Celia; Xue, Wei-Feng; Lynch, Iseult; Lindman, Stina; Thulin, Eva et al. (2007): Nucleation of protein fibrillation by nanoparticles. In: *Proceedings of the National Academy of Sciences* 104 (21), S. 8691–8696. DOI: 10.1073/pnas.0701250104.

Loch, Joanna I.; Polit, Agnieszka; Bonarek, Piotr; Olszewska, Dominika; Kurpiewska, Katarzyna; Dziedzicka-Wasylewska, Marta; Lewiński, Krzysztof (2012): Structural and thermodynamic studies of binding saturated fatty acids to bovine β-lactoglobulin. In: *International Journal of Biological Macromolecules* 50 (4), S. 1095–1102. DOI: 10.1016/j.ijbiomac.2012.03.002.

Loveday, Simon M.; Anema, Skelte G.; Singh, Harjinder (2017): β-Lactoglobulin nanofibrils. The long and the short of it. In: *International Dairy Journal* 67, S. 35–45. DOI: 10.1016/j.idairyj.2016.09.011.

Macchi, Francesca; Hoffmann, Søren V.; Carlsen, Martin; Vad, Brian; Imparato, Alberto; Rischel, Christian; Otzen, Daniel E. (2011): Mechanical stress affects glucagon fibrillation kinetics and fibril structure. In: *Langmuir : the ACS journal of surfaces and colloids* 27 (20), S. 12539–12549. DOI: 10.1021/la202125c.

Mantovani, Raphaela Araujo; Pinheiro, Ana Cristina; Vicente, António Augusto; Cunha, Rosiane Lopes (2017): In vitro digestion of oil-in-water emulsions stabilized by whey protein nanofibrils. In: *Food research international (Ottawa, Ont.)* 99 (Pt 1), S. 790–798. DOI: 10.1016/j.foodres.2017.06.049.

Marengo, Mauro; Miriani, Matteo; Ferranti, Pasquale; Bonomi, Francesco; Iametti, Stefania; Barbiroli, Alberto (2016): Structural changes in emulsion-bound bovine beta-lactoglobulin affect its proteolysis and immunoreactivity. In: *Biochimica et Biophysica Acta (BBA) - Proteins and Proteomics* 1864 (7), S. 805–813. DOI: 10.1016/j.bbapap.2016.04.007.

Moro, Andrea; Báez, Germán D.; Ballerini, Griselda A.; Busti, Pablo A.; Delorenzi, Néstor J. (2013): Emulsifying and foaming properties of β-lactoglobulin modified by heat treatment. In: *Food Research International* 51 (1), S. 1–7. DOI: 10.1016/j.foodres.2012.11.011.

Mudgal, P.; Daubert, C. R.; Foegeding, E. A. (2011a): Effects of protein concentration and CaCl2 on cold-set thickening mechanism of β-lactoglobulin at low pH. In: *International Dairy Journal* 21 (5), S. 319–326. DOI: 10.1016/j.idairyj.2010.11.014.

Mudgal, Prashant; Daubert, Christopher R.; Clare, Debra A.; Foegeding, E. Allen (2011b): Effect of disulfide interactions and hydrolysis on the thermal aggregation of β-lactoglobulin. In: *Journal of agricultural and food chemistry* 59 (5), S. 1491–1497. DOI: 10.1021/jf101893v.

Ng, Shy Kai; Nyam, Kar Lin; Nehdi, Imededdine Arbi; Chong, Gun Hean; Lai, Oi Ming; Tan, Chin Ping (2016): Impact of stirring speed on β-lactoglobulin fibril formation. In: *Food Sci Biotechnol* 25 (S1), S. 15–21. DOI: 10.1007/s10068-016-0093-8.

Oboroceanu, Daniela; Wang, Lizhe; Magner, Edmond; Auty, Mark A.E. (2014): Fibrillization of whey proteins improves foaming capacity and foam stability at low protein

concentrations. In: *Journal of Food Engineering* 121, S. 102–111. DOI: 10.1016/j.jfoodeng.2013.08.023.

Ozmen, Mustafa; Can, Keziban; Akin, Ilker; Arslan, Gulsin; Tor, Ali; Cengeloglu, Yunus; Ersoz, Mustafa (2009): Surface modification of glass beads with glutaraldehyde. Characterization and their adsorption property for metal ions. In: *Journal of hazardous materials* 171 (1-3), S. 594–600. DOI: 10.1016/j.jhazmat.2009.06.045.

Peng, Dengfeng; Yang, Jinchu; Li, Jing; Tang, Cuie; Li, Bin (2017): Foams Stabilized by β-Lactoglobulin Amyloid Fibrils. Effect of pH. In: *Journal of agricultural and food chemistry* 65 (48), S. 10658–10665. DOI: 10.1021/acs.jafc.7b03669.

Perriman, Adam W.; Henderson, Mark J.; Holt, Stephen A.; White, John W. (2007): Effect of the air-water interface on the stability of beta-lactoglobulin. In: *The journal of physical chemistry. B* 111 (48), S. 13527–13537. DOI: 10.1021/jp074777r.

Pronchik, Jeremy; He, Xianglan; Giurleo, Jason T.; Talaga, David S. (2010): In vitro formation of amyloid from alpha-synuclein is dominated by reactions at hydrophobic interfaces. In: *Journal of the American Chemical Society* 132 (28), S. 9797–9803. DOI: 10.1021/ja102896h.

Sasso, L.; Suei, S.; Domigan, L.; Healy, J.; Nock, V.; Williams, M. A. K.; Gerrard, J. A. (2014): Versatile multi-functionalization of protein nanofibrils for biosensor applications. In: *Nanoscale* 6 (3), S. 1629–1634. DOI: 10.1039/c3nr05752f.

Schrader, Marcel; Pommerehne, Kathrin; Wolf, Silas; Finke, Benedikt; Schilde, Carsten; Kampen, Ingo et al. (2019): Design of a CFD-DEM-based method for mechanical stress calculation and its application to glass bead-enhanced cultivations of filamentous Lentzea aerocolonigenes. In: *Biochemical Engineering Journal* 148, S. 116–130. DOI: 10.1016/j.bej.2019.04.014.

Serfert, Y.; Lamprecht, C.; Tan, C.-P.; Keppler, J. K.; Appel, E.; Rossier-Miranda, F. J. et al. (2014): Characterisation and use of β-lactoglobulin fibrils for microencapsulation of lipophilic ingredients and oxidative stability thereof. In: *Journal of Food Engineering* 143, S. 53–61. DOI: 10.1016/j.jfoodeng.2014.06.026.

Shezad, Khurram; Zhang, Kejun; Hussain, Mubashir; Dong, Hai; He, Chuanxin; Gong, Xiangjun et al. (2016): Surface Roughness Modulates Diffusion and Fibrillation of Amyloid-β Peptide. In: *Langmuir : the ACS journal of surfaces and colloids* 32 (32), S. 8238–8244. DOI: 10.1021/acs.langmuir.6b01756.

Sluzky, V.; Tamada, J. A.; Klibanov, A. M.; Langer, R. (1991): Kinetics of insulin aggregation in aqueous solutions upon agitation in the presence of hydrophobic surfaces. In: *Proceedings of the National Academy of Sciences* 88 (21), S. 9377–9381. DOI: 10.1073/pnas.88.21.9377.

van der Linden, Erik; Venema, Paul (2007): Self-assembly and aggregation of proteins. In: *Current Opinion in Colloid & Interface Science* 12 (4-5), S. 158–165. DOI: 10.1016/j.cocis.2007.07.010.

vandenAkker, Corianne C.; Schleeger, Michael; Bruinen, Anne L.; Deckert-Gaudig, Tanja; Velikov, Krassimir P.; Heeren, Ron M. A. et al. (2016): Multimodal Spectroscopic Study of Amyloid Fibril Polymorphism. In: *The journal of physical chemistry. B* 120 (34), S. 8809–8817. DOI: 10.1021/acs.jpcb.6b05339.

Ye, Xinchen; Hedenqvist, Mikael S.; Langton, Maud; Lendel, Christofer (2018): On the role of peptide hydrolysis for fibrillation kinetics and amyloid fibril morphology. In: *RSC Adv.* 8 (13), S. 6915–6924. DOI: 10.1039/C7RA10981D.

5.8. Supplementary Material

TAB S5-3 Temperature log of the temperature of the liquid measured inside the shake flask over a period of 5 hours. A, B and C present the left, middle and right spot in the incubation oven adjusted to 80° C.

Time [h]	*A*	*B*	*C*
0	25,5°C	25,9°C	25,6°C
0,5	68,5°C	65,1°C	66,3°C
1	70,1°C	66,0°C	68,1°C
2	71,4°C	67,0°C	69,7°C
3	71,5°C	67,0°C	70,0°C
4	71,5°C	66,8°C	70,0°C
5	71,6°C	67,0°C	70,0°C

TAB S5-4 Adsorbtion of pH 3.5 aggregates on modified and unmodified particle surfaces [6.6 µm]. Adsorbtion of the protein on particle surface [%] was calculated by the decrease of absorption at 280 nm measured by UV/VIS spectroscopy.

Time [h]	***unmodified***		***modified***	
	Mean [%]	*SD*	*Mean [%]*	*SD*
0.5	0,0	0,0	0,0	0,0
1	11,7	1,0	14,9	0,4
2	11,3	2,3	20,8	0,1
3	12,2	6,0	26,7	2,4
4	20,8	11,2	31,3	4,9
5	12,2	4,9	35,8	4,5

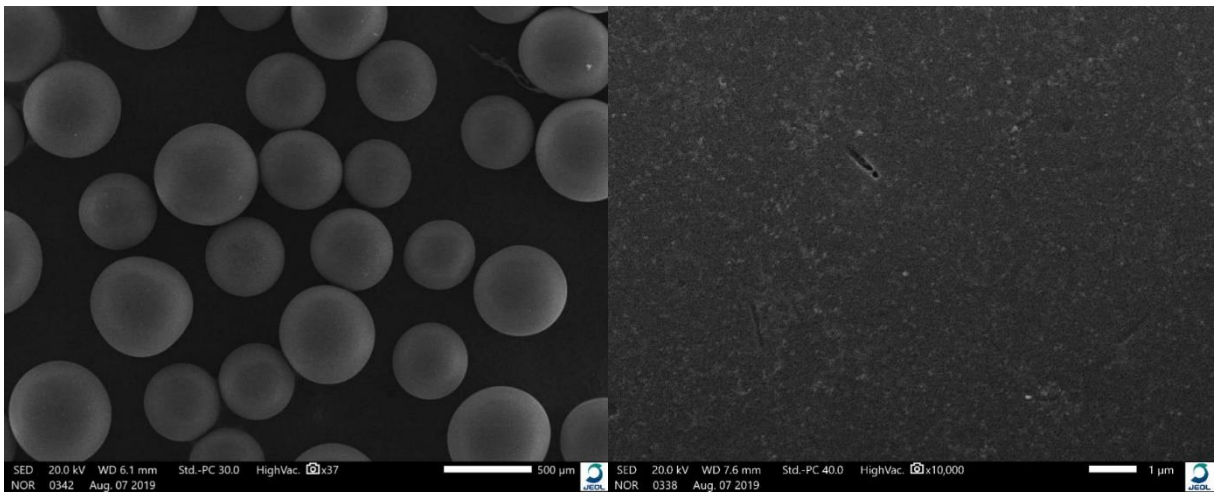

FIG S5-8 unmodified glass beads measured by scanning electron microscope (SEM)

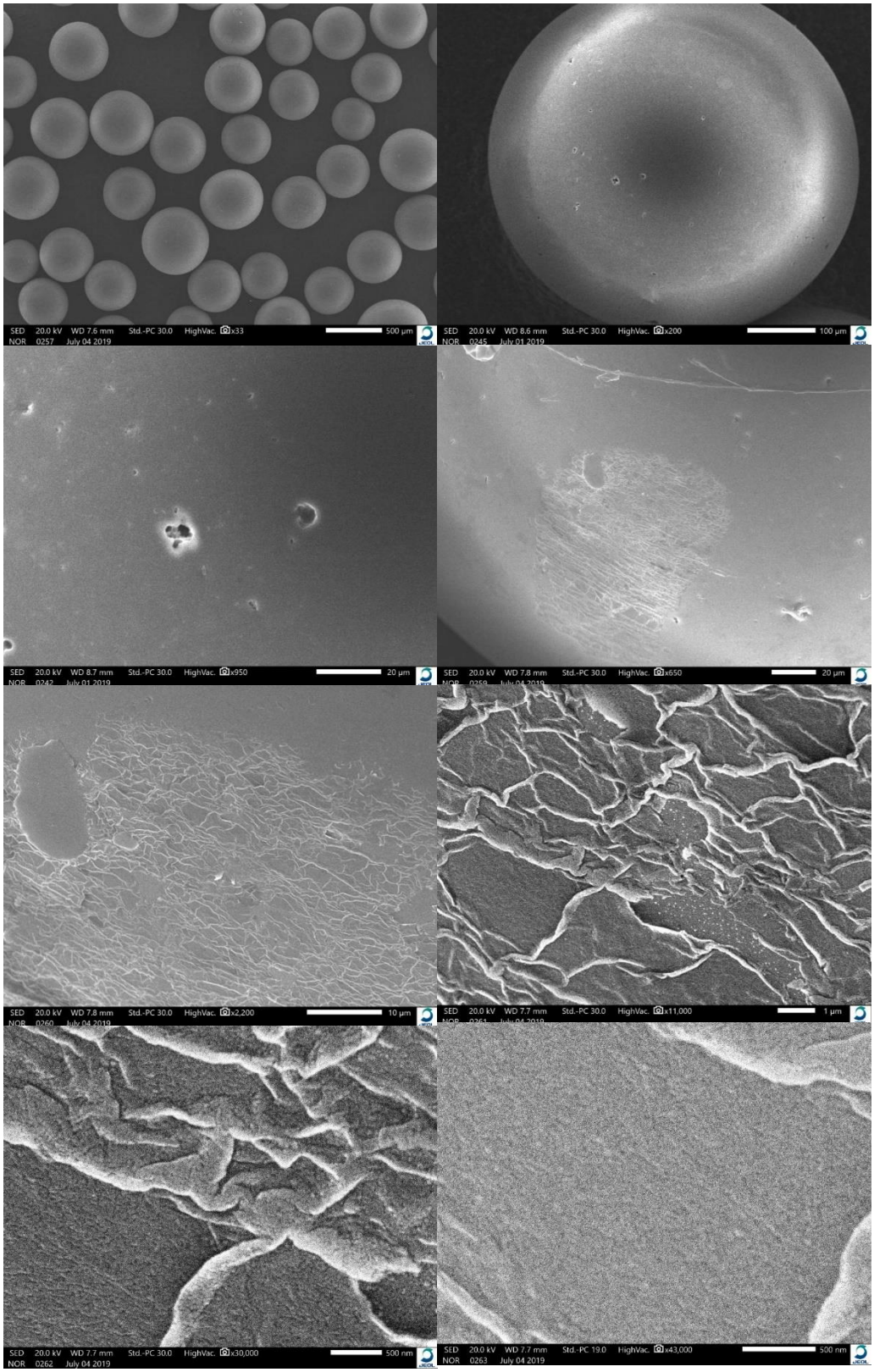

FIG S5-2 unmodified glass beads after fibril formation process (5h at pH 2 and ~70 °C) measured by scanning electron microscope (SEM)

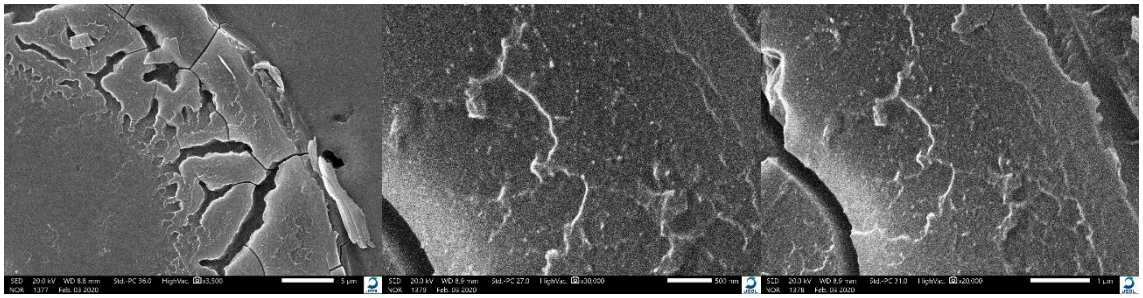

FIG S5-9 modified glass bead surfaces after fibril formation process (5h at pH 2 and ~70 °C) measured by scanning electron microscope (SEM)

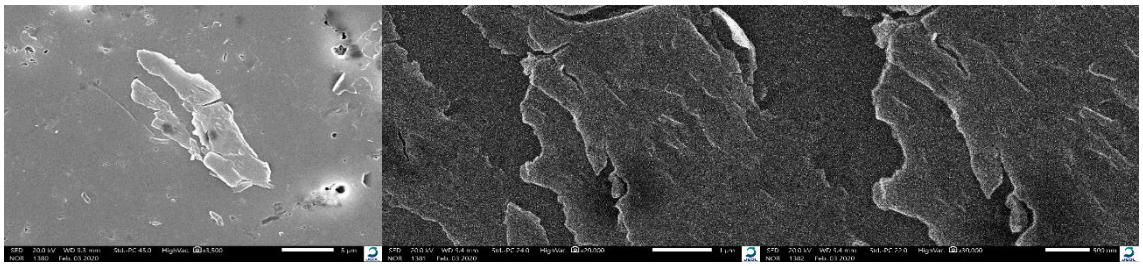

FIG S5-10 modified glass bead surfaces after fibril formation process (5h at pH 3.5 and ~70 °C) measured by scanning electron microscope (SEM)

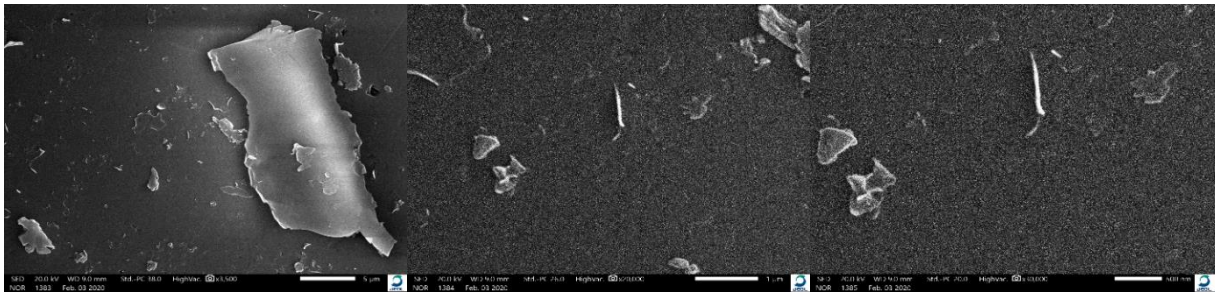

FIG S5-11 unmodified glass bead surfaces after fibril formation process (5h at pH 2 and ~70 °C) measured by scanning electron microscope (SEM)

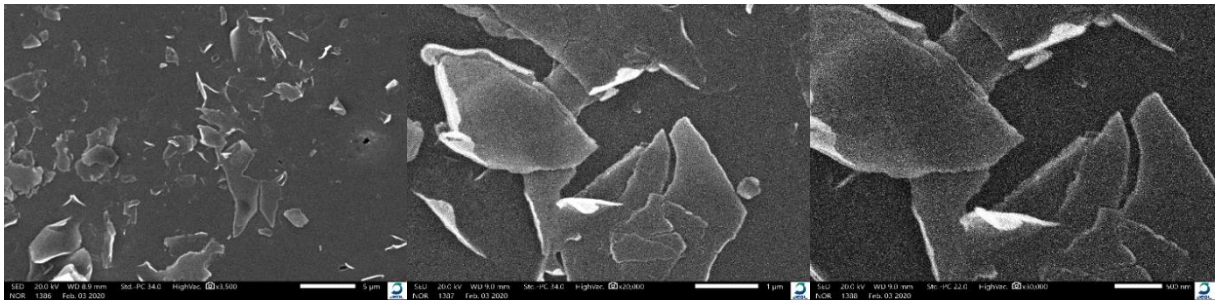

FIG S5-12 unmodified glass bead surfaces after fibril formation process (5h at pH 3.5 and ~70 °C) measured by scanning electron microscope (SEM)

6. Manuscript 4 – Process stability of amyloid and amyloid-like aggregates in oil-water systems under varying shear stress

Whey protein (amyloid)-aggregates in oil-water systems: The process-related comminution effect

Timon R. Heyn[a], Maximilian J. Uttinger[b], Arno Kwade[c], Wolfgang Peukert[b], Julia K. Keppler[a,d]*, Karin Schwarz[a]

Submitted previously to Journal of Food Engineering (2020): Heyn, Timon R.; Mayer, Julian; Neumann, Hendrikje R.; Selhuber-Unkel, Christine; Kwade, Arno; Schwarz, Karin; Keppler, Julia K. (2020): The threshold of amyloid aggregation of beta-lactoglobulin. Relevant factor combinations. Article reference: JFOODENG-D-21-00032.

Reproduced with permission from Elsevier

[a] Institute of Human Nutrition and Food Science, Department of Food Technology, Kiel University, 24118 Kiel, Germany

[b] Institute of Particle Technology, Interdisciplinary Center for Functional Particle Systems, Friedrich-Alexander Universität Erlangen-Nürnberg, Erlangen, Germany

[c] Institute for Particle Technology, Technical University Braunschweig, 38104 Braunschweig, Germany

[d] Laboratory of Food Process Engineering, Wageningen University, Bornse Weilanden 9, 6708WG, Wageningen, P.O. Box 17, 6700 AA, Wageningen, the Netherlands

6.1. Abstract

Amyloid fibrils and amyloid-like aggregates from beta-lactoglobulin were stressed by rotor-stator- or ultra-sonic processing in the presence and absence of an oil phase to simulate processing steps typical for emulsion preparation.

Straight fibrils produced at pH 2 and worm-like aggregates produced at pH 3.5 during 5 h incubation at 90 °C were stressed under increasing calorimetrically measured energy intakes. Rotor-stator-application was performed from 0.3 to 43 J ml^{-1}, while sonication was applied from 27 to 76 J ml^{-1}. Experiments were conducted with or without 18 % rapeseed oil. Influences on fibril length were measured by atomic force microscopy (AFM), dynamic light scattering (DLS) and analytical ultracentrifugation. Changes of the beta-sheet structure was analysed by fluorescence-assay (ThT) and infrared spectroscopy (FTIR).

Fibrils (pH 2) decreased in length in dependence of the mechanical energy input applied by rotor-stator-shear and sonication, whereas worm-like aggregates were only affected by sonication. The addition of oil led to reduced aggregate length at lower energy intakes for all aggregates. No effects on the amyloid(-like) structure itself were observed. The results can be used to adjust process parameters in order to avoid destruction of fibrils or worm-like aggregates during emulsion preparation.

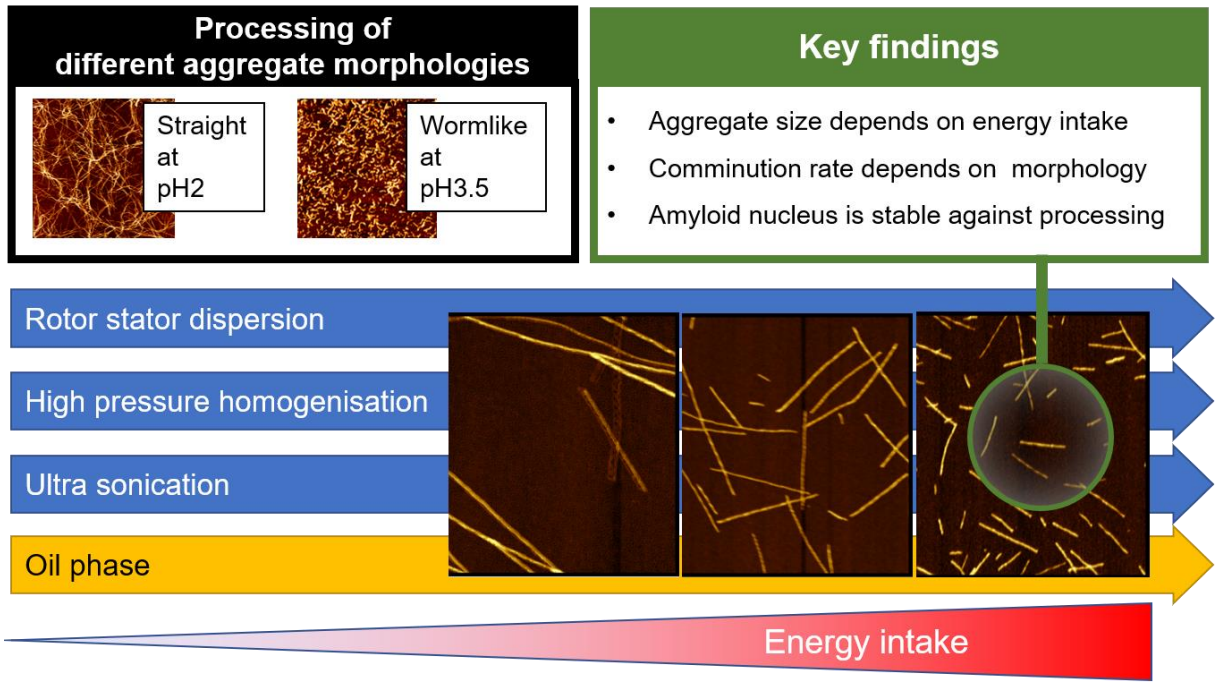

Abbreviations

BLG, Beta-Lactoglobulin

E_V, volume specific energy

N, Rotational number

RPM, Rounds per minute

ThT, Thioflavin-T

AFM, Atomic Force Microscopy

AUC, Analytical Ultracentrifugation

DLS, Dynamic Light Scattering

d.nm, Diameter in Nanometer

6.2. Introduction

Amyloid fibrils from whey protein beta-lactoglobulin (BLG) exhibit valuable functional properties due to their high aspect ratio and stiffness as well as their collective ordering features (Cao and Mezzenga, 2019). BLG is a safe and nutritionally valuable protein (Bateman et al., 2010). Therefore, the implementation of functional BLG fibrils into new materials such as biosensors or hybrid membranes are highly promising application areas (Knowles and Mezzenga, 2016). Up to now, it has been demonstrated that BLG fibrils can increase the physical stability of gels (Mohammadian and Madadlou, 2016), foams (Oboroceanu et al., 2014) and emulsions (Gao et al., 2017). Using BLG fibrils as emulsifier can further improve the oxidative stability of the emulsified oil phase (Serfert et al., 2014).

However, these long protein filaments are subject to length reduction upon shearing (Serfert et al., 2014), e.g., during emulsification. This shortening might also induce changes of the functionality (Koo et al., 2018). Fibrils produced at pH 2 are stiff and semi-flexible (Adamcik et al., 2010). In contrast, the amyloid-like aggregates produced at pH 3.5 have a shorter and more flexible structure (Heyn et al., 2019). So far, the influence of the fibril morphology on its size reduction upon processing is still unclear. Furthermore, the role of other emulsification factors such as the presence of oil affecting the morphology of fibrils during mixing are not yet clear. However, this is of particular importance, since different emulsification processes and conditions can potentially alter the protein aggregate size.

In order to investigate the size reduction kinetics of fibril lengths by shear forces, straight fibrils formed at pH of 2 were exposed to different pressure drops in a high pressure homogenizer and to different rotational speeds of a rotor-stator system, as the volume specific energy (E_V) scales with the drop of pressure ($E_V = \Delta p$) as well as the cube of the rotational number ($E_V \sim N^3$) (Uttinger et al., 2020). Moreover, the influence of cavitation on fibril fragmentation was investigated by use of ultrasonication. Ultrasound imposes high stresses on the dispersed particles in form of shear forces, strong static pressure fluctuations and cavitation bubbles (Sutariya et al., 2018). E_V induced by either shear or cavitation can be quantified by calorimetry directly in solution ($E_V \sim E_C$) (Özcan-Taşkın et al., 2011; Shen et al., 2017; Romdhane et al., 1995).

To further investigate the influence of liquid interface formation under process relevant conditions during emulsion processing on fibril comminution, the rotor-stator and ultrasonic

treatment were also performed with 18 wt% oil as the dispersed phase, which is frequently used in whey protein emulsions (Keppler et al. 2018, Keppler et al. 2017, Serfert et al. 2014).

All experiments were repeated with amyloid-like (worm-shaped) aggregates, which form at pH 3.5, to analyse the robustness of these more flexible morphologies in great detail. The change in aggregate size was observed using comprehensive analytical tools, namely atomic force microscopy (AFM), analytical ultracentrifugation (AUC) and dynamic light scattering (DLS).

Finally, influences of processing (rotor-stator systems, ultra-sonication) on the protein secondary structure, more specifically on the amyloid beta-sheet structure of all morphologies was monitored by Thioflavin-T (ThT-) assay and Fourier transformation infrared spectroscopy (FTIR).

Based on these findings, the size reduction kinetics of fibrils is derived from E_V. Our results provide a suitable basis for estimation of the effect of industrial processing and the influence of shear forces on the length of different aggregate morphologies (i.e., fibrils and worm-like aggregates). In addition, the emulsification process with protein aggregates can be adapted based on the presented results in order to obtain the desired aggregate size and length.

6.3. Materials and Methods

6.3.1. Materials

Beta-lactoglobulin (BLG) was obtained from *Davisco Foods International Inc.* (Eden Prairie, US) with 97 % protein and 96 % BLG in dry matter. Calculated NaCl content was 49.6 µmol g^{-1} protein. Thioflavin-T (ThT > 95 %) acid was obtained *from EMD Chemicals Inc.* All other chemicals were of analytical grade and obtained from *Sigma Aldrich Inc.* All experiments were conducted with ultra-pure water (> 17 MΩ; total oxidizable carbon < 5ppb).

6.3.2. Amyloid aggregate preparation

25 mg/ml BLG fibril solutions were prepared as described by (Heyn et al., 2019). Prior to all processing steps, fibril dispersions were diluted to 10 mg/ml.

6.3.3. Processing of fibrils

6.3.3.1. Processing via Ultra-turrax

Shear treatment of fibrils were performed by an ultra turrax equipped with a S 25 N – 25 F dispersion tool (*IKA® - Werke GmbH & CO.KG*, Staufen, Germany). 100 ml fibril solution were stressed with ω_{stress} for 60 s at 3 – 25 KRPM with and without 18 wt% oil. The samples

were placed in ice during processing to avoid thermal induced changes in the system. E_V was measured by calorimetry with a 150 ml water solution without protein in a thermally insulated vessel (by an aluminium foil). The protein solution had slightly higher viscosity compared to water (~1.1 mPas s) (Heyn et al. 2020) and showed shear-thinning properties, therefore the use of water without protein was considered sufficient for measuring E_V. The increase in temperature was measured with a digital thermometer and E_V was calculated using the specific thermal capacity of water (4185.1 J kg^{-1}). The calculated mechanical and measured calometric energy intakes listed in the **supporting material TAB S6-2**.

6.3.3.2. Processing via sonication

The sonication treatment was performed using a UW 2070 ultrasound device with MS 73 sonotrode (*Bandelin electronic,* Berlin, Germany). A Bandelin Sonopuls GM 2070 (*Bandelin electronic*, Berlin, Germany) was used as high frequency generator of 20 kHz +- 500 Hz with 0.9 s pulses and 0.1 s interruption. 5 ml fibril solution was stressed for 60 s at 10, 20, 40, and 70 % of the maximal amplitude with and without 18 wt% oil. Samples were placed on ice during processing to ensure a constant temperature. E_V was measured in thermally insulated plastic tubes with 15 ml water. The temperature increase rate was protocolled with a thermometer and the energy was calculated using the specific thermal capacity of water (4185.1 J kg^{-1}). Calculated and measured energy intakes listed in the **supporting material TAB S6-3**.

6.3.3.3. Processing by high pressure homogenisation

Fibril solutions were stressed in a high pressure system at 50, 400 or 800 bar as described by (Gothsch et al., 2016), corresponding to the E_V of 5, 40 and 80 J ml^{-1}. Two different geometries were used. The "straight" geometry GE07 is equipped with a channel of 2.5 cm length, a width of 500 µm and a depth of 54 µm. The "orifice" geometry E021B is equipped with an additional orifice in the middle of the channel, which reduced the channel width to 80 µm over a length of 300 µm. Both geometries are illustrated in the **supporting material FIG S6-9.** In dependence of fibril morphology, pressure level and geometry, various volume flows were observed (**supporting material TAB S6-4**).

6.3.4. Characterization of the fibril length and aggregate size

6.3.4.1. Atomic force microscopy (AFM)

Fibril morphology was investigated using AFM (*NanoWizard 3, JPK Instruments AG*, Berlin, Germany) following the protocol of (Serfert et al., 2014) and (Adamcik et al., 2010). For tapping mode, ACTA-Cantilevers (spring constant 40 N/m, resonance frequency 300 kHz; *Applied Nano-Structures, Inc.*, Mountain View, USA) were used at a scan rate of 0.5 Hz. The analysis tool Gwyddion 2.53 was used for data visualization. Statistical values of fibril lengths were determined manually from ~150 fibrils of three individual samples with an implemented software tool.

6.3.4.2. Analytical ultracentrifugation (AUC)

The sedimentation analysis of fibril solutions via AUC was carried out according to the protocol established by (Uttinger et al., 2020). Prior to the measurements via AUC, the samples were diluted with ultrapure water at the respective pH value. Directly before the sedimentation analysis, the sample concentration was controlled by measuring the absorbance of the samples at 280 nm and 290 nm Genysis 10S UV-VIS spectrometer (*ThermoFisher Scientific*, Waltham, United States). For the experiments within this manuscript, a modified preparative centrifuge, type Optima L-90 K, available from Beckman Coulter, equipped with an integrated UV/visible multiwavelength detector has been used (Walter et al., 2014). For our sedimentation velocity (SV) experiments, the rotor speed was set to 30 KRPM and held constant for the entire experiment. Sedimentation data were acquired for wavelengths between 260 nm and 400 nm. The buffer solution was taken as a reference when converting intensity data to absorbance. The temperature was set to 20° C throughout the measurements. Titanium centerpieces with an optical path length of 12 mm were used for all experiments. Further details of the applied multiwavelength optics and the data evaluation of the rotor speed gradient experiments can be found in literature (Walter and Peukert, 2016). Sedimentation data was extracted from the recorded data at a wavelength with a sample signal of unity. Data analysis of SV experiments was performed using the c(s) method implemented in SEDFIT (Version 16.1) (Schuck and Rossmanith, 2000).

6.3.4.3. Dynamic light scattering (DLS)

The change of the protein aggregate size was measured by dynamic light scattering in a Zetasizer Nano ZS (*Malvern Instrument GmbH*, Herrenberg, Germany) using disposable

cuvettes DTS0012 at a protein concentration of 1 mg ml^{-1}. Temperature was set to 25 °C and a viscosity of 0.8872 cP and a material refractive index of 1.450 was used.

6.3.5. Characterization of secondary structure

In order to monitor the aggregate structure stability, the influence of shear stress and cavitation on amyloid beta-sheets was analysed by ThT-assay and ATR-FTIR. All respective experiments were carried out following the protocol of Heyn et al. (2019): For ThT-assay, 48 µl of the sample was added to 4 ml of a 3.0 mM ThT solution, the mixture was vortexed and incubated for 60 s prior to measurement in a fluorescence spectrophotometer (*Cary Eclipse, Varian GmbH,* Darmstadt, Germany) at 440 Ex. and 482 Em.. The change of beta-sheets was investigated with the Confocheck^{TM} FTIR system, using a Tensor 2 (*Bruker Optik GmbH,* Ettlingen, Germany) fitted with a thermally controlled BioATR II Cell. 20 µl of the 1 wt% protein solution were pipetted onto the ATR crystal. 120 scans at a resolution of 0.7 cm^{-1} were recorded and averaged. The spectra were corrected for the absorbance of CO_2 and H_2O (vapour and solute) and vector-normalized, afterwards the 2nd derivation was calculated with 9 smoothing points using OPUS Software (*Bruker Optik GmbH,* Ettlingen, Germany).

6.3.6. Statistical analysis

Statistical analysis of the collected data was conducted by GraphPad PRISM (version 8.4.3, *GraphPad Software,* San Diego, USA). A significant decrease in aggregate length was verified by two-way ANOVA with Tukey's multiple comparison test at the 0.05- significance level. AFM, AUC, DLS, ThT and FTIR measurements were conducted in triplicate.

6.4. Results

6.4.1. Influence of high pressure homogenisation on aggregate length scale

Straight fibrils prepared at pH 2 were processed for reference purposes using a high-pressure homogenization system. The fibril solution was pressed through the two different microchannels at 50, 400 or 800 bar, corresponding to the E_V of 5, 40 and 80 J ml^{-1}. One microchannel had an orifice valve to induce particularly high dynamic pressures with resulting cavitation. The fibril length distributions caused by this process were determined by AFM (**FIG 6-1 A**). The results show that a distinct decrease in fibril length for pressure increase from 5 to 80 J ml^{-1}. The corresponding sedimentation coefficients were determined (**FIG 6-1 B (AFM)**) and compared with the sedimentation coefficients measured by AUC. The standard deviations

of the sedimentation coefficients in **FIG 6-1 B (AUC)** correspond to the measured width of the sedimentation coefficient distributions. Notably, the measured distribution from AUC are broader than the results from statistical AFM analysis. This can be attributed to small differences in the height of the fibrils, which directly affect the sedimentation properties. This was analysed in detail by Uttinger et al. (Uttinger et al. 2020). As shown in **FIG 6-1**, a trend between the increase of the applied pressure and the decrease of the observable fibril length, sedimentation constant, and z-average (**Supporting material TAB S6-5**) could be observed. The use of the microchannel with orifice plate leads to an even stronger reduction of the average fibril length at the respective pressures. Notably, the relationship of the sedimentation coefficient and the fibril length is given by a root function (Uttinger et al. 2020). Conclusively, the width of the sedimentation coefficient distribution cannot be directly related to the width of the respective length distribution.

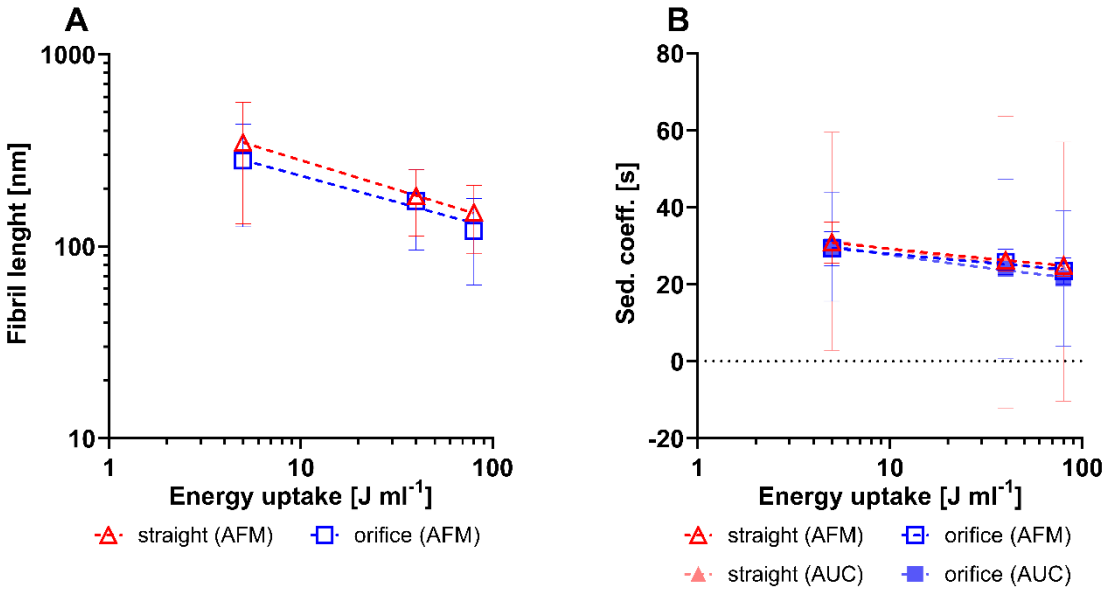

FIG 6-1 (**A**) Mean and standard deviation of the length distribution on atomic force microscopy images and (**B**) sedimentation coefficient determined by analytical ultracentrifugation and atomic force microscopy of high-pressure homogenised pH 2 fibril solution. Fibril solutions were diluted to 1 wt% and processed at different volume specific energy uptakes (EV) (i.e., 5, 40 or 80 J ml-1) and with different microchannel geometries (straight or orifice).

6.4.2. Influence of rotor stator dispersion on aggregates with and without oil

The unprocessed straight fibrils formed at pH 2 showed a length of 5 to 10 µm measured by AFM, which is in the range of our previous studies (Heyn et al., 2019). The rotor-stator dispersion led to a reduction of the fibril length with increasing shear force and E_V (**FIG 6-2 A**), whereby the time was kept constant. The decrease in fibril length observed by AFM was further confirmed by the measurement of aggregate size by DLS (**FIG 6-2 A**) as well as an

auxiliary analysis of the sedimentation coefficient distributions via AUC (**Supporting material FIG S6-8 A**). For AFM, AUC and DLS based on the power function relationship a *size reduction exponent* of 0.65, 0.36 and 0.26 was calculated, respectively (**FIG 6-3**). The differences between the size reduction exponents between AFM and AUC are due to the fact that the AUC cannot take sufficient account of fibril lengths above 700 nm (Uttinger et al. 2020) and thus underestimates the real lengths at lower E_V, i.e., the slope flattens. Therefore, for this higher fibril length range only results from AFM were used statistical analysis. Moreover, DLS measurements was only used to support the characterization of fibrils, since the z-average hydrodynamic diameter cannot fully take into account the changes of the fibril lengths. This is attributed to the fact that the change of fibril length and diameter does not linearly change with the hydrodynamic diameter.

The addition of oil to the aqueous solution led to even smaller fibril length at lower rotational speeds up to 1.19E+05 (23.88 J ml^{-1}) (**Supporting material TAB S6-7**). Although the length of fibrils in the presence of oil droplets decreased to ~800 nm at the lowest rotational number (**FIG 6-2 A**), increasing the shear stress to E_V of 24 to 43 J ml^{-1} led to similar mean fibril length of 294 to 256 nm compared to experiments without oil phase (222 to 250 nm). Therefore, the slope (*size reduction exponent*) was lowered to 0.27 (AFM) and 0.20 (AUC) for the mean fibril length (equation 1) (**FIG 6-3 A**). DLS measurements supported a slight decrease in aggregate size in dependence of E_V when oil was added (**FIG 6-2 A**).

Unprocessed worm-like aggregates, which are formed at pH 3.5, have a mean contour length of 73 nm and a maximum length of ~240 nm (**Supporting material TAB S6-7**). Applying various shear forces, the mean or median aggregate length and aggregate size did not decrease depending on E_V (**FIG 6-2 B**). However, a slight reduction of the fibril length as function of the E_V was observable when oil was added. According to DLS, the z-average of the aggregates increased when worm-like aggregates were sheared together with oil, which can be attributed to structural changes within the aggregates or an agglomeration of the aggregates by the oil droplets. These changes directly reflect upon changes in the hydrodynamic diameter of a corresponding volume equivalent sphere.

Monitoring the amyloid properties of both types of aggregates via ThT-assay demonstrated a slight reduction of fluorescence intensity for fibril solutions processed at $E_V > 2$ J ml^{-1} compared to the unprocessed ones (**FIG 6-4 A**). However, this decrease remained constant for all shear levels. Analysis with FTIR gave no evidence of conformational changes of the processed pH 2 samples without oil (**FIG 6-4 C**). However, when oil was added, a slight increase in the 1620

cm^{-1} waveband, indicative for intermolecular beta-sheets, was observed (**FIG 6-4 C**). This hints at further protein aggregate formation.

For worm-like aggregates, no significant decrease of the fluorescence intensity after stressing at lowest shear levels was evident (**FIG 6-4 B**). However, the addition of oil led to a decrease of the fluorescence intensity after processing with 0.43 J mol^{-1}. No alteration at the 1620 cm^{-1} waveband was observed in FTIR, neither of other secondary structure elements (intramolecular beta-sheets at 1630 cm^{-1}, second beta-sheet band at 1688 cm^{-1} and alpha helix at 1655 cm^{-1} (Keppler et al., 2017; Kavanagh et al., 2000) (**FIG 6-4 D**), as the level of aggregate structures in pH 3.5 BLG solutions was relatively high.

6.4.3. Influence of processing by sonication with and without oil

The minimal ultrasonication amplitude was 21.2 µm (10 % of the max. amplitude of 212 µm), which led to an E_V of 27 J ml^{-1} in the fibril solution, while the highest conducted sonication amplitude of 148.4 µm led to an E_V of 76 J ml^{-1}. The different sonication levels led to a decrease of fibril length at pH 2 from 161 nm to 107.2 nm (**FIG 6-5 A**) with a *size reduction exponent* of 0.49 (AFM) and a reduction of the aggregate size with a *size reduction exponent* of 0.27 (DLS) (**FIG 6-6**)**.** The decrease of aggregate size with increasing E_V was confirmed with DLS (**FIG 6-5 A)** The addition of oil before sonication led to an even lower decrease of mean fibril length. However, analysis via DLS demonstrated an increase of the z-average with increased E_V, probably due to agglomeration of the aggregates.

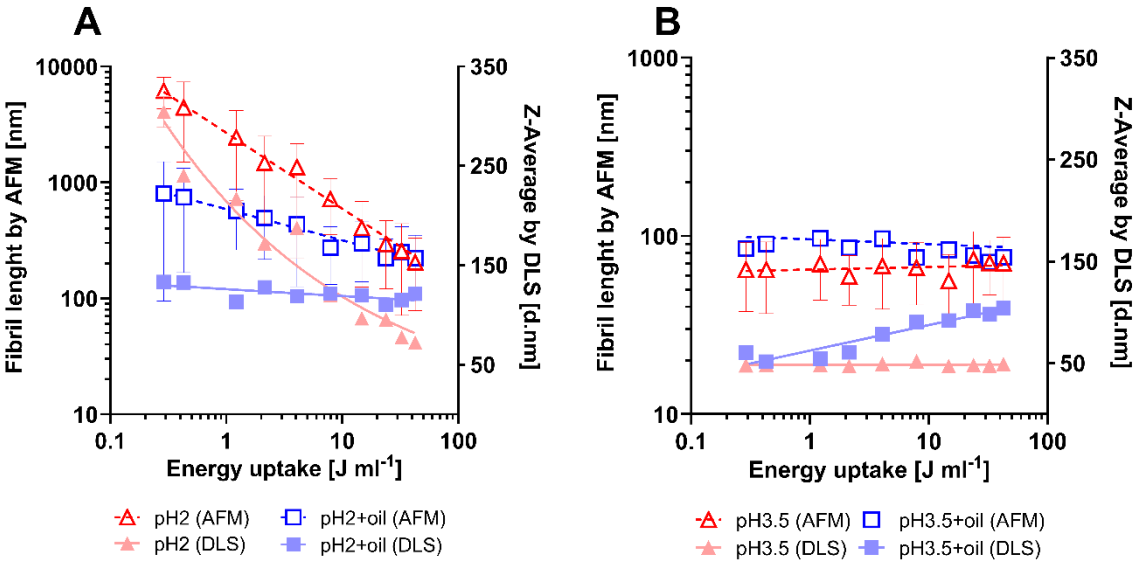

FIG 6-2 Mean and standard deviation of length distribution [nm] and Z-average of the particle diameter [d.nm] of rotor-stator-sheared straight fibrils formed at pH2 (A) and wormlike aggregates formed at pH3.5 (B) measured by atomic force microscopy (AFM) and dynamic light scattering (DLS), respectively: Measured volume specific energy uptakes (EV) was increased from 0.29 J ml-1 to 42.71 J ml-1 in dependence of rotational number N. Oil was removed by three centrifugation steps at 24 000*g before the analysis was conducted. Notably, the measured fibril lengths may be underestimated due to the fact that fibrils extend beyond the detection section (= 10 µm x 10 µm), hence cannot be taken into account adequately.

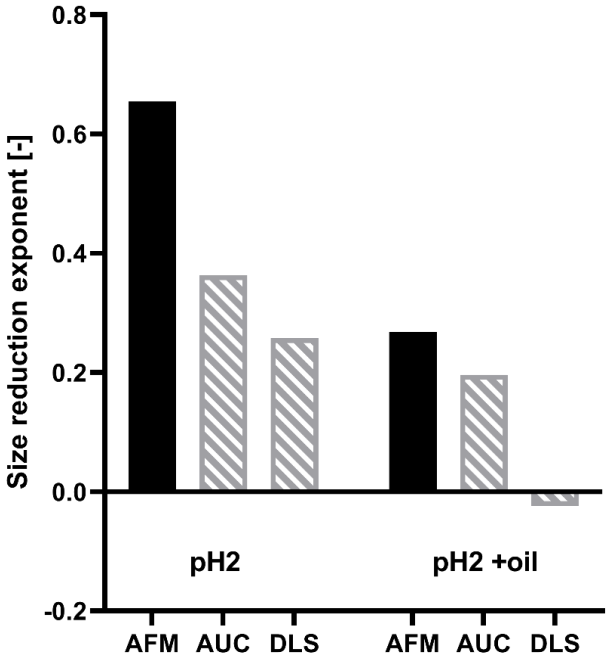

FIG 6-3 Size reduction exponent b ($-\boldsymbol{b} = \frac{\log \boldsymbol{L}(\boldsymbol{E_V})}{\log(\boldsymbol{E_V}+\boldsymbol{y})}$) of rotor-stator-sheared straight fibrils formed at pH2 with and without oil, analysed with atomic force microscopy (AFM), analytical ultracentrifugation (AUC) and dynamic light scattering (DLS).

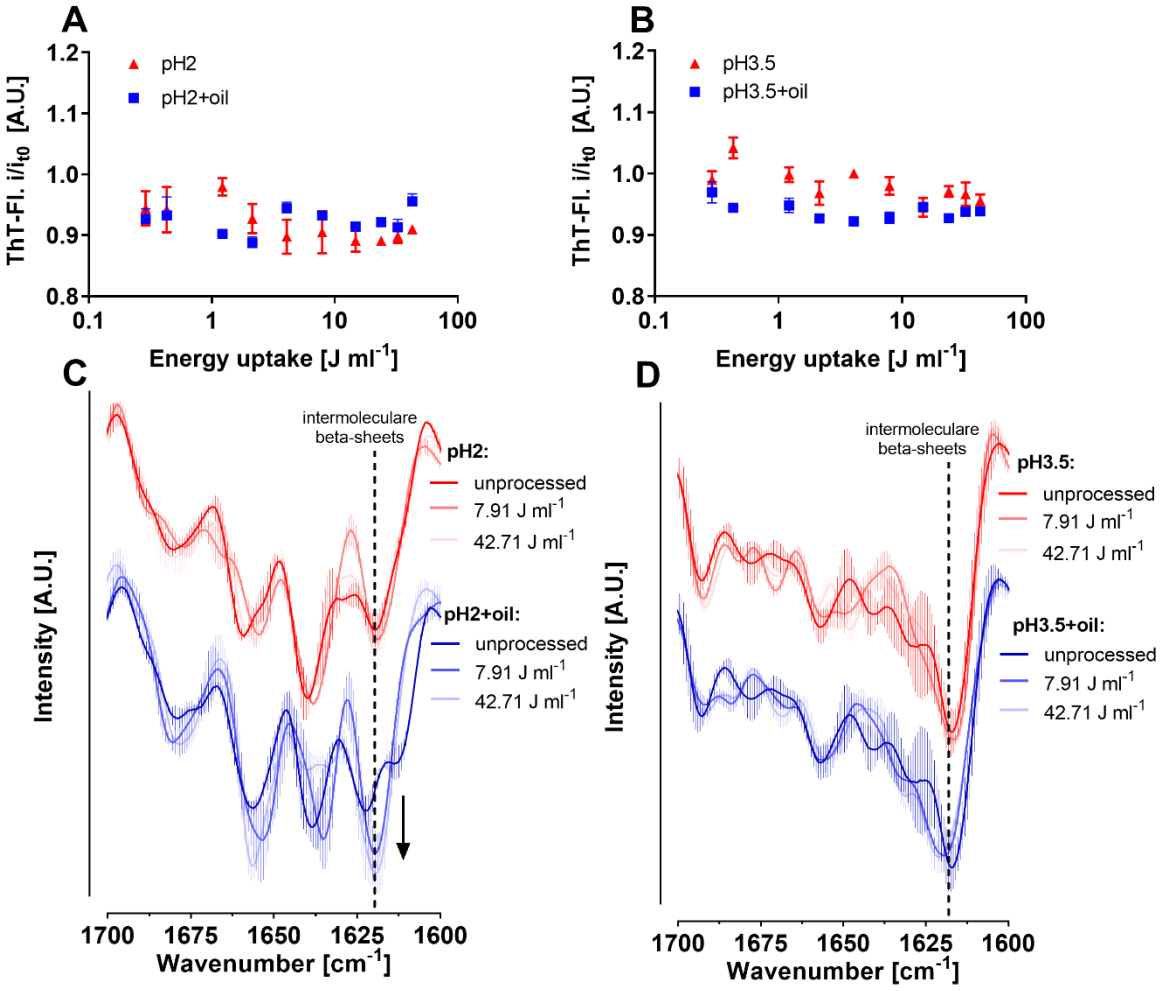

FIG 6-4 Normalized ThT-fluorescence (**A and B**) and second derivation of amide I spectra (**C and D**) analysed by FTIR of rotor-stator-sheared straight fibrils formed at pH2 (**A and C**) and wormlike aggregates formed at pH3.5 (**B and D**). Volume specific energy uptakes (E_V) increased from 0.29 J ml^{-1} to 42.71 J ml^{-1} in dependence on rotational number N. Oil was removed by three centrifugation steps at 24 000**g* before the analysis was conducted.

The AFM analysis of ultrasonicated worm-like aggregates revealed a decrease of the mean contour length after treatment with an E_V of 27 J ml^{-1} to 76 J ml^{-1} from 102 nm to 50 nm (**FIG 6-5 B**). Notably, the observed fibril length in the solution treated at the lowest stress level was even higher as in the unprocessed solution (**Supporting material TAB S6-8**). However, a decrease in aggregate size was not observed with DLS. The addition of oil to the pH 3.5 aggregate solution led to a reduction of the contour length at smaller amplitudes, but had no effect at higher sonication levels (**FIG 6-5 B**). Analysis with DLS confirms the occurrence of large particles in solution when an amplitude of 148.4 µm was used.

Analysis of the amyloid structure by ThT-assay indicated no significant loss of cross-beta-sheets stacks in the pH 2 fibril solutions with and without oil after ultra-sonication (**FIG 6-7 A**). However, FTIR revealed an increase of aggregated material when fibrils were sonicated in

the presence of the oil phase at an amplitude of 84.4 µm (**FIG 6-7 C**) (i.e., increase of the 1620 cm^{-1} waveband intensity). Sonication of worm-like aggregates without oil had no effect on the ThT fluorescence (**FIG 6-7 B**). However, the addition of 18 wt% oil led to a decreased fluorescence intensity with rising E_V and also to the formation of a very viscous gel when E_V exceeds ~34 J ml^{-1}. Still, no effect on the aggregate structure itself was observable with FTIR for worm-like aggregates sonicated with and without oil (**FIG 6-8 D**).

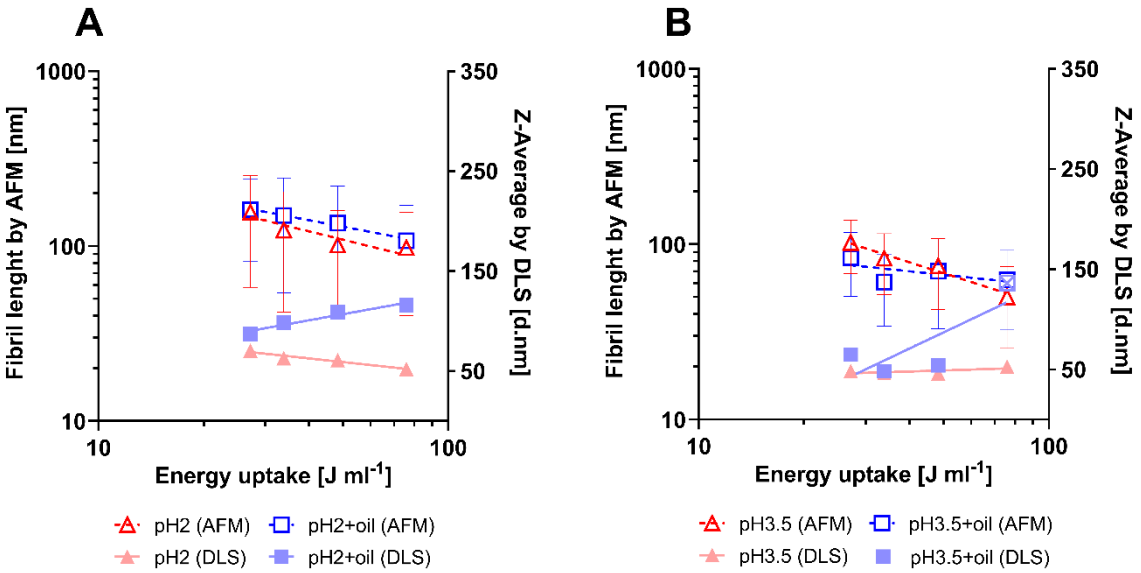

FIG 6-5 Mean and standard deviation of length distribution and Z-Average of sonication treated straight fibrils formed at pH2 (A) and wormlike aggregates formed at pH3.5 (B) measured by atomic force microscopy (AFM) and dynamic light scattering (DLS), respectively: Measured volume specific energy uptake (E_V) increased from 27.2 J ml^{-1} to 76.0 J ml^{-1} in dependence on sonication amplitude. Oil was removed by three centrifugation steps at 25 000*g before the analysis was conducted.

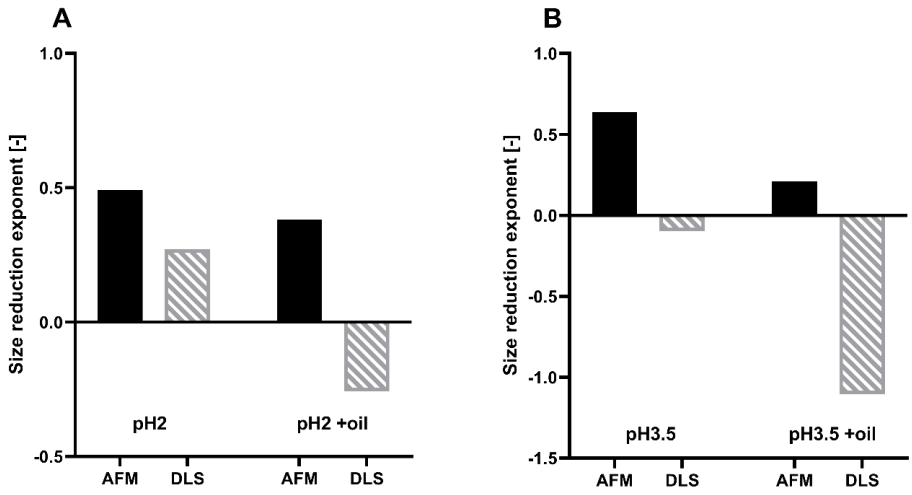

FIG 6-6 Size reduction exponent b ($-\boldsymbol{b} = \frac{\log \boldsymbol{L}(\boldsymbol{E_V})}{\log(\boldsymbol{E_V}+\boldsymbol{y})}$) of sonication treated straight fibrils formed at pH2 (A) and wormlike aggregates formed at pH3.5 (B) analysed with atomic force microscopy (AFM) and the auxiliary method dynamic light scattering (DLS).

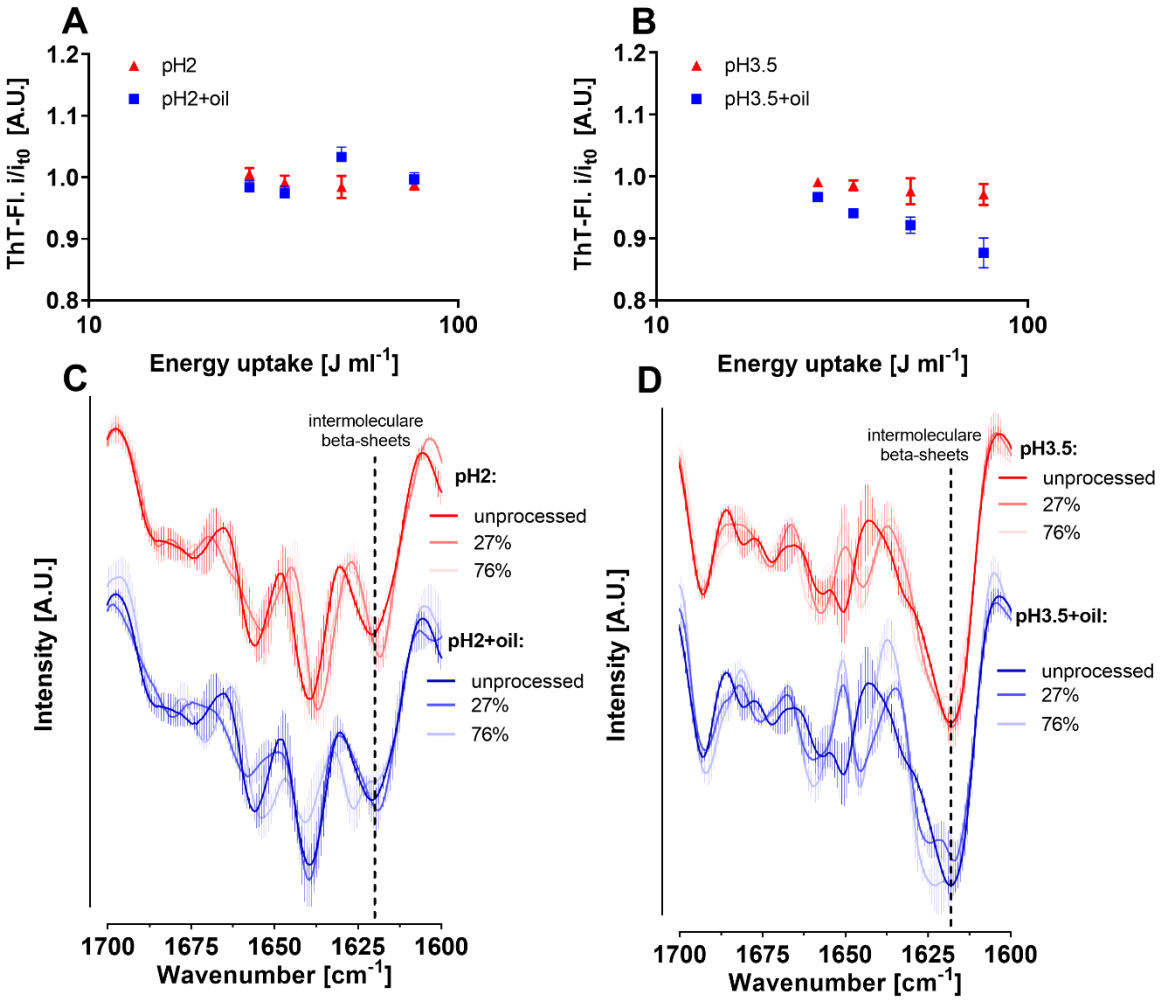

FIG 6-7 Normalized ThT-Fluorescence (**A – D**) and second derivation of amide I spectra (E-H) analysed by FTIR of rotor-stator-sheared fibril solution: At pH 2 without oil (A/E), at pH 2 with 18 % oil (B/F) at pH 3.5 without oil (**C/G**) and at pH 3.5 with 18 % oil (**D/H**). The volume specific energy uptake (E_V) was increased in dependence of sonication amplitude from 27.2 J ml^{-1} to 76.0 J ml^{-1}. Oil was removed by three centrifugation steps at 24 000*g before the analysis was conducted.

6.5. Discussion

6.5.1. Influence of shear on amyloid(-like) aggregates

The shear stress, derived from the volume specific energy input (E_V), can be considered as the product of the stress number (S_N ~ t) and the stress intensity (S_I ~ τ). The presented investigations via AFM demonstrated a reduction of the mean fibril length at pH 2 depending on E_V (**FIG 6-2 and 6-3**) which was confirmed by AUC and DLS measurements. This is in line with previous findings, which demonstrated that the aggregate comminution in rotor-stator processes directly correlates with E_V (Schönstedt et al., 2015). E_V was be estimated using

calorimetric methods and correlated to binding energies (Özcan-Taşkın et al., 2011). For a wide parameter range the fibril length reduction can be expressed as a function of E_V according to the well-known power law (Zhang et al., 2012; Häffele et al., 2018):

EQU 6-1 Length distribution in dependence of the energy intake

$$\mathrm{L} = a * {E_V}^{-b}(1), for\ a = y^{-b}$$

$$\Leftrightarrow$$

$$\log L\,(E_V) = -b * \log(E_V + y)$$

$$\Leftrightarrow$$

$$-b = \frac{\log L\,(E_V)}{\log(E_V + y)}$$

A power law relationship between shear stress and the resulting length of semi-flexible BLG fibrils has been shown in previous works (Kroes-Nijboer et al., 2010; Uttinger et al., 2020). The comminution rate exponent of b = 0.65 for pH 2 fibrils in rotor-stator dispersion is in line with findings by Uttinger et al. (2020) for BLG-fibril fragmentation in a similar device. Our findings in terms of the size reduction exponent agree with the previous results from comminution of particles from different materials and shapes through emulsification by colloid mills, high pressure homogenization and ultrasound (b = 0.3 - 0.8) (Halbig et al., 2016). Therefore, it can be suggested that the shortening of protein fibrils at pH 2 follows similar rules as the comminution of other materials and shapes.

Based on the constant decrease in ThT fluorescence (**FIG 6-4 A**) with increasing stress, it is hypothesized that there is a fraction of beta-sheet stacks in pH 2 fibrils or protofibrils that is unstable to even the lowest applied E_V of 0.29 J ml^{-1}. However, since this decrease is independent of E_V, it was not possible to detect a lower number than five strands (~18.8 Å) for the remaining beta-sheet stacks in this system which is required for ThT binding (Krebs et al., 2005). Therefore, it can be suggested that even the highest implemented stress intensity cannot reduce the length of the fibrils below 1.8 nm.

In contrast to pH 2 fibrils, the average length of worm-like aggregates at pH 3.5 was independent of E_V (**FIG 6-2 B**). This might be caused by their smaller mean length and the resulting lower shear force compared with semi-flexible fibrils produced at pH 2. Thus, the

shear force and in turn the stress intensity is probably to small to reduce the length of the amyloid aggregates further. Additionally, their morphology is considered to be more flexible and thin (Heyn et al., 2019), which may lead easier to an alignment in the shear field, expressed by shear angle sin (alpha) (**EQU 6-2**). The shear stress τ depends on the applied force F, the contact area A and the angle between the vector F and the area A in the relation of:

EQU 6-2 Shear stress calculated by force vector, contact area and shear angle

$$\tau = F A^{-1} sin(\alpha)$$

According to equation (4), the shear stress is reduced due to the adjustment of the shear angle to less than 45°, while the lower diameter reduces the area A of the aggregates.

The flexible structure of the worm-like aggregates indicates lower binding energies between the protein molecules (Eisenberg and Sawaya, 2017). A reason could be a larger distance or a decreased shape complementation between the associated beta-sheets (Lawrence and Colman, 1993) caused by interfering random coil segments of unhydrolyzed BLG (Heyn et al., 2019). Another possibility is the existence of areas in the amyloid-like aggregate where the beta-sheet stacks are interrupted and a potential unstructured protein junction is located (Lux et al., 2021). In the former case, the amyloid aggregate would potentially be dissociated more quickly through the mechanical energy input, which was evidently not the case. In the second case, these "predetermined interconnected joints" would give way and convert the applied specific comminution energy into kinetic energy without any real destruction of the aggregate structure. This could explain the conservation of their size irrespective of the applied energy intake.

6.5.2. Influence of cavitation on amyloid(-like) aggregates

In contrast to rotor-stator dispersion, sonication of fibrils and worm-like aggregates led to a reduction of the mean aggregate length for both morphologies (**FIG 6-5**). The decrease in aggregate size as function of E_V (*size reduction exponent*) is even greater for pH 3.5 worm-like aggregates *(b=0.64)* than for pH 2 fibrils *(b=0.49)* when processed by sonication. These observations give evidence that there is a further decrease in fibril length up to 30-50%, when E_V by sonication was further increased up to 76 J ml^{-1}, compared to the maximum of 42.7 J ml^{-1} applied by rotor-stator-dispersion. Furthermore, sonication (76.0 J ml^{-1}) caused shorter mean fibril length ~107 nm as high-pressure homogenisation (121 - 150 nm) at an E_V of 80 J ml^{-1} (**FIG 6-1 vs FIG 6-5**). This may be due to higher stress intensities during ultrasonic application compared to high pressure homogenization.

It was mentioned that for sonication any mechanical stress is related to the occurrence of cavitation bubbles (Halbig et al., 2016). It can be expected that cavitation appears at all amplitude levels, which are applied in the present work (Behrend et al., 2000). When the cavitation bubbles implode, a high shear flow is generated in the surrounding liquid (Nacken et al., 2017). Nacken et al. (2017), who worked on the delamination of graphite sheets, mentioned, that the principle of cavitation induced energy transfer to rod like structures based on liquid to surface friction, which is caused by shear flow over the length of the structure. Since the induced shear stress is at its maximum in the immediate vicinity of interfaces (here water-gas), it can be explained how the ultrasonically induced energy (at similar E_V) led to a stronger fractionation of the fibrils compared to the rotor-stator system. In rotor-stator-systems, the maximal surface friction only occurs next to the surfaces of the rotor and stator gear rim and the vessel walls. Therefore, it can be suggested that for the size reduction of worm-like aggregates the applied shear stress must be maximal, which could be induced for example by additional surfaces (Li et al., 2018).

However, it has also to be noted that during cavitation very high local temperatures of ~10,000 K can occur (Gogate, 2011), which might have an effect on the protein/amyloid structure. However, no effects were observed by ThT-assays and ATR-FTIR (**FIG 6-7**).

6.5.3. Influence of Water-Oil Interfaces in amyloid(-like) aggregates

The addition of oil led to increased reduction of semiflexible fibrils at lower E_V (**FIG 6-2 A vs C**), when sheared in a rotor stator system. A reduction of the mean fibril length after addition of oil was also observed for sonicated fibrils and worm-like aggregates (**FIG 6-5**) in the lower energy range. Due to the smaller aggregate sizes at lower E_V and a similar aggregate size at higher E_V, fitting of the aggregate size against E_V led to decreased slopes and therefore smaller size reduction exponents b for the experiments with added oil, compared to the experiments without added oil (**FIG 6-3 and** 6-**6**).

Compared to aqueous solutions most water/oil dispersions were found to have an increased viscosity with shear-thinning behaviour (Otsubo and Prud'homme, 1994; Brewer et al., 2016). An enhancement of particle comminution during emulsification process at higher viscosities has been described previously (Behrend et al., 2000). The viscosity is related to the shear stress acting on the fibrils (Heyn et al., 2020). Accordingly, the shear stress is increased especially at lower shear rates (low E_V) compared to aqueous solutions without oil addition (**FIG 6-2 A**). This may explain the significant decrease in fibril length at low E_V in solutions with oil, whereas

this effect is diminished at higher E_V. While this maximum stress intensity during rotor-stator dispersion might be still too low for the fragmentation of flexible aggregates formed at pH 3.5, sonication provides sufficient stress intensity levels (**FIG 6-2 B vs. FIG 6-5 B**). At higher levels of E_V, the oil particle comminution might consume the provided comminution power, which is why the degree of aggregate comminution cannot be further increased.

Additionally, it can be expected that the introduction of the oil phase will result in a firm attachment of the fibrils or aggregates at the interface (Xu et al., 2018; Jordens et al., 2013). Fibrils build an interfacial multilayer which is kept stable by electrostatic repulsion forces (Jordens et al., 2014b). A higher interfacial viscosity has been described for pH 2 fibrils than for non-aggregated BLG (Rühs et al., 2013b; Rühs et al., 2013a). The relatively high immobility of the fibrils at the liquid interface increases the shear stress on the fibrils when the surface of the oil droplets is exposed to shear regarding equation (2).

Interactions between the fibril and the oil interface can also lead to deformation of the fibrils which could cause its fragmentation (Jordens et al., 2014a). Decomposition of BLG fibrils have been described after attachment to an MCT-water interface (Jordens et al., 2014b).

Using the highest E_V by shear or sonication led to some new intermolecular beta-sheets according to ATR-FTIR (**FIG 6-4 and 6-7**). Indeed, measurements via AUC revealed very small aggregates in rotor-stator-sheared samples with added oil, which were not evident in the absence of oil (**Supporting material FIG S6-8 A vs B**). However, this finding can also be linked to very strongly fragmented fibrils. Measurements by DLS revealed the increase of particle size with increasing E_V during shear and sonication (**FIG 6-2 and 6-5**). Thus, it might be possible that the oil-water interface induces aggregation of free peptides or BLG monomers during processing. Finally, the presence of residual oil droplets in the analysis solution despite careful centrifugation can be an explanation.

6.6. Conclusion

TAB 6-1 Comminution rate (SRE) and mean aggregate length received at the highest conducted volume specific energy intake (MAS) after rotor-stator-dispersion and ultra-sonication, with and without added oil. High-pressure-homogenization was conducted at 80 J ml^{-1} for comparison.

			production process				
			rotor-stator-dispersion		ultra-sonication		HP-homogenisation
			without oil	with oil	without oil	with oil	without oil
morphology	pH 2 fibril	*SRE*	*0.65*	*0.27*	*0.48*	*0.38*	*0.27 (orifice) 0.30 (straight)*
		MAS [nm]	**204**	**222**	**107**	**98**	**121 (orifice) 150 (straight)**
	pH 3.5 worm-like	*SRE*	*n.r.*	*n.r.*	*0.64*	*0.21*	*n.r.*
		MAS [nm]	**70**	**86**	**50**	**63**	**n.r.**

SRE: Size reduction exponent;
MAS: minimal aggregate size;
HP: High-pressure
n.r..: no result

The results of the present study primarily indicate that the way of processing influences the comminution of amyloid fibrils or amyloid-like aggregates. The observed comminution rate not only depends on the applied E_V but also on the aggregate morphology and whether the processing is conducted in the presence of an oil phase. While fibrils are shortened by the application of rotor-stator shear in dependence of the E_V, no effect on worm-like aggregates was observed. Ultra-sonication leads to the local occurrence of very high shear effects by cavitation, to which even the worm-like aggregates were unstable. Thus, it can be concluded that the highest fragmentation of amyloid fibrils and amyloid-like aggregates was reached by sonication, followed by high-pressure homogenisation, while the processing with rotor-stator-dispersion resulted in the lowest size reduction of the aggregates (**TAB 6-1**). Especially the differences in the stress intensity level in the different processes may have been the determining factor here. The different process stabilities of fibrillar and amyloid-like aggregates further confirms the structural differences between the different morphologies. This indicates a loose, flexible structure of the pH 3.5 aggregates, which is only disrupted when the shear stress locally exceeds a specific value. Addition of oil led to reduced aggregates sizes at low E_V, but had low effects at high E_V. Thus, the choice of a specific emulsification technology (high-pressure homogenization, ultrasonic or rotor-stator dispersion) could be adapted to the corresponding aggregate morphology in order to preserve the aggregate size and thus possible functionality. At the same time, it can be seen that the oil phase also influences the aggregates in the process and can therefore be an important process parameter in terms of its quantity and viscosity. In

the future, more studies are needed that determine the effect of oil on fibril comminution. None of the studied processes led to a marked reduction in the quantity of ThT-fluorescence and intermolecular beta-sheets. This indicates that the amyloid structures themselves are not completely degraded, but possibly remain in the solution as seeds, which could allow the post-process-formation of new mature fibrils and aggregates. This might alter the viscosity and other functionalities of the product in the following process chain, which needs to be evaluated in the future.

Acknowledgement
This project was funded by DFG SPP 1934 DiSPBiotech (Project no. 315456892, 315396049 and 315460011). We are grateful to Jesco Reimers of the Food Technology Division, CAU Kiel for his supporting work in the laboratory and Stephanie Michel from the Institute for Particle Technology, TU Braunschweig for the preparation of the atomic force microscope images.

6.7. References

Adamcik, Jozef; Jung, Jin-Mi; Flakowski, Jérôme; Los Rios, Paolo de; Dietler, Giovanni; Mezzenga, Raffaele (2010): Understanding amyloid aggregation by statistical analysis of atomic force microscopy images. In: *Nature nanotechnology* 5 (6), S. 423–428. DOI: 10.1038/nnano.2010.59.

Bateman, Libei; Ye, Aiqian; Singh, Harjinder (2010): In vitro digestion of beta-lactoglobulin fibrils formed by heat treatment at low pH. In: *Journal of agricultural and food chemistry* 58 (17), S. 9800–9808. DOI: 10.1021/jf101722t.

Behrend, O.; Ax, K.; Schubert, H. (2000): Influence of continuous phase viscosity on emulsification by ultrasound. In: *Ultrasonics sonochemistry* 7 (2), S. 77–85. DOI: 10.1016/S1350-4177(99)00029-2.

BREWER, David Ramirez; FRANCO, José Maria; GARCIA-ZAPATEIRO, Luis Alberto (2016): Rheological properties of oil-in-water emulsions prepared with oil and protein isolates from sesame (Sesamum Indicum). In: *Food Sci. Technol* 36 (1), S. 64–69. DOI: 10.1590/1678-457X.6761.

Eisenberg, David S.; Sawaya, Michael R. (2017): Structural Studies of Amyloid Proteins at the Molecular Level. In: *Annual review of biochemistry* 86, S. 69–95. DOI: 10.1146/annurev-biochem-061516-045104.

Gao, Zhiming; Zhao, Junjun; Huang, Ying; Yao, Xiaolin; Zhang, Ke; Fang, Yapeng et al. (2017): Edible Pickering emulsion stabilized by protein fibrils. Part 1. Effects of pH and fibrils concentration. In: *LWT - Food Science and Technology* 76, S. 1–8. DOI: 10.1016/j.lwt.2016.10.038.

Gogate, Parag R. (2011): Hydrodynamic Cavitation for Food and Water Processing. In: *Food Bioprocess Technol* 4 (6), S. 996–1011. DOI: 10.1007/s11947-010-0418-1.

Gothsch, T.; Richter, C.; Beinert, S.; Schilcher, C.; Schilde, C.; Büttgenbach, S.; Kwade, A. (2016): Effect of cavitation on dispersion and emulsification process in high-pressure microsystems (HPMS). In: *Chemical Engineering Science* 144, S. 239–248. DOI: 10.1016/j.ces.2016.01.034.

Häffele, Florian; Mende, Susann; Jaros, Doris; Rohm, Harald; Nirschl, Hermann (2018): Relationship between shear energy input and sedimentation properties of exopolysaccharide-producing Streptococcus thermophilus strains. In: *Separation and Purification Technology* 202, S. 21–26. DOI: 10.1016/j.seppur.2018.03.031.

Halbig, Christian E.; Nacken, Thomas J.; Walter, Johannes; Damm, Cornelia; Eigler, Siegfried; Peukert, Wolfgang (2016): Quantitative investigation of the fragmentation process and defect density evolution of oxo-functionalized graphene due to ultrasonication and milling. In: *Carbon* 96, S. 897–903. DOI: 10.1016/j.carbon.2015.10.021.

Heyn, Timon R.; Garamus, Vasil M.; Neumann, Hendrikje R.; Uttinger, Maximilian J.; Guckeisen, Tobias; Heuer, Monique et al. (2019): Influence of the polydispersity of pH 2 and pH 3.5 beta-lactoglobulin amyloid fibril solutions on analytical methods. In: *European Polymer Journal* (120), S. 109211. DOI: 10.1016/j.eurpolymj.2019.08.038.

Heyn, Timon R.; Mayer, Julian; Neumann, Hendrikje R.; Selhuber-Unkel, Christine; Kwade, Arno; Schwarz, Karin; Keppler, Julia K. (2020): The threshold of amyloid aggregation of beta-lactoglobulin. Relevant factor combinations. In: *Journal of Food Engineering* 283, S. 110005. DOI: 10.1016/j.jfoodeng.2020.110005.

Jordens, Sophia; Isa, Lucio; Usov, Ivan; Mezzenga, Raffaele (2013): Non-equilibrium nature of two-dimensional isotropic and nematic coexistence in amyloid fibrils at liquid interfaces. In: *Nature communications* 4, S. 1917. DOI: 10.1038/ncomms2911.

Jordens, Sophia; Riley, Emily E.; Usov, Ivan; Isa, Lucio; Olmsted, Peter D.; Mezzenga, Raffaele (2014a): Adsorption at Liquid Interfaces Induces Amyloid Fibril Bending and Ring Formation. In: *ACS nano* 8 (11), S. 11071–11079. DOI: 10.1021/nn504249x.

Jordens, Sophia; Rühs, Patrick A.; Sieber, Christine; Isa, Lucio; Fischer, Peter; Mezzenga, Raffaele (2014b): Bridging the gap between the nanostructural organization and macroscopic interfacial rheology of amyloid fibrils at liquid interfaces. In: *Langmuir : the ACS journal of surfaces and colloids* 30 (33), S. 10090–10097. DOI: 10.1021/la5020658.

Kavanagh, Gaynor M.; Clark, Allan H.; Ross-Murphy, Simon B. (2000): Heat-Induced Gelation of Globular Proteins. 4. Gelation Kinetics of Low pH β-Lactoglobulin Gels. In: *Langmuir* 16 (24), S. 9584–9594. DOI: 10.1021/la0004698.

Keppler, Julia Katharina; Martin, Dierk; Garamus, Vasil M.; Berton-Carabin, Claire; Nipoti, Elia; Coenye, Tom; Schwarz, Karin (2017): Functionality of whey proteins covalently modified by allyl isothiocyanate. Part 1 physicochemical and antibacterial properties of native and modified whey proteins at pH 2 to 7. In: *Food Hydrocolloids* 65, S. 130–143. DOI: 10.1016/j.foodhyd.2016.11.016.

Knowles, Tuomas P. J.; Mezzenga, Raffaele (2016): Amyloid Fibrils as Building Blocks for Natural and Artificial Functional Materials. In: *Advanced materials (Deerfield Beach, Fla.)* 28 (31), S. 6546–6561. DOI: 10.1002/adma.201505961.

Koo, Charmaine K.W.; Chung, Cheryl; Ogren, Thaddao; Mutilangi, William; McClements, David Julian (2018): Extending protein functionality. Microfluidization of heat denatured whey protein fibrils. In: *Journal of Food Engineering* 223, S. 189–196. DOI: 10.1016/j.jfoodeng.2017.10.020.

Kroes-Nijboer, Ardy; Venema, Paul; Baptist, Harry; van der Linden, Erik (2010): Fracture of protein fibrils as induced by elongational flow. In: *Langmuir : the ACS journal of surfaces and colloids* 26 (16), S. 13097–13101. DOI: 10.1021/la1025262.

Lawrence, M. C.; Colman, P. M. (1993): Shape complementarity at protein/protein interfaces. In: *Journal of molecular biology* 234 (4), S. 946–950. DOI: 10.1006/jmbi.1993.1648.

Li, Chen; Qin, Rongrong; Liu, Ruirui; Miao, Shuting; Yang, Peng (2018): Functional amyloid materials at surfaces/interfaces. In: *Biomaterials science* 6 (3), S. 462–472. DOI: 10.1039/c7bm01124e.

Lux, Jacqueline; Azarkh, Mykhailo; Fitzner, Laura; Keppler, Julia K.; Schwarz, Karin; Drescher, Malte; Steffen-Heins, Anja (2021): Amyloid aggregation of spin-labeled β-lactoglobulin. Part II. Identification of spin-labeled protein and peptide sequences after amyloid aggregation. In: *Food Hydrocolloids* 112, S. 106174. DOI: 10.1016/j.foodhyd.2020.106174.

Mohammadian, Mehdi; Madadlou, Ashkan (2016): Cold-set hydrogels made of whey protein nanofibrils with different divalent cations. In: *International Journal of Biological Macromolecules* 89, S. 499–506. DOI: 10.1016/j.ijbiomac.2016.05.009.

Nacken, Thomas J.; Halbig, Christian E.; Wawra, Simon E.; Damm, Cornelia; Romeis, Stefan; Walter, Johannes et al. (2017): Structural factors controlling size reduction of graphene oxide in liquid processing. In: *Carbon* 125, S. 360–369. DOI: 10.1016/j.carbon.2017.09.066.

Oboroceanu, Daniela; Wang, Lizhe; Magner, Edmond; Auty, Mark A.E. (2014): Fibrillization of whey proteins improves foaming capacity and foam stability at low protein concentrations. In: *Journal of Food Engineering* 121, S. 102–111. DOI: 10.1016/j.jfoodeng.2013.08.023.

Otsubo, Y.; Prud'homme, R. K. (1994): Rheology of oil-in-water emulsions. In: *Rheola Acta* 33 (1), S. 29–37. DOI: 10.1007/BF00453461.

Özcan-Taşkın, Gül; Kubicki, Dominik; Padron, Gustavo (2011): Power and flow characteristics of three rotor-stator heads. In: *Can. J. Chem. Eng.* 89 (5), S. 1005–1017. DOI: 10.1002/cjce.20553.

Romdhane, M.; Gourdon, C.; Casamatta, G. (1995): Development of a thermoelectric sensor for ultrasonic intensity measurement. In: *Ultrasonics* 33 (2), S. 139–146. DOI: 10.1016/0041-624X(94)00019-L.

Rühs, P. A.; Scheuble, N.; Windhab, E. J.; Fischer, P. (2013a): Protein adsorption and interfacial rheology interfering in dilatational experiment. In: *Eur. Phys. J. Spec. Top.* 222 (1), S. 47–60. DOI: 10.1140/epjst/e2013-01825-0.

Rühs, Patrick A.; Affolter, Christine; Windhab, Erich J.; Fischer, Peter (2013b): Shear and dilatational linear and nonlinear subphase controlled interfacial rheology of β-lactoglobulin fibrils and their derivatives. In: *Journal of Rheology* 57 (3), S. 1003–1022. DOI: 10.1122/1.4802051.

Schönstedt, Björn; Jacob, Hans-Joachim; Schilde, Carsten; Kwade, Arno (2015): Scale-up of the power draw of inline-rotor–stator mixers with high throughput. In: *Chemical Engineering Research and Design* 93, S. 12–20. DOI: 10.1016/j.cherd.2014.04.004.

Schuck, Peter; Rossmanith, Peter (2000): Determination of the sedimentation coefficient distribution by least-squares boundary modeling. In: *Biopolymers* 54 (5), S. 328–341. DOI: 10.1002/1097-0282(20001015)54:5<328::AID-BIP40>3.0.CO;2-P.

Serfert, Y.; Lamprecht, C.; Tan, C.-P.; Keppler, J. K.; Appel, E.; Rossier-Miranda, F. J. et al. (2014): Characterisation and use of β-lactoglobulin fibrils for microencapsulation of lipophilic ingredients and oxidative stability thereof. In: *Journal of Food Engineering* 143, S. 53–61. DOI: 10.1016/j.jfoodeng.2014.06.026.

Shen, Xue; Zhao, Changhui; Guo, Mingruo (2017): Effects of high intensity ultrasound on acid-induced gelation properties of whey protein gel. In: *Ultrasonics sonochemistry* 39, S. 810–815. DOI: 10.1016/j.ultsonch.2017.05.039.

Uttinger, Maximilian J.; Heyn, Timon R.; Jandt, Uwe; Wawra, Simon E.; Winzer, Bettina; Keppler, Julia K.; Peukert, Wolfgang (2020): Measurement of length distribution of beta-lactoglobulin fibrils by multiwavelength analytical ultracentrifugation. In: *European biophysics journal : EBJ. DOI:* 10.1007/s00249-020-01421-4.

Walter, Johannes; Löhr, Konrad; Karabudak, Engin; Reis, Wieland; Mikhael, Jules; Peukert, Wolfgang et al. (2014): Multidimensional analysis of nanoparticles with highly disperse properties using multiwavelength analytical ultracentrifugation. In: *ACS nano* 8 (9), S. 8871–8886. DOI: 10.1021/nn503205k.

Walter, Johannes; Peukert, Wolfgang (2016): Dynamic range multiwavelength particle characterization using analytical ultracentrifugation. In: *Nanoscale* 8 (14), S. 7484–7495. DOI: 10.1039/c5nr08547k.

Xu, Hua-Neng; Li, Ying-Hao; Zhang, Lianfu (2018): Driving Forces for Accumulation of Cellulose Nanofibrils at the Oil/Water Interface. In: *Langmuir : the ACS journal of surfaces and colloids* 34 (36), S. 10757–10763. DOI: 10.1021/acs.langmuir.8b02310.

Zhang, Jinli; Xu, Shuangqing; Li, Wei (2012): High shear mixers. A review of typical applications and studies on power draw, flow pattern, energy dissipation and transfer properties. In: *Chemical Engineering and Processing: Process Intensification* 57-58, S. 25–41. DOI: 10.1016/j.cep.2012.04.004.

6.8. Supplementary material

TAB S6-2 Calculated energy input and measured energy uptake per volume (EV) implemented by shear with Ultra-turrax and rotational numbers from 1.88*104 to 1.57*105 (3 to 25 KRPM).

Rotational Number N [rad s^{-1}]	*Calculated energy input per volume[a] [J ml^{-1}]*	*Measured energy uptake per volume[b] [J ml^{-1}]*
1.88E+04	0.11	0.29
2.51E+04	0.26	0.43
3.77E+04	0.87	1.22
5.03E+04	2.07	2.14
6.28E+04	4.04	4.07
8.17E+04	8.87	7.91
1.01E+05	16.53	14.77
1.19E+05	27.68	23.88
1.38E+05	42.97	32.56
1.57E+05	63.05	42.71

[a] E_V = P*t / V and Ne = P / $n^3 d^5 \rho_S$ = f(Re). The Newton number (Ne) remains constant for reynolds numbers above 10^4* in turbulent flow. *Therefore,* the *Energyintake is a function of the rotationnumber n (Uttinger et al. 2020).
[b] Energy uptake was calculated by the increase in temperature [K] / Mass H_2O [kg] and the specific thermal capacity of water (4185.1 J/kg) during the 60 s of the experiment.

TAB S6-3 Measured volume specific energy intakes (EV) implemented by ultra sonication and a soundwave amplitude from 21.2 µm to 148.4 µm.

Amplitude [μm_{ss}]	*Measured energy per volume[b] [J ml^{-1}]*
21.2	27.2 ± 3.5
42.4	33.9 ± 2.2
84.8	48.3 ± 1.3
148.4	76.0 ± 1.3

[b] Energy uptake (E_V) was calculated by the increase in temperature [K] / Mass H_2O [kg] and the specific thermal capacity of water (4185.1 J/kg) during the 60 s of the experiment.

TAB S6-4 Flow rate (ml s-1) during stressing at different pressure levels in a high-pressure homogenisation system in dependence of geometry and fibril morphology.

Geometrie	*Pressure level [bar]*	*Flow rate [ml s^{-1}]*	
		Morphologie	
		Straight (pH 2)	Worm-like (pH 3.5)
Orifice	50	0.28	0.35
	400	0.98	1.02
	800	1.43	1.43
Straight	50	0.70	0.68
	400	1.95	2.04
	800	2.78	2.38

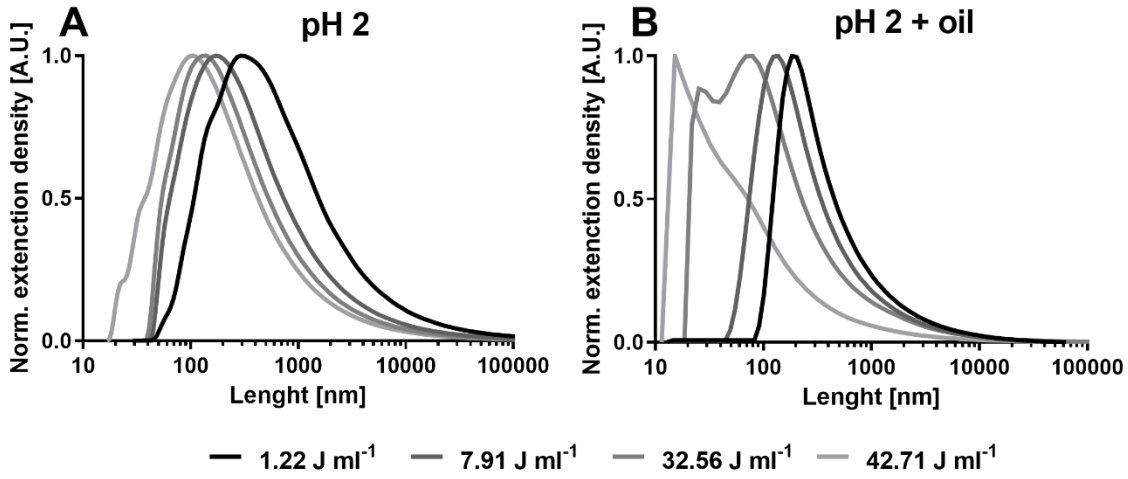

FIG S6-8 Length distribution [nm] of rotor-stator-sheared fibril solutions analysed with analytical ultracentrifugation: At pH 2 without oil (A) and with 18 wt% oil (B). Volume specific energy intakes (EV) was increased in dependence of rotational number N from 1.22 J ml-1 to 42.71 J ml-1. Oil was removed by three centrifugation steps at 24 000*g before the analysis was conducted.

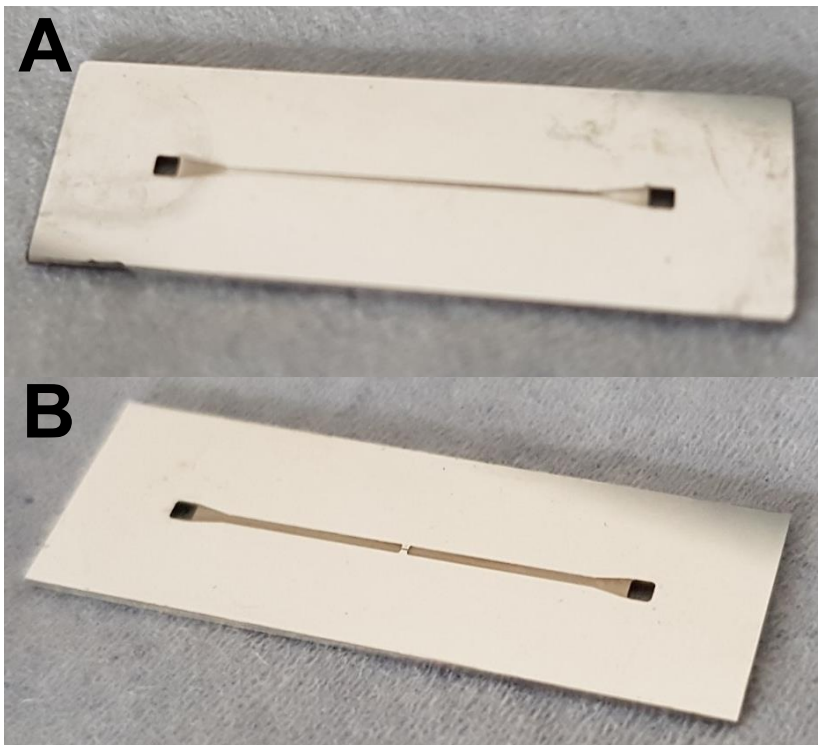

FIG S6-9 Straight (**A**) "GE07" and orificed (**B**) "E021B" microchannel geometry used for high pressure homogenisation.

TAB S6-5 fibril length (atomic force microscopy), sedimentation coefficient (analytical ultracentrifugation) and aggregate size (dynamic light scattering) measured after high pressure homogenisation at different pressure levels and orifice geometries.

Geometry	E_V *[J ml^{-1}]*	***AFM*** *Mean length ± SD [nm]*	***AUC*** *Sed. Coef. ± SD [s]*	***DLS*** *Z-Average ± SD [nm]*
Straight	5	347 ± 216	31 ± 28	101 ± 14
	40	182 ± 69	26 ± 38	79 ± 8
	80	150 ± 58	23 ± 34	58 ± 8
Orifice	5	280 ± 153	30 ± 14	78 ± 2
	40	173 ± 77	24 ± 23	56 ± 2
	80	121 ± 57	22 ± 18	53 ± 3

TAB S6-6 Sedimentation coefficient [s] of rotor-stator sheared pH 2 fibrils analysed by analytical ultracentrifugation

Setting	E_V *[J ml^{-1}]*	*1.22*	*7.91*	*32.56*	*42.71*
pH 2 without oil	Mean (s)	29.77	25.65	23.28	21.54
	Standart Deviation (s)	14.20	37.94	33.68	17.62
pH 2 with oil	Mean (s)	24.44	22.47	12.00	9.39
	Standart Deviation (s)	4.82	5.63	9.41	11.26

TAB S6-7 Fibril length (nm) of rotor-stator sheared fibrils analysed by atomic force microscopy images.

Setting	*E_V [J ml^{-1}]*	*unpr.*	*0.29*	*0.43*	*1.22*	*2.14*	*4.07*	*7.91*	*14.77*	*23.88*	*32.56*	*42.71*	*b*	*R^2*
pH 2 without oil	Mean (nm)	*7043*	6155	4414	2434	1469	1350	716	404.5	294.5	256.4	204.3	-0.654	0.994
	Median (nm)	*8010*	6213	3938	1931	1253	1230	652.4	384.6	285.7	210.2	187.6	-0.741	0.985
	Minimum (nm)	*1020*	1422	251.8	169.5	91.13	191	155.5	26.94	61.42	72.35	33.47	----	----
	Maximum (nm)	*13300*	9273	9464	8155	4809	4346	2315	1114	682.2	928.6	557.2	----	----
pH 2 with oil	Mean (nm)	----	801	744.2	568.6	491.9	434.3	274.2	297.2	222.4	250.7	222.2	-0.268	0.983
	Median (nm)	----	680.0	648.3	501.2	436.3	347.8	249.7	277.8	210.5	212.7	191.5	-0.260	0.985
	Minimum (nm)	----	39	65.6	48.03	104.3	93	39.58	77.63	51.51	57	62.94	----	----
	Maximum (nm)	----	5014	4823	1542	2361	2636	754.3	924	620.7	1220	630.1	----	----
pH 3.5 without oil	Mean (nm)	*73.55*	64.57	64.53	69.65	59.21	67.76	66.26	55.85	73.57	70.52	70.23	0.014	0.094
	Median (nm)	*64.48*	57.15	57.73	67.76	58.23	62.31	59.81	55.89	71.03	67.43	69.53	0.030	0.330
	Minimum (nm)	*16.80*	15.25	14.19	27.58	16.92	15.66	24.53	4.303	16.38	32.77	22.85	----	----
	Maximum (nm)	*243.7*	134.6	152.5	209.1	101.3	131.6	146.9	120.6	193.8	146.5	162.4	----	----
pH 3.5 with oil	Mean (nm)	----	92.99	96.66	103.5	91.57	100.2	86.21	91.95	86.36	82.77	86.49	-0.0227	0.444
	Median (nm)	----	84.80	90.18	96.90	85.80	96.49	75.80	83.48	77.71	71.19	75.83	-0.038	0.436
	Minimum (nm)	----	15.25	23.84	19.53	13.57	14.83	9.475	6.356	2.996	6.7	7.639	----	----
	Maximum (nm)	----	269.3	249.2	254.2	237.6	271.9	576.3	527	292.7	388.8	376.4	----	----

TAB S6-8 Fibril length (nm) of ultrasonic processed fibrils analysed by atomic force microscopy images

Setting	*E_V [J ml^{-1}]*	unprocessed	*27.2*	*33.9*	*48.3*	*76.0*	*b*	*R^2*
pH 2 without oil	Mean (nm)	*7043*	161.4	149.7	135.2	107.2	-0.492	0.8454
	Median (nm)	*8010*	135.5	96.11	89.50	83.96	-0.470	0.7192
	Minimum (nm)	*1020*	26.38	18.61	7.198	14.34	----	----
	Maximum (nm)	*13300*	440.2	574.8	393.2	318.3	----	----
pH 2 with oil	Mean (nm)	-----	156	123.1	101.4	97.83	-0.382	0.9821
	Median (nm)	-----	150.1	125.6	112.1	88.12	-0.501	0.9154
	Minimum (nm)	-----	11.59	19.14	17.47	6.232	----	----
	Maximum (nm)	-----	616.1	528.9	351.6	276.6	----	----
pH 3.5 without oil	Mean (nm)	*73.55*	102.2	83.16	75.1	49.99	-0.638	0.9613
	Median (nm)	*64.48*	98.28	76.65	71.86	46.37	-0.659	0.9347
	Minimum (nm)	*16.80*	20.97	26.55	19.07	15.28	----	----
	Maximum (nm)	*243.7*	221.2	177	179.3	136.7	----	----
pH 3.5 with oil	Mean (nm)	**----**	83.56	60.88	70.09	62.52	-0.209	0.3681
	Median (nm)	**----**	81.40	57.87	62.33	59.36	-0.256	0.4271
	Minimum (nm)	**----**		11.41	10.8	14.83	8.735	----	----
	Maximum (nm)	**----**		190.7	166.8	295.7	146.9	----	----

7. General discussion

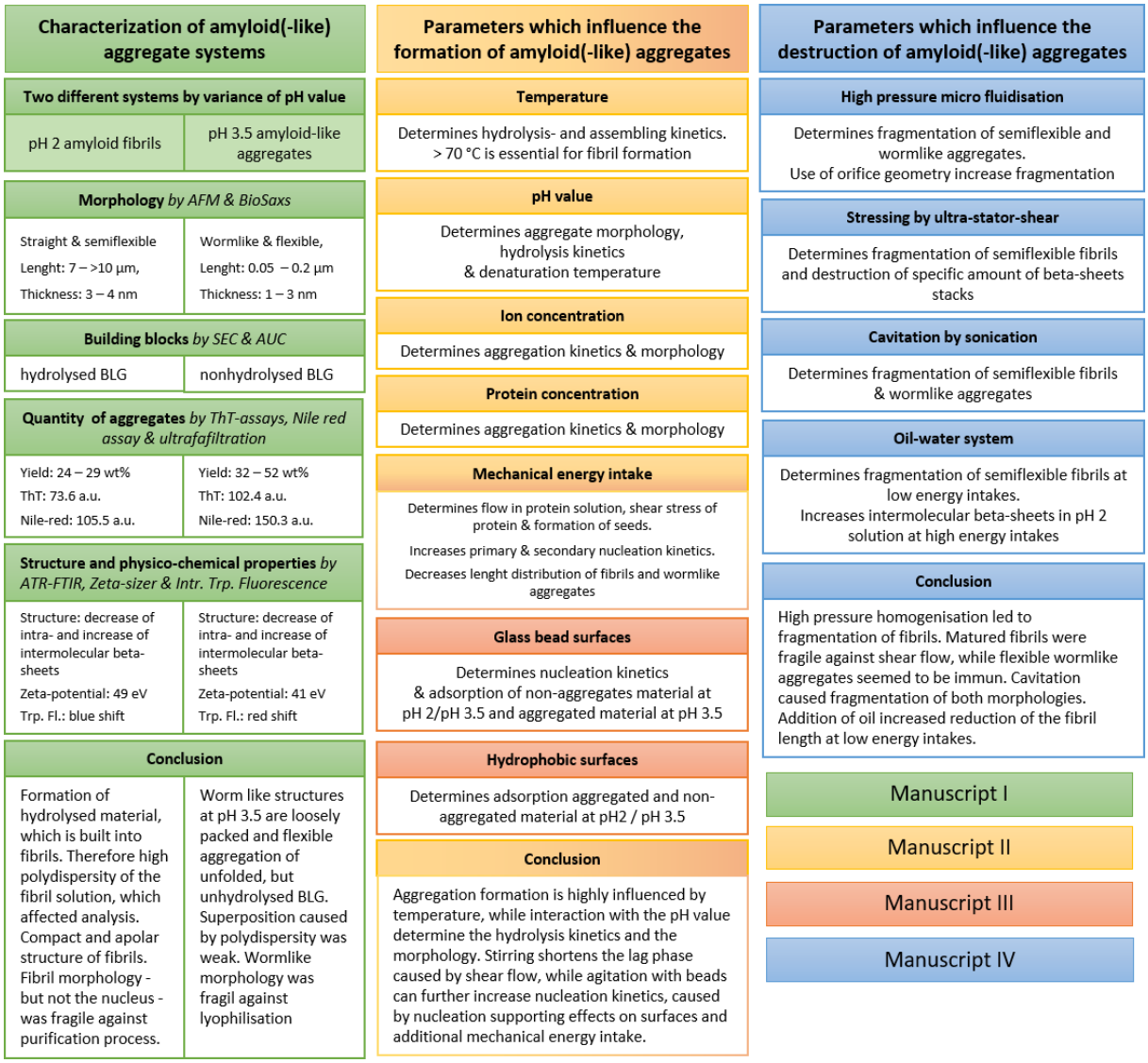

FIG 7-1 Schematic structure of the presented thesis with selected results**.**

The topic of this thesis was the investigation of parameters which influence the formation and degradation of amyloid or amyloid-like structures from beta-lactoglobulin (BLG) in one or two-phase systems. The most important results of **manuscripts 1 to 4** are summarized in **FIG 7-1**. From the comparison in the first column (green) first, the **terminology** of aggregates formed at pH 2 and the aggregates formed at pH 3.5 and which were used in this thesis can be derived (**chapter 7.1)**. Second, the **hypothesis** from **chapter 1** will be addressed directly (**chapter 7.2**). Third the most important findings regarding the two different morphologies: fibril and worm-like aggregation, will be compared and discussed in **chapter 7.3**. From this, answers to the question of relevance for food processing can be derived: Is the occurrence of amyloid or amyloid-like aggregation possible in the food production chain (**chapter 7.4**) and how can the

suitability and value of the two morphologies for processed food be deduced on the basis of the results obtained (**chapter 7.5**)?

7.1. Terminology of the aggregates formed at pH 2 and pH 3.5 after heating

Amyloid structures base on a compact cross-beta-sheet structure characterized by beta-sheet stacks parallel to a fibril axis (**chapter 2.2.2**).

For **BLG aggregates formed at pH 2**, this structure has been demonstrated in the past (Cao and Mezzenga 2019), which is why they are referred to as **amyloid fibrils, fibrils or amyloid aggregates** in the present work. Here, the detection was performed with the help of the dye Thioflavin-T (ThT), which binds to the surface of beta-sheet stacks and subsequently reaches higher fluorescence intensities (Krebs et al. 2005). The aggregation process correlates further with the increase of intermolecular beta-sheets, which could be detected by Fourier transform infrared spectroscopy (FTIR) (Zandomeneghi et al. 2004).

For **BLG aggregates formed at pH 3.5**, an increase in ThT fluorescence (ThT FL) as well as an increase in intermolecular beta-sheets was detected (**FIG 7-1**), this is why they can be linked to an amyloid structure. Through analysis with atomic force microscopy (AFM) it was demonstrated that these aggregates do not have an ordered fibril axis (**FIG 3-1**). Furthermore, the exact beta-sheet arrangement of the aggregates at pH 3.5 is still unknown. There are indications that no proper cross-beta-sheet structures can be formed from unhydrolyzed BLG (Nicolai et al. 2011). For this reason, the aggregates that were formed at pH 3.5 are referred as **amyloid-like aggregates or worm-like aggregates**.

7.2. Addressing the hypotheses

Hypothesis 1. *It was expected that fibrils and worm-like aggregates formed at pH 2 and pH 3.5, respectively, consist of different building blocks*. Observations by size exclusion chromatography (SEC) and analytical ultracentrifugation (AUC) described in **manuscript 1**, revealed that aggregates formed at pH 2 consist of hydrolysed BLG-peptides, while at pH 3.5 non-hydrolysed BLG assemble to aggregates.

Hypothesis 2: *It was hypothesized that isolated amyloid fibrils and amyloid-like aggregates at pH 2 and pH 3.5, respectively, have different physico-chemical properties and differences in sample composition interfere with their analysis.* Findings by ThT-assay, Nile-red-assay, intr. Trp. fluorescence, zeta-potential, FTIR and small angle X-ray scattering (SAXS) of isolated aggregate fraction illustrated in **manuscript 1**, as well as the surface behaviour of the

aggregates shown in **manuscript 3,** indicated that amyloid fibrils and amyloid-like aggregates have different physico-chemical properties. However, the analysis of the non-amyloid(-like) fractions or non-isolated solutions have shown slight, but also extreme differences in the results.

Hypothesis 3: *It was assumed that the temperature is the most important process parameter for BLG amyloid fibril formation, and that factor-interaction may affect the aggregation kinetics at different temperatures.* The results of the statistical designed experiments in **manuscript 2** indicated that temperature has the highest influence on the aggregation kinetics during fibril formation and determines the threshold of fibril formation. It was found that other parameters, such as pH value and shear stress interact with the temperature regarding the aggregation kinetics, which was evaluated by differential scanning calorimetry and computational fluid dynamics, respectively.

Hypothesis 4: *It was suggested that the application of additional mechanical energy and specific surface area by agitated particles accelerated the formation of aggregates and that this effect is different for amyloid(-like) aggregates at pH 2 and pH 3.5, respectively.* The results presented in **manuscript 3** demonstrated that the agitation with glass beads increase the aggregation kinetics of the amyloid fibrils at pH 2, but not for amyloid-like aggregates at pH 3.5, and this effect depends on the bead size and shaking speed. At high specific surface areas effects on the lag phase of amyloid formation were observed. The experiments with chemical modified bead surfaces indicated that the bead surface hydrophobicity and roughness has a strong influence on the nucleation of the amyloids and therefore the aggregation kinetics.

Hypothesis 5: *It was hypothesized that shear stress and cavitation affect the fragmentation of BLG amyloid and amyloid-like aggregates in oil-water systems to a different extent.* Findings of **manuscript 4** revealed the decrease of the mean length of fibrils by rotor-stator-shear, but not for worm-like aggregates. It was found that cavitation implemented by high pressure micro fluidisation and sonication led to an even stronger fragmentation of fibrils and worm-like aggregates at comparable amounts of dissipated energy. The presence of an oil-phase led to stronger fragmentation at lower energy intakes.

7.3. Differences between amyloid(-like) aggregation formed at pH 2 or pH 3.5

To characterize two different aggregation systems with similar parameter settings, amyloid fibrils and worm-like amyloid-like aggregates from BLG were compared in this thesis. The parameter that cause a variance in the morphology is the difference between a pH values of 2 (fibrils) and 3.5 (worm-like aggregates) as described first by Serfert et al. (2014). In addition to the morphology, differences in the structure was discovered in **manuscript 1**. Referring to **hypothesis 1**, the different building blocks as the reason for different level of hydrolysis were revealed by size exclusion chromatography (SEC). The increased hydrolysis in the pH 2 protein solution caused a higher degree of polydispersity compared to the pH 3.5 solution, which led to a stronger superposition effects (**hypothesis 2**). The different ways of building blocks assembling and formation of amyloid (kind) structures (**manuscript 1 to 3**) also causes a different dependence on process parameters (**hypothesis 3 and 4**), stability against process influences (**hypothesis 5**) of e.g. shear (**manuscript 3 and 4**), cavitation (**manuscript 4**) and interfaces (**manuscript 3 and 4**). While fibril structures have been well investigated due to their high relevance for a wide range of applications, the pH value depending worm-like aggregates, their differences to the semi-flexible fibrils and their potential for applications have hardly been described so far.

7.3.1. Differences in polydispersity at pH 2 and pH 3.5

Due to acid hydrolysis kinetics dependence on the pH value, it was suggested that there is a different level of hydrolysis during the formation of aggregates at pH 2 and pH 3.5. This could lead to a higher degree of polydispersity in the proteins solution (**hypothesis 1**). Investigations of **manuscript 1 and 2** allow now to derive the following compositions for the different systems: At pH 2 and 90 °C for 5 h, ~60 % of the BLG was proteolysed into peptides (**FIG 4-5**), while 40 – 60 % of this peptide material is incorporated into the fibrils (Keppler et al. 2019). This implies that ~30% of the total protein mass present in the solution is amyloid aggregated material, ~40 % is (supposedly) monomeric (Townend et al. 1960) BLG and ~30 % are non-aggregated peptides. Findings by SEC illustrated in **FIG 3-2 B**, indicated there was only low level of hydrolysis after 5 h at pH 3.5 and 90 °C < 5 %. The existence of hydrolysed material was validated by AUC (**FIG 3-3 B**) which showed the presence of particles < 18 kDa and by experiments over 24 h to 72 h (published by Keppler et al. (2019), mentioned a similar level of hydrolysis in pH 3.5 and pH 2 solutions when heated over this time period. Although, after 5 h the solution contains only small amount of peptides (6.6 kDa and 4.3 kDa), which were not incorporated into the aggregates (**FIG 3-2 B**), 32 – 52 % aggregated material >300 kDa

(measured by UF in **FIG 3-4 D**) and therefore ~45 – 75 % monomer, dimer or oligomer BLG material (< 300 kDa). Because of the higher amount of peptides at pH 2 solution after heating, this system was mentioned in **manuscript 1** to be more polydisperse and caused a higher extent of superposition effects (**see chapter 7.3.2**), especially for unspecific analysis, such as intrinsic TRP fluorescence (**FIG 3-6**) and FTIR (**FIG 3-5**) compared to the heated solution at pH 3.5.

As there might be synergistic effects between peptides and fibrils when accumulate at interfaces (Lux et al. 2020c; Jung et al. 2010), this polydispersity has also relevance for the investigations in **manuscript 3 and 4**, when interfaces (glass bead surfaces, bound steric acid surfaces, oil droplets) were part of the experiments. Additionally, as there was the detection of very high hydrophobic peptides or peptide aggregates in the pH 2 fibril solution (Lux et al., 2020b), this special fraction could be an important factor for the fibril interaction with the hydrophobic stearic acid surfaces (**FIG 5-1 B**). According to Kroes-Nijboer et al. (2011) and Arosio et al. (2012) the assembly of the building blocks depends on their availability in the solution. A "negative assembly", i.e. a dissociation of the fibril building blocks according to thermodynamic effects— as demonstrates for other amyloid fibril before (Carulla et al. 2005; O'Nuallain et al. 2005)—might be conceivable if their availability due to purification approaches zero. From the different polydispersity or hydrolysate quantities in heated pH 2 and pH 3.5 solutions, further relevance's for the technical functionality or food safety can be derived which are discussed in **chapter 7.5**

7.3.2. Differences in structure of amyloid fibrils and amyloid-like aggregates

Structure of pH 2 semiflexible fibrils based on the assembling of hydrolysed BLG (Akkermans et al. 2008c; Ye et al. 2018; Kroes-Nijboer et al. 2011), which degree and size during 72 h of incubation was first time investigated, described and compared to conditions at pH 3.5 in **manuscript 1 and manuscript 2** as well as work published by Keppler et al. (2019) and which specific findings was brought together in **chapter 7.3.1**

The structure of pH 2 fibrils is mostly known and have been described in the theoretical background in **chapter 2.2.2.** However, regarding **hypothesis 2,** fractionation by ultrafiltration with subsequent lyophilisation of the polydisperse fibril solution (**chapter 7.3.1**) led to a more specific analysis of the aggregated and non-aggregated fraction. Due to this, the detection of the compact and apolar structure of semiflexible fibrils were able by intrinsic TRP fluorescence (**FIG 3-6 A**), which is usually superposed by the non-aggregated and/or hydrolysed BLG and led to misinterpretation of findings in the past (Hettiarachchi et al. 2012). Additionally, due to the prepurification the pure character of intermolecular beta-sheets stacks in the fibrils were

able to detect by ATR-FTIR (**FIG 3-3 A)** which absorbance at band 1620 cm^{-1} (amid I) is usually lowered by non-aggregated material. The measurements indicated that there is a proportional increase of intermolecular beta-sheets and therefore absorbance at this band in dependence of the fibril yield. Therefore, the absorbance of purified fibrils helped to calculate the fibril yield by the measured absorbance at this band as it was done in **manuscript 2**.

Because the electrostatic interactions are very relevant for the ordered and firm aggregation of the nucleus (Loveday et al. 2017; Akkermans et al. 2006; Dave et al. 2014), a detailed investigation of the zeta-potential of the different fractions at pH 2 and pH 3.5 was conducted (**FIG 3-4 C**) and revealed a higher zeta-potential of the non-aggregated fraction at both pH values.

To compare the findings on pH 2 semiflexible fibrils with another aggregate morphology, most of the experiments and analyses (**manuscript 1, 3 and 4**) were also conducted for short worm-like aggregates formed at high temperatures and pH 3.5. The structures formed at pH 3.5 are less well investigated. (Mudgal et al. 2009; Mudgal et al. 2011b; Mudgal et al. 2011a; Mudgal et al. 2011c) described short flexible strands fibrils at pH 3.35. However, there are also parallels to amorphous aggregates and worm-like aggregates obtained from BLG at high temperature and a pH value of 7 (Jung et al. 2008; Gosal et al. 2004) (**FIG-S 4-9**) or from ovalbumin at pH 2 (Lara et al. 2012). Short flexible proteins strands can also be obtained by increasing the ion concentration by adding NaCl or $CaCl_2$ (Loveday et al. 2010) or the protein concentration (vandenAkker et al. 2011; Ye et al. 2018). Although, it has to be noted that the ionic strength also increases with protein concentration (Nicolai and Durand 2013). Similar to the short flexible strand described by Lara et al. (2012), the findings by ThT-assay on purified aggregates in **manuscript 1** revealed a much lower beta-sheet of the pH 3.5 aggregates compared to the fibrils formed at pH 2 (**FIG 3-4 A and FIG 3-5 E**). By Nicolai and Durand (2013) it was mentioned, that the initial aggregation of intact proteins or the electrostatic interactions inhibited formation of semi-flexible fibrils and therefore flexible short strands might occur. Indeed, measurements of the aggregate building blocks by SEC revealed a much lower hydrolysis kinetics at pH 3.5 (**FIG 3-2**) and measurements by zeta-sizer a decreased zeta-potential (**FIG 3-4 C)** compared to pH 2 fibrils. Investigations of Ramshini et al. (2011) on the protein yeast hexokinase-B (55 kDa) revealed that this flexible strands indeed have the ability to bind ThT (but weaker as semiflexible fibrils), and have a significant amount of beta-sheets structure (analysed with far-UV CD and X-ray fibre diffraction), which is parallel to the findings illustrated in **manuscript 1** by ThT-assay (**FIG 3-4 A)** and by FTIR (**FIG 3-5 E)** for the

worm-like aggregates found at pH 3.5. They suggested that the flexible aggregates have the germ of amyloid structure, but that the large size of the building blocks prevents them from acquiring in an ordered and regular cross-beta-sheet structure typical of real amyloid fibrils (Ramshini et al. 2011). Investigation with electron paramagnetic resonance (EPR) of the pH 3.5 morphologies by Lux et al. (2020b) revealed a "pearl chain structure with centipedes' properties". The pearls are the intermolecular beta-sheet connected BLG molecules, while the centipedes are the C- or N terminal protein strands protrude out of this chain. These explains many of the differences between pH 2 and pH 3.5 aggregates made in this thesis, not only regarding the structure, but also the resulting aggregation kinetics (**manuscript 2 and 3**), adsorption behaviour and stability against process influences (**manuscript 3 and 4**).

7.3.3. Differences in aggregation kinetics at pH 2 and pH 3.5

The formation of pH 2 semiflexible fibrils and its classification in lag- nucleus and termination phase has already been described in detail in **chapter 2.2.3.** The results provided in **manuscript 2 and 3** have given new insights into the interactions between relevant influencing factors in the low temperature range, the dependence of the aggregation kinetics of building blocks and, above all, the detailed comparison of the formation of pH 2 fibrils with the aggregation behaviour of worm-like aggregates formed at pH 3.5.

It was found that the essential threshold temperature for fibril formation is > 70 °C (**FIG 4-4**), which is the denaturation temperature of BLG (Loveday 2016; Keppler et al. 2014). It was hypothesized that this threshold can be reduced by further process factors (**hypothesis 3**). In fact, no significant reducing (or increasing) effect could be detected by varying protein concentration, ion concentration, stirring speed or pH value (**TAB 4-3**). Although parameters such as pH value led to a reduction in denaturation temperature (**TAB 4-4**), this only increased the aggregation kinetics at > 72.5 °C (**FIG 4-4 G and H**).

Alcohol induced effect on protein nativity, which led to aggregation < 70 °C were mentioned before (Kayser et al. 2020; Gosal et al. 2004). However, the resulting morphologies were worm-like and consisted of unhydrolyzed BLG (Kayser et al. 2020). Since the morphology is determined by the size of the building blocks (**chapter 7.3.1**), among other things, a more semi-flexible and amyloid germ structure under the influence of alcohol and lower temperatures could be possible if the hydrolysed material is provided in advance. However, alcohol-induced aggregation is extremely fast (e.g. < 0.5 h at 30 °C and 30 vol% ethanol/TFE) (Kayser et al. 2020; Yamaguchi et al. 2006; Schmittschmitt and Scholtz 2003), while hydrophobic interactions—which also determine the stability of intermolecular beta-sheets—are reduced in

the case of apolar solvents (Nikolaidis et al. 2017). Therefore, an orderly stacking of the building blocks to an amyloid cross beta-sheet structure with the help of alcohol should be considered critically.

As described in **chapter 2.1.2**, the mechanical energy input can also lead to a denaturation of proteins and therefore to the reduction of the threshold of fibril formation, which was taken up in **hypothesis 3**. In **manuscript 3** an additional loading of the protein was achieved by agitation of glass beads and induce additional mechanical stress by shear, impact and rolling of the beads against each other (Schrader et al. 2019). It was found that the aggregation kinetics at a temperature of ~70 °C is increased compared to a moderately stirred system at 72.5 °C (**FIG 5-4 vs. FIG 4-2 C**). However, the assurance of a constant temperature was limited due to the heating system used for the agitation experiments.

However, there is an important indication that the increased aggregation kinetic is not based on a mechanical denaturation of the protein. Aggregation kinetics studies on the formation of worm-like aggregates at pH 3.5 showed that their formation depends on temperature as well as for the pH 2 fibrils (**FIG 7-2 A**), although no hydrolysis is necessary for the formation of these morphologies (**manuscript 1**). It was shown that the aggregation kinetics at pH 3.5 were completely independent of the size of the beads or the shaking speed, or even when there were no beads or shaking. (**FIG 5-4**). Since it is to be expected that at pH 3.5 the protein is exposed to the same forces as at pH 2, it can be deduced that the stress on the protein at pH 2 is not a denaturation effect, but rather one that influences the nucleation of the fibril building blocks.

At the same time, the comparison of the aggregation kinetics of pH 2 fibrils and pH 3.5 aggregates indicates that this nucleation-accelerating effect through mechanical energy input by agitation with beads or stirring (**manuscript 2 and 3**) may not be transferred on the worm-like aggregates (**manuscript 3 and FIG 7-2 C**). This leads to the conclusion that 1st the mechanical stress only benefits the formation kinetics of amyloid nuclei and 2nd confirms that worm-like aggregates at pH 3.5 do not have an amyloid germ. It remains to be investigated whether mechanical stress may increase the aggregation kinetics of worm-like aggregates from peptides, such as those found at pH 2 and higher protein or salt concentration.

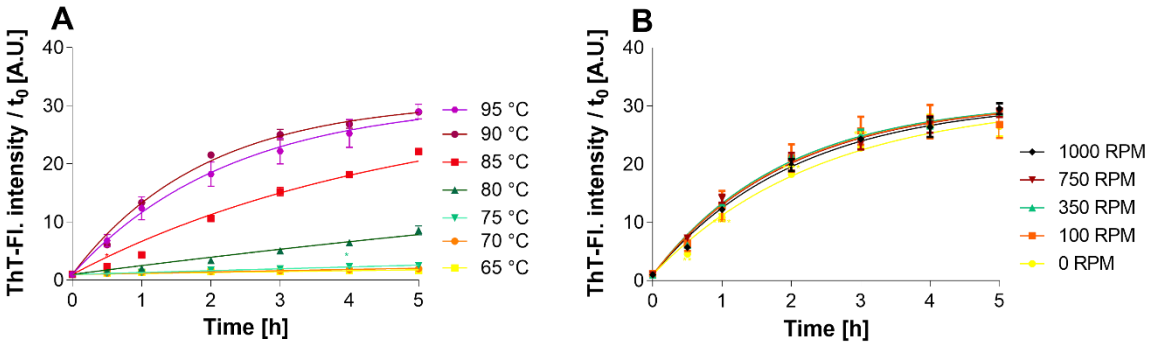

FIG 7-2 Increase in ThT-Flourescence intensity (normalized) in a pH 3.5 BLG-solution using different temperatures (A) or different stirring velocities (B). Other process parameters (protein concentration, ion concentration, used stirring bar and glass container), were the same as used in manuscript 1 and 2 (Adapted from: Anika Ziemer, 2020).

7.3.4. Differences in stability of fibrils and worm-like aggregates

As discussed in **chapter 7.1.2** the structure of pH 2 fibrils is compact, semiflexible and stabilised by hydrogen bonds and steric zipper spines, while structures at pH 3.5 connected by intermolecular beta-sheets, which creates loose and flexible characteristics, but also a short morphology. This leads to different stability properties during exposition to different processes such as ultrafiltration (**manuscript 1**), freeze-drying (**manuscript 1**), stirring (**manuscript 2**), glass beads (**manuscript 3**), hydrophobic surfaces (**manuscript 3**), oil phase (**manuscript 4**), high pressure homogenization (**manuscript 4**), rotor-stator dispersion (**manuscript 4**) or ultrasound (**manuscript 4**). An overview of made observations is listed in **TAB 7-1** supplemented with findings from the literature. The processing of semi-flexible fibrils for common industrially relevant processes (high pressure homogenization, rotor-stator dispersion, ultrasound) has already been applied by different working groups (Serfert et al. 2014; Jung et al. 2010; Oboroceanu et al. 2011; Rogers et al. 2005; Mantovani et al. 2018). However, the processing of worm-like structures has only been described very incompletely (Mudgal et al. 2011b; Koo et al. 2018) and never for amyloid-like structures formed at pH 3.5.

TAB 7-1 Overview of observations made in this thesis and described in literature on influences of mechanical processing on semiflexible amyloid fibrils and worm-like flexible aggregations.

Observation of destructive effect

Process	Semiflexible fibrils	Worm-like aggregates	Reference
Ultrafiltration	Fragmentation	No effect	**Manuscript 1** (*supporting material*)
Lyophilisation	Clusters Fragmentation[a]	Fragmentation to spherical pieces Increased thickening function[b] No effect (pH 2, 80 mM $CaCl_2$ curly fibrils)[a]	**Manuscript 1** (*supporting material*) [a](Loveday et al. 2012) [b](Mudgal et al. 2011b)
Stirring	No effect Secondary nucleation[a]	No effect	**Manuscript 2;** [a](Bolder et al. 2007)
Agitation with glass beads	Fragmentation	Fragmentation to spherical pieces, adsorbance and precipitation	**Manuscript 3**
Agitation with hydrophobic surfaces	Fragmentation	no effect, adsorbance	**Manuscript 3**
Oil	Increased fragmentation at low shear stress.	Moderate fragmentation during shear and sonication	**Manuscript 4**
High pressure homogenization/ micro fluidisation	Strong fragmentation[a]	Fragmentation to spherical pieces, Low effect of flexible strands (pH 2 >5% BLG)[b]	**Manuscript 4** (*supporting material*); [a](Serfert et al. 2014; Jung et al. 2010; Jung and Mezzenga 2010; Oboroceanu et al. 2011; Oboroceanu et al. 2014) [b](Koo et al. 2018)
Rotor stator dispersion	Fragmentation[a] Low effect at 5000 rpm[b]	No effect	**Manuscript 4;** [a](Serfert et al. 2014; Uttinger et al. 2020; Oboroceanu et al. 2014) [b](Mantovani et al. 2018)
Ultrasound	Strong Fragmentation[a]	Fragmentation	**Manuscript 4** [a](Mantovani et al. 2018)
Pressure	Dissociation (lysozyme fibril) at 4500 bar		(Shah et al. 2012)
Elongational flow	Fragmentation		(Kroes-Nijboer et al. 2010)
Shear in rheometer	Small effects on length distribution ($200s^{-1}$)[a] Shortens of fibrils (337 s^{-1}; 505 s^{-1} and 673 s^{-1})[b]		[a](Akkermans et al. 2006) [b](Akkermans et al. 2008a)
Dialysis	No effect		(Jung et al. 2010)
Foaming	Fragmentation[a] No effect of fibril length, but on fibril thickness[b]		[a](**Lux et al. 2020c**) [b](Oboroceanu et al. 2014)

When different observations were described, the link to the corresponding reference is marked (a, b)

The comparison of the studies shown here and observations from the literature (**TAB 7-1**) demonstrates that stressing of straight or worm-like structures is associated by their shortening to a certain minimum length. Methods used in this work have revealed a minimum length of 6 – 33 nm (straight) and 7 – 15 nm (worm-like).

So far, the decrease in ThT FL or intermolecular beta-sheets by FTIR has not been described for one of them here (**manuscript 1 and 4**) or in literature. This reveals, that the aggregate structures cannot be reduced below the beta-sheet stack length of 4 beta-sheets (Krebs et al. 2005), when implicate mechanical stress. Taking into account the maximum distance of 12 Å (0.1 nm) between the beta-sheets (Sunde et al. 1997), only a decrease of the fibril length to below 4.8 nm would lead to a loss of ThT-fluorescence. This constancy of the minimum stack length is also given if the original filamentous morphology is manipulated by lyophilisation (**manuscript 1**) or by changing the pH value (**FIG 7-3**). Although the stability of compact fibrillar and loosely packed worm-like structures was thought to be different (**hypothesis 5**), they are very similar in this specific case. Although a large similarity between pH 2 and pH 3.5 aggregates can be found here, it was shown that the flexible morphologies are not shortened in shear flow (rotor-stator, ultrafiltration), but can be reduced in higher extent by other forms of stress, such as freeze-drying (**manuscript 1**) and cavitation (ultrasound treatment, micro fluidisation) (**manuscript 4**). It was mentioned that the process lability of worm-like structures formed at different process condition (e.g., pH 2 but > 7 wt% protein or addition of 80 mM $CaCl_2$) might also be different (Koo et al. 2018; Loveday et al. 2012) . However, as the length distribution of the aggregates affects their functionality (Oboroceanu et al. 2014; Jung et al. 2010; Koo et al. 2018), the optimal application of processing should be discussed (**chapter 7.5**).

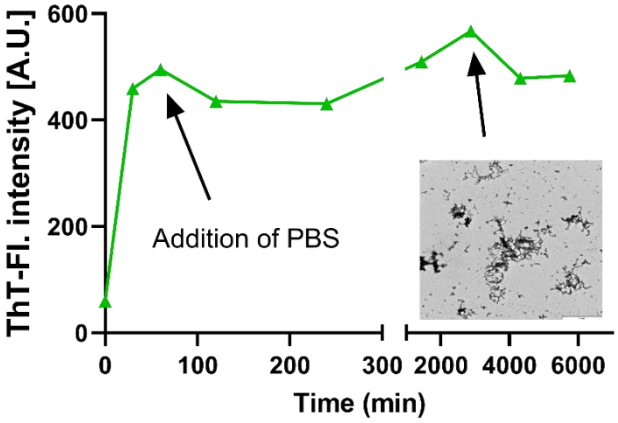

FIG 7-3 Thioflavin-T fluorescence and fibril morphology after adjustment of pH value to 7 by addition of phosphate buffered saline (PBS). Green line shows the ThT-Flourescence intensity [A.U] in dependency of time. Transmission electron microscopy images were obtained after 2 days of incubation (Investigations by Bisher Eymsh, internal communication).

7.3.5. Concluding remarks

The findings on the differences between pH 2 fibrils and pH 3.5 worm-like aggregates concerning of structure, polydispersity, aggregation kinetics and process stability can be summarized as followed: At pH 2 and 90 °C a polydisperse system of rigid and compact fibrils as well as non-aggregated material is formed. The aggregation kinetics depends on mechanical factors and the temperature-related hydrolysis and assembling of the building blocks. When introduced into industrial processes, fractionation and thus a change in functionality can be expected. Worm-like aggregates, as they are formed at pH 3.5, aggregate from BLG monomers depending on the temperature. This flexible BLG concentration seems to be connected by intermolecular beta-sheets and to be independent of shear flow. Therefore, it would be possible to use shear stress during processing, if intrinsically attacking forces such as cavitation or freeze-drying are avoided.

7.4. Possibility of spontaneously amyloid(-like) aggregation during the food's lifetime

Based on the previous findings and the discussion in **chapter 7.3**, the question can now be discussed whether accidental amyloid(-like) aggregate formation can occur during food processing. This discussion is currently focused on the whey protein BLG but could also be applied to many other proteins which aggregate amyloidly under similar conditions (**chapter 2.2.1**). The answer to this question is particularly relevant with regard to food safety (toxicity of amyloid structures, altered nutritional value, or allergic reactions) and the altered technological properties. Because of the immense differences in the process parameters, especially with respect to build-up and degradation factors, a distinction is made between the stages of the food processing/use chain: production, storage and consumption. The investigations of this thesis focused on the processing of whey protein during an emulsification process. This process can be found in industrial processing during the homogenization of milk or when whey protein is used as an emulsifier. In order not to exclude any hypothetical possibilities, the conditions of further processes are also included in the following discussion.

7.4.1. Amyloid(-like) aggregation during processing

During processing, the presence of high temperatures (Guyomarc'h 2006; Chandrapala et al. 2015; Kelly et al. 2002; Mokoonlall et al. 2016; Oldfield et al. 2005; Singh 2004), pressures (Hayes et al. 2005; Kelly et al. 2002), shear forces (Brantley et al. 2002; Mokoonlall et al. 2016; Quevedo et al. 2020) and interfaces (Novalin et al. 2005) as well as the presence of different

proteins (Mokoonlall et al. 2016; Oldfield et al. 2005), ions (Affsprung and Gehrke 1956) or proton concentrations (Guyomarc'h 2006; Chandrapala et al. 2015; Grunwald and Petz 2003; Singh 2004) must be expected. The conditions for the formation of an amyloid structure or an amyloid germ were estimated in this work to be > 70 °C and a pH value of < 3.0 (**manuscript 2**). A further decisive factor is the time required for hydrolysis, nucleation and assembling. For amyloid-like (ThT-binding) structures, the pH value ranging up to 7 is possible and no hydrolysis, but growth time for the aggregates is needed (**chapter 7.3.3**).

The first limiting factor that probably prevents the formation of amyloid aggregates is the extremely acidic pH value (< 3.0), which is not used for sensory reasons, but also to protect the machines from corrosion (Podobaev and Avdeev 2001). Even pH values of 3.5 are very rare (acid whey minimum is 3.55 (Gami et al. 2016)). This means that even if the temperature is maintained at > 70 °C for some time and increased shear forces or surfaces could accelerate nucleation, the pH in the solution would not be sufficient enough to cause adequate hydrolysis as a prerequisite for the amyloid structure. However, as the proton activity (Iuchi et al. 2009) and therefore the pH value in the micro environment of hydrophobic interfaces can differ from solution conditions, the hydrolysation of BLG and a subsequent amyloid association by nucleation supporting effects is conceivable, anyway.

As mentioned in intern an unpublished work (Schild, 2019), the kind of acid such as sulphuric acid or formic acid—which are both uncommon acids in food—is also of high relevance for fibril formation. However, the formation of amyloid-like worm-like structures at pH 3.5 or pH 7 from unhydrolysed BLG would be conceivable (**Chapter 7.3.2**), taking into account the presence of process temperatures above 70 °C for a rather longer time, because the aggregation of these structures cannot be accelerated by shearing or interfaces (**manuscript 3**). Due to the shear forces during the process, the formation of very short amyloid structures is generally to be expected (**manuscript 4**). As the fibril formation from BLG during processing might be rare, other milk proteins such as alpha$_{s2}$-caseins, have milder fibril formation conditions (e.g. 37 °C at pH 6.5) (Thorn et al. 2008; Thorn et al. 2005; Pan and Zhong 2015) and their assembling to amyloid fibrils could be therefore of high relevance.

7.4.2. Amyloid(-like) aggregation during storage

If it were hypothetically assumed that an amyloid germ would be formed during the processing of a BLG-containing food, due to extremely acidic conditions (e.g., at charged interfaces) combined with high temperatures and shear effects, it could be expected that in subsequent storage, there would be sufficient time for this germ to grow into a fibril. Nevertheless, the first

limitation for this process would be the adequate availability of peptide building blocks (**manuscript 1 and 2**). To improve probiotic effects (Mccomas and Gilliland 2003) or to reduce allergenic potential (Kim et al. 2018), however, these could have been added to the product before. Further, there is a second barrier, which is the lack of acidic pH value (**manuscript 2**)—causing the orderly assembly due to electrostatic interactions (**manuscript 1**)—apart from the disturbing (**manuscript 2**) high neutralizing ion density in the product (Affsprung and Gehrke 1956). In addition, the product is stored at low temperatures (Mokoonlall et al. 2016), which in turn would keep the possible aggregation kinetics extremely low (**manuscript 2**). It would be theoretically possible that worm-like aggregates are formed due to the milder conditions (**see Chapter 7.3**) and even contribute to a desired product property. Long storage periods, coupled with moderate temperatures, occur during the incubation and gelation phase of yoghurt (Lucey and Singh 1997; Sodini et al. 2006; Karam et al. 2013), but also a pH value range of 6.7 to 4.6. Therefore, the desired gel-forming properties of casein may be supported by gel-forming properties of amyloid like BLG aggregates (Nicolai et al. 2011; Mudgal et al. 2009).

7.4.3. Amyloid(-like) aggregation after oral ingestion

Regarding to findings of the present work, a potential phase in which whey proteins could undergo amyloid aggregation would be after oral consumption. The gastric juice is acidified to a pH of 1 to 4 by the presence of HCl. At the same time, proteolytic cleaving enzymes present help to form potential amyloid building blocks (Deng et al. 2020). The stomach motor activity that takes place allows a comparison with moderate stirring or shaking (**manuscript 2 and 3**). According to the evidence in **manuscript 2**, the prevailing temperature of 37 °C would only lead to very low aggregation kinetics. However, this could potentially be accelerated by the presence of alcohol (Kayser et al. 2020), so that the first worm-like (amyloid-like) aggregates (**Chapter 7.3.3**) could already have formed after 30 min, if whey protein and a subsequent sufficient amount of ethanol-containing drink were dosed.

7.4.4. Concluding remarks

It can be concluded that the formation of “true” amyloid structures from BLG during food production is limited due to the lack of extreme conditions such as pH (adjusted by non-food acids), low ion concentration and high temperatures in the solution, combined over a long period of time. However, because of the nucleation supporting effects of interfaces, the formation of small amounts of amyloids is conceivable. Furthermore, the formation of worm-like amyloid-like aggregates would be possible, due to milder circumstances. In this case,

monitoring for amyloid structures in relevant processes using experimental setups would be of relevance.

7.5. Which form of aggregation is more favourable for the food application?

Results have shown that physico-chemical properties, but also aggregations kinetics and stability of pH 2 fibrils and pH 3.5 aggregates differ. The findings presented in this thesis give the opportunity to evaluate their application and functionality in processed food under new aspects.

7.5.1. Application of amyloid and worm-like aggregates

As already described in **chapter 2.2.1**, there are numerous applications for fibrils in the field of new materials or food technology. Here, the high aspect ratio of the protein filaments plays an important role (Cao and Mezzenga 2019). As worm-like aggregates do not share this elementary property (**FIG 3-1**), it is to be expected that fibrils and worm-like aggregates can differ massively in their functionality and therefore the suitable areas of application. In addition to these morphological differences, it has been shown that there are also major differences in the physico-chemical properties (**chapter 7.3.2**). Fibrils seem to have very hydrophobic areas, which can ensure a strong attachment to oil-water interfaces (**FIG 3-4**). However, Lux et al. (2020a) and other working groups (Jung et al. 2010; Rühs et al. 2013; Jordens et al. 2014) have also shown that the improved stabilization of hydrophobic interfaces is achieved by the interaction of unaggregated, rapidly diffusing peptide material and the interface viscoelasticity increasing stiffer fibrils. This degree of synergistic effect is not expected for the worm-like aggregates due to a missing or very small amount of peptides (**manuscript 1**). On the other hand, improved hydrophobic properties of the worm-like aggregates could be demonstrated in comparison to the fibrils using Nile red-assays (**FIG 3-4 B**). In combination with the lower zeta-potential (**FIG 3-4 C**) and the increased flexibility (**TAB 3-1**), an increased attachment at interfaces can be assumed for these structures, as it was also demonstrated in **manuscript 3**. Assuming that the worm-like structures in this work and the flexible morphologies at pH 3.35 (Mudgal et al. 2009; Mudgal et al. 2011b; Mudgal et al. 2011c; Mudgal et al. 2011a) could show similar behaviour, the formation of so-called microgels (Mudgal et al. 2011b) at interfaces could be deduced from smaller inter-particle distances (compared to pH 2 fibrils). Observations of ultrasonic expansion of pH 3.5 aggregates at higher sound levels and 18 % oil interestingly showed the formation of a pasty emulsion, which was not found for the fibril solution (**data not shown**), although the aggregates were strongly fragmented (**Manuscript 4**). Due to the intact primary structure of the pH 3.5 aggregates and the lower electrostatic repulsion between the

molecules, there could be a higher degree to intermolecular cross-linking, which encloses the oil droplets and thus leads to increased stability. So far, however, there is still a lack of comprehensive studies in which the functionality of pH 3.5 aggregates as emulsifiers were evaluated. Due to the observation, that the hydrophobicity of BLG aggregates is increased, their use in oleogels could also be of relevance.

7.5.2. Differences in production cost of fibrils and worm-like aggregates

Product costs are the sum of invested material, energy and time. The use of BLG fibrils offers the possibility to achieve improved functional properties (e.g. gel or foam stability) (Peng et al. 2017; Mudgal et al. 2009) with less use of the rather demanded protein (Elzoghby et al. 2015; Cao and Mezzenga 2019). At the same time, the synthesis of fibrils is only possible by using high temperatures over a fairly long period of time (**manuscript 2**). The results of this work show the same energy-intensive relationship for worm-like aggregates (**manuscript 1 and 3**). However, further literature and investigations showed that fast and cold aggregation to worm-like structures can be achieved by using alcohol (Yamaguchi et al. 2006; Schmittschmitt and Scholtz 2003; Kayser et al. 2020). Even so, it is still unclear whether the physico-chemical properties can be preserved after removal of the alcohol, or if the same properties as those of non-alcoholic amyloid aggregates can be achieved. Investigations for this are still pending. In the case of pH 2 fibrils, a seeding effect could be used to accelerate the synthesis of the fibrils, in which the initial provision of activated nuclei leads directly to fibril growth without a storage phase (Loveday et al. 2012; Mahul-Mellier et al. 2015; Morozova-Roche et al. 2000; Krebs et al. 2000). This time saving effect probably plays a role in the stirring and use of glass particles in the present work (**manuscript 2 and 3)**. However, it is still necessary to generate the building blocks by hydrolysis at high temperatures (**manuscript 1 and 2**). So far, no fibril assembly of BLG peptide building blocks from enzymatic proteolysis has been described.

7.5.3. Key challenges of the process

The investigations of the present work have demonstrated the high process lability of the amyloid and amyloid-like structures (**see chapter 7.3.4**). However, other studies have shown that despite the process and the resulting fragmentation of aggregates, the advantageous properties of the amyloid or amyloid-like structures can still be obtained (Serfert et al. 2014; Arosio et al. 2012; Gao et al. 2017; Mantovani et al. 2017). Even so, if one considers the entire chain of fibril production, storage and product use, certain challenges can be identified: The use of high acidity during production can contribute to severe damage to production equipment (Podobaev and Avdeev 2001). An important point is therefore stabilisation of the fibrils, even

if the pH value is raised to sensory acceptable parameters (**FIG 7-3**) (Akkermans et al. 2008b; Wu et al. 2016; Loveday et al. 2011). Various methods to increase stability have already been investigated (Loveday et al. 2011; Hettiarachchi et al. 2016; Mudgal et al. 2011b). However, it can be assumed that their use in a complex food system will bring further challenges. A further point concerns the stabilization of the fibrils for storage. For hygienic, but also logistical reasons, storage of the amyloid(-like) aggregates in solution is not recommended. However, the (freeze) drying of the aggregates leads to a very strong fragmentation (**manuscript 1**), which is reflected in various modifications of the physico-chemical properties (**FIG 3-4 and FIG 3-5**) and an observable decrease in viscosity (Mudgal et al. 2011b; Loveday et al. 2012).

7.5.4. Concluding remarks

For many material-related applications, fibrils may be more suitable due to their specific morphology. For food, however, the amyloid-like aggregates might be more attractive due to their higher stability against shear-forces and their formation at higher pH values. At the same time, their very fast and energy-efficient synthesis could be realized by adding ethanol. The effect of alcohol on fibril formation has not been clarified, as a hydrolysis step is required prior to aggregation. For worm-like aggregates, however, the actual evaluation for applications that go beyond gel formation is missing. Therefore, it is difficult to draw a clear conclusion.

7.6. Outlook

Based on the presented findings, the following research questions can be raised for future investigations:

Regarding **hypothesis 1**, it should be investigated whether peptides at pH 3.5 also aggregate in a worm-like morphology and whether these aggregates have altered physico-chemical properties compared to fibrils at pH 2 and worm-like aggregates produced from non-hydrolysed BLG. It could be possible that worm-like aggregates transformed to straight fibrils, when a higher degree of hydrolysis occur over time (Keppler et al. 2019).

Regarding **hypothesis 2,** the exact structure of worm-like aggregates at pH 3.5 is not clear so far. With the help of techniques such as cryo-electron microscopy and solid-state nuclear magnetic resonance, further clarification of the exact structure of aggregates could be validated in order to be able to classify them more clearly as amyloid, amyloid-like or amorphous aggregates.

Regarding **hypothesis 3**, it was found that temperature determines the assembly kinetics of peptide building blocks. The experiments here were extended to a duration of 5 h. By extending the test duration to 24 to 72 h, influences on growth and termination phase and thus maximum fibril yield could be investigated. Since a solvent-supported, cold assembly of unhydrolyzed BLG has been described, the influence of solvents on the assembly kinetics of peptide building blocks should also be investigated to close this knowledge gap.

Regarding **hypothesis 4,** the parameter of energy input and the resulting partitioning into stressing by shear, impact and rolling should be investigated in more detail. For this purpose, a computational fluid dynamic (CFD) simulation can be used, as already applied in manuscript 2. In addition, a further variance of surface chemistry by other forms of carboxylic acids would be interesting to further investigate the influence of interface parameters for the optimal formation but also the lowest possible fragmentation of fibrils and worm-like aggregates.

Regarding **hypothesis 5,** a shortening of the aggregate length, but no reduction of the ThT-reactive amyloid components, as well as of the intermolecular beta sheets detected by FTIR, could be achieved. Investigations at even higher energy inputs over an even longer period of time or with the addition of low concentrations of dissociative additives (e.g. guanidine HCl and DTT) could provide insights into the energies that are practically necessary to initiate the dissociation of amyloid structures.

Finally, this work offers interesting new insights into the comparison of amyloid fibrils and amyloid-like aggregates with respect to structure, physico-chemical properties, aggregation kinetics and process stability. These findings should now be transferred to food (or material) applications by means of further experimental setups.

7.7. References

Affsprung, H.E., & Gehrke, C.W. (1956). Electrochemical Measurements on Milk with Cation and Anion Sensitive Membrane Electrodes. *J Dairy Sci*, 39(4), 345–55. http://dx.doi.org/10.3168/jds.S0022-0302(56)94759-2.

Akkermans, C., van der Goot, A.J., Venema, P., van der Linden, E., & Boom, R.M. (2008a). Formation of fibrillar whey protein aggregates. *Food Hydrocolloids*, 22(7), 1315–25. http://dx.doi.org/10.1016/j.foodhyd.2007.07.001.

Akkermans, C., van der Goot, A.J., Venema, P., van der Linden, E., & Boom, R.M. (2008b). Properties of protein fibrils in whey protein isolate solutions. *International Dairy Journal*, 18(10-11), 1034–42. http://dx.doi.org/10.1016/j.idairyj.2008.05.006.

Akkermans, C., Venema, P., Rogers, S.S., van der Goot, A.J., Boom, R.M., & van der Linden, E. (2006). Shear Pulses Nucleate Fibril Aggregation. *Food Biophysics*, 1(3), 144–50. http://dx.doi.org/10.1007/s11483-006-9012-5.

Akkermans, C., Venema, P., van der Goot, A.J., Gruppen, H., Bakx, E.J., & Boom, R.M., et al. (2008c). Peptides are building blocks of heat-induced fibrillar protein aggregates of beta-lactoglobulin formed at pH 2. *Biomacromolecules*, 9(5), 1474–9. http://dx.doi.org/10.1021/bm7014224.

Arosio, P., Beeg, M., Nicoud, L., & Morbidelli, M. (2012). Time evolution of amyloid fibril length distribution described by a population balance model. *Chemical Engineering Science*, 78, 21–32. http://dx.doi.org/10.1016/j.ces.2012.04.031.

Bolder, S.G., Sagis, L.M.C., Venema, P., & van der Linden, E. (2007). Effect of stirring and seeding on whey protein fibril formation. *J Agric Food Chem*, 55(14), 5661–9. http://dx.doi.org/10.1021/jf063351r.

Brantley JD, Hurwitz MF, Geibel SA, Mahmoud Reyad JC. Shear seperation method and system. 21 p.; November 12, 2002.

Cao, Y., & Mezzenga, R. (2019). Food protein amyloid fibrils. *Adv Colloid Interface Sci*, 269, 334–56. http://dx.doi.org/10.1016/j.cis.2019.05.002.

Carulla, N., Caddy, G.L., Hall, D.R., Zurdo, J., Gairí, M., & Feliz, M., et al. (2005). Molecular recycling within amyloid fibrils. *Nature*, 436(7050), 554–8. http://dx.doi.org/10.1038/nature03986.

Chandrapala, J., Duke, M.C., Gray, S.R., Zisu, B., Weeks, M., & Palmer, M., et al. (2015). Properties of acid whey as a function of pH and temperature. *J Dairy Sci*, 98(7), 4352–63. http://dx.doi.org/10.3168/jds.2015-9435.

Dave, A.C., Loveday, S.M., Anema, S.G., Jameson, G.B., & Singh, H. (2014). Glycation as a Tool To Probe the Mechanism of β-Lactoglobulin Nanofibril Self-Assembly. *J. Agric. Food Chem.*, 62(14), 3269–78. http://dx.doi.org/10.1021/jf405441g.

Deng, R., Janssen, A.E.M., Vergeldt, F.J., van As, H., Graaf, C. de, & Mars, M., et al. (2020). Exploring in vitro gastric digestion of whey protein by time-domain nuclear magnetic resonance and magnetic resonance imaging. *Food Hydrocolloids*, 99, 105348. http://dx.doi.org/10.1016/j.foodhyd.2019.105348.

Elzoghby, A.O., Elgohary, M.M., & Kamel, N.M. (2015). Implications of protein- and Peptide-based nanoparticles as potential vehicles for anticancer drugs. *Adv Protein Chem Struct Biol*, 98, 169–221. http://dx.doi.org/10.1016/bs.apcsb.2014.12.002.

Gami S, Godwin G, Czymmek K, Ganoe K, Ketterings Q. Acid Whey pH and Nutrient Content; 2016.

Gao, Z., Zhao, J., Huang, Y., Yao, X., Zhang, K., & Fang, Y., et al. (2017). Edible Pickering emulsion stabilized by protein fibrils. Part 1. *LWT - Food Science and Technology*, 76, 1–8. http://dx.doi.org/10.1016/j.lwt.2016.10.038.

Gosal, W.S., Clark, A.H., & Ross-Murphy, S.B. (2004). Fibrillar beta-lactoglobulin gels. *Biomacromolecules*, 5(6), 2430–8. http://dx.doi.org/10.1021/bm0496615.

Grunwald, L., & Petz, M. (2003). Food processing effects on residues. *Analytica Chimica Acta*, 483(1-2), 73–9. http://dx.doi.org/10.1016/S0003-2670(02)01405-8.

Guyomarc'h, F. (2006). Formation of heat-induced protein aggregates in milk as a means to recover the whey protein fraction in cheese manufacture, and potential of heat-treating milk at alkaline pH values in order to keep its rennet coagulation properties. A review. *Lait*, 86(1), 1–20. http://dx.doi.org/10.1051/lait:2005046.

Hayes, M.G., Fox, P.F., & Kelly, A.L. (2005). Potential applications of high pressure homogenisation in processing of liquid milk. *J Dairy Res*, 72(1), 25–33. http://dx.doi.org/10.1017/s0022029904000524.

Hettiarachchi, C.A., Melton, L.D., Gerrard, J.A., & Loveday, S.M. (2012). Formation of β-lactoglobulin nanofibrils by microwave heating gives a peptide composition different from conventional heating. *Biomacromolecules*, 13(9), 2868–80. http://dx.doi.org/10.1021/bm300896r.

Hettiarachchi, C.A., Melton, L.D., McGillivray, D.J., Loveday, S.M., Gerrard, J.A., & Williams, M.A.K. (2016). β-Lactoglobulin nanofibrils can be assembled into nanotapes via site-specific interactions with pectin. *Soft Matter*, 12(3), 756–68. http://dx.doi.org/10.1039/c5sm01530h.

Iuchi, S., Chen, H., Paesani, F., & Voth, G.A. (2009). Hydrated excess proton at water-hydrophobic interfaces. *J Phys Chem B*, 113(13), 4017–30. http://dx.doi.org/10.1021/jp805304j.

Jordens, S., Rühs, P.A., Sieber, C., Isa, L., Fischer, P., & Mezzenga, R. (2014). Bridging the gap between the nanostructural organization and macroscopic interfacial rheology of amyloid fibrils at liquid interfaces. *Langmuir*, 30(33), 10090–7. http://dx.doi.org/10.1021/la5020658.

Jung, J.-M., Gunes, D.Z., & Mezzenga, R. (2010). Interfacial activity and interfacial shear rheology of native β-lactoglobulin monomers and their heat-induced fibres. *Langmuir*, 26(19), 15366–75. http://dx.doi.org/10.1021/la102721m.

Jung, J.-M., & Mezzenga, R. (2010). Liquid Crystalline Phase Behavior of Protein Fibres in Water. *Langmuir*, 26(1), 504–14. http://dx.doi.org/10.1021/la9021432.

Jung, J.-M., Savin, G., Pouzot, M., Schmitt, C., & Mezzenga, R. (2008). Structure of heat-induced beta-lactoglobulin aggregates and their complexes with sodium-dodecyl sulfate. *Biomacromolecules*, 9(9), 2477–86. http://dx.doi.org/10.1021/bm800502j.

Karam, M.C., Gaiani, C., Hosri, C., Burgain, J., & Scher, J. (2013). Effect of dairy powders fortification on yogurt textural and sensorial properties. *J Dairy Res*, 80(4), 400–9. http://dx.doi.org/10.1017/S0022029913000514.

Kayser, J.J., Arnold, P., Steffen-Heins, A., Schwarz, K., & Keppler, J.K. (2020). Functional ethanol-induced fibrils. *Journal of Food Engineering*(270), 109764. http://dx.doi.org/10.1016/j.jfoodeng.2019.109764.

Kelly, J., Kelly, P.M., & Harrington, D. (2002). Influence of processing variables on the physico-chemical properties of spray dried fat-based milk powders. *Lait*, 82(4), 401–12. http://dx.doi.org/10.1051/lait:2002019.

Keppler, J.K., Heyn, T.R., Meissner, P.M., Schrader, K., & Schwarz, K. (2019). Protein oxidation during temperature-induced amyloid aggregation of beta-lactoglobulin. *Food Chem*, 289, 223–31. http://dx.doi.org/10.1016/j.foodchem.2019.02.114.

Keppler, J.K., Sönnichsen, F.D., Lorenzen, P.-C., & Schwarz, K. (2014). Differences in heat stability and ligand binding among β-lactoglobulin genetic variants A, B and C using (1)H NMR and fluorescence quenching. *Biochim Biophys Acta*, 1844(6), 1083–93. http://dx.doi.org/10.1016/j.bbapap.2014.02.007.

Kim, H., Ahn, S.-I., Jhoo, J.-W., & Kim, G.-Y. (2018). Comparison of Allergic Parameters between Whey Protein Concentrate and Its Hydrolysate in Rat Basophilic Leukemia (RBL)-2H3 Cells. *Korean J Food Sci Anim Resour*, 38(4), 780–93. http://dx.doi.org/10.5851/kosfa.2018.e16.

Koo, C.K.W., Chung, C., Ogren, T., Mutilangi, W., & McClements, D.J. (2018). Extending protein functionality. *Journal of Food Engineering*, 223, 189–96. http://dx.doi.org/10.1016/j.jfoodeng.2017.10.020.

Krebs, M.R., Wilkins, D.K., Chung, E.W., Pitkeathly, M.C., Chamberlain, A.K., & Zurdo, J., et al. (2000). Formation and seeding of amyloid fibrils from wild-type hen lysozyme and a peptide fragment from the beta-domain. *J Mol Biol*, 300(3), 541–9. http://dx.doi.org/10.1006/jmbi.2000.3862.

Krebs, M.R.H., Bromley, E.H.C., & Donald, A.M. (2005). The binding of thioflavin-T to amyloid fibrils. *J Struct Biol*, 149(1), 30–7. http://dx.doi.org/10.1016/j.jsb.2004.08.002.

Kroes-Nijboer, A., Venema, P., Baptist, H., & van der Linden, E. (2010). Fracture of protein fibrils as induced by elongational flow. *Langmuir*, 26(16), 13097–101. http://dx.doi.org/10.1021/la1025262.

Kroes-Nijboer, A., Venema, P., Bouman, J., & van der Linden, E. (2011). Influence of protein hydrolysis on the growth kinetics of β-lg fibrils. *Langmuir*, 27(10), 5753–61. http://dx.doi.org/10.1021/la104797u.

Lara, C., Gourdin-Bertin, S., Adamcik, J., Bolisetty, S., & Mezzenga, R. (2012). Self-assembly of ovalbumin into amyloid and non-amyloid fibrils. *Biomacromolecules*, 13(12), 4213–21. http://dx.doi.org/10.1021/bm301481v.

Loveday, S.M. (2016). β-Lactoglobulin heat denaturation. *International Dairy Journal*, 52, 92–100. http://dx.doi.org/10.1016/j.idairyj.2015.08.001.

Loveday, S.M., Anema, S.G., & Singh, H. (2017). β-Lactoglobulin nanofibrils. *International Dairy Journal*, 67, 35–45. http://dx.doi.org/10.1016/j.idairyj.2016.09.011.

Loveday, S.M., Su, J., Rao, M.A., Anema, S.G., & Singh, H. (2011). Effect of calcium on the morphology and functionality of whey protein nanofibrils. *Biomacromolecules*, 12(10), 3780–8. http://dx.doi.org/10.1021/bm201013b.

Loveday, S.M., Su, J., Rao, M.A., Anema, S.G., & Singh, H. (2012a). Whey protein nanofibrils. *J Agric Food Chem*, 60(20), 5229–36. http://dx.doi.org/10.1021/jf300367k.

Loveday, S.M., Wang, X.L., Rao, M.A., Anema, S.G., Creamer, L.K., & Singh, H. (2010). Tuning the properties of β-lactoglobulin nanofibrils with pH, NaCl and CaCl2. *International Dairy Journal*, 20(9), 571–9. http://dx.doi.org/10.1016/j.idairyj.2010.02.014.

Lucey, J.A., & Singh, H. (1997). Formation and physical properties of acid milk gels. *Food Research International*, 30(7), 529–42. http://dx.doi.org/10.1016/S0963-9969(98)00015-5.

Lux, Jacqueline; Heyn, Timon R.; Kampen, Ingo; Schwarz, Karin; Keppler, Julia K.; Steffen-Heins, Anja (2021a): Amyloid aggregation of spin-labeled β-lactoglobulin. Part I. Influence of spin labeling on amyloid aggregation. In: *Food Hydrocolloids* 112, S. 106178. DOI: 10.1016/j.foodhyd.2020.106178.

Lux, Jacqueline; Azarkh, Mykhailo; Fitzner, Laura; Keppler, Julia K.; Schwarz, Karin; Drescher, Malte; Steffen-Heins, Anja (2021b): Amyloid aggregation of spin-labeled β-lactoglobulin. Part II. Identification of spin-labeled protein and peptide sequences after amyloid aggregation. In: *Food Hydrocolloids* 112, S. 106174. DOI: 10.1016/j.foodhyd.2020.106174.

Mahul-Mellier, A.-L., Vercruysse, F., Maco, B., Ait-Bouziad, N., Roo, M. de, & Muller, D., et al. (2015). Fibril growth and seeding capacity play key roles in α-synuclein-mediated apoptotic cell death. *Cell Death Differ*, 22(12), 2107–22. http://dx.doi.org/10.1038/cdd.2015.79.

Mantovani, R.A., Figueiredo Furtado, G. de, Netto, F.M., & Cunha, R.L. (2018). Assessing the potential of whey protein fibril as emulsifier. *Journal of Food Engineering*, 223, 99–108. http://dx.doi.org/10.1016/j.jfoodeng.2017.12.006.

Mantovani, R.A., Pinheiro, A.C., Vicente, A.A., & Cunha, R.L. (2017). In vitro digestion of oil-in-water emulsions stabilized by whey protein nanofibrils. *Food Res Int*, 99(Pt 1), 790–8. http://dx.doi.org/10.1016/j.foodres.2017.06.049.

Mccomas, K.A., & Gilliland, S.E. (2003). Growth of Probiotic and Traditional Yogurt Cultures in Milk Supplemented with Whey Protein Hydrolysate. *J Food Sci*, 68(6), 2090–5. http://dx.doi.org/10.1111/j.1365-2621.2003.tb07024.x.

Mokoonlall, A., Nöbel, S., & Hinrichs, J. (2016). Post-processing of fermented milk to stirred products. *Trends in Food Science & Technology*, 54, 26–36. http://dx.doi.org/10.1016/j.tifs.2016.05.012.

Morozova-Roche, L.A., Zurdo, J., Spencer, A., Noppe, W., Receveur, V., & Archer, D.B., et al. (2000). Amyloid fibril formation and seeding by wild-type human lysozyme and its

disease-related mutational variants. *J Struct Biol*, 130(2-3), 339–51. http://dx.doi.org/10.1006/jsbi.2000.4264.

Mudgal, P., Daubert, C.R., Clare, D.A., & Foegeding, E.A. (2011a). Effect of disulfide interactions and hydrolysis on the thermal aggregation of β-lactoglobulin. *J Agric Food Chem*, 59(5), 1491–7. http://dx.doi.org/10.1021/jf101893v.

Mudgal, P., Daubert, C.R., & Foegeding, E.A. (2009). Cold-set thickening mechanism of β-lactoglobulin at low pH. *Food Hydrocolloids*, 23(7), 1762–70. http://dx.doi.org/10.1016/j.foodhyd.2009.03.009.

Mudgal, P., Daubert, C.R., & Foegeding, E.A. (2011b). Effects of protein concentration and CaCl2 on cold-set thickening mechanism of β-lactoglobulin at low pH. *International Dairy Journal*, 21(5), 319–26. http://dx.doi.org/10.1016/j.idairyj.2010.11.014.

Mudgal, P., Daubert, C.R., & Foegeding, E.A. (2011c). Kinetic study of β-lactoglobulin thermal aggregation at low pH. *Journal of Food Engineering*, 106(2), 159–65. http://dx.doi.org/10.1016/j.jfoodeng.2011.04.025.

Nicolai, T., Britten, M., & Schmitt, C. (2011). β-Lactoglobulin and WPI aggregates. *Food Hydrocolloids*, 25(8), 1945–62. http://dx.doi.org/10.1016/j.foodhyd.2011.02.006.

Nicolai, T., & Durand, D. (2013). Controlled food protein aggregation for new functionality. *Current Opinion in Colloid & Interface Science*, 18(4), 249–56. http://dx.doi.org/10.1016/j.cocis.2013.03.001.

Nikolaidis, A., Andreadis, M., & Moschakis, T. (2017). Effect of heat, pH, Ultra-sonication and ethanol on the denaturation of whey protein isolate using a newly developed approach in the analysis of difference-UV spectra. *Food Chem*, 232, 425–33. http://dx.doi.org/10.1016/j.foodchem.2017.04.022.

Novalin, S., Neuhaus, W., & Kulbe, K.D. (2005). A new innovative process to produce lactose-reduced skim milk. *J Biotechnol*, 119(2), 212–8. http://dx.doi.org/10.1016/j.jbiotec.2005.03.018.

Oboroceanu, D., Wang, L., Kroes-Nijboer, A., Brodkorb, A., Venema, P., & Magner, E., et al. (2011). The effect of high pressure microfluidization on the structure and length distribution of whey protein fibrils. *International Dairy Journal*, 21(10), 823–30. http://dx.doi.org/10.1016/j.idairyj.2011.03.015.

Oboroceanu, D., Wang, L., Magner, E., & Auty, M.A.E. (2014). Fibrillization of whey proteins improves foaming capacity and foam stability at low protein concentrations. *Journal of Food Engineering*, 121, 102–11. http://dx.doi.org/10.1016/j.jfoodeng.2013.08.023.

Oldfield, D.J., Taylor, M.W., & Singh, H. (2005). Effect of preheating and other process parameters on whey protein reactions during skim milk powder manufacture. *International Dairy Journal*, 15(5), 501–11. http://dx.doi.org/10.1016/j.idairyj.2004.09.004.

O'Nuallain, B., Shivaprasad, S., Kheterpal, I., & Wetzel, R. (2005). Thermodynamics of A beta(1-40) amyloid fibril elongation. *Biochemistry*, 44(38), 12709–18. http://dx.doi.org/10.1021/bi050927h.

Pan, K., & Zhong, Q. (2015). Amyloid-like fibrils formed from intrinsically disordered caseins. *Soft Matter*, 11(29), 5898–904. http://dx.doi.org/10.1039/c5sm01037c.

Peng, D., Yang, J., Li, J., Tang, C., & Li, B. (2017). Foams Stabilized by β-Lactoglobulin Amyloid Fibrils. *J Agric Food Chem*, 65(48), 10658–65. http://dx.doi.org/10.1021/acs.jafc.7b03669.

Podobaev, N.I., & Avdeev, Y.G. (2001). Temperature and Time Effects on the Acid Corrosion of Steel in the Presence of Acetylenic Inhibitors. *Protection of Metals*, 37(6), 529–33. http://dx.doi.org/10.1023/A:1012855211234.

Quevedo, M., Kulozik, U., Karbstein, H.P., & Emin, M.A. (2020). Kinetics of denaturation and aggregation of highly concentrated β-Lactoglobulin under defined thermomechanical treatment. *Journal of Food Engineering*, 274, 109825. http://dx.doi.org/10.1016/j.jfoodeng.2019.109825.

Ramshini, H., Parrini, C., Relini, A., Zampagni, M., Mannini, B., & Pesce, A., et al. (2011). Large proteins have a great tendency to aggregate but a low propensity to form amyloid fibrils. *PLoS ONE*, 6(1), e16075. http://dx.doi.org/10.1371/journal.pone.0016075.

Rogers, S.S., Venema, P., Sagis, L.M.C., van der Linden, E., & Donald, A.M. (2005). Measuring the Length Distribution of a Fibril System. *Macromolecules*, 38(7), 2948–58. http://dx.doi.org/10.1021/ma0474224.

Rühs, P.A., Affolter, C., Windhab, E.J., & Fischer, P. (2013). Shear and dilatational linear and nonlinear subphase controlled interfacial rheology of β-lactoglobulin fibrils and their derivatives. *Journal of Rheology*, 57(3), 1003–22. http://dx.doi.org/10.1122/1.4802051.

Schmittschmitt, J.P., & Scholtz, J.M. (2003). The role of protein stability, solubility, and net charge in amyloid fibril formation. *Protein Sci*, 12(10), 2374–8. http://dx.doi.org/10.1110/ps.03152903.

Schrader, M., Pommerehne, K., Wolf, S., Finke, B., Schilde, C., & Kampen, I., et al. (2019). Design of a CFD-DEM-based method for mechanical stress calculation and its application to glass bead-enhanced cultivations of filamentous Lentzea aerocolonigenes. *Biochemical Engineering Journal*, 148, 116–30. http://dx.doi.org/10.1016/j.bej.2019.04.014.

Serfert, Y., Lamprecht, C., Tan, C.-P., Keppler, J.K., Appel, E., & Rossier-Miranda, F.J., et al. (2014). Characterisation and use of β-lactoglobulin fibrils for microencapsulation of lipophilic ingredients and oxidative stability thereof. *Journal of Food Engineering*, 143, 53–61. http://dx.doi.org/10.1016/j.jfoodeng.2014.06.026.

Shah, B.R., Maeno, A., Matsuo, H., Tachibana, H., & Akasaka, K. (2012). Pressure-accelerated dissociation of amyloid fibrils in wild-type hen lysozyme. *Biophys J*, 102(1), 121–6. http://dx.doi.org/10.1016/j.bpj.2011.10.041.

Singh, H. (2004). Heat stability of milk. *Int J Dairy Tech*, 57(2-3), 111–9. http://dx.doi.org/10.1111/j.1471-0307.2004.00143.x.

Sodini, I., Mattas, J., & Tong, P.S. (2006). Influence of pH and heat treatment of whey on the functional properties of whey protein concentrates in yoghurt. *International Dairy Journal*, 16(12), 1464–9. http://dx.doi.org/10.1016/j.idairyj.2005.03.014.

Sunde, M., Serpell, L.C., Bartlam, M., Fraser, P.E., Pepys, M.B., & Blake, C.C. (1997). Common core structure of amyloid fibrils by synchrotron X-ray diffraction. *J Mol Biol*, 273(3), 729–39. http://dx.doi.org/10.1006/jmbi.1997.1348.

Thorn, D.C., Ecroyd, H., Sunde, M., Poon, S., & Carver, J.A. (2008). Amyloid fibril formation by bovine milk alpha s2-casein occurs under physiological conditions yet is prevented by its natural counterpart, alpha s1-casein. *Biochemistry*, 47(12), 3926–36. http://dx.doi.org/10.1021/bi701278c.

Thorn, D.C., Meehan, S., Sunde, M., Rekas, A., Gras, S.L., & MacPhee, C.E., et al. (2005). Amyloid fibril formation by bovine milk kappa-casein and its inhibition by the molecular chaperones alphaS- and beta-casein. *Biochemistry*, 44(51), 17027–36. http://dx.doi.org/10.1021/bi051352r.

Townend, R., Weinberger, L., & Timasheff, S.N. (1960). Molecular Interactions in β-Lactoglobulin. IV. The Dissociation of β-Lactoglobulin below pH 3.5 2. *J Am Chem Soc*, 82(12), 3175–9. http://dx.doi.org/10.1021/ja01497a047.

Uttinger, M.J., Heyn, T.R., Jandt, U., Wawra, S.E., Winzer, B., & Keppler, J.K., et al. (2020). Measurement of length distribution of beta-lactoglobulin fibrils by multiwavelength analytical ultracentrifugation. *Eur Biophys J*. http://dx.doi.org/10.1007/s00249-020-01421-4.

vandenAkker, C.C., Engel, M.F.M., Velikov, K.P., Bonn, M., & Koenderink, G.H. (2011). Morphology and persistence length of amyloid fibrils are correlated to peptide molecular structure. *J Am Chem Soc*, 133(45), 18030–3. http://dx.doi.org/10.1021/ja206513r.

Wu, X., Nishinari, K., Gao, Z., Zhao, M., Zhang, K., & Fang, Y., et al. (2016). Gelation of β-lactoglobulin and its fibrils in the presence of transglutaminase. *Food Hydrocolloids*, 52, 942–51. http://dx.doi.org/10.1016/j.foodhyd.2015.09.012.

Yamaguchi, K.-i., Naiki, H., & Goto, Y. (2006). Mechanism by which the amyloid-like fibrils of a beta 2-microglobulin fragment are induced by fluorine-substituted alcohols. *J Mol Biol*, 363(1), 279–88. http://dx.doi.org/10.1016/j.jmb.2006.08.030.

Ye, X., Hedenqvist, M.S., Langton, M., & Lendel, C. (2018). On the role of peptide hydrolysis for fibrillation kinetics and amyloid fibril morphology. *RSC Adv.*, 8(13), 6915–24. http://dx.doi.org/10.1039/C7RA10981D.

Zandomeneghi, G., Krebs, M.R.H., McCammon, M.G., & Fändrich, M. (2004). FTIR reveals structural differences between native beta-sheet proteins and amyloid fibrils. *Protein Sci*, 13(12), 3314–21. http://dx.doi.org/10.1110/ps.041024904.

Unpublished References

Lux, J., Schestkowa, H., Koop, J., Neumann H. R., Selhuber-Unkel, C., Schwarz, K., Drusch, S., Keppler, J.K., Steffen-Heins, A. (2020c) (unpublished). Surface activity and foaming properties of whey protein isolate amyloid and non-amyloid fractions and their synergistic effects.

Schild, K. (2019), Edible functional fibrils – Influence of protein modification on amyloid aggregation of whey protein beta-lactoglobulin, Master thesis at institute of human nutrition and food science, Department of food technology

Ziemer, A., (2020), Modellierung des Einflusses von chemischen und physikalischen Prozessparametern auf die Bildung von amyloiden Aggregaten aus Beta-Lactoglobulin, Master thesis at institute of human nutrition and food science, Department of food technology

8. Summary

The aim of this work is to investigate the influence of process factors on the formation and fragmentation of amyloid and amyloid-like aggregates from whey protein beta-lactoglobulin (BLG).

The specific characteristic of amyloid structures is the stacking of proteinogenic beta-strands to so-called cross-beta sheets. At a pH value of 2 and sufficiently high temperatures, low ion and moderate protein concentration, BLG forms long, semi-flexible amyloid fibrils. Under the same process conditions, but at a pH value of 3.5, flexible worm-like aggregates are formed, which can be described as amyloid-like. While the structure of BLG fibrils is well studied, there is little structural information on the worm-like aggregates at pH 3.5. Furthermore, to date, no comparison of the different morphologies with respect to physico-chemical properties, as well as formation kinetics and stability as a function of mechanical stress or interfaces has been performed.

This information is relevant to estimate the value of the respective aggregates for different applications, such as new kind of materials and medical applications as well as for innovative food technology applications. It was mentioned, that the interfacial properties of amyloid aggregates are different from those of non-aggregated BLG. For example, the application of fibrils leads to a higher physical and chemical stabilization of oil-water emulsions and foams. The high aspect ratio of fibrils lead to higher capillary forces and larger elastic and loss moduli at interfaces compared to spherical particles, which makes the fibrils to an innovative additive for pickering emulsions. However, in the production of emulsions the protein structures are exposed to high shear forces and cavitation in combination with a high specific surface area of the oil-water interface. These process factors can contribute to the degradation of the amyloid aggregates. Furthermore, shear forces and interfaces—in addition to parameters such as temperature, pH value and ion concentration—also have a high relevance for the formation of amyloid structures.

So far, the scenarios of formation and degradation have not been compared yet and detailed investigation of the relevant process factors are lacking. However, findings in this area are important to optimise the formation of amyloid aggregates, to minimise their degradation in processing operations or to prevent their unwanted formation amyloid aggregation in food processing chains.

The first step in the present thesis was the analysis of the structure and the physico-chemical properties of the different aggregates. It was indicated that in contrast to fibrils, which are formed from peptides, worm-like morphologies at pH 3.5 formed from unhydrolysed BLG. After fractionation of aggregated and non aggregated protein, a higher proportion of beta-sheets, a higher compactness, a higher zeta-potential and a lower hydrophobicity of the fibrils compared to the worm-like aggregates could be observed.

In a second step, the dependence of aggregation kinetics on various process parameters such as temperature, pH value, protein concentration, ion concentration and stirring speed in the incubation vessel was investigated. Temperature was identified as the most important factor. Interactions of temperature with pH value and stirring speed were be determined, which are related to the pH-dependent reduction of the denaturation temperature and the viscosity-dependent shear stress.

In further steps, the influence of mechanical energy input and surfaces on the aggregation kinetics was investigated by using chemically modified glass beads in the shaking incubator. It was demonstrated that the aggregation kinetics of amyloid fibrils is strongly dependent on the mechanical energy input and surface chemistry, whereas amyloid-like aggregates are independent of both factors. A shortening of the aggregation length was observed by using glass beads during incubation. In the next step, the length of the aggregates was investigated in more detail using rotor-stator-dispersion and ultra-sonication in one- or two-phase (oil-water) systems. A dependence of the fibril fragmentation on the rotor-stator-shear could be determined, while the worm-like aggregates remained unaffected. A high fragmentation of both aggregates was achieved by the application of cavitation. In two-phase systems, shorter aggregate lengths were observed at lower energy inputs, which indicates a shear force maximizing influence of the interfaces.

In conclusion, this thesis could demonstrates that amyloid and amyloid-like aggregates have different structures, physico-chemical properties, formation kinetics and process stability, which makes them suitable for different technological applications. The application of worm-like aggregates might result in new kind of materials or new functionalities in food products in the future. The innovative approach to produce amyloid fibrils by glass bead-assisted agitation may lead to a more efficient way of fibril production in the future.

9. Zusammenfassung

Das Ziel dieser Arbeit ist die Untersuchung des Einflusses von Prozessparametern auf die Bildung und den Abbau von amyloiden und amyloidartigen Aggregaten aus beta-Lactoglobulin (BLG).

Amyloide Strukturen zeichnet die Stapelung von beta-Strängen zu sogenannten cross-beta-Faltblättern aus. Bei einem pH-Wert von 2 und ausreichend hohen Temperaturen, niedriger Ionen- und moderater Proteinkonzentration bilden sich aus dem Proteinmolekül lange, semiflexible amyloide Fibrillen. Bei den gleichen Prozessbedingungen, aber bei einem pH-Wert von 3,5, entstehen flexible wurmartige Aggregate, die als amyloidartig bezeichnet werden können. Während die BLG Fibrillen bezüglich ihrer Struktur relativ gut untersucht sind, gibt es wenig Informationen bezüglich der Struktur der wurmartigen Aggregate bei pH 3,5. Darüber hinaus wurde bisher kein Vergleich der unterschiedlichen Morphologien hinsichtlich physikalisch-chemischer Eigenschaften sowie Bildungskinetik und Stabilität in Abhängigkeit von mechanischer Belastung oder Grenzflächen durchgeführt.

Diese Information ist relevant, um den Wert der jeweiligen Aggregate für unterschiedliche Anwendungen, wie z.B. neue Materialien oder medizinische Anwendungen, sowie für innovative lebensmitteltechnologische Applikationen einschätzen zu können. In der Vergangenheit konnten bereits die, im Vergleich zum Ausgangsprotein veränderten, Grenzflächeneigenschaften belegt werden. So führt z.B. die Anwendung von Fibrillen zu höherer physikalischer und chemischer Stabilisierung von Öl-Wasser-Emulsionen und Schäumen. Das hohe Längen-Breiten-Verhältnis der Fibrillen erzeugt höhere Kapillarkräfte und größere Elastizitäts- und Verlustmodule an den Grenzflächen, wodurch BLG-Fibrillen idealerweise in innovativen Pickering-Emulsionen eingesetzt werden können. Bei der Emulsionsherstellung sind die Proteinstrukturen allerdings hohen Scherkräften und z.T. Kavitation in Kombinationen mit einer hohen spezifischen Oberfläche der Öl-Wasser Grenzfläche ausgesetzt. Diese Prozessfaktoren können zu einem Abbau der amyloiden Aggregate beitragen. Andererseits haben Scherung und Grenzflächen – neben anderen Faktoren wie Temperatur, pH-Wert und Ionenkonzentration – auch eine hohe Relevanz für die Entstehung von amyloiden Strukturen.

Bis jetzt wurden die Szenarien der Aggregatbildung und des -abbaus nicht gegenübergestellt und auch noch keine tiefergehende Untersuchung der relevanten Prozessfaktoren angestellt. Erkenntnisse hierüber sind aber von Bedeutung, um z.B. die Bildung von amyloiden

Aggregaten zu optimieren, ihren Abbau in verarbeitenden Prozessen zu minimieren oder ihre ungewollte Bildung in lebensmittelverarbeitenden Prozessketten zu verhindern.

In dieser Arbeit erfolgte als erster Schritt die Untersuchung der Struktur und der physikalisch-chemischen Eigenschaften der unterschiedlichen Aggregate. Es konnte gezeigt werden, dass im Gegensatz zu den Fibrillen, die aus Peptiden entstehen, bei pH 3,5 unhydrolysiertes BLG zu den wurmartigen Morphologien assembliert. Nach der Fraktionierung von aggregierten und unaggregierten Proteinen konnte ein höherer Anteil an beta-Faltblättern, eine höhere Kompaktheit, eine höhere Oberflächenladung und eine geringere Hydrophobizität der Fibrillen im Vergleich zu den wurmartigen Aggregaten festgestellt werden.

Im zweiten Schritt wurde die Abhängigkeit der Aggregationskinetik von verschiedenen Prozessparametern, wie Temperatur, pH-Wert, Proteinkonzentration, Ionenkonzentration und Rührgeschwindigkeit im Inkubationsgefäß untersucht. Die Temperatur konnte als wichtigster Faktor identifiziert werden. Es konnten außerdem Wechselwirkungen der Temperatur mit pH-Wert und der Rührgeschwindigkeit festgestellt werden. Diese basierten auf der pH-abhängigen Reduzierung der Denaturierungstemperatur sowie der viskositätsabhängigen Schubspannung. In weiteren Schritten wurde der Einfluss von mechanischen Energieeinträgen und Oberflächen auf die Aggregationskinetik durch den Einsatz von chemisch modifizierten Glaskugeln im Schüttelinkubator untersucht. Es zeigte sich, dass die Aggregationskinetik von amyloiden Fibrillen eine starke Abhängigkeit vom mechanischen Energieeintrag und von der Oberflächen-Chemie aufweist, während amyloidartige Aggregate gegenüber beiden Faktoren unabhängig sind. Bereits durch den Einsatz der Glaskugeln konnte eine Verkürzung der Aggregatlänge festgestellt werden, welche im nächsten Schritt unter Einsatz von Rotor-Stator-Dispersion und Ultraschall in ein- oder zweiphasigen (Öl-Wasser) Systemen tiefergehend untersucht wurde. Hierbei konnte eine Abhängigkeit der Fibrillenverkürzung von der Rotor-Stator-Scherung festgestellt werden, während die wurmartigen Aggregate unverändert blieben. Eine hohe Fragmentierung von beiden Aggregaten wurde durch Applikation von Kavitation erreicht. In zweiphasigen Systemen wurden geringere Aggregatlängen bereits bei niedrigeren Energieeinträgen erreicht, was auf einen scherkraft-maximierenden Einfluss der Grenzflächen hinweist.

Zusammenfassend konnte diese Arbeit zeigen, dass beide Aggregationsformen unterschiedliche Eigenschaften hinsichtlich ihrer Struktur, physikalisch-chemischen Eigenschaften, Bildungskinetik und Prozessstabilität aufweisen, was sie für unterschiedliche technologische Anwendungen geeignet macht. Die Verwendung von wurmartigen Aggregaten

könnte zu neuen Materialien oder Funktionalitäten in Lebensmittelprodukten führen. Der innovative Ansatz amyloide Fibrillen mit Hilfe von freibeweglichen Glaskugeln beim Schütteln herzustellen, kann zu einer effizienteren und kostensparenderen Möglichkeit der Fibrillen-Produktion führen.

10. Supplemental

10.1. Thioflavin T assay

Background

Thioflavin T (ThT) is a cationic benzothiazole dye (**FIG 10-1 A**) (Biancalana and Koide, 2010; Krebs et al., 2005). Unbounded ThT in aqueous solution has only a low fluorescence intensity with a maximum excitation wavelength of 350 nm and emission wavelength of 440 nm (Krebs et al., 2005). The dye is able to bind to β sheet-rich regions in proteins (LeVine III, 1999; Naiki et al., 1989). This aggregation shifts the excitation and emission maxima to 450 nm and 482 nm and the fluorescence intensity increases significantly (**FIG 10-1 B**) (Biancalana and Koide, 2010). This increase is probably caused by the partially restricted mobility of the ThT conformers. Due to a low energy barrier in solution, the benzylamine and benzothiazole can rotate freely via their common carbon bond. This rotation ensures a fast extinction of the excited state and thus results in low emission. After binding, the conformers are not able to rotate, thus the excited state is maintained longer and therefore the fluorescence intensity is significantly increased (Krebs et al., 2005). How exactly the binding between the secondary structure and the dye occurs is not clear to date (Biancalana and Koide 2010). A possible alignment of ThT to beta-sheet structure is illustrated in **FIG 10-1 C.**

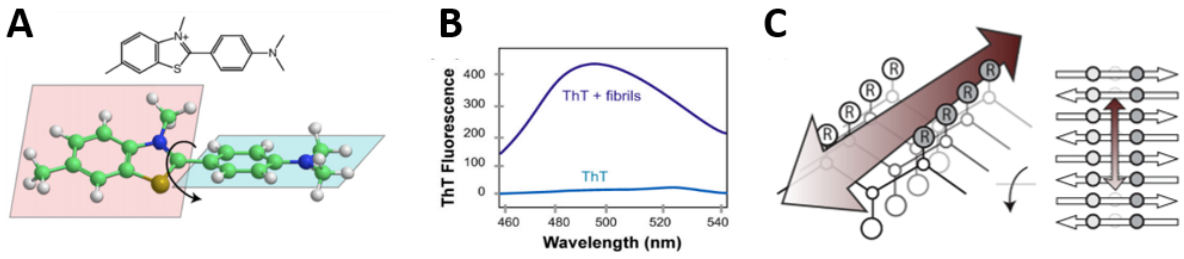

FIG 10-1 Chemical structure of ThT (**A**), the ThT-fluorescence before and after binding (**B**) and alignment of ThT at the surface of beta-sheet-structures (**C**) (Biancalana and Koide, 2010).

Implementation

The 3.0 mM ThT-Stock solution was prepared by solution of 8.766 NaCl and 18 mg ThT in 1 000 ml of a 10 mM phosphate buffer. The samples were first diluted to 1% protein with milli-Q water adjusted to the corresponding pH value and then the ThT-assay was performed according to Loveday et al., (2012). For this 48 µl of the diluted sample were added to 4 ml of the previously prepared ThT-solution, vortexed for about 20 seconds and were incubated for 60 s at room temperature. The fluorescence intensity was then measured in a fluorescence spectrophotometer (*Cary Eclipse, Varian GmbH,* Darmstadt, Germany) at 440 Ex. and 482 Em. wavelenght. A 10mm, four-sided ground quartz cells High Precision Cell from *Hellma*

Analytics were used. Each sample was subjected to a triple determination. To ensure that only the formation of amyloid aggregates is measured and to compensate for slight variations in protein content, the mean value of the fluorescence intensities of the corresponding unheated sample (t0) was subtracted.

10.2. Attenuated total reflection - Fourier transform infrared spectroscopy

Background

Infrared spectroscopy was utilized to receive information about the secondary structure of the proteins and amyloid(-like) aggregates. By Fourier transformation a complete spectrum in the mid-infrared range can be generated in a very short time (Barth, 2007). For Attenuated total reflection the infrared beam pass a crystal, where it is reflected several times and interacts with the sample at the interface between sample and crystal. The sample absorbs part of the energy, which leads to attenuation of the beam. Ultimately the beam reaches the detector, which measures the intensity. From the measured intensities and the interferogram without sample interaction the infrared spectrogram can be calculated. Proteins have a characteristic spectrum at 1600 – 1,700 cm^{-1} (Amid I) and 1500 – 1600 cm^{-1} (Amid II), which are linked to the amino acid residues. The absorption of the amide I band is caused by stretching vibrations of the C=O bonds, while the amide II band is caused by bending vibrations of the N-H bonds. Since both bonds are involved in hydrogen bonds, information about the secondary structure of proteins can be obtained via the two bands (Byler and Susi, 1986). During amyloid formation, structural changes occur, which leads structural changes, especially at the 1630 cm^{-1} (intramolecular beta-sheets) and 1620 cm^{-1} (intermolecular beta-sheets) (Moran and Zanni, 2014).

Implementation

Changes of the protein beta-sheet conformation were investigated with the Confocheck™, a specialized protein in solution FTIR System, using a Tensor 2 System from *Bruker Optik GmbH, Ettlingen, Germany* fitted with a thermally controlled BioATR Cell 2. Protein samples at pH 2 or pH 3.5 were diluted to 0.5 or 1 % protein concentration and 20 µl of the sample volume was pipetted onto the ATR crystal. The sample was equilibrated for several minutes to adapt to the target temperature which was set to 25 °C.

The spectra were acquired and averaged over 120 scans at a resolution of 0.7 cm^{-1}. After atmospheric correction for absorbance of CO_2 and H_2O as vapour and solute, respectively, the protein spectra from 4000 cm^{-1} to 900 cm^{-1} were vector-normalized. The amid I band (1590 – 1700 cm^{-1}) was cut out from the whole spectra. For 2nd derivation spectra the second derivation was calculated with 9 smoothing points. To obtain numerical values for the relative changes in

beta-sheets, respective changes in the intensities of the second derivative of FTIR wavenumber 1632 cm^{-1} (intramolecular beta-sheets) and FTIR band wavenumber 1622 cm^{-1} (intermolecular beta-sheets) were determined. From the numerical intensity values at the respective wavenumbers at time t_i, the intensity values of the same wavenumber at time t_0 of the respective measurement series were subtracted.

10.3. Size exclusion chromatography

Background

The size exclusion chromatography (SEC) separates molecules in the solution by molecular weight. The effect of separation bases on the different diffusion volumes of different sized molecules. Smaller molecules can enter the porous polymers of the stationary phase, which increase their available diffusion volume, while larger molecules do not fit in (Kostanski et al., 2004). Because of this larger molecules will eluent in the beginning and the small ones in the end. The stationary phase are porous polymers, such as cross-linked dextran or agarose or copolymers such as dextran-methylenbisacrylamid. The polymer particles have a size of 3 to 35 µm, and pore diameters of 6 to 200 nm (Kuga, 1981).

Implementation

As SEC column a Superdex™ 200 10/300 GL from *GE Healthcare* (*Bio-Sciences AB*, Uppsala, Sweden) was used. The utilised HPLC-system was an Agilent 1100 HPLC equipped with a diode array detector set to 205 nm, 214 nm, 278 nm and 280 nm. The eluent was 0.15 M Tris-HCl buffer pH 8. The flow rate was 0.3 ml/min. Sample injection volume was 50 µl. The column was run at 25 °C. Calibration was conducted for molecular weights between 6,500 and 75,000 Da.

For an analysis of the sample building blocks using the SEC a protocol of Akkermans et al., (2008) was implemented: To obtain a BLG concentration of 0.4 %, 420 µl of the guanidine HCl, DTT and TRIS HCl buffer pH 8 solution were mixed with 200 µl of the 1 wt% protein/fibril solution. The solution was then vortexed and incubated for 60 minutes at room temperature under agitation at 140 RPM. A 0.2 µl cellulose syringe filter was used during transfer of the sample to the HPLC vial.

10.4. References

Akkermans C, Venema P, van der Goot AJ, Gruppen H, Bakx EJ, Boom RM, et al. Peptides are building blocks of heat-induced fibrillar protein aggregates of beta-lactoglobulin formed at pH 2. Biomacromolecules 2008; 9(5): 1474–9.

Barth A. Infrared spectroscopy of proteins. Biochim Biophys Acta 2007; 1767(9): 1073–101.

Biancalana M, Koide S. Molecular mechanism of Thioflavin-T binding to amyloid fibrils. Biochim Biophys Acta 2010; 1804(7): 1405–12.

Byler DM, Susi H. Examination of the secondary structure of proteins by deconvolved FTIR spectra. Biopolymers 1986; 25(3): 469–87.

Kostanski LK, Keller DM, Hamielec AE. Size-exclusion chromatography-a review of calibration methodologies. J Biochem Biophys Methods 2004; 58(2): 159–86.

Krebs MRH, Bromley EHC, Donald AM. The binding of thioflavin-T to amyloid fibrils. J Struct Biol 2005; 149(1): 30–7.

Kuga S. Pore size distribution analysis of gel substances by size exclusion chromatography. Journal of Chromatography A 1981; 206(3): 449–61.

LeVine III H. Quantification of β-sheet amyloid fibril structures with thioflavin T 1999; 1999: 274–84.

Loveday SM, Wang XL, Rao MA, Anema SG, Singh H. β-Lactoglobulin nanofibrils. Food Hydrocolloids 2012; 27(1): 242–9.

Moran SD, Zanni MT. How to Get Insight into Amyloid Structure and Formation from Infrared Spectroscopy. J Phys Chem Lett 2014; 5(11): 1984–93.

Naiki H, Higuchi K, Hosokawa M, Takeda T. Fluorometric determination of amyloid fibrils in vitro using the fluorescent dye, thioflavine T. Analytical Biochemistry 1989; 177(2): 244–9.